1-1-1975

Fundamentals of liquid drop generation with respect to solid capture in wet scrubbers.

Vinod R. Marwaha
University of Windsor

FUNDAMENTALS
OF
LIQUID DROP GENERATION
WITH RESPECT TO
SOLID CAPTURE IN WET SCRUBBERS

A Thesis
Submitted to the Faculty of Graduate Studies
Through the
Department of Chemical Engineering
in Partial Fulfillment of the Requirements
for the Degree of
Master of Applied Science
at the
University of Windsor
by

Vinod R. Marwaha

University of Windsor

1975

APPROVED BY: Alex Empfp

L. P. Matthews

E. A. Pierce

ACKNOWLEDGEMENTS

The author is indebted to his advisors Professor A. W. Gnyp and Professor C. C. St. Pierre, for their continued help, invaluable guidance and counselling during the course of the research reported here.

Financial support which made this work possible was provided by the Ministry of the Environment, Province of Ontario.

The assistance of Mr. V. K. Bewtra for computer work and Mrs. Betty Sheehan for typing the lengthy manuscript is acknowledged.

ABSTRACT

This critical review of theoretical and experimental studies on the atomization of liquids provides a basis for the interpretation of wet scrubber performance. The different methods of generating liquid drops and the experimental techniques used for determining drop size distribution have been described in some detail. Mathematical representations of drop size distribution are discussed and illustrated by application to standard drop size data.

Of the fifty-seven equations available for predicting mean drop diameters seventeen were selected for evaluation. Their accuracy for predicting mean drop diameter was determined by using the data of Ingebo and Foster as a basis for comparison. Penetration, trajectory and dispersion of a transverse jet of scrubbing liquid in a turbulent air stream have also been reported for the data of the same investigators.

Most of the predictive equations for mean drop diameter are empirical, giving highly erroneous results when used outside the range for which they were developed. The more promising predictions appear to be based on

theoretical equations which still need further development. Future work on mathematical representations of drop size distributions calls for better correlation of the amounts of liquid injected and conditions of atomization.

CONTENTS

LIST OF FIGURES

LIST OF TABLES

I. INTRODUCTION

This report outlines the progress made during the 16 month period from 1 September, 1973 to 31 December, 1974 on the research grant "Continuation and Extension of the Evaluation of Wet Collector Performance for Particulate Removal" awarded by the Ontario Ministry of the Environment to the air pollution research group in the Department of Chemical Engineering at the University of Windsor.

A. Aims

The objective of the 1973-74 research program, as determined by Ontario Ministry of the Environment priorities, was to continue the development of a design manual that would permit the evaluation of performance characteristics of industrial wet gas cleaning devices. Under the terms of the grant, the research personnel were

i. to continue the collection and critical evaluation of literature pertinent to the operation of wet collectors

ii. to develop a detailed theoretical analysis of the chemical and physical processes involved in the operation of wet collectors and

iii. to develop a preliminary outline of a design manual that can be used for the analysis of

the performance characteristics of industrial wet gas cleaning equipment.

B. Program Development

In order to achieve the desired aims, the research group was organized to permit investigations on

i. Fundamentals of Gaseous-Particulate Flow Around Solid and Liquid Spherical Obstructions

ii. Atomization and Generation of Liquid Droplets With Respect to Solid Capture

iii. Solid Particle Collection in Wet Scrubbers by Thermophoretic and Diffusiophoretic Effects Including Condensation and Evaporation and

iv. Fundamentals of Venturi Scrubber Performance.

II. INFORMATION SEARCH

A. Open Literature

To date, a total of 2000 references pertaining to the evaluation of gas cleaning equipment performance have been collected and critically evaluated.

B. Conferences

The following conferences, where relevant papers were presented, were attended:

Twelfth Annual Purdue Air Quality Conference
Indianapolis, Indiana 6-8 Nov., 1973

Fourth Annual Environmental Engineering and Science Conference
Louisville, Kentucky 4-5 March, 1974

Pollution Control Association of Ontario Educational Seminar
Toronto, Ontario 14 March, 1974

Ministry of the Environment Research Seminar
Toronto, Ontario 21 March, 1974

Ontario Section APCA Spring Meeting
Waterloo, Ontario 6-8 May, 1974

Canadian Symposium on Fluid Dynamics
London, Ontario 21 June, 1974

University of Waterloo Special Lecture Series
Waterloo, Ontario 26 June, 1974

In addition, papers were obtained from the following conferences which were not attended:

The New York Academy of Sciences Conference on Odors: Evaluation, Utilization and Control New York, New York	1-3 October, 1973
Sixty-Sixth Annual Meeting, AIChE Philadelphia, Pennsylvania	11-15 November, 1973
ASHRAE 1974 Semi-Annual Meeting Los Angeles, California	3-7 February, 1974
State-of-the-Art of Odor Control Technology Conference, APCA Pittsburgh, Pennsylvania	7-8 March, 1974
Seventy-Sixth National Meeting, AIChE Tulsa, Oklahoma	7-14 March, 1974
American Industrial Hygiene Conference Miami Beach, Florida	12-17 May, 1974
Seventy-Seventh National Meeting, AIChE Pittsburgh, Pennsylvania	2-5 June, 1974
Sixty-Seventh Annual Meeting, APCA Denver, Colorado	9-13 June, 1974

C. Advanced-Seminars

In its effort to remain knowledgeable on the current state of technology associated with stack sampling for gaseous and particulate pollutants, the research group offered six stack sampling courses during the past year. Two of these were tailored specifically for members of the Ontario Ministry of the Environment. A third was designed to fulfill the needs of 18 officials selected from across the country by the Air Pollution Control Directorate of Environment Canada.

Interactions with engineers, chemists, technicians and administrators from industrial and regulatory organizations provide the group with added insight into the problems related to testing and performance of gas cleaning devices.

D. Equipment Manufacturers and Suppliers

A significant effort has been made to up-date the collection of trade literature available from manufacturers and suppliers of gas cleaning equipment and related components. This will be particularly important to future work involving the assessment of the performance of typical commercially available wet collectors.

E. Regulatory Agencies

Mutually profitable contacts were maintained during this period with personnel at:

Ontario Ministry of the Environment	Toronto, Ontario
U.S. Environmental Protection Agency Office of Air Programs	Research Triangle Park, North Carolina
Air Pollution Control Directorate, Environment Canada	Ottawa, Ontario
Montreal Urban Community	Montreal, Quebec

F. Universities and Research Institutes

Correspondence and personal visits were maintained with individuals at:

University of Waterloo Waterloo, Ontario	Chemical Engineering
University of Western Ontario London, Ontario	Dr. J. M. Beeckmans
University of British Columbia Vancouver, British Columbia	Chemical Engineering
The University of Texas Austin, Texas	Chemical Engineering
Oakland University Rochester, Michigan	School of Engineering
University of Bristol Bristol, England	Aeronautical Engineering
Illinois Institute of Technology	Odor Sciences Centre
Lawrence Livermore Laboratory University of California Livermore, California	Technical Information Department
University of Bridgeport Bridgeport, Connecticut	Dr. E. S. Tillman, Jr.
The University of Leeds Leeds, England	Prof. N. Dombrowski
Indian Institute of Science Banglore, India	Prof. R. Kumar

Jet Propulsion Laboratory California Insitute of Technolgoy Pasadena, California	George A. Mitchell, Document Review Group
Syracuse Univeristy Dept. of Chemical Engg. and Materials Science Syracuse, New York	Dr. R. Rajagopalan
Environmental Protection Agency Air Pollution Technical Information Centre Research Triangel Park North Carolina	Johon E. Knight
Research Centre The British Petroleum Company Limited Sunburn on Thames Middlesex, United Kingdom	Dr. E. L. Howe
Dept. of Chemical Engg. Iowa State University Ames, Iowa	Dr. J. C. Hill

III. FUNDAMENTALS

A. Definitions

The term "atomization", according to Romp [1], was introduced in 1875 by Isherwood who made a study of oil burning. The etymology of the word, as explained by Castleman [2] implies the formation of drops that are so fine that they are indivisible. Such a concept has a definite physical significance for liquid jets, Castleman claims, because of the limit to drop fineness that is implied. Since "atomization" denotes the formation of very fine droplets, Castleman recommends that the term "disintegration" be used when the drop sizes are larger than the limiting value of seven microns. Although "atomization" as the connotation of "reducing liquid to atoms", is a very exaggerated term for the formation of sprays of liquids, it is, nevertheless, a term now generally used in all English speaking countries and will be used in this report.

The recent literature tends to make a distinction between "atomizing nozzles" and "spray nozzles". The former are two fluid or pneumatic type devices that use air or steam to accomplish atomization. The second category represents pressure-type nozzles in which the pressure on the liquid supplies the energy for "breakup". The use of the adjective

"atomizing" for two-fluid nozzles probably results from the fact that they usually generate smaller droplets than those formed by pressure type "spray nozzles".

The concept of "breakup" refers to the initial separation of a liquid jet. "Disintegration" implies the formation of more or less coarse drops while "atomization" describes the formation of very fine droplets.

B. Background

Atomization of a liquid, usually water, is considered to be one of the most important steps in the separation of suspended matter from gas streams in wet collectors. Suspended matter includes dusts, aerosols, fumes and mists. In most wet scrubbers the liquid is dispersed through the gas so that collection of suspended matter is the result of particulate interaction with the individual droplets of the scrubbing liquid.

One of the most efficient and widely used wet devices is the Venturi scrubber. In its simplest form, it consists of a constriction in the duct carrying the dirty gas. Scrubbing liquor is introduced at the constriction in the form of low velocity jets. The accelerating liquid drops capture suspended matter at very high collection efficiencies, for even finer particles.

In chamber scrubbers the dirty gases are influenced by one or more spray nozzles or mechanical spray generators in which liquid jets impinge upon rotating disks. Sometimes the gases are forced to follow a torturous path that provides for repeated contact with scrubbing liquid through appropriate baffling. Another form of particulate-drop contacting utilizes gravity sprays with counter current flow of dirty gases. Sometimes the scrubbing liquid is supplied in the form of a high velocity jet directed along the axis of a Venturi nozzle. Centrifugal motion can be imparted to the gas stream by introducing it tangentially into the scrubber. Scrubbing liquid is often introduced through nozzles injecting circumferentially or radially. In inertial orifice scrubbers the scrubbing liquid is atomized at the expense of the kinetic energy of the gas stream.

Because the removal of suspended matter in wet collectors depends primarily on liquid drop characteristics, it is of utmost importance to determine the drop diameter for which maximum collection can be expected, for a given size range of particulate matter. Having established the optimum drop size, the problem then is to generate such a spray and to uniformly distribute the appropriate drops in a gas stream for maximum collection efficiency with minimum use of energy. Since it is practically difficult, if not impossible, to generate a

a spray in which each drop has the same optimum size, it is essential to know the range over which the drop diameters will vary for any set of conditions, simulating those which exist in wet scrubbers.

For a Venturi scrubber, the overall cleaning mechanism is not fully understood, although it is considered to be an extremely effective device. The venturi, classified as an inertial impaction type of gas scrubber as well as an absorber or extractor, has been widely used industrially [3-8]. It is considered to be as efficient as the electrostatic precipitator [9]. Although the venturi system is simple to install and maintain, it is expensive to operate because of the high air pumping costs. If correct scrubbing fluid atomization details were known, it should be possible to reduce the operating costs and, perhaps, to improve collection efficiencies. In this inertial impaction type of scrubber, it is desirable to generate drops, which are uniformly distributed over the cross-section of the throat and diffuser.

This work provides a review and evaluation of the investigations carried out on atomization, with reference to wet scrubbers in general, and Venturi scrubbers in particular. Several hundred papers and reports on the atomization of liquids, for many different purposes, have been analyzed.

Studies dealing with generation of sprays for

i. agricultural and insecticidal uses

ii. therapeutic aerosols

iii. internal combustion, jet and rocket engine fuel-air mixtures

iv. humidification operations

v. drying of solids suspended in liquids

have been related to the literature concerned with continuous injection of liquids into gases, as applied to wet scrubbers.

C. Organization

1. Liquid Drop Generation

In any wet gas cleaning device it is necessary to atomize and distribute the scrubbing liquid. The performance of the equipment is critically dependent on the drop size produced by the atomizer and the manner in which the gaseous medium mixes with the generated drops. Thus, a study of the characteristics of different atomizers is important if an optimum selection is to be made for any specific need.

Seven different means of atomizing liquids into drops have been reported. Pressure nozzles, pneumatic atomizers, rotating disks or cups, vibrating devices, impingement with a solid surface and electrical atomization appear to be promising techniques for drop generation.

2. Drop Size Analysis

The ultimate spray from any nozzle consists of a spectrum of polydisperse droplets which vary over a wide size range. On the basis of free fall, the maximum possible drop diameter for a water spray or rain has been reported as 8000-9000 microns [10]. For a suddenly applied sonic velocity of 340 m/sec, which might be encountered in an air atomizer, the survival diameter is 6-7 microns [2, 10] although drops smaller than 1 micron have also been reported [11]. This means this liquid spray encompasses a 10^3 fold range of drop sizes, a 10^6 fold range of drop areas, and a 10^9 fold range of drop volumes. Furthermore, because of the complex nature of the breakup mechanism, any one spray represents at least a ten fold range of drop sizes and a thousand fold range of drop volumes.

The direct method of analysis involves trapping a representative portion of the spray for counting and sizing the droplets. The sizes are separated into class

intervals and the number of droplets ΔN in each class interval is counted. There are several ways of representing these data graphically according to

i. a histogram of ΔN vs $\bar{X}_i$, the class mid point diameter

ii. a cumulative graph of total number fraction of drops less than diameter X

iii. a cumulative volume fraction of sprayed liquid with drop diameter less than X

A typical analysis of drop size data has been included in Chapter V.

3. Drop Size Distribution Correlations

It is sometimes convenient to select an empirical functional form for the distribution of drop sizes which will satisfy available data. Such a function should be easy to manipulate mathematically and should have a minimum number of arbitrary constants. The constants, which are obtained from an analysis of the size distribution, characterize the distribution of a particular spray. They are different for different sprays. Usually the number of arbitrary constants is restricted to two. One represents some average diameter and the other a uniformity or spreading index, which

is a measure of the size homogeneity. The ultimate test of a good distribution function (but one which is rarely applied because of the scarcity of reliable data) is that the arbitrary constants correlate as functions of the operating conditions, the geometry of the spraying device, and the physical properties of the spray liquid.

Several mathematical representations of drop size distribution have been discussed in the main text, with special emphasis focussed on the Nukiyama-Tanasawa expression and the log-normal distribution. The use of these functions is illustrated with standard drop size data.

4. Prediction of Mean Drop Diameter

In most wet scrubbers the liquid is dispersed through the dirty gas. The collection of suspended matter is the result of particulate interaction with the dispersed droplets of the scrubbing liquid. Thus, the effectiveness of any wet collector is due to the sum of all possible interactions of all the droplets with the suspended matter.

Fundamental analysis of the collection of small particles reveals that, in general, for particles of normal density in the micron and submicron ranges of size, the important collection mechanisms are due to

i. gravitational forces

ii. centrifugal forces

iii. electrostatic forces

iv. magnetic forces

v. inertial impaction

vi. direct interception

vii. Brownian diffusion

viii. thermophoretic forces

ix. diffusiophoretic forces

x. wake entrainment.

The importance of drop size to particulate removal in wet collectors can be illustrated in terms of the inertial impaction and direct interception mechanisms.

A particle, carried along by a gas stream on approaching an obstruction such as a liquid droplet tends to follow the gas stream around the obstacle but may strike the droplet because of an inertial effect. In Figure 3.1 the solid lines represent the fluid streamlines around a droplet of diameter X. The dotted lines represent the paths of particles which initially followed the fluid stream lines.

For a flow around a droplet, the quantity D/X, where D is the distance between limiting streamlines A and B, represents the fraction of particles initially present in

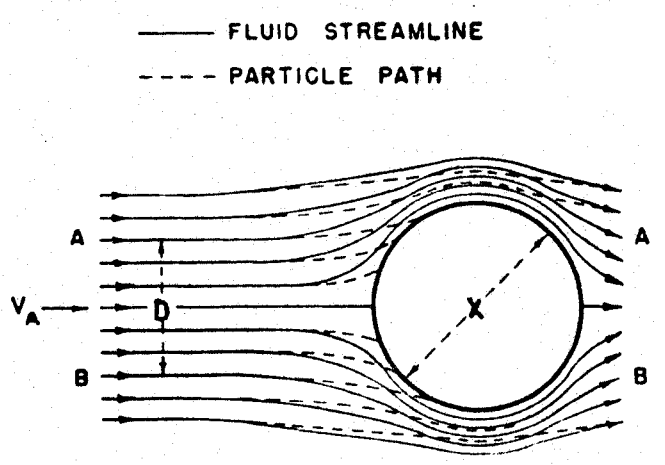

FIGURE 3.1: Inertial Impaction Upon Single Liquid Drop

a volume swept by the droplet which will be removed by inertial impaction. Normally the particle paths represent the trajectories of particle centres or point masses.

The trajectory of the centre of any relatively large particle may not intersect with the droplet, however the particle may pass close enough for the surface of the particle to touch the collecting drop and be arrested by it.

It follows, from what has been discussed, that liquid drop diameter, X, is an essential parameter in the estimation of the collection efficiency of a single drop. The overall scrubber efficiency is then evaluated by summing up the collection on the entire drop spectrum in a spray. In the past an actual polydisperse droplet spray was modelled by a fictitous monodisperse spray with every drop having a hypothetical mean diameter, X, which was used for the evaluation of collection efficiency in any wet scrubber.

The present work is an attempt to correlate the existing literature pertaining to prediction of mean drop diameters. Seventeen equations, reported in the main text, provide means of anticipating mean drop diameters when a liquid is injected in a flowing gas stream.

REFERENCES

1. Romp, H. A., Oil Burning, Martinus Nijhoff (The Hague), 1937.

2. Castleman, R. A., Jr., The Mechanism of the Atomization Accompanying Solid Injection, NACA Report No. 440, 12 (1932).

3. Anonymous, Scrubber Ends Coker's Napthalene Woes, Chemical Engineering, 65, (10), 78 (1958).

4. Basse, B., Gases Cleaned by Use of Scrubbers, Blast Furnace and Steel Plant, 44, (11), 1307-1310 and 1312 (1956).

5. Bishop, C. A., Campbell, W. W., Hunter, D. L., and Lightner, M. W., Successful Cleaning of Open Hearth Exhaust Gas With a High-Energy Venturi Scrubber, APCA Journal 11, (2), 83-87 (1961).

6. Eberhardt, J. E., and Graham, H. S., The Venturi Washer for Blast Furnace Gas, Iron and Steel Engineer, 32, 63-71 (1955).

7. Shah, I. S., New Flue Gas Scrubbing System Reduces Air Pollution, Chemical Engineering 74, (7), 84 (1967).

8. Willet, H. P., and Pike, D. E., Venturi Scrubber for Cleaning Oxygen Steel Process Gases, Iron and Steel Engineer 38, 126-31 (1961).

9. Stern, A. C., Air Pollution, Chapter 46 by S. Calvert 2nd Ed. Vol III, Academic Press (1968).

10. Ranz, W. E., On Sprays and Spraying, Department of Chemical Engineering Research, The Pennsylvania State University, University Park, Pennsylvania, 1956.

11. Dombrowski, N., Spray Drying in Biochemical and Biological Engineering Science, Vol. 2, editor N. Blakebrough, Academic Press (1968).

IV. LIQUID DROP GENERATION AND SIZE MEASUREMENT

A. Liquid Drop Generation

Liquids can be disintegrated into droplets by seven different methods [1, 2]. Atomization techniques include:

i. solid injection using pressure nozzles

ii. pneumatic breakup involving disintegration of a liquid encountering a high velocity gas stream. This is commonly called two fluid atomization.

iii. use of rotating disks or cups, from the periphery of which the liquid is discharged at high velocity

iv. vibrating devices employing sonic or mechanical vibrations

v. impinging jets, providing collision of two liquid streams

vi. impingement of a liquid jet against a solid surface, and

vii. application of high voltage electricity.

1. Solid Injection

The most widely used method for atomizing liquids is solid injection by pressure atomizers. In a typical pressure atomizer a liquid is forced under pressure through an orifice.

The form of the resulting spray can be controlled by varying the direction of flow towards the orifice and the applied pressure. Conical and flat spray sheets are produced by this method.

Joyce [3] points out that there are two basic types of pressure jet atomizers. The

a. plain orifice type, which may employ pressures as high as 5000 psi, is used in diesel and other internal-combustion engines
b. centrifugal swirl type, which requires low pressures, is used in several industrial applications such as spray painting, spray drying, insecticide spraying, food processing and air and water pollution control.

a. Plain Orifice

Discussions will be limited to plain orifice nozzles employing low pressures.

The simplest method of effecting liquid disintegration is through the application of pressure. When a stream of an inviscid liquid issues from an orifice into a gas at relatively low velocity, the most likely length into which the liquid will break, as shown by Rayleigh [4], is about 4.5 times the diameter of the liquid jet. Rayleigh predicted the conditions necessary for the collapse of a liquid jet

issuing at low velocity. Assuming irrotational flow of a non-viscous jet, he deduced that a small disturbance, symmetrical about the axis of the jet, as suggested in Figure 4.1, would cause breakup when the amplitude of the disturbance grew to one-half the diameter of the undisturbed liquid jet.

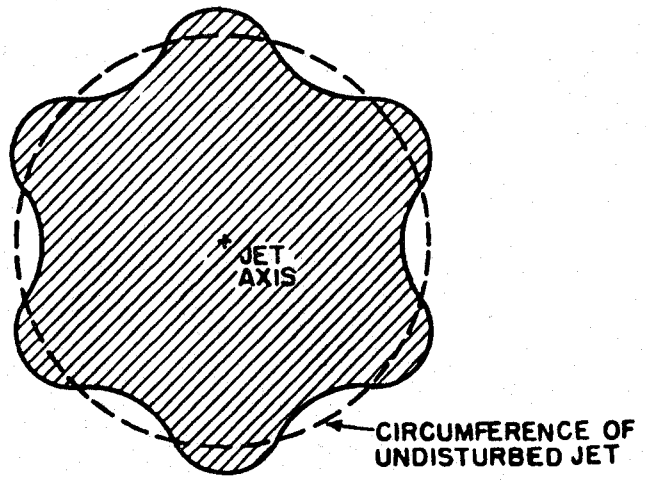

FIGURE 4.1: Idealized Representation of Initial Symmetrical, Circumferential Disturbance Around a Liquid Jet [2]

This behavior may be represented by the equation

$$\alpha = \alpha_o e^{qt} \qquad 4.1$$

where

α = amplitude of the disturbance at time t, cm

α_o = initial amplitude of the disturbance, cm

q = time rate of growth of the amplitude of disturbance, which is a function of liquid surface tension, density, jet diameter, and wave length of the disturbance, seconds^{-1}

t = time, seconds

Figure 4.2 shows an idealization of the Rayleigh breakup of a

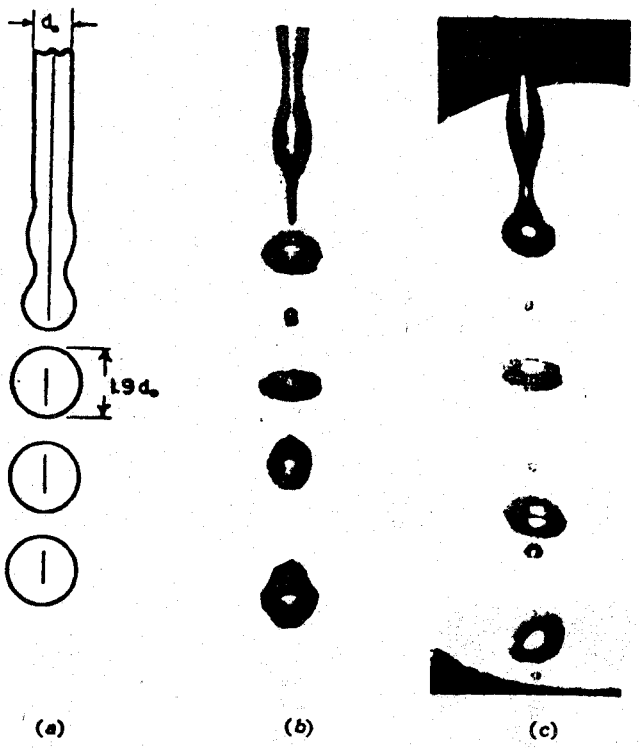

FIGURE 4.2: (a) Idealized Jet Breakup Suggesting Uniform Drop Diameter and no Satellites.

(b) and (c) Actual Breakup of a Water Jet as Shown by High-Speed Photographs [2].

falling liquid jet according to equation 4.1 and breakup as it actually occurs. It will be noted in Figure 4.2(a)

that a liquid jet, disintegrating simply as a result of inertial forces, first starts to neck down and eventually collapses to form drops. In Figure 4.2(b) and (c) the drops are interspersed with small satellite drops at the point of necking down. The theory of Rayleigh [4] does not predict the occurrence of these small satellite drops. Although it attributes droplet formation to interfacial tension forces alone, the Rayleigh theory does predict reasonable results for low-viscosity, high interfacial tension liquids.

In a more general mathematical analysis of the disintegration of a viscous jet, Weber [5] developed a general differential equation for the breakup motion of a jet when both viscous and inertial forces offer significant resistance. His analysis essentially extended Rayleigh's work to include the effect of viscous forces on jet breakup. From Weber's analysis the ratio ℓ/d, required to produce maximum stability for viscous jets, is given by the expression

$$\ell/2R = \ell/d = \pi \sqrt{2} \left[1 + \frac{3\mu}{\sqrt{\rho_L \sigma_L d}}\right]^{\frac{1}{2}} \qquad 4.2$$

where

ℓ = wave length of disturbance, cm

R = initial jet radius = $\frac{d}{2}$ cm

μ = viscosity of liquid, poise

ρ_L = density of liquid, gm /cm^3

σ_L = surface tension of liquid, dynes/cm

Haenlein [6] presented experimental evidence to support Weber's theoretical analysis. His studies of the breakup lengths of fluids of various viscosities and surface tensions indicated that for liquids having a viscosity of the order of 860 centipoises the ratio of wave length to jet diameter producing maximum instability could range from 30 to 40, in contrast to the value of 4.5 predicted by the Rayleigh theory for nonviscous jets. Haenlein [6] showed five characteristic forms of disintegration distinguished by

i. surface disturbances resulting from imperfections in the jet, vibrations of the nozzle, or from particles of dust or air bubbles. Figures 4.3(a) and 4.3(b) show the most important rotationally symmetric disturbances. Figure 4.3(c) illustrates the one-sided wave-like disturbances that occur for wave length to jet diameter ratios of approximately 20

ii. drop formation without the influence of surrounding air. This occurs at low velocities, when the air does not appreciably affect the shape of the

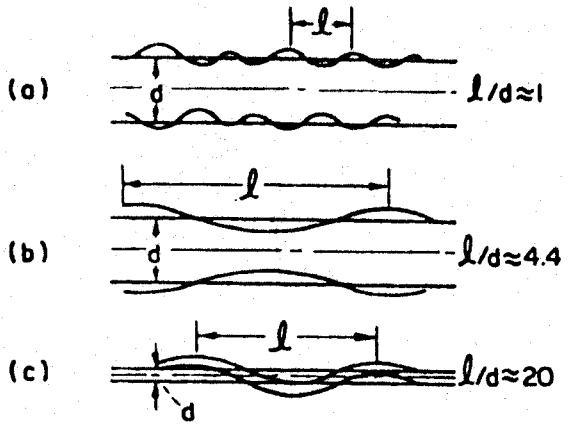

FIGURE 4.3: Surface Disturbances of a Jet. (a) and (b) Rotationally Symmetric, (c) One-Sided Wavelike [6]

jet. Figure 4.4(a) represents the disintegration of a jet without air influence for an initial disturbance of $\ell/d = 4.42$

iii. drop formation with the influence of air as shown in Figure 4.4(b). The aerodynamic forces act similarly to wind blowing over water and produce a definite initial disturbance. The air velocity increases over the wave crests and decreases over the troughs. At the same time, the pressure decreases over the crests and increases over the troughs so that the wave motion is intensified and drops are formed

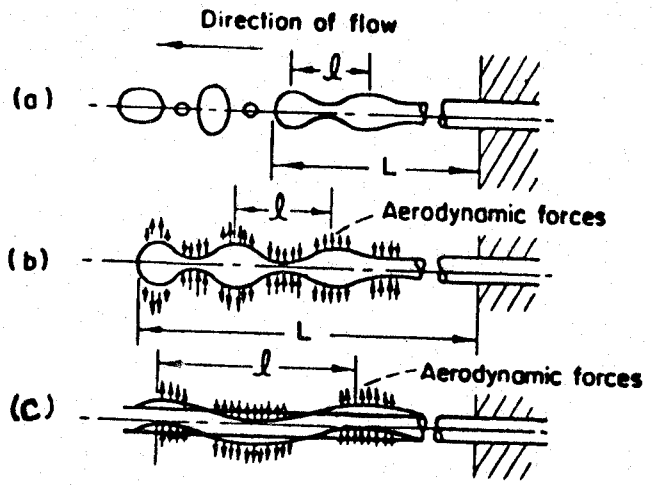

FIGURE 4.4: Disintegration Phenomena. (a) Drop Formation Without Air Influence, (b) Drop Formation With Air Influence, (c) Wave Formation Through Air Influence [6].

iv. wave formation due to action of air. This occurs when the velocity is further increased, and the initial disturbances become one-sided under the augmented influence of the air, as shown in Figure 4.4(c).

v. complete disintegration of the jet. This occurs when the velocity is further increased and the jet loses all regularity of form. Haenlein offered

no explanation concerning the mechanics of this last and most important form of disruption of the jet.

The experimental data of Haenlein [6] were correlated by Ohnesorge [7] who studied the mechanism of atomization from the standpoint of dimensional analysis. For the case of atomization of a liquid jet without the influence of the surrounding air, the mechanism of breakup could be expected to depend on jet diameter, jet velocity, liquid density, surface tension, and viscosity. The breakup mechanism of a jet, as predicted by dimensional analysis, would appear to be a function of the jet Reynolds number, $Ud\,\rho_L/\mu$, and a dimensionless group, $\mu/\sqrt{\sigma_L \rho_L\, d}$, sometimes referred to as the z-number where

U = liquid velocity of jet, cm/sec

d = diameter of liquid jet, cm

ρ_L = liquid density, gm/cm^3

μ = liquid viscosity, poise

The Ohnesorge [7] plot of z-number vs Reynolds number classified the modes of atomization into four groups according to the rapidity of drop formation. His four categories included

i. slow dripping from an orifice without jet formation

ii. the Rayleigh mechanism of jet breakup wherein an axially symmetric disturbance produces breakup, as described previously

iii. breakup caused by disturbances which are symmetrical about a helical axis starting at the orifice (as treated by Haenlein and Weber)

iv. the so-called atomization of the jet

The Ohnesorge classifications apply to the breakup of a jet issuing from an orifice as a solid stream of liquid with only one principal velocity component. Atomizers used in industrial applications, however, may produce breakup by imparting to the liquid both translational and rotational velocity components, which produce liquid sheets and ligaments that become unstable in a manner quite similar to that of the jets just discussed.

b. Centrifugal Swirl Type Atomizer

This type of atomizer can produce conical or fan spray sheets.

i. Swirl Type Atomizers Producing Conical Sheets

Figure 4.5 shows the design principles of a simple swirl type atomizer. The liquid, under pressure, is fed through tangentially disposed ducts, slots, or channels leading to a circular space called the vortex or swirl chamber. As the liquid spins or swirls around, its angular velocity increases inversely as the radius of swirl. This leads to the formation of an air core throughout the nozzle. The rotating mass of liquid is forced forward, around the core of air, towards the discharge orifice, which has a small diameter compared to that of the swirl chamber. The swirling liquid is under the influence of two main forces. A translational force moves the liquid axially forward. A centrifugal or spinning component makes the liquid fly tangentially outwards immediately after it emerges from the restricting boundary wall of the orifice.

1. Tangential Feed Ducts
2. Air Core
3. Vortex or Swirl Chamber
4. Discharge Orifice
5. Cone Angle of Spray

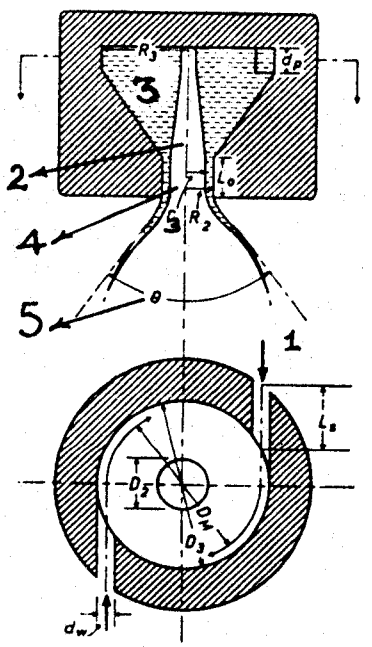

FIGURE 4.5: Principle of a Simple Swirl Type Atomizer

As a result of these two forces the liquid emerges from the orifice as a divergent cone which forms a rapidly thinning conical sheet [3]. Various designs of swirl spray nozzles in current use are shown in Figure 4.6.

The form of the conical sheet depends upon the working pressure. At low pressures the liquid first forms a bubble as shown in Figure 4.7(a). With increasing pressures the bubble opens to form a hollow cone according to Figure 4.7(b). As the pressure is increased further, the curved surface straightens, with the region of disintegration moving closer towards the orifice as depicted in Figure 4.7 (c) and (d). The pressure at which each stage occurs depends on the nozzle design and physical properties of the liquid, particularly the viscosity and surface tension. Tanasawa and Kobayasi [8] have shown that for the nozzle design illustrated in Figure 4.6(b), the last stage corresponds to normal operating conditions. This occurs when the Reynolds Number,

$$N_{Re} = U_i \, R_3/\nu \qquad 4.3$$

is greater than 2800, where

N_{Re} = Reynolds number

U_i = liquid velocity at inlet to swirl chamber, cm/sec

R_3 = swirl chamber radius, cm

$\nu = \frac{\mu}{\rho_L}$ = fluid kinematic viscosity, cm^2/sec

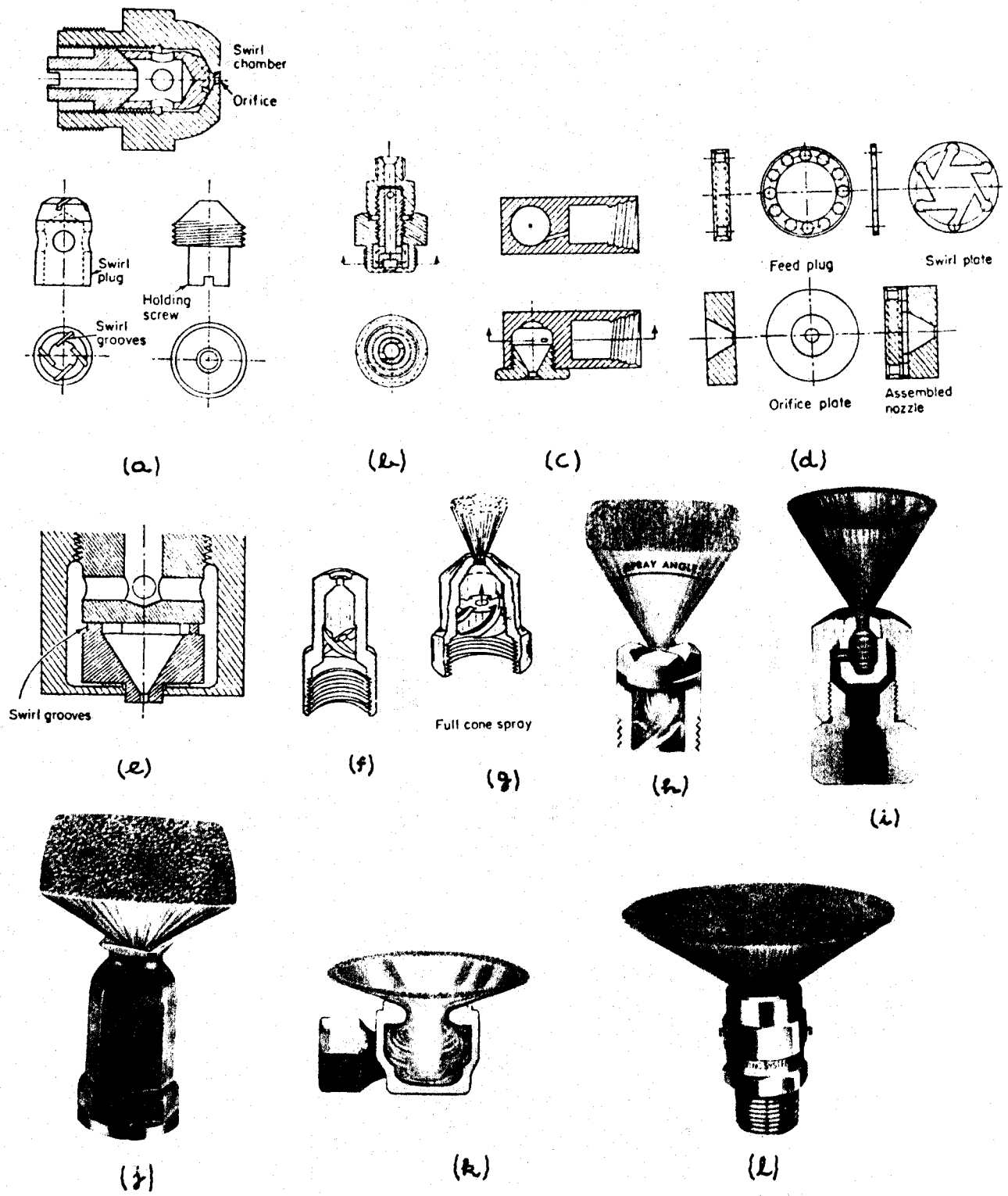

FIGURE 4.6: Characteristic Design of Swirl Spray Nozzles

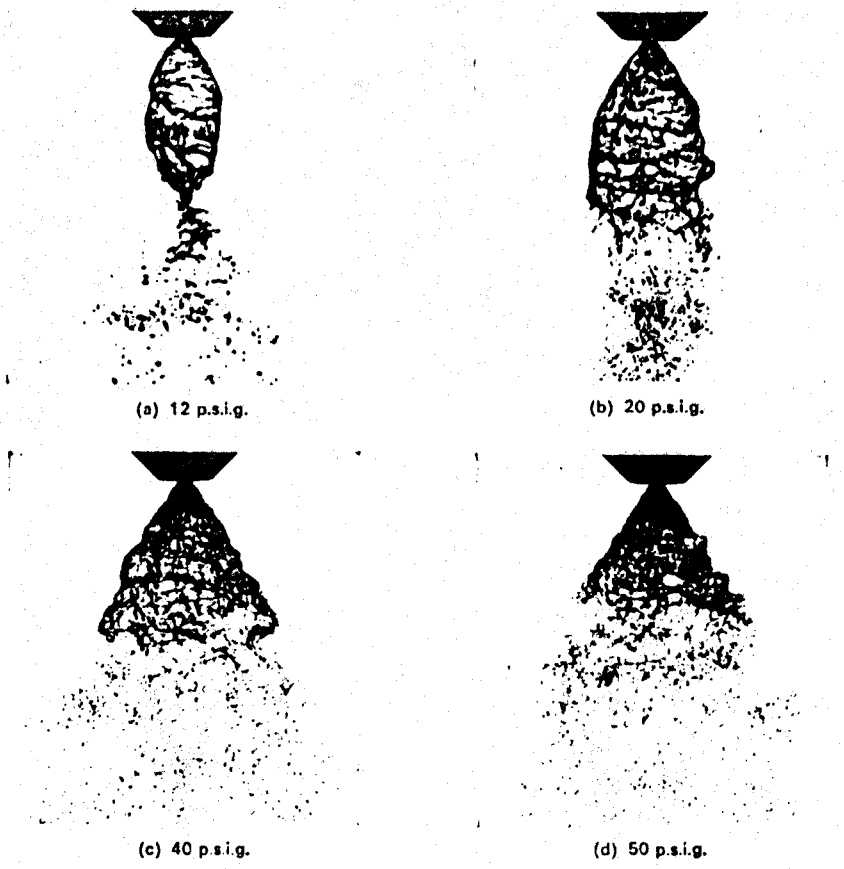

FIGURE 4.7: Development of Conical Sheet with Differential Ejection Pressure [1]

The discharge coefficient, C_Q, and spray angle, θ, are two important parameters which determine the character of the conical spray. These have been shown to be functions of the dimensionless group $\Delta' = A_s/(D_2 D_M)$ whose

A_s = total area of swirl grooves, cm^2

D_2 = orifice diameter, cm

D_M = mean diameter of swirl chamber, cm

The discharge coefficient, C_Q, relates to volumetric flow rate, Q_v, to the pressure drop across the atomizer, ΔP, and orifice area, A, by the usual relationship

$$Q_v = C_Q A\sqrt{\frac{2\Delta P}{\rho_L}} \qquad 4.4$$

Figure 4.8 provides the relationships between spray angle θ, discharge coefficient C_Q, and nozzle dimensionless group Δ' as reported by several workers.

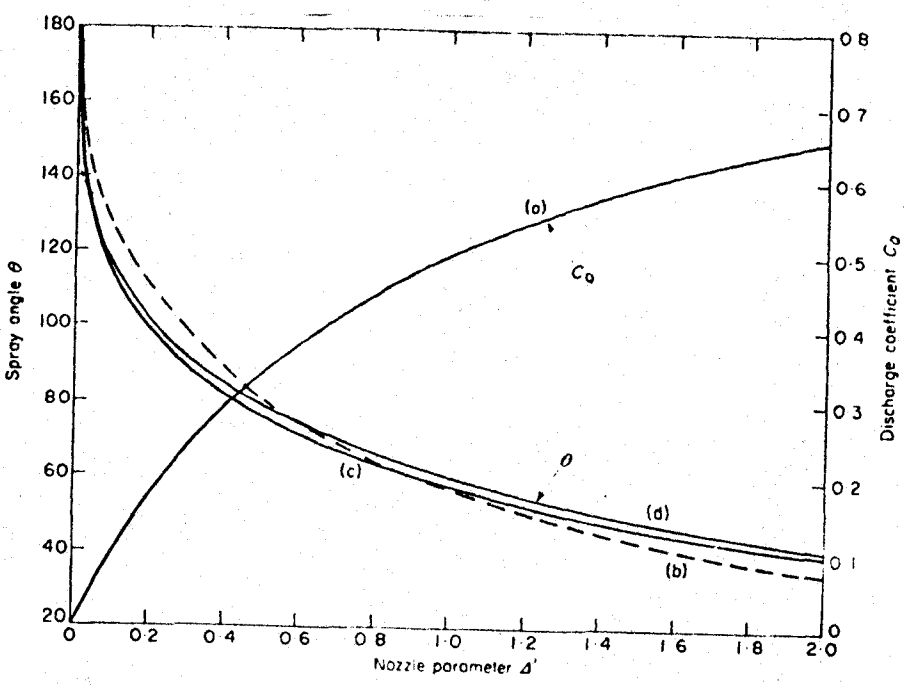

FIGURE 4.8: Variation of Spray Angle and Discharge Coefficient with Nozzle Parameter and Comparison with Various Ideal Theories. (a) Taylor [9], Watson [10], Novikov [11], Sohngen and Grigull [12], (b) Novikov [11], Sohngen and Grigull [12], (c) Taylor [9], (d) Watson [10]. Adapted From [1].

The cone angle, θ, is the maximum angle of the conical sheet as it emerges from the orifice as shown in Figure 4.5. This angle is practically independent of ambient conditions. However, the angle of the spray curtain varies with distance from the nozzle, the plane in which the nozzle is spraying, the differential pressure, the ambient fluid density and the nozzle throughput. Figure 4.9 compares the spray pattern of a nozzle operating with a flow rate of 43 gallons/min. at 3 psig with that of a nozzle having an output of 0.7 gallons/hour at 100 psig.

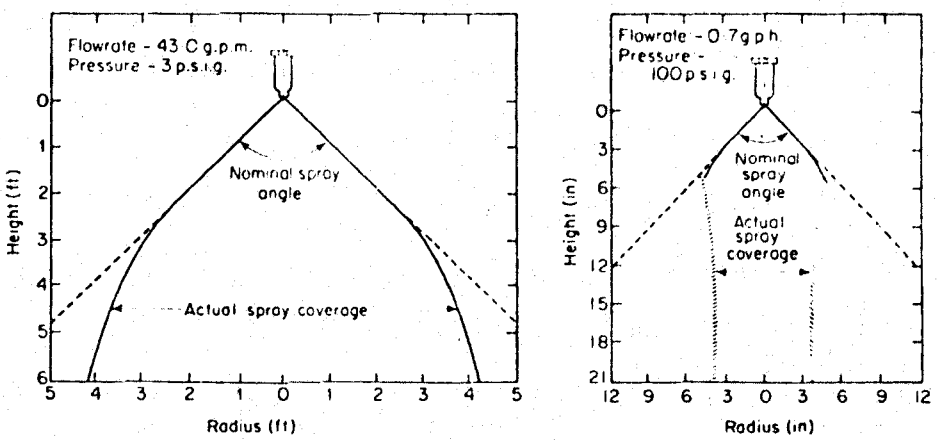

FIGURE 4.9: Spray Patterns for Large and Small Output Nozzles Discharging in Ambient Air [1]

Tanasawa and Kobayasi [8] suggested empirical relations for C_O and θ for the nozzle design shown in Figure 4.6(b). For sharp-edged orifices

$$C_Q = 1 - \frac{2}{\pi} \tan^{-1} \left\{ 2.13 \left[\frac{\frac{4}{\pi} \Delta'' + 1.2}{\left(\frac{4}{\pi} \Delta'' + 1\right)^2 - 1} \right] e^{-0.271(R_3/d_o)} \right\} \quad 4.5$$

where

C_Q = discharge coefficient for sharp edged orifice, dimensionless

Δ'' = $A_s(D_2D_3)$, dimensionless

R_3 = $D_3/2$ = swirl chamber radius, cm

D_2 = orifice diameter, cm

A_s = total area of swirl grooves, cm^2

d_o = diameter of swirl groove equivalent in area to total area of swirl groove, cm

and

$$\theta = 180° - 2 \tan^{-1} \left\{ \frac{4}{\pi} \Delta'' \, (1.37 + 26.9e)^{-4.92(d_o/R_3)} \right\} \quad 4.6$$

C_Q and θ vary with Lo/D_2 according to

$$\frac{C_Q'}{C_Q} = e^{-0.018(Lo/D_2)} \quad 4.7$$

where

Lo = orifice length (see Figure 4.5) cm

C_Q' = discharge coefficient for orifice of finite length Lo, dimensionless

and

$$\frac{\theta'}{\theta} = 0.232\, e^{-3.94(Lo/D_2)} + 0.768\, e^{-0.0185(Lo/D_2)} \qquad 4.8$$

where

θ' = full spray angle for orifice of finite length Lo, degrees

These workers also correlated θ with viscosity according to

$$\frac{\theta}{\theta_{Re=\infty}} = e^{-(550/N_{Re})} \qquad 4.9$$

where

$$U_i = (r_3/R_2)(R_2/R_3)(2\Delta P/\rho_L)^{0.5} \text{ cm/sec} \qquad 4.10$$

where

r_3 = air core radius, cm

ΔP = differential ejection pressure, dynes/cm^2

and where the variation of (r_3/R_2) with Δ" is given according to Figure 4.10.

Hasson [13] showed that if the equation of conservation of angular momentum is expressed by the general relation for the tangential velocity distribution in a vortex in the form

$$V(r)^n = \text{Constant} \qquad 4.11$$

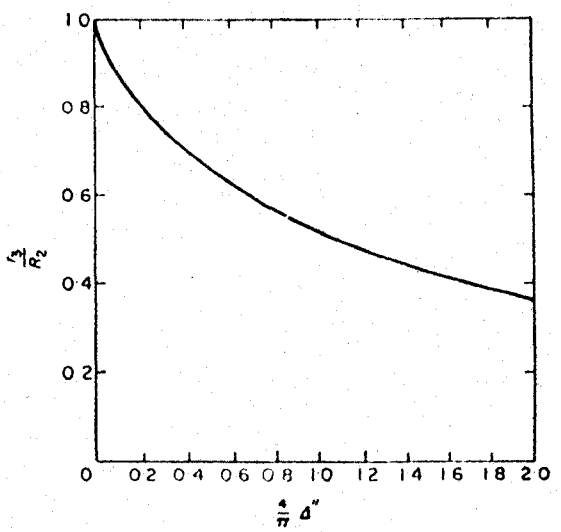

FIGURE 4.10: Relation Between Air Core Radius, Orifice Radius and Nozzle Parameter $\frac{4\Delta''}{\pi}$ [1]

where

V = tangential velocity, cm/sec

r = radius, cm

n = constant varying from + 1 for a free vortex to -1 for a forced vortex

then the nozzle variables $A_s/(D_2D_M) = \Delta'$ and D_M/D_2 could be combined into the single parameter $(\Delta')(\frac{D_M}{D_2})^{1-n}$

On this basis, experimental data obtained by different workers were correlated by selecting an appropriate value of n for each nozzle design. Figure 4.11 shows a correlation of discharge coefficients with $(\Delta')(D_M/D_2)^{1-n}$.

Corresponding correlations for the spray angles are illustrated in Figure 4.12. Note that the discharge coefficient is relatively insensitive to Lo/D_2, but the spray angles are segregated according to this parameter.

According to equation 4.4 the flow rate varies with

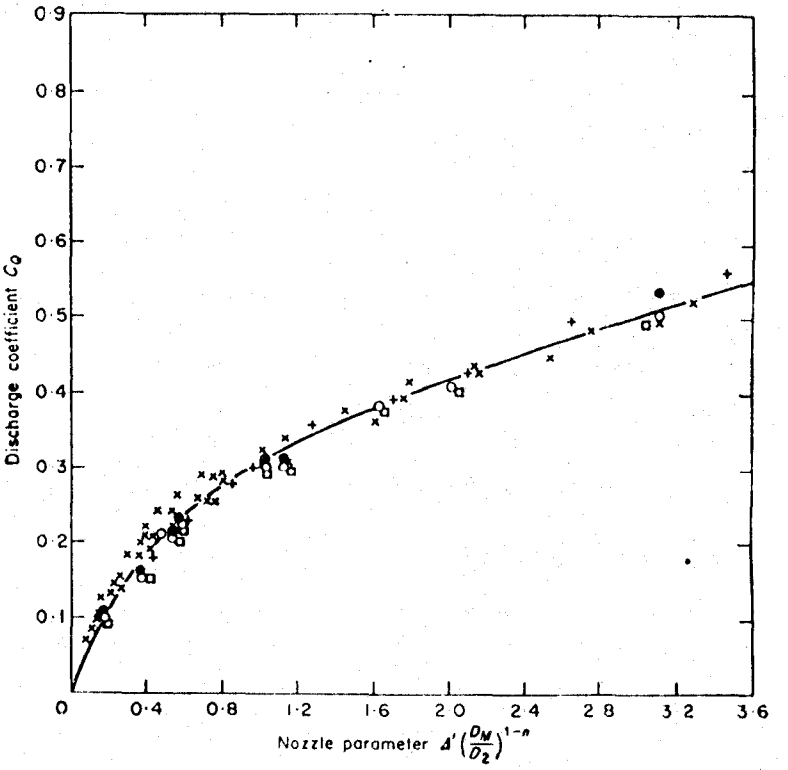

Nozzle	Lo/D_2	n
+ Figure 4.6c	0.12 - 0.23	0.1
× Figure 4.6d	--	0.1
● Figure 4.6e	0.125	0.5
o Figure 4.6e	0.51	0.5
□ Figure 4.6e	0.91	0.5

FIGURE 4.11: Correlation of Discharge Coefficients [1]

the square root of the pressure drop. As a result pressure nozzles are somewhat inflexible since large changes of flow rate require excessive variations in differential pressure. For example, for an atomizer operating satisfactorily at

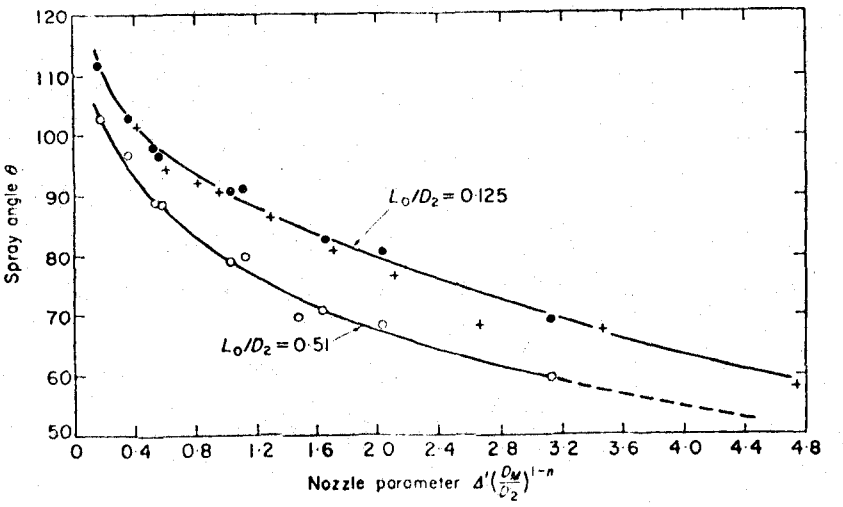

FIGURE 4.12: Correlation for Spray Angles [1]

	Nozzle
+	Figure 4.6c
●,○	Figure 4.6e

25 psi, a pressure differential of 2500 psi is required to increase the flow rate to some ten times the initial value. These limitations, inherent in all pressure-type nozzles, have been overcome in swirl spray nozzles by the development of the spill, duplex, variable port and multiple orifice atomizers illustrated in Figure 4.13. For these nozzles, ratios of maximum to minimum outputs in excess of 50 can be easily achieved.

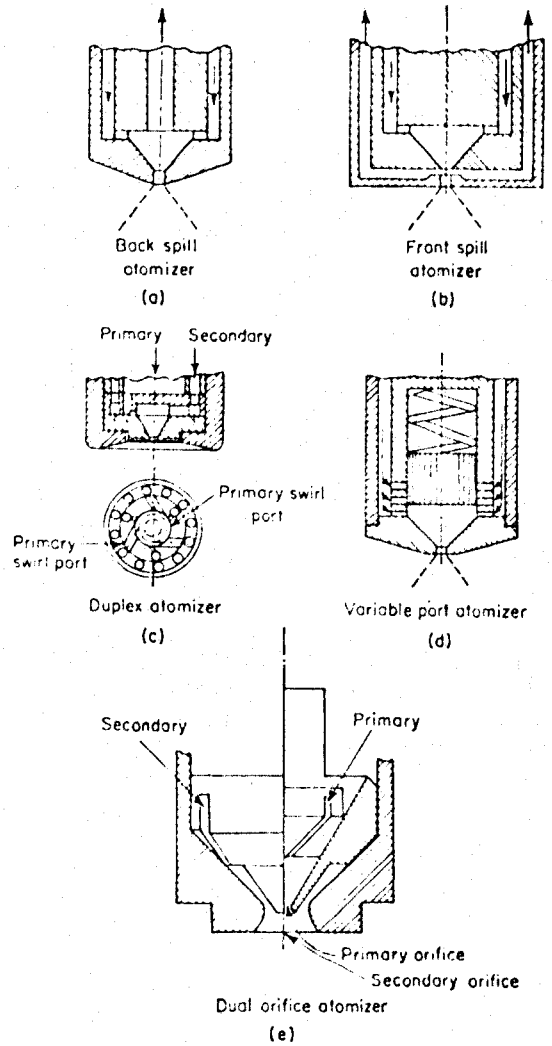

FIGURE 4.13: Swirl Spray Nozzles Capable of Providing Large Throughput Variations [1]

ii. Swirl Type Atomizers Producing Fan Spray Sheets

In the single orifice fan spray nozzle, two streams of liquid are made to impinge behind an orifice by specially designed approach passages. As a result, a liquid sheet is formed in a plane perpendicular to the plane of the streams. The principle, illustrated in Figure 4.14(a), involves liquid flowing through a rectangular orifice at the end of a rectangular tube. Under these conditions the flow through the orifice is constricted in only one plane and the streamlines converge to form a region of pressure behind the orifice. A flat sheet is produced as the liquid freely spreads through the orifice, limited only by the side walls. The spreading angle of the sheet can be increased further by extending the opening to the sides of the orifice as in figure 4.14(b). Figure 4.14(c), (d), (e) and (f) shows commercial nozzles designed on this principle.

In a fan spray nozzle the extent of the sheet is controlled at the boundary by the equilibrium between the momentum along the streamlines and the contraction of the edges as a result of the action of surface tension [14]. For liquids of low viscosity, the boundary is controlled by the differential ejection pressure, sheet thickness and surface tension and is independent of liquid density. The sheet develops as it travels from the orifice, but its velocity remains constant, independent of viscosity, and its thickness,

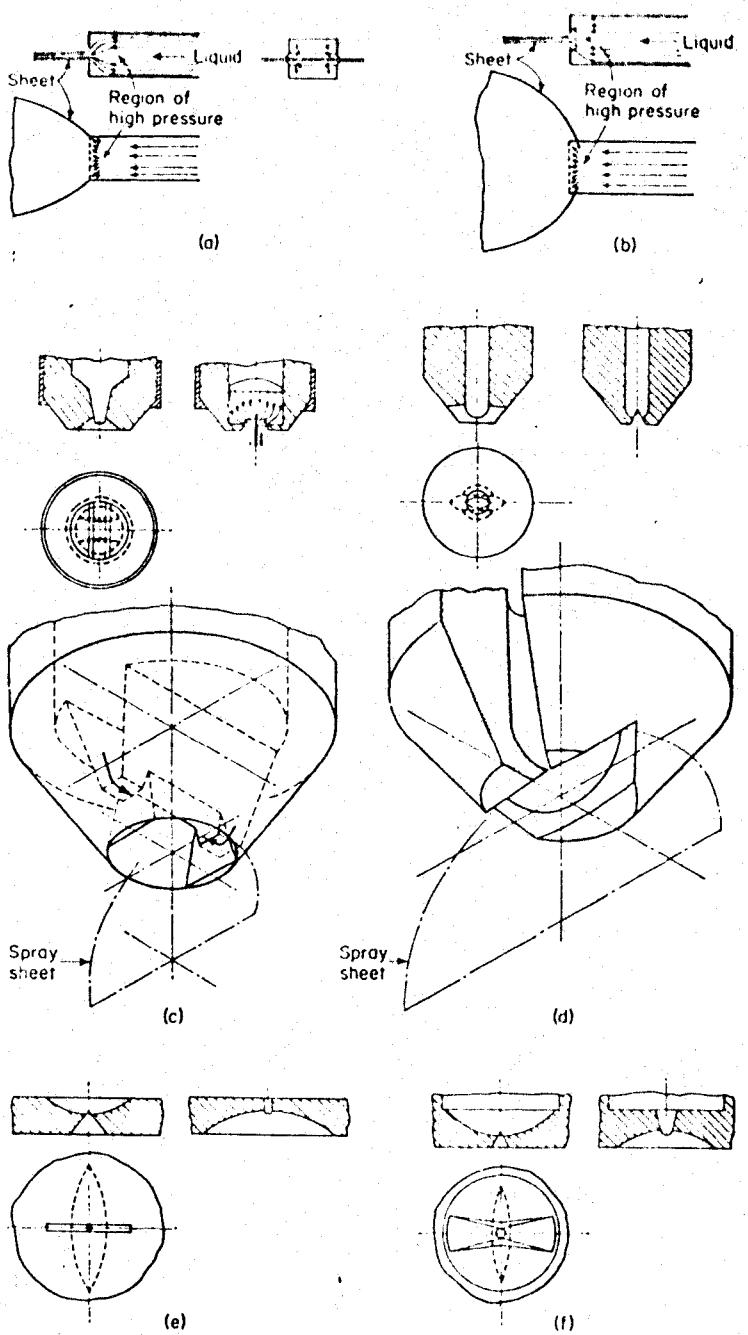

FIGURE 4.14: Characteristic Designs of Fan Spray Nozzles [1]

therefore, diminishes.

The characteristic development of a flat sheet of liquid from a single-orifice fan spray nozzle with increasing pressure is illustrated in Figure 4.15. This behaviour corresponds to the phenomena observed with swirl spray nozzles.

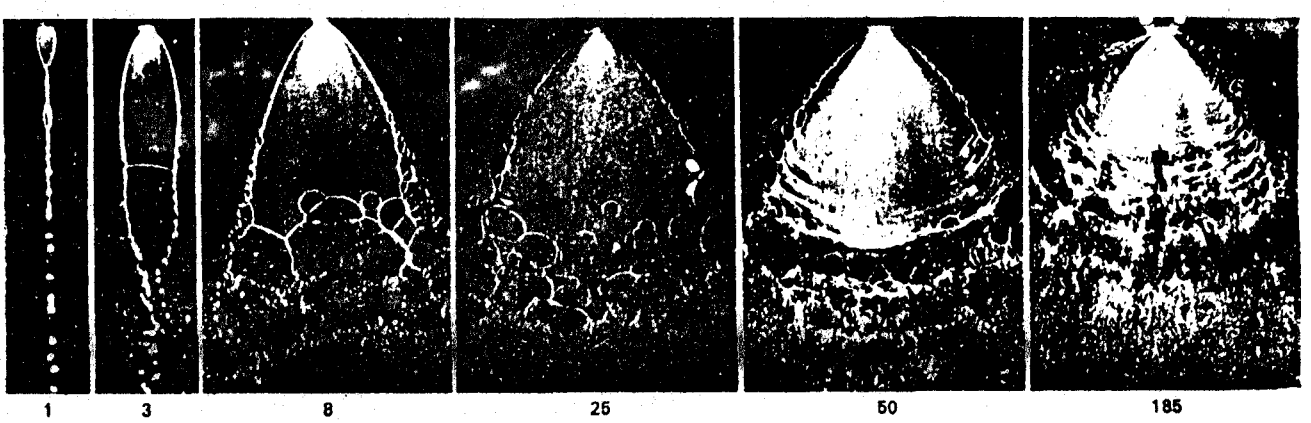

FIGURE 4.15: Development of Fan Spray Sheet with Differential Ejection Pressure (Pressure in lbs/in^2 as Shown by Figures)

At low pressure differences (1 psi) a small sheet is formed. It is bounded by thick rims which are drawn together by surface tension. The impinging rims then form another closed sheet at right angles to the first. This effect is repeated until the velocity of the liquid in the rims is reduced so that a plane jet is formed which breaks up into large drops. At 3 psi pressure, the area of the sheet increases with a

resultant decrease in thickness. Oscillations start to develop in the rims and become evident about half-way down the sheet. Accordingly, the rims disintegrate regularly. As the pressure is increased further, the sheet continues to open until a pressure of 25 psi is reached. The length of a freely moving liquid sheet is determined by the controlling mechanism of disintegration and depends, among other things, on the nature of the liquid. For the oil/water emulsion used it attained a maximum distance at 25 psi after which it receded.

2. Pneumatic Atomization

In pneumatic atomization, the liquid is broken up, by impingement, with a high velocity gas stream, usually air, which may be flowing either inside or outside of the atomizer. This method has been called air stream, air blast, twin fluid, gas or air injection atomization by various investigators.

The simplest arrangement, for effecting this type of fluid disintegration, discharges the liquid into the center of the gas stream as illustrated in Figure 4.16. The selected frames from high speed motion photography [2] shown in Figure 4.17 illustrate the violent turbulence created during pneumatic atomization.

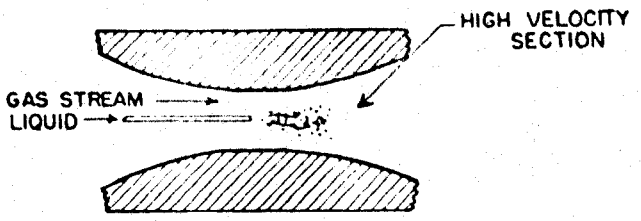

FIGURE 4.16: Pneumatic Atomization by Injection of Liquid into a Venturi Throat

Limper [15] made a study of a venturi atomizer in which the liquid was injected into a high speed gas stream in the throat of a convergent divergent diffuser. Axial injection at the center of the throat (which should not be more than one throat diameter in length as suggested by Limper) was found to be the most efficient arrangement. When the exit velocity was greater than 400 ft/sec, there was no evidence of unatomized liquid leaving the discharge end. Limper concluded that, when using this method of atomization, the velocity of the liquid stream should be as low as possible to ensure complete atomization in the throat section. Furthermore he suggested that the degree of atomization is improved by adding a straight length of throat section.

The other forms of pneumatic atomizers in general use are shown in Figure 4.18. In the more common designs, illustrated by Figure 4.18(a-g), the gas impinges on a solid jet of liquid. Some control over the resulting spray pattern is obtained by imparting a swirl to the gas stream. When the

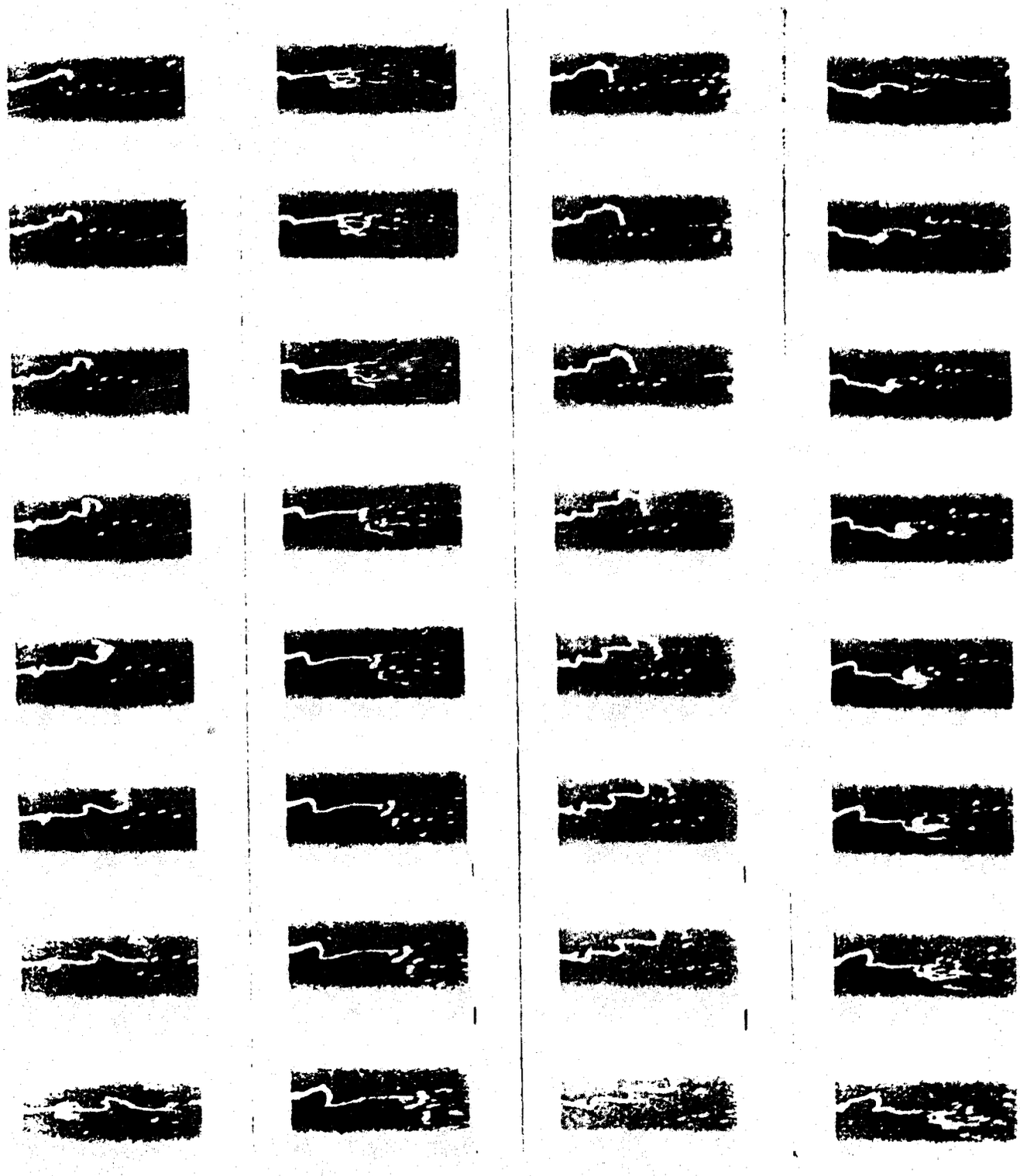

FIGURE 4.17: Selected Frames of a High-Speed Motion Picture Showing the Mechanism of Venturi Atomization [2]. Air Velocity = 134 ft/sec. Liquid Rate = 10 ft/sec. Liquid Jet Diameter = 320μ

required liquid flow rate is high, the liquid jet diameter must be increased. Under these conditions, the energy transfer

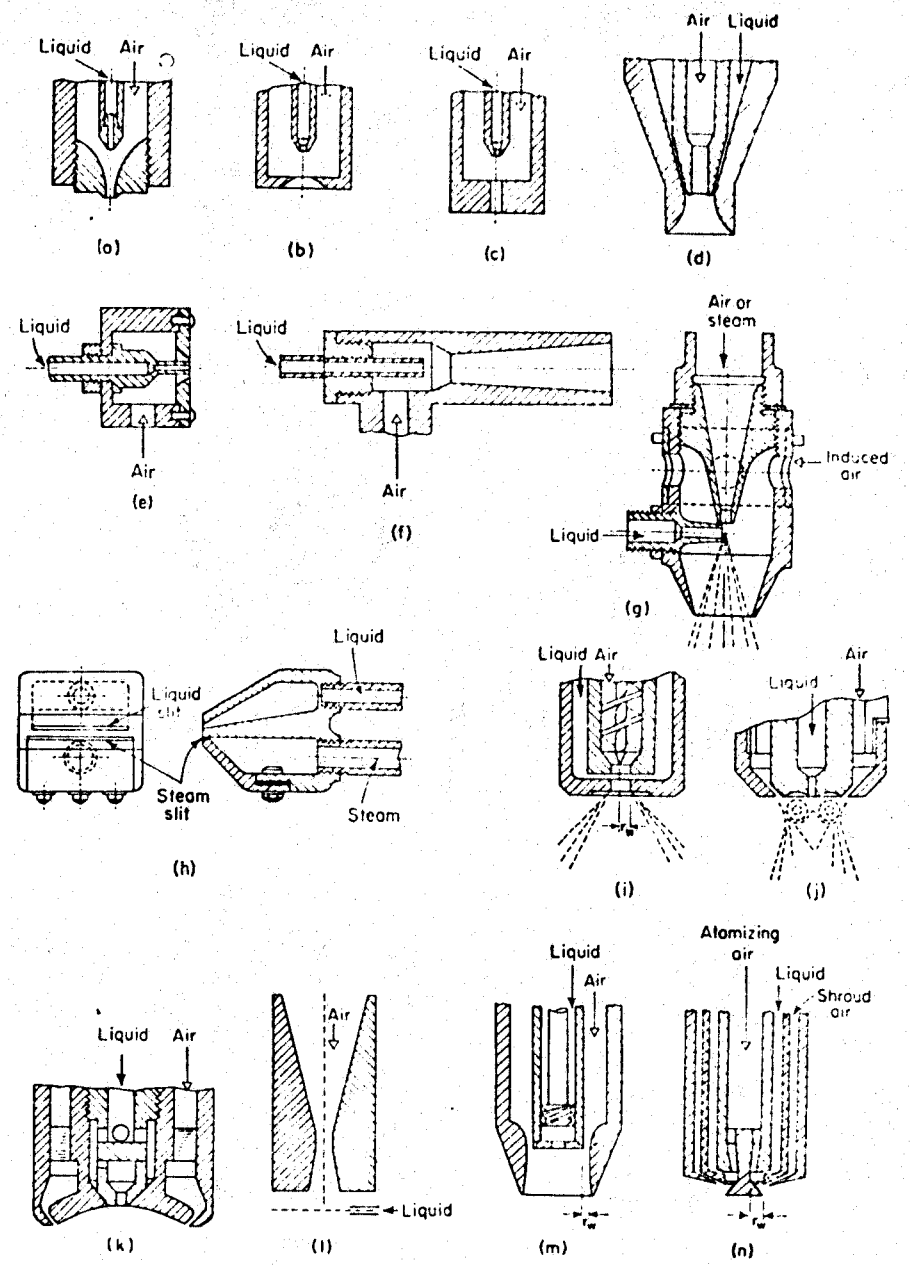

FIGURE 4.18: Typical Designs of Pneumatic Atomizers

from gas to liquid becomes very inefficient [1]. One method of overcoming this difficulty involves using multi-hole nozzles or prefilming the liquid jet before it is impacted by the gas stream. Numerous ways of prefilming liquids have been devised. Figure 4.18(h) shows the drooling or weir type atomizer in which liquid emerges from a slit and falls onto a high velocity gas blast. Figure 4.18(i) illustrates the design devised by Clare and Radcliff [16], which directs liquid radially inwards into a high velocity swirling gas stream. In the method used by Fraser [17] the liquid is aerodynamically spread out on a surface. According to Figure 4.18(j), the gas issues from an annulus surrounding, but some distance away from, the central liquid orifice. A vortex ring is formed in the central liquid orifice. This vortex ring causes the air immediately around the orifice to travel in a direction opposite to the liquid leaving the orifice. By this means the liquid flow is constrained along the surface of the cup shaped depression around the orifice. It spreads outwards as a sheet towards the periphery to meet the high velocity air stream which directs the flow towards the nozzle axis. The air pattern outside the nozzle can be compared to an inverted hollow conical sheet of gas constraining a vortex ring against the face of the nozzle. The liquid is forced to rotate on the boundaries

of the vortex ring until it can escape through the conical sheet of air and be propelled forward. Thus the contact time for atomization is greatly increased. This improves the energy transfer between the gas and liquid streams.

In the device depicted by Figure 4.18(k) a swirl spray nozzle is placed inside a cup in order to produce a conical sheet. A rotary motion is imparted to the gas stream so that the resulting spray angle can be easily controlled. Figure 4.19 shows photographs of the operation of this atomizer. The spray sheet produced by the swirl spray nozzle in still air is depicted in Figure 4.19(a). Figure 4.19(b) portrays the finer atomization achieved with a cocurrent air blast of approximately 750 ft/sec.

Marshall stated, in 1954, that pneumatic atomization was the only commercial method for producing fine sprays in which the diameters of all droplets would be less than 15μ. The application of this type of atomization to Venturi scrubbers is handicapped by the difficulty of breaking up large streams of liquid in an efficient manner to attain a desired drop size distribution. Fraser et al [18] have confirmed that air flow patterns may be considerably modified in the presence of liquid sheets and thus affect the transfer of energy between the two fluids. This will be discussed in Chapter VI.

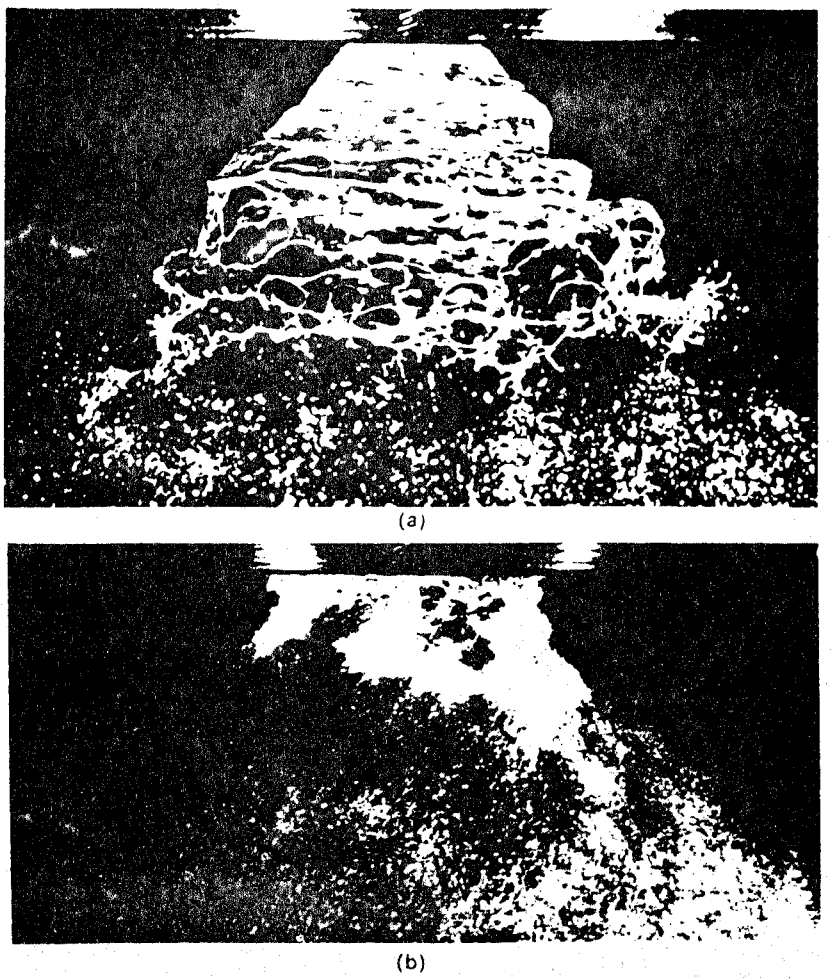

FIGURE 4.19: Atomization of a Conical Sheet (a) In Still Air (b) In an Air Blast [1]

3. Rotating Disks and Cups

Devices based on this method of atomization are frequently referred to as "Centrifugal Atomizers". However, this terminology often leads to some confusion with "Centrifugal Nozzles" of the swirl type previously shown in Figure 4.5. The two methods of liquid disintegration are distinctly different although both employ centrifugal forces to accomplish atomization. To avoid confusion, the term rotating will be used to designate atomization employing disks, cones, bowls, cups or other shapes rotated at high speeds.

Figure 4.20 shows a representation of a section of a rotating disk atomizer.

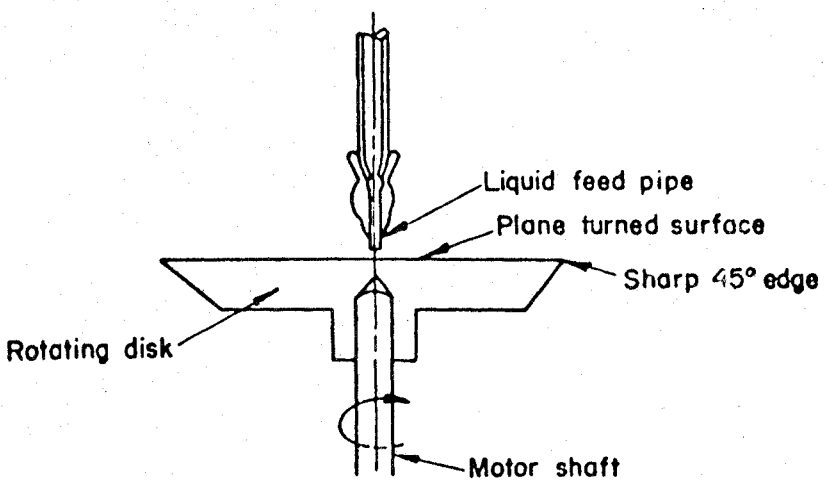

FIGURE 4.20: Rotating Disk Atomizer [19]

The liquid, fed from a small-bore tube onto the center of the rotating surface, spreads to the periphery in a thin film. Care must be taken to ensure that the feed is centrally located and continuous. If the rotor surface is not completely wetted by the liquid, uneven film formation will lead to non-uniform dispersion. Some typical rotary atomizers are shown in Figure 4.21.

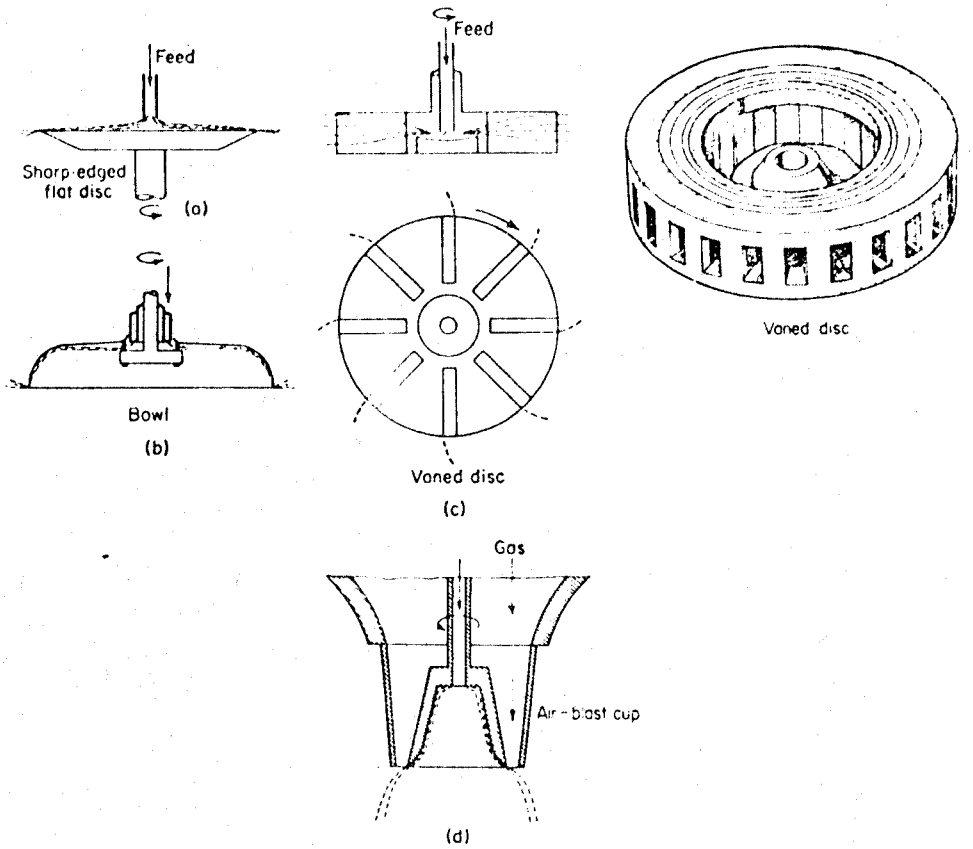

FIGURE 4.21: Typical Rotary Atomizers (a) Sharp Edge Flat Disc, (b) Bowl, (c) Vaned Disc, (d) Air-Blast Cup.

The thickness and uniformity of the free edge of the liquid, formed at the rim of a spinning disc or cup, can be controlled by regulating the centrifugal force through the liquid flow rate and/or the speed of the disc. Because the film is in contact with a solid surface, flow disturbances are reduced. As a result the diameters of the threads and drops formed under these conditions are more uniform [19, 20, 21, 22].

At very low flow rates (i.e. $2\frac{1}{2}$ lb/hr) the liquid spreads out towards the cup lip where it forms a ring. As liquid continues to flow onto the ring, its inertia increases and overcomes the restraining surface tension. Figure 4.22 demonstrates the disturbances which appear on the outer edge and grow in size until liquid is spun off as discrete drops

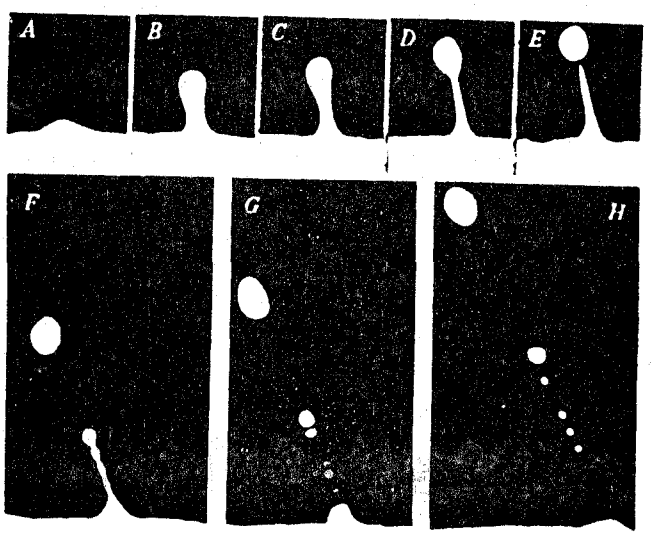

FIGURE 4.22: Rim Disintegration From Spinning Disc [1]

of uniform size which initially remain attached to the rim by the fine attenuating threads illustrated in Figure 4.23(a). When a drop is finally detached, the thread breaks down into a chain of small satellite drops. Since the satellite drops constitute only a small proportion of the total liquid flow rate, any device operating under these conditions effectively produces a mono-disperse spray on a mass or volume basis, but not on a number basis.

When the liquid flow rate is increased the retaining threads grow in thickness and form long jets as illustrated in Figure 4.23(b). As these jets extend into the surroundings, they stretch and finally break down into strings of drops, the diameters of which are smaller than those formed by the low flow rate mechanism of drop formation.

With still higher flow rates, the jets are unable to remove all of the liquid. Consequently a ring of liquid is forced beyond the edge to produce a thin sheet that extends around the cup lip as shown in Figure 4.23(c). If this occurs at low peripheral speeds and flow rates, (100 rpm and 28 lb/hr for a 2-in diameter cup) a relatively undisturbed sheet is formed. It extends from the cup lip until a position of equilibrium is achieved. When the kinetic energy of the advancing sheet exceeds the surface tension contraction force per unit film thickness, at the free edge, disintegration begins.

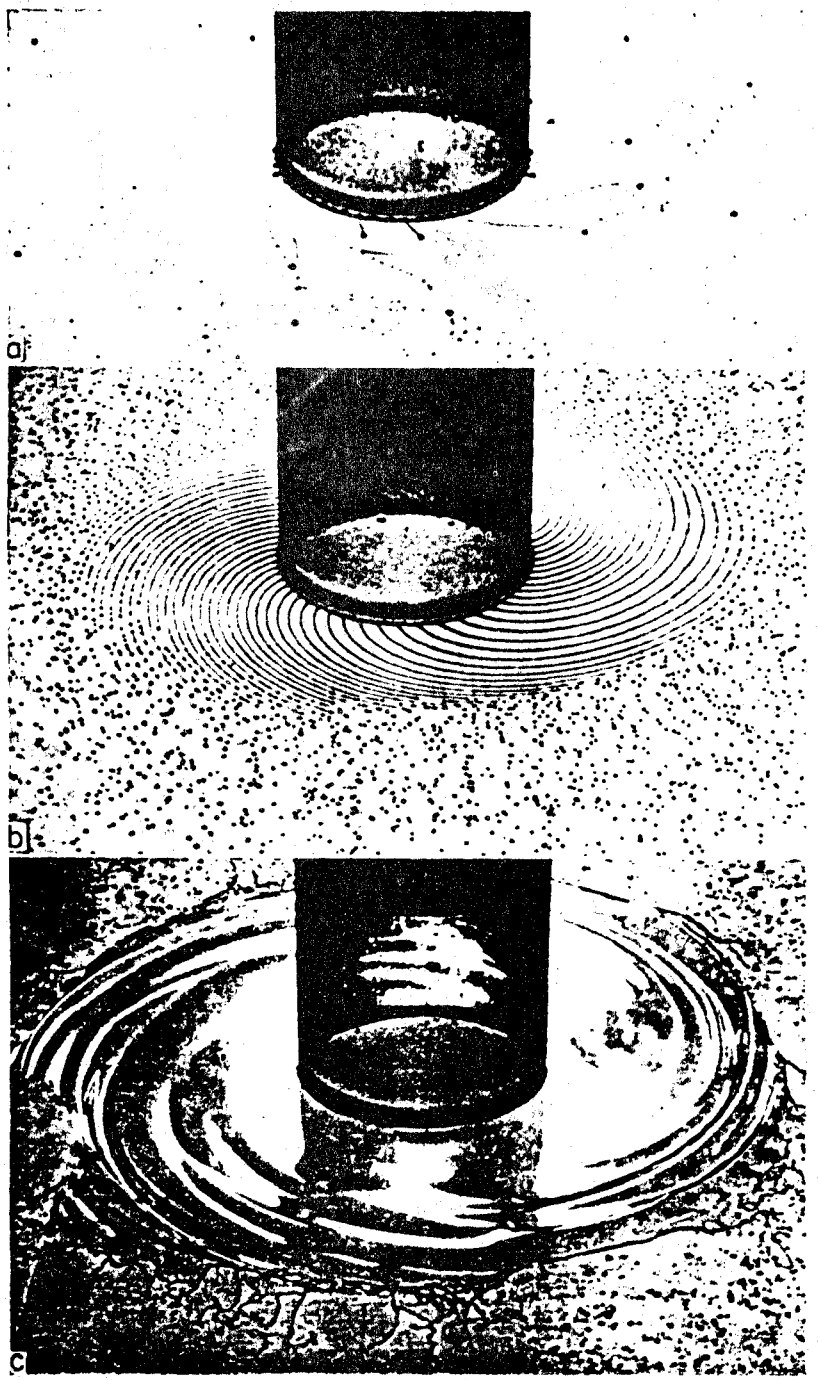

FIGURE 4.23: Mechanism of Drop Formation from Rotating Cups. (Clockwise Rotation 2-in Diameter, 165 Centistokes viscosity). (a) Direct Drop Formation, (b) Breakdown of Threads Produced from Cup Lip, (c) Sheet Disintegration [23].

Essentially a thick rim is produced and then breaks into threads. Since the rim has no controlling solid surface the threads are irregular in their formation and size.

May [24] employed the rotating disk method of atomization using a high speed spinning top operated by compressed air. He found that water, because of its high surface tension, is more difficult to spray than oils. By applying a suction field around the rotor, May was able to withdraw the satellite droplets while a crossflow of air carried off the main drops. In this way, homogeneous oil mists, having uniform drop diameters as small as six microns, were produced. When spraying low surface tension liquids, such as oils or organic solvents which readily wet the rotor, May reported that 90% of all the drops fell within a band width of five percent of the length mean diameter. Also the minimum observed drop size was only six percent smaller than this mean.

Fraser, Dombrowski and Routley [18, 23, 25], in a series of investigations, studied the flow mechanics of the sheet. They showed that, since the liquid streamlines follow an approximately tangential path, the sheet rapidly reduces in thickness with increasing radial distance according to the relation.

$$m = \frac{162\ Q_m}{\rho_L V_R [d_L^2\ U_m^2/4V_R^2) + a\ d_L + a^2]^{1/2}} \qquad 4.12$$

where

m = sheet thickness, microns

Q_m = liquid mass flow rate, lb/hr

ρ_L = liquid density, lb/ft^3

V_R = at radial distance a, the resultant sheet velocity equal to $\sqrt{V_T^2 + U_m^2}$, ft/sec

V_T = tangential component of sheet velocity, ft/sec

d_L = cup diameter at lip, in

U_m = mean radial velocity of liquid along wall of cup, ft/sec

a = radial extent of sheet measured from cup lip, in

The geometry of the liquid sheet is shown in Figure 4.24.

Figure 4.25 demonstrates the rapid reduction in sheet thickness for a 2-in diameter cup operating with a liquid viscosity of 45 centistokes at various flow rates and rotational speeds. These workers also found that, except for a limited range of operating conditions, a spinning cup is not capable of smoothing out the flow of liquid over its surface under the action of the centrifugal force. Their studies also indicated that the sheet uniformity is critically dependent on the method of feed distribution. The limits of operation for various types of feed distribution are shown in Figure 4.26.

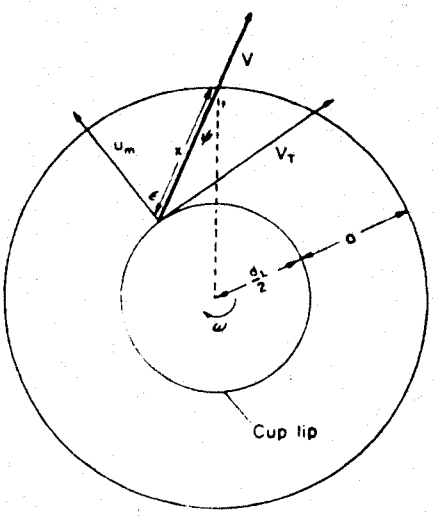

ε = angle between the radial velocity component and the resultant liquid velocity of the sheet at the cup lip

ψ = angle between the resultant sheet velocity and the sheet diameter at the free edge of the sheet

w = angular speed of cup

FIGURE 4.24: Geometry of a Liquid Sheet Advancing From a Spinning Cup [23]

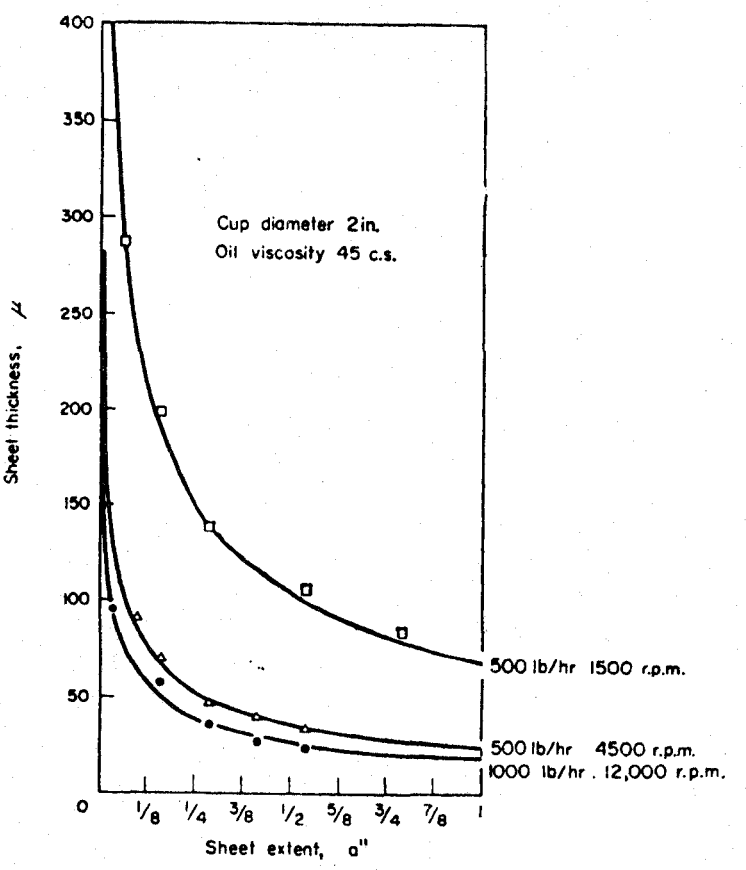

FIGURE 4.25: Comparison of Measured and Calculated Values of Sheet Thickness [23].

4. Methods Based on Vibrations

Less common methods of atomization employing sonic or mechanical vibrations have been reported.

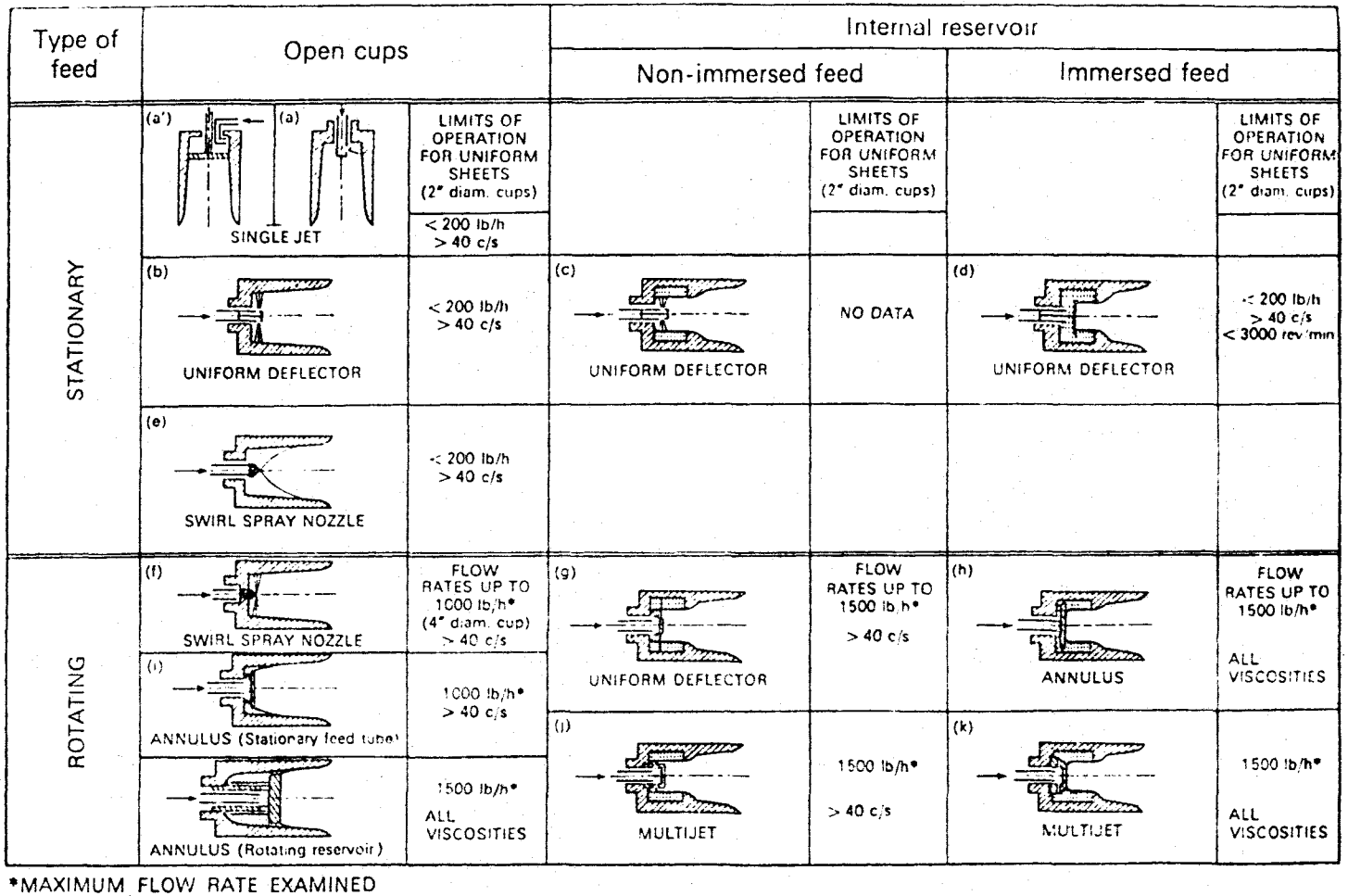

*MAXIMUM FLOW RATE EXAMINED

FIGURE 4.26: Basic Methods of Distributing Liquid in a Rotating Cup [1]

In ultrasonic atomization, liquid breakup results when a beam of ultrasonic energy from an electromagnetically activated vibrating reed is directed along the liquid stream, into a resonant cavity, or when the beam is directed at the air or gas interface. Under proper conditions a dense fog may be produced. Significant investigations in this field are those of Lang [26], Mizutani, Uga and Nishimoto [27] and Rudakov et al [28]. Alliger [29] has recently reported on an ultrasonic spray device used for air pollution abatement. The dense fog created by this atomizing process is illustrated in Figure 4.27.

Joeck [30] has patented a method of liquid atomization based on delivering a beam of ultrasonic energy into a chamber that is resonant to the frequency of the driver. A stream of liquid is subjected to the ultrasonic sound vibrations within the chamber to produce finely divided droplets.

Dimmock [31] described a method of producing a stream of droplets of uniform size by means of a vibrating hollow reed actuated by a small electromagnet. Although primary and subsidiary droplets were formed, uniform drop diameters ranging from 10 to 300 microns could be obtained, by appropriate adjustment of operating conditions. Dimmock suggested that the size uniformity in a single stream of drops from this apparatus was greater than that obtained with a rotating disk type sprayer, however, it had the disadvantage of producing

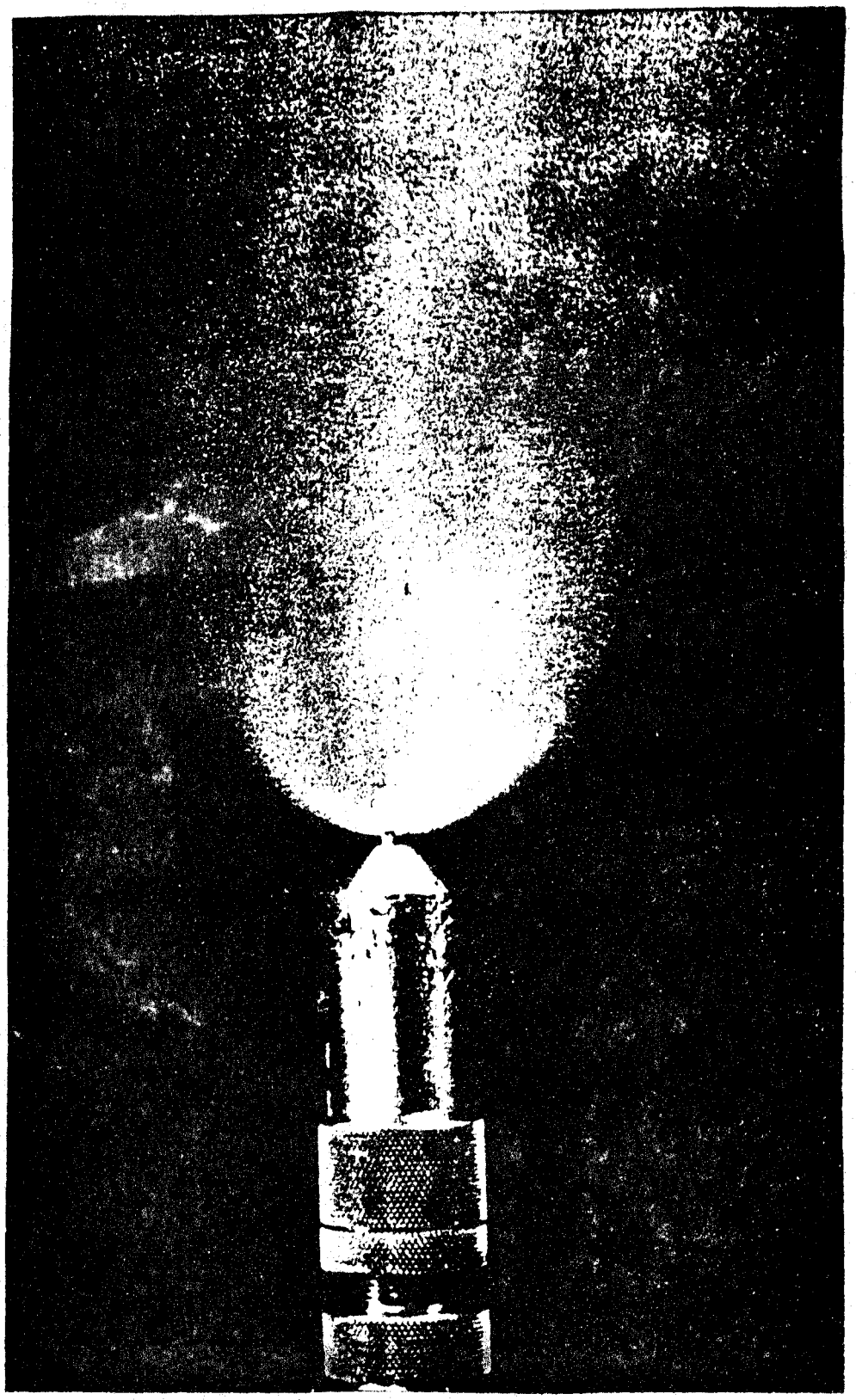

FIGURE 4.27: An Ultrasonic Spray [29]

only a limited quantity.

Wissema and Davies [32] described conditions for the formation of uniformly sized drops using vibration atomization. Their investigation focussed on the effect of amplitude and frequency of vibration on drop size and break up length of the jet.

Sliepcevich et al [33] studied the characteristics of a vibrating type nozzle in which the liquid was forced through an annular passage formed by a valve in an orifice. The valve stem was held under tension by an adjustable spring. A valve head, having a tapered portion, sits externally on the orifice. Figure 4.28 illustrates the basic nozzle design

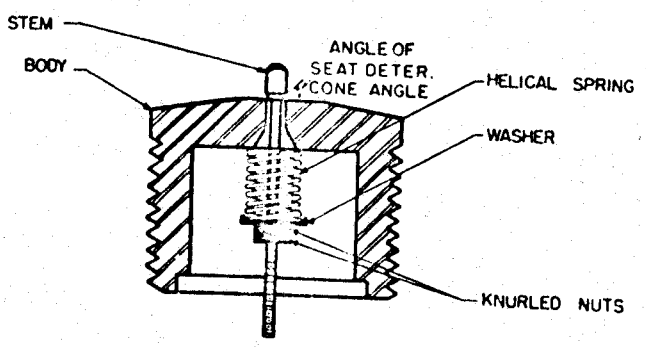

FIGURE 4.28: Vibrating Type of Nozzle Studied by Sliepcevich et al [33]

in which the liquid, under pressures as high as 3000 lbs/in^2, forces the tapered head from its seat to create a pressure drop. As the valve endeavors to reseat, the pressure builds

up again. This sequence of actions produces a condition of "self excited vibrations", according to the authors.

Sliepcevich et al [33] reported capacity-pressure relationships, cone angles, and relative spray fineness evaluations. It was observed that the cone angle was determined by the angle of the valve head taper and was, in fact, equal to this angle. The frequencies of the vibrations were in the audible range, varying from 200 to 800 cycles/sec. For any given nozzle, the most uniform and finely dispersed sprays were obtained when the vibrations were clearly audible. It was observed from light absorption measurements on the spray that a finer dispersion was obtainable with the vibrating type of nozzle than with the usual non vibrating swirl type for any given capacity. This suggests the necessity of vibration for good atomization. Correlations of capacity vs. pressure were also reported for various conditions of valve-stem-orifice diameter ratios and various spring tensions.

5. Impinging Liquid Jets

The principle of operation of the impinging jet nozzle is similar to that of the fan spray nozzle with the exception that two or more independent liquid jets are made to impinge against one another. Consider two cylindrical and equal jets of radius R flowing at the same velocity Vo,

in the directions shown in Figure 4.29. If the two jets collide obliquely at a total included angle of 2θ, it is found that the liquid spreads into a flat sheet flowing in a plane perpendicular to that containing the axes of the two jets.

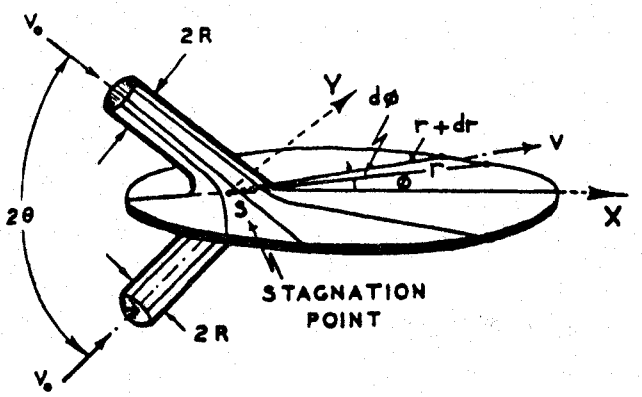

FIGURE 4.29: Equal Thickness Contour of Sheet Formed by Impinging Jets [34]

Hasson and Peck [34], who analyzed the flow patterns for this system, related the variation of sheet thickness to

i. the radial distance from the point of impact
ii. the angular position from the sheet axis
iii. the jet diameters
iv. the angle of impingement of the two jets

Heidmann and Humphrey [35] made an extensive investigation of the flow characteristics and spray patterns formed by the impingement of two liquid jets. The formation of sprays, resulting from the impingement of two water jets, was studied by visual, photographic, and photoelectric techniques. High speed motion pictures and microflash photographs, taken of the spray pattern, indicated that the formation of liquid drops is an intermittent, rather than a continuous process. Upon impingement a ruffled sheet of liquid, which disintegrates intermittently to form groups of liquid drops, is formed perpendicularly to the plane of the two jets. This process resembles waves propagating from an origin at the point of impingement. The experimental data provided quantitative evaluations of wave frequencies, wave intensities and the mass of atomized liquid per unit volume for a typical spray. The frequency of wave formation was observed to be constant over a finite time interval under constant operating conditions. For the range of test conditions used, the frequency varied between 1000 and 4000 cps.

Heidmann and Foster [36] extended the studies to two water jets impinging at angles varying from 10° to 90° into an airstream moving at 100 ft/sec. Drop size distribution data showed bimodal characteristics with a mass median diameter of 300 microns for one mode and 900-1200 microns for the other. The most significant effect of impingement

angle and liquid jet velocity on the distributions was a change in the relative number of drops in each mode and in the geometric mean deviation of the larger drop size mode. An increase in impingement angle produced an increase in the number of small drops and a decrease in the deviation of the larger drop size mode. This effect was most pronounced at low jet velocities.

Another significant investigation on impinging liquid jets was carried out by Ryan [37]. Working with directly opposed jets, formed by sharp edged orifices meeting in an environment of atmospheric air, Ryan made a preliminary study of the mechanism of jet impingement. His data disclosed that

i. the point of impingement could not be stabilized between the two orifices unless the momentum flux per unit cross-sectional area was the same for both jets

ii. the efficiency of impingement, defined as the ratio of kinetic energy of the liquid leaving the point of impingement to that of the jet entering, was essentially unity.

6. Impingement Against a Solid Surface

When a liquid drop collides with a solid surface at a relative velocity approaching 1000 ft/sec, the drop first spreads as a flat disk over the surface. The perimeter of the disk subsequently breaks into radial filaments and ultimately into a mist of fine droplets. For a water drop initially about 2 mm in diameter, the mist droplets range from 4 to 25μ in diameter [38].

The basic method involves directing a liquid jet at high velocity against a solid target [2]. The resulting impact and thinning of the liquid film caused by the change in direction of the jet produce disintegration. In one commercial nozzle, this principle is realized by locating a hook or pin at the axis of the nozzle orifice so that the liquid jet impinges on the end of the obstruction as shown in figure 4.30. Liquid break up appears to be better effected if the jet has started to collapse just before impacting on the target.

7. Electrical Atomization

If a potential of several thousand volts is applied to drops of a liquid flowing slowly from a fine tipped glass tube, the drops will become smaller and flow more rapidly. Under appropriate conditions of potential,

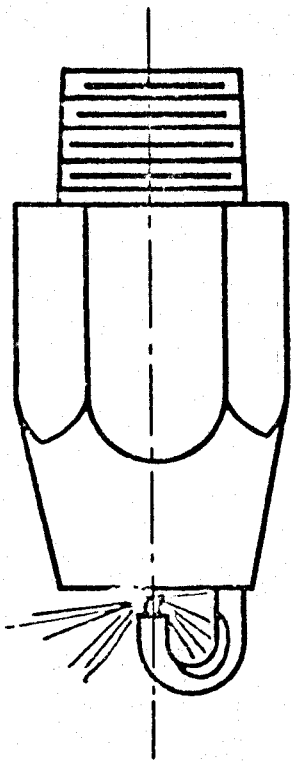

FIGURE 4.30: Impingement Type Nozzle [2]

liquid pressure, conductivity, interfacial tension and dielectric constant as well as tip shape and capillary radius, the liquid will stream from the tube in a fine thread that rapidly breaks into a cloud of droplets [39].

This phenomenon is a manifestation of the instability of electrified liquid surfaces [40]. Specifically it results from a reduction in interfacial tension [41]. When a liquid is subjected to an applied potential, its surface

acquires electrical charges. Consequently, an outward pressure is developed because of the repulsion of like charges. In the case of a charged droplet the pressure is counter balanced by the interfacial tension forces. For a liquid flowing from a capillary, the greatest charge intensity is at the leading surface. This pulls the liquid out into a fine thread which eventually breaks to form droplets [42]. Essentially mono-disperse droplets can be obtained at low production rates, but the range of droplet sizes is narrow under most other operating conditions.

Marshall [2] has mentioned the use of a commercial electrical atomizing system in conjunction with spinning disk atomizers to produce paint sprays.

B. Measurement Techniques

The analysis of liquid sprays in terms of drop size distributions is important to all studies of atomization, especially when applied to wet scrubber performance. A liquid spray is a dynamic system whose drop size distribution varies with time.

The size spectrum of a polydisperse spray depends on the distance from the point of generation, the initial direction of the spray and the nature of imposed or induced air currents. Coalescence or disintegration of drops may take place [43, 44], depending upon the air stream

velocity and the spatial drop concentrations [1]. Therefore the position at which a spray is sampled must be related to the manner in which the results will be used.

Numerous experimental methods have been used to measure the drop size distribution of sprays. These experimental approaches include

i. microscopic examination of drops
ii. freezing of spray drops followed by sieving
iii. direct photographic evaluations
iv. optical methods based on the scattering or absorption of light
v. electronic and radioautographic techniques
vi. cascade impactor sizing

Because each method has its advantages and disadvantages, none is completely satisfactory. The most common objection to any technique is that it is too tedious and time consuming. Drop size determinations are complicated by the fact that

i. significant errors are introduced as a result of disturbing the spray where a sample is collected
ii. most sizing techniques are not capable of measuring drops over a large size

range and generally discriminate against small droplets

iii. calibration of measuring devices is difficult or uncertain

iv. complex equipment is involved

v. results are unreliable once obtained

Sampling of a spray is one of the more difficult steps in the experimental procedures that require collection of an actual sample. Unfortunately the importance and difficulty of obtaining a sufficiently representative sample have not been fully appreciated by some investigators.

1. Collection on Slides or in Cells

By far the most frequently employed method of drop size determination has been the collection of droplets on a glass slide which is passed rapidly through a spray and examined with a microscope having a calibrated eye piece. Although attempts are made to collect at least 1000 drops on the slide a serious objection to this approach is that it is difficult, if not impossible, to obtain a sufficiently representative sample. The tendency for the smaller droplets to follow the air stream past the slide, rather than to be collected, biases the size determination towards larger drops.

Use of narrow slides reduces discrimination against small drops, but the effect is not completely eliminated until the slide width approaches drop dimensions. Another objection to this method is that collected droplets are subject to distortion because of adherence to the slide. Also evaporation may occur from all sizes, but most rapidly from the smaller drops.

Although drop spreading may occur during collection on a slide, its magnitude may be determined and accounted for by a so-called spread factor [45]. Slides coated with thin films of grease or oil tend to prevent water drop spreading. On such prepared surfaces collected drops tend to be more nearly spherical at the time of measurement. Other coatings such as lampblack (produced by holding the slide over a kerosene flame) or magnesium oxide (from a burning ribbon of magnesium) help to minimize evaporation effects.

Drop evaporation can be greatly reduced if the spray is collected in an immiscible liquid. Consequently dishes or cells containing thin layers of oil or kerosene [46, 47, 48] have been used instead of coated slides for catching spray drops. When the sprayed liquid is just slightly denser than the collecting fluid, the spray drops remain very nearly spherical. Drops may be made more readily visible by incorporating a dye into the sprayed liquid [49].

The shatter of large drops upon contacting the collecting liquid surface and the failure of the smallest sizes to impact can lead to significant errors in drop size evaluation.

Rupe [63, 64] and others [48-62, 65, 66] have used techniques based on collection by cells or slides to measure drop size distributions in sprays.

2. Freezing of Drops

An obvious means of reducing drop deformation and evaporation is by freezing them immediately upon collection. Holroyd [67] suggested the use of this method for liquids that would solidify before coming in contact with any solid surface. With this technique drops could be studied at leisure. Holroyd, who atomized melted beeswax with some success, suggested the use of low melting point alloys. The frozen drop method was more fully developed by Longwell [68], who collected fuel oil spray drops in an immiscible liquid which was maintained at a sufficiently low temperature to freeze the collected drops. The drop sizes were determined by means of standard sieving of the formed solids. This technique was extended by Taylor and Harmon [69] to the capture of water sprays by hexane at dry ice temperature. The sizes of the drops were determined from their rate of sedimentation.

The wax method was perfected by Joyce [3] who used paraffin wax to simulate the physical properties of fuel oil. Small liquid wax droplets, solidifying rapidly in air, were directed into a funnel-like bath of flowing water, from which a sample of the water-borne wax spray was collected in a suitable vessel. The same technique was used by Fraser [70], Fraser et al [18], and by Radcliff and Clare [71] to study the performance of an air blast atomizer. Wetzel [72] examined venturi atomization by using a low melting point alloy, whereas, Turner and Moulton [73] sprayed benzoic acid and beta-naphthol. Kim and Marshall [74] worked with micro-crystalline wax to determine drop size distributions from a pneumatic atomizer. The total spray was frozen and collected to provide a sample for size determinations. The capture of spray droplets in liquid nitrogen has also been reported [75, 76]. Experimentally liquid nitrogen is attractive because its temperature is sufficiently low to ensure immediate freezing of most sprays and because its low surface tension of 8.3 dynes/cm permits easy penetration by the drops.

3. Photographic Analysis

Determinations of drop size distributions based on photographing the undisturbed spray have been discussed by several investigators [77-86]. Clearly the results of such approaches are not biased by an interference with the spray.

If photography is accomplished immediately after drop formation negligible errors due to evaporation or coalescence should be involved.

Experimental difficulties must be expected, because fast moving droplets, of the order of 20μ in diameter or less, are not readily photographed. In addition determining, from any photograph, which droplets are in focus and which are not can present significant problems. Unfortunately, the photograph records the spatial distribution of drops, that is, the size distribution in the volume included within the field of focus. However, the information usually needed is the temporal distribution, that is, the size distribution of drops passing a cross-sectional area in a unit of time. To obtain the latter, droplet velocities must be determined from double exposures over short known time intervals. Fluorescent dyes can be added to a liquid before atomizing to aid in droplet photography [87] or pattern examination [88].

Holographic techniques, developed by Thompson et al [89] and [90], have been applied to the determination of drop sizes and velocities throughout an undisturbed gas stream.

4. Optical Methods

Optical techniques involve measuring the intensity, the colour or the polarization of light scattered by a spray

as well as light transmission and diffraction upon passage of a light beam through a spray [91, 92]. These rapid and relatively simple methods do not disturb the spray pattern. In general, optical techniques are better suited to aerosols and extremely fine mists or sprays. Without elaborate auxiliary equipment such as settling chambers, they give only mean (surface volume) diameters [93].

Evaluation of small particle and droplet sizes from measurements of the scattering of light is based primarily on the theory developed by Gustav Mie in 1908. The complete details are given in compact form by Stratton [94] with pertinent equations outlined by Sinclair and La Mer [95].

The applications of optical methods have been illustrated by several investigators [96-104].

5. Electronic and Radioautographic Methods

Electronic size analysers are based on electrostatic charging, light scattering and electrical resistivity.

Guyton [105] developed an electronic counter that depended upon the electrostatic charging of small particles forced, at high velocities, through a fine jet to impinge upon a metallic collector. Electrical pulses, imparted to the collector by particles of 2.5 microns or larger, were amplified to operate a mechanical counter. Guyton found that,

for solid particles that did not conduct electricity, the pulse amplitude was proportional to the square of the particle diameter.

Gucker and O'Konski [106] used a combination of light-scattering and electronic principles. A fine stream of small particles, protected by a flowing sheath of pure air, was passed through a spot under intense dark-field illumination and flashes of light scattered forward upon a photocell. Each particle, about 0.6 micron or more in diameter. created an electrical pulse that could be sufficiently amplified to operate a mechanical counter. The apparatus was capable of counting particles weighing 5×10^{-13} gm at rates up to 1000 per minute and determining their sizes by means of an electronic discriminator.

Geist [107, 108] developed an electronic spray analyzer somewhat similar in principle to Guyton's device. His apparatus consisted of a charged wire inserted or moving through a suspension of droplets. Electronic circuits amplified, classified and counted the electrical pulses created by impaction of the drops on the charged wire probe.

In a number of instruments [109, 110, 111], spray characteristics have been developed on the basis of drops passing through a small light beam. The resulting interruptions

are recorded for analysis after undergoing electronic discrimination.

Completely automatic scanning instruments have been reported. They make it possible to rapidly measure large numbers of drops on slides or represented on photo-micrographs [84, 112]. Semiautomatic scanning could be advantageously employed when larger numbers of drops are to be sized. Typical of this class is a caliperlike device [113] having a number of electrical contacts corresponding to various openings. It makes measuring and recording of particle or drop diameters from photographs or micrographs an easier task.

6. Cascade Impactor Sizing

A cascade impactor [114] is essentially a series, or cascade, of flat surfaces mounted directly in front of ports, or jets, through which a spray may be drawn. The jets decrease in size as the spray progresses through the device. As the gas velocity increases the smaller droplets find it increasingly difficult to pass the obstacles. Finally, when essentially all of them are caught, their capture position is related to their size.

Multistage impactors are built usually for solid particle analysis [115, 116, 117] but at least one impaction system has been designed especially for spray nozzle analysis [118].

Levine and Klienknecht [119] adapted the cascade impactor method to a study of droplet sizes in clouds sampled from aeroplanes. The air, containing the droplets, was slowed down from flight speed to the inlet-air velocity of the impactor by a diffuser. This cascade impactor consisted of four stages. The slides on each stage were coated with a layer of magnesium oxide whose thickness was much less than the drop diameters. Levine and Klienknecht used coatings that were thinner than those of May [114]. This made it possible to observe impressions made by droplets as small as four microns in diameter.

C, Spray Characterization

Almost all atomization processes produce a polydispersed drop size distribution in which drop diameters may normally range from 10 to 1000 microns [1]. In order to conveniently describe the spray, in a qualitative manner, two characterization terms are introduced. The first, uniformity, indicates the size range over which the drop diameters vary. The second, fineness, relates to the actual drop diameters or quality of atomization. However, in order to fully analyze the properties of a spray system, a more quantitative approach is required. This is usually achieved by interpreting the drop size data in terms of a distribution equation with two parameters; one of which is a mean diameter

to account for spray fineness, and the other is a measure of the dispersion of the spray or deviation from the mean diameter.

Houghton's [120] drop size distribution data, for water droplets in natural fogs and clouds, can be used to illustrate a typical drop size analysis. Table 4.1 summarizes the drop spectrum data. For each class interval, ΔX_i, the number of drops counted, ΔN_i, called the frequency per class interval, is reported. A common method of graphically representing the classified data is by means of a histogram. The histogram for Houghton's [120] data is shown in Figure 4.31. Conventionally the abscissa represents the class interval ΔX_i, while the ordinate represents the frequency per class interval ΔN_i. When ΔN_i is divided by the total number of drops in the entire spray sample, N, the relative class frequency, $\Delta N_i/N$ is obtained. Sometimes the class intervals ΔX_i are not of equal size. In such situations the relative class frequency, $\Delta N_i/N$ is normalized by dividing by the class interval, ΔX_i. This normalized relative class frequency, $\frac{\Delta N_i/N}{\Delta X_i}$, when plotted vs the class interval midpoint, gives the frequency function of the drop size distribution. Figure 4.32 illustrates the drop size frequency curves on both a number and volume basis. There is a significant disparity between the drop diameter at which the largest number of drops occur and the drop diameter at which most of the sprayed liquid volume appears.

1	2	3	4	5	6	7
Class Interval	Frequency	Class Mid-Point Diameter	Normalized Relative Class Frequency on Number Basis	Normalized Relative Class Frequency on Volume Basis	Cumulative Relative Class Frequency on Number Basis	Cumulative Relative Class Frequency on Volume Basi
ΔX_i, μ	ΔN_i	$\overline{X_i}$	$f(X) = \frac{(\Delta N_i/\Delta X_i)}{N}$	$f(X^3) = \frac{(\Delta V_i/\Delta X_i)}{V}$	$F(X) = \sum_{i=1}^{h} \frac{(\Delta N_i/\Delta X_i)}{N} \Delta X_i$	$F(X^3) = \sum_{i=1}^{w} \frac{(\Delta V_i/\Delta X_i)}{V} \Delta X$
1.5-2.5	390,000	2	0.4068	.00317	0.4068	.00317
2.5-7.5	340,000	5	0.0709	.00864	0.7613	.04637
7.5-12.5	165,000	10	0.0344	.03357	0.9333	.21422
12.5-17.5	40,200	15	0.0083	.02760	0.9748	.35222
17.5-22.5	11,680	20	0.0024	.01901	0.9868	.44727
22.5-27.5	4.970	25	0.0010	.01579	0.9918	.52622
27.5-32.5	2,160	30	0.0004	.01186	0.9938	.58552
32.5-37.5	1,730	35	0.00036	.01509	0.9956	.66097
37.5-42.5	1,080	40	0.00022	.01406	0.9967	.73127
42.5-47.5	650	45	0.00013	.01205	0.9973	.79152
47.5-55.0	430	50	0.00008	.01093	0.9977	.84617
55.0-65.0	350	60	0.00003	.00769	0.998	.92307
65.0-75.0	220	70	0.00002	.00767	1.000	1.0000
	N = 958470					

TABLE 4.1: Houghton's [124] Drop-Size Data

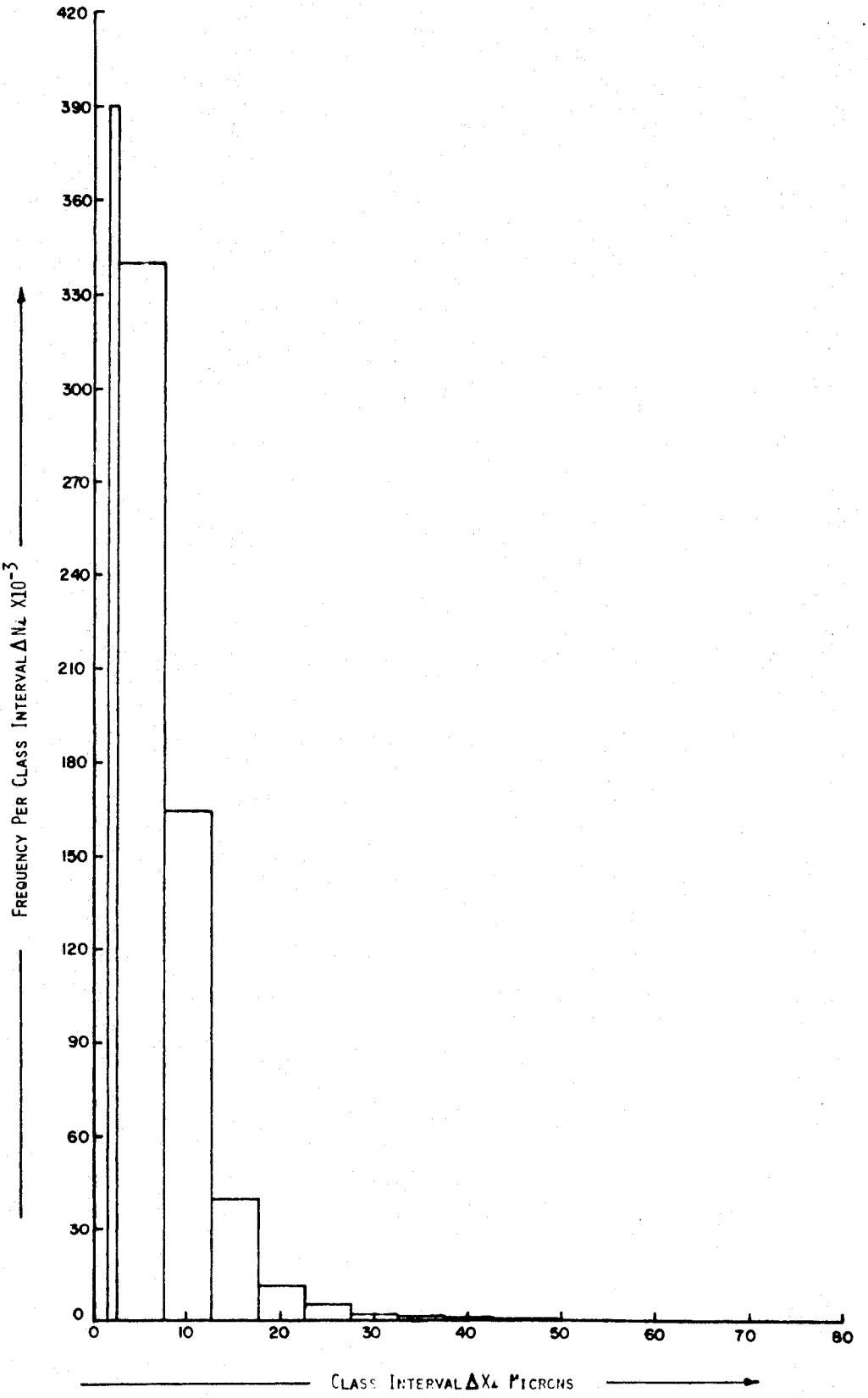

FIGURE 4.31: Histogram for Houghton's [124] Data on Number Basis

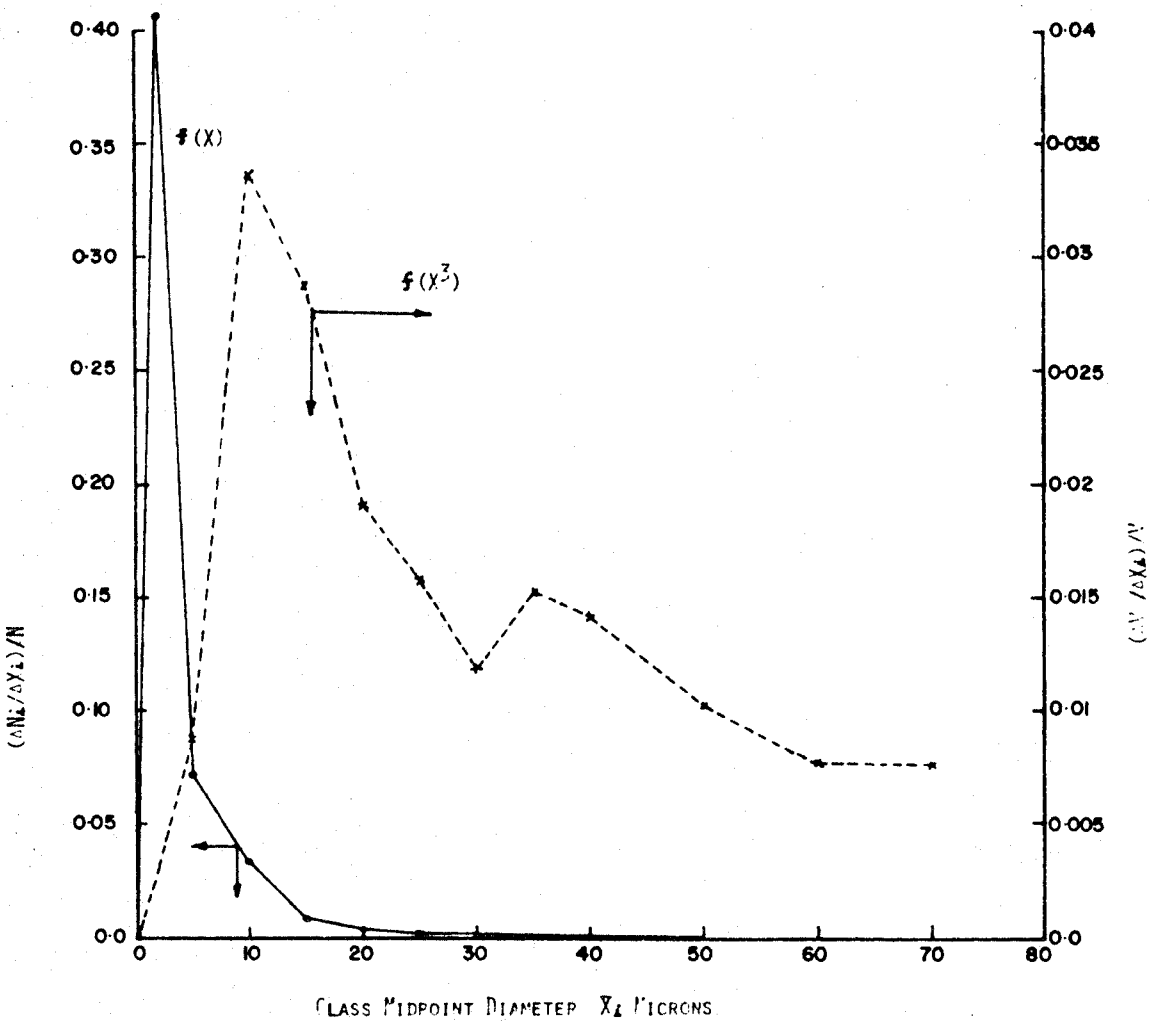

FIGURE 4.32: DROP SIZE FREQUENCY CURVES ON NUMBER AND VOLUME BASIS FOR HOUGHTON'S [124] DATA

A sample distribution function of Houghton's data is illustrated in Figure 4.33. A distribution function is a cumulative relative class frequency considered as a function of the class midpoints. The frequency function characterizes the given spray sample in detail. From this function, two important constants, the sample mean diameter and the sample variance, can be computed.

The length mean diameter of the sample spray or the sample length mean diameter, $\bar{X}_{10}$, is defined by

$$X_{10} = \frac{1}{N} \sum_{i=1}^{h} \Delta N_i \, \overline{X_i} \qquad 4.13$$

where

h = number of class intervals in which the drop size data are classified

This is, however, only one of many relevant drop mean diameters encountered in spray analyses. Additional mean diameters will be defined in the next chapter.

The variance of the sample or sample variance σ, based on the length mean diameter, $\bar{X}_{10}$, is defined by

$$\sigma^2 = \frac{1}{N-1} \sum_{i=1}^{h} (\bar{X}_i - \bar{X}_{10})^2 \qquad 4.14$$

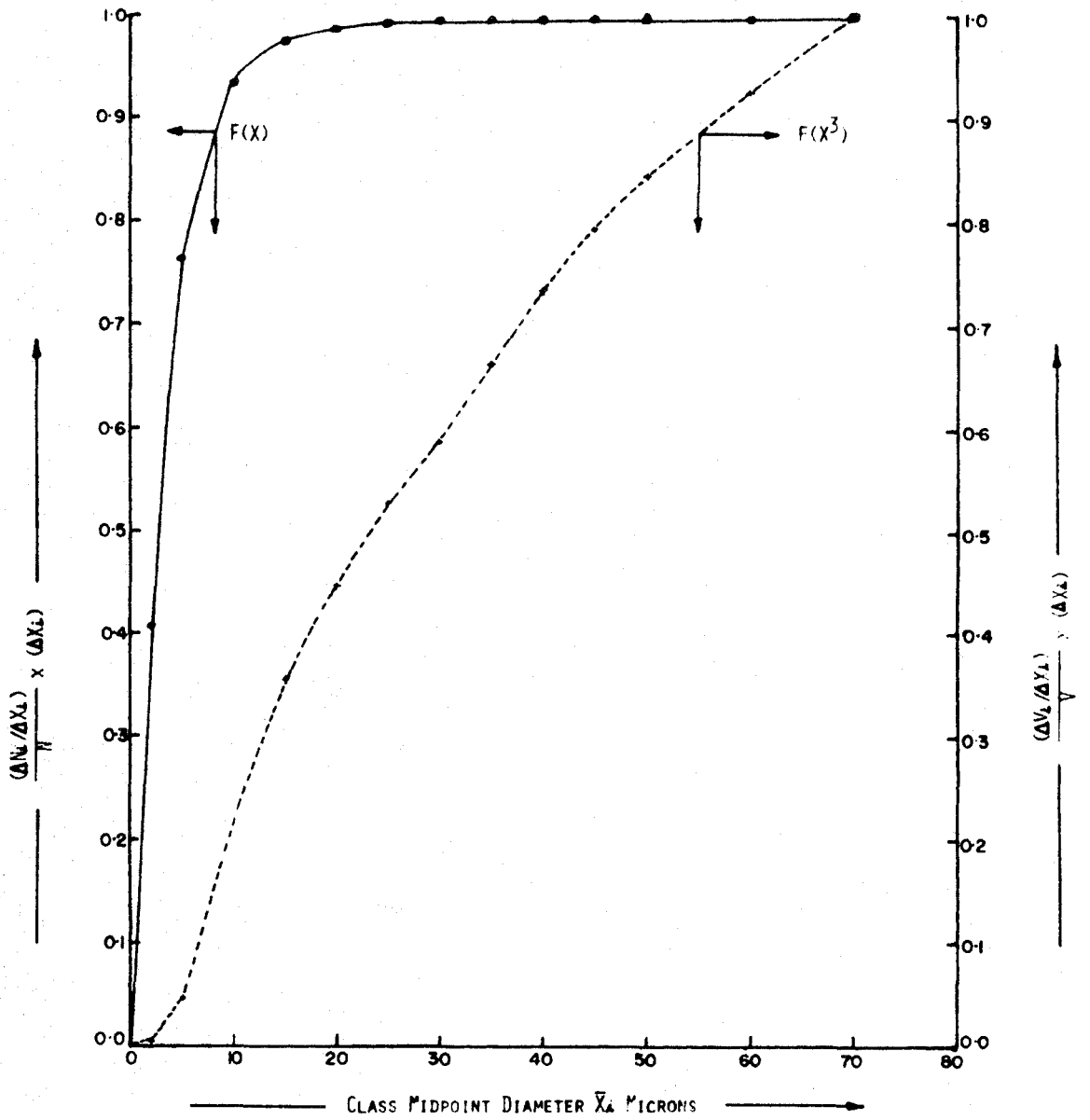

FIGURE 4.33: CUMULATIVE DROP SIZE DISTRIBUTION ON NUMBER AND VOLUME BASIS FOR HOUGHTON'S [12] DATA

A distribution function is a concise mathematical representation modelling the drop diameters and size range encountered in the spray sample. A number of purely empirical and statistically based functions have been proposed as representations of experimental drop size distributions. These distribution functions have been fitted to experimental drop size data for various atomizers in terms of the mean diameter and sample variance. By analyzing a large number of samples obtained at various positions in the spray, an accurate distribution can be obtained. Such a distribution function allows intelligent discussion of the drop spectrum uniformity and fineness in terms of sample variance and mean diameter respectively.

REFERENCES

1. Dombrowski, N., and Munday, G., Spray Drying, Biochemical and Biological Engineering Science, Edited by N. Blakebrough, Volume 2, Academic Press 1968.

2. Marshall, W. R., Atomization and Spray Drying, Chemical Engineering Progr. Monograph Series, No. 2, Vol. 50 (1954).

3. Joyce, J. R., The Atomization of Liquid Fuels for Combustion, Journal Inst. Fuel, 22 (124), 150 (1949).

4. Lord Rayleigh, On the Instability of Jets, Proc. London Math Soc., 10, 4-13 (1878).

5. Weber , C., Zum Zerfall eines Fluessigkeitsstrahles, Z. Agnew Math Mech, 11, 136-154 (1931).

6. Haenlein, A., Forsch. Gebiete Ingenieurw., Forschungsheft, 2, 139 (1931); Translation, Nat. Advisory Comm. Aeronaut, Tech. Mem. 659 (1932).

7. Ohnesorge, W. Z., Angew Math U. Mech., 16, 355, (1936).

8. Tanasawa, Y., and Kobayasi, K., Technology Rep. Tohoku University 20, 27 (1955).

9. Taylor, G. I., Int. Congr. Appl. Mech. 2, 280 (1948).

10. Watson, E. A., Joseph Lucas Research Laboratory Report No. L2671 (1947).

11. Novikov, I. I., Soviet Phys. Tech. Phys. 18, 345 (1948); Transl. Eng. Digest, 10, 72 (1949).

12. Sohngen, E. and Grigull, U., Forsch. Geb. Ing. Wes. 17, 77 (1951).

13. Hasson, D. Ph. D. Thesis, University of London (U.K.) 1956.

14. Dombrowski, N., Hasson, D., and Ward, D. E., Some Aspects of Liquid Flow Through Fan Spray Nozzles, Chemical Engg. Sci., 12, 35-50 (1960).

15. Limper, A. F., Atomization of Liquids by Injection into High Velocity Gas Streams, M.S. Thesis, Department of Chemical Engineering, University of Illinois, May 1947.

16. Clare, H. and Radcliffe, A., J. Inst. Fuel 27, 510 (1954).

17. Fraser, R. P., Brit. Patent 405, 308 (1934).

18. Fraser, R. P., Dombrowski, N., and Routley, J. M., The Atomization of a Liquid Sheet by an Impinging Air Stream, Chemical Engineering Science, 18, 339-353 (1963).

19. Walton, W. H., and Prewett, W. C., The Production of Sprays and Mists of Uniform Drop Size by Means of Spinning Disc-Type Sprayers, Proc. Phys. Soc., Vol. 62, 341 (1949).

20. Dombrowski, N and Fraser, R. P., A Photographic Investigation into the Disintegration of Liquid Sheets, Phil. Trans. Roy. Soc. London A247, 101-130 (1954).

21. Hinze, J. O. and Melborn, H. J., Appl. Mech. 17, 145 (1950).

22. Straus, R., Ph.D. Thesis, University of London (1949).

23. Fraser, R. P., Dombrowski, N., and Routly, J. H., The Filming of Liquids by Spinning Cups, Chem. Engg. Sci., 18, 323-337 (1963).

24. May, K. R., An Improved Spinning Top Homogeneous Spray Apparatus, Journal Applied Phys., Vol. 20, 932, October 1949.

25. Fraser, R. P., Dombrowski, N., and Routley, J. H., The Production of Uniform Liquid Sheets from Spinning Cups, Chemical Engineering Sci., 18, 315-321 (1963).

26. Lang, R. J., Ultrasonic Atomization of Liquids, J. Acoust Soc. Am., 34, 6-8 (1962).

27. Mizutani, Y., Uga, Y., and Nishimoto, T., An Investigation on Ultrasonic Atomization, Bulletin of Japan Soc. Mech. Engrs. 15 (83), 620-627 (1972).

28. Rudakov, Ya D., Geller, Z. I., Gaponenko, A. M., Rudakov, G. Ya., Experimental Investigation of Atomization of Liquid by Acoustic Atomizers, Teploenergetika 19 (10) 81-83 (1972).

29. Alliger, H., A New Air Pollution Abatement Device, Paper presented at American Chemical Society Meeting, Available from Heat Systems - Ultrasonics Inc., 38 East Hall, Plain View, New York 11803.

30. Joeck, Thomas, D., Method for Atomizing by Supersonic Sound Vibrations, U. S. Patent 2, 532, 554, December 5, 1950.

31. Dimmock, N. A., Production of Uniform Droplets, Nature Vol. 166, No. 4225, October 21, 686, (1950.

32. Wissema, J. G., and Davies, G. A., The Formation of Uniformly Sized Drops by Vibration - Atomization, Can. J. Chemical Engineering, Vol. 47, 530-535 (1969).

33. Sliepcevich, C. M., Consiglio, J. A., and Kurata, Fred; Operating Characteristics of a Vibrating-Type Atomizing Nozzle, Ind. Eng. Chem., 42 (11), 2353 (1950).

34. Hasson, D., and Peck, R. E., Thickness Distribution in a Sheet Formed by Impinging Jets, AIChE Journal 10 (5), 752-754 (1964).

35. Heidmann, M. F., and Humphrey, J. C., Fluctuations in a Spray Formed by Two Impinging Jets, NACA Technical Note 2349, April 1951, 35 pp. Also in J. of Amer. Rocket Soc., Vol. 22, 127-131, (1952).

36. Heidmann, M. F., and Foster, H. H., Effects of Impingement Angle on Drop-Size Distribution and Spray Pattern of Two Impinging Water Jets, NASA Technical Note D-872, July 1961.

37. Ryan, N. W., Mixing and Atomization by Impingement of Unconfined Liquid Jets, D. Sc. Thesis, Department of Chemical Engineering Mass. Inst. of Tech., Dec. 30, 1948.

38. Jenkins, D. C., and Booker, J. D, A Photographic Study of the Impact Between Water Drops and a Surface Moving at High Speed, Aeronautic Research Centre, Great Britain, Paper 501 (1960).

39. Vonnegut, B., and Neubauer, R. L., Production of Monodisperse Liquid Particle by Electrical Atomization, J. Colloid Sci. 7, 616-622 (1952).

40. Zeleny, J., On the Conditions of Instability of Electrified Drops, with Applications to the Electrical Discharge from Liquid Points, Proc. Cambridge Phil. Soc., 18, 71-83 (1916).

41. Johnson, C., Production of Liquid Drops, Nature, 197, 1092-1093 (1963).

42. Green, H. L., and Lane, W. R., Particulate Clouds, Dusts, Smokes, and Mists, New York: Van Nostrand, 1957.

43. Hopkinson, J. L., Shell Technical Report ICT/6, 1946.

44. Hasson, D., and Mizrahi, J., The Drop Size of Fan Spray Nozzles: Measurements by the Solidifying Wax Method Compared With Those Obtained by Other Sizing Techniques. Trans. Instn. Chem. Engs. 39, 415-432 (1961).

45. Harris, W. J., Method For Size Distribution Determinations of Non-Volatile Droplets by Electron Microscopy, Brit. J. Applied Phys., 10, pp. 139-140 (1959).

46. Dimmock, N. A., Production of Uniform Droplets, Nature 166, p. 686 (1950).

47. Tate, R. W., Immersion Sampling of Spray Droplets, AIChE Journal, 7, 574-577 (1961).

48. Doble, S. M., Design of Spray Nozzles, Engineering, 159, pp. 21-23, 61-63, 103-104, (1945).

49. Merrington, A. C., and Richardson, E. C., The Breakup of Liquid Jets, Proc. Phys., Soc. (London), 59, 1-13 (1947).

50. Pigford, R. L., and Pyle, C., Performance Characteristics of Spray-Type Absorption Equipment, Ind. Engg. Chem. 43, 1649 (1951).

51. Kuhn, R., Atomization of Liquid Fuels, NACA Technical Memorandum No. 329, 330 and 331, September 1925. Translated from Der Motorwagen, July 10 and 20, 1924, October 10 and 20, 1924, November 30, 1924, December 10, 1924, January 20, 1925 and February 10, 1925.

52. Sauter, J., Determining Size of Drops in Fuel Mixtures of Internal Combustion Engines, NACA Technical Memorandum No. 390, December 1926. Translation from Zeitschrift des Vereines deutscher Ingenieure, July 31, 1926.

53. Lee, D. W., The Effect of Nozzle Design and Operating Conditions on the Atomization and Distribution of Fuel Sprays, NACA Report 425, 1932.

54. De Juhasz, Kalman, J., Zahn, O. F., and Schweitzer, P. H., On the Formation and Dispersion of Oil Sprays, Bull No. 40, Engr. Expt. Sta., The Pennsylvania State College, August 22, 1932, 93 pp.

55. Nukiyama, S. and Tanasawa, Y., An Experiment on the Atomization of Liquids by Means of an Air Stream (1st Report); Trans. Soc. Mech. Engs., Japan, 4, No. 14, 86-93, (1938).

56. Houghton, H. G., and Radford, W. H., On the Measurement of Drop Size and Liquid Water Content in Fogs and Clouds; Papers in Physical Oceanography and Meteorology, published by Mass. Inst. Tech., and Woods Hole Oceanographic Inst., Vol. 6, No. 4, November 1938, 31 pp.

57. Burdette, Robert C., Some of the Principles Governing the Production of Air-Floated Oil Particles and Their Relation to the Toxicity of Contact Oil Sprays to Insects; Bulletin No. 632, New Jersey Agricultural Experiment Station, New Brunswick, N. J., January 1938, 31 pp.

58. Pierce, N. C., Efficiency of Hydraulic Nozzles for Atomization, M.S. Thesis, University of Illinois, 1947, 46 pp.

59. Limper, A. F., Atomization of Liquids by Injection into High Velocity Gas Streams, M.S. Thesis, University of Illinois, 1947, 78 pp. (ATl No. 13087).

60. Maxwell, R. W., Study of Air Atomization, M.S. Thesis, Mass. Inst. of Technology, May 21, 1948.

61. Lewis, H. C., Edwards, D. G., Goglia, M. J., Rice, R. I., and Smith, L. W., Atomization of Liquids in High Velocity Gas Streams, Ind. Eng. Chem., 40, 67, (1948).

62. Conroy, E. H., Jr., and Johnstone, H. F., Combustion of Sulfur in a Venturi Spray Burner; Ind. Eng. Chem., Vol. 41, 41, 2741 (1949).

63. Rupe, J. H., A Technique for the Investigation of Spray Characteristics of Constant Flow Nozzles, Part I; Presented at Conference on Fuel Sprays, University of Michigan, March 30-31, 1949, 14 pp.

64. Rupe, J. H., A Semi-Automatic Size Differentiating Droplet Counter, Progress Report No. 20-162, Jet Propulsion Lab., Cal. Inst. of Tech., February 26, 1952, (ATl No. 148916), 28 pp.

65. Golitzine, J., Method for Measuring the Size of Water Droplets in Clouds, Fogs, and Sprays, Note 6, National Aeronautical Establishment, Ottawa, Canada, 1951, 13 pp.

66. Gretzinger, J., and Marshall, W. R., Jr., Characteristics of Pneumatic Atomization, AICHE Journal, 7(2), 312-318 (1961).

67. Holroyd, H. B., On the Atomization of Liquid Jets, Jour. of the Franklin Inst., 215, 93. (1933).

68. Longwell, J. P., Fuel Oil Atomization, D. Sc. Thesis, Mass. Inst. Tech., 1943, 167 pp.

69. Taylor, E. H., and Harmon, D. B., Jr., Measuring Drop Sizes in Sprays, Ind. Eng. Chem., Vol. 46, (7), 1455-1457 (1954).

70. Fraser, R. P., Proceedings of 2nd Industrial Conference, Fermhurst Research Station, London, England (1957).

71. Radcliffe, A., and Clare, H., A Correlation of the Performance of Two Air Blast Atomizers with Mixing Sections of Different Size, National Gas Turbine Establishment, Report No. R144, October 1953.

72. Wetzel, H., Ph.D. Thesis, University of Wisconsin, Madison (1951).

73. Turner, G. M., and Moulton, R. W., Chem. Eng. Progr., 49, 185 (1953).

74. Kim, K. Y., and Marshall, W. R., Drop Size Distributions from Pneumatic Atomizers, AIChE Journal, 17 (3) 575-584, (1971).

75. Choudpur, A. P. R., Lamb, G. G. and Stevens, W. F., Determination of Drop Size Distribution, Trans. Indian Inst. Chem. Engrs., 10, 21-24 (1957-58).

76. Nelson, P. A., Stevens, W. F., Size Distribution of Droplets from Centrifugal Spray Nozzles, AIChE Journal, 7, 80-86 (1961).

77. Ingebo, R. D., Relation of Atomization and Rocket Combustor Performance, Chemical Engineering Progr., 58, 74-76 (1962).

78. Ingebo, R. D., Size Distribution and Velocity of Ethanol Drops in a Rocket Combustor Burning Ethanol and Liquid Oxygen, Amer. Rocket Soc. Jour., 31, 540-541 (1961).

79. Priem, R. J., Breakup of Water Drops and Sprays with a Shock Wave, Jet Propulsion, 27, 1084-1087, 1093 (1957).

80. Gilman, S., A Photographic Method of Determining the Size Distribution of Small Particles, M.S. Thesis, University of Pittsburgh, 1942.

81. Stubbs, H. E., and York, J. L., Photographic Analysis of Sprays, Paper Presented at the Annual Meeting of the American Soc. of Mech. Engrs., Atlantic City, N.J., November 25-30, 1951.

82. McCullough, S., and Perkins, P. J., Flight Camera for Photographing Cloud Droplets in Natural Suspension in the Atmosphere, NACA Research Memorandum RME50K01a, June 29, 1951.

83. Hesketh, H. E., Cloud Type Atomization of a Liquid Stream by a Gas Stream in a Venturi Scrubber, Ph.D. Thesis, Pennsylvania State University, 1968.

84. Adler, C. R., Mark, A. M., Marshall, W. R., and Parent, R. J., A Scanning Device for Determining the Size of Spray Droplet Images, Chemical Engineering Progr., 50 (1), 14-23 (1954).

85. Clark, C. J. amd Dombrowski, N., On the Photographic Analysis of Sprays, Journal Aerosol Sci., 4(1), 27-33 (1973).

86. Browning, J. A., Literature of the Combustion of Petroleum, Advances in Chemistry Series No. 20, American Chemical Society, 1958.

87. Benson, G. M., El. Wakil, M. M., Myers, P. S., Uyehara, O. A., Fluorescent Technique for Determining the Cross-Sectional Drop Size Distributions of Liquid Sprays, Amer. Rocket Soc. Jour., 30, 447-454

88. Staniland, L. N., Simple Daylight Detectors for the Examination of Fluorescent Traced Sprays, Chem. & Ind. (London), 502-503 (1961).

89. Thompson, B. J., Parrent, G. B., Ward, J. H., and Justh, B., J. Appl. Meteor.5, 434 (1966).

90. Fourney, M. E., Matkin, J. H., and Waggoner, A. P., Aerosol Size and Velocity Determination via Holography, Rev. Sci. Instr. 40 (2), 205-213 (1969).

91. Sinclair, D., Optical Properties of Aerosols, Handbook on Aerosols, Washington, D. C.: U. S. Atomic Energy Commission, 1950, Chap. 7.

92. Sinclair, D., Measurement of Particle Size and Size Distribution, Handbook on Aerosols, Washington, D. C.; U. S. Atomic Energy Commission, 1950, Chap. 8.

93. Dombrowski, N., and Wolfsohn, D. L., Measurement of the Surface Volume Mean Diameter of Sprays, Journal Aerosol Sci., 2, 405-412 (1971).

94. Stratton, J. A., Electromagnetic Theory, McGraw Hill, p. 563, 1941.

95. Sinclair, D., and La Mer, V. K., Light Scattering as a Measure of Particle Size in Aerosols, Chem. Rev., 44, 245 (1949).

96. Durbin, E. J., Optical Methods Involving Light Scattering for Measuring Size and Concentration of Condensation Particles in Supercooled Hypersonic Flow, NACA Technical Note 2441, August 1951.

97. Schmidt, J. M., Measurement of Droplet Size by the Diffraction Ring Method, Progr. Report No. 3-18, Jet Propulsion Lab., Calif. Inst. of Tech., July 27, 1948.

98. Schmidt, J. M., A Preliminary Investigation of the Atomization of Liquids Injected into an Air Stream, Prog. Report No. 4-101, Jet Propulsion Lab., Calif. Inst. Tech., May 23, 1949.

99. Sauter, J., Investigation of Atomization in Carburetors, NACA Technical Memorandum, No. 518, June 1929. Translation from Zeitschrift des Vereines deutscher Ingenieure, November 3, 1928.

100. Schmidt, J. M., Application of the Photoelectric Photometer to the Study of Atomization, Progr. Report No. 3-15, Jet Propulsion Lab., Calif. Inst. of Tech., July 30, 1946.

101. Mehlig, H., Zur Physik der Brennstoff-strahlen in Diesselmaschinen, Automobiltechnische Zeitschrift (Germany), 37, 411-421, (1934).

102. Dieck, R. H., and Roberts, R. L., Appl. Opt. 9, 2007, (1970).

103. Dobbins, R. A., Crocco, L. and Glassman, I., Measurement of Mean Particle Sizes of Sprays from Diffractively Scattered Light, AIAA Journal, 1 (8), 1882-1886 (1963).

104. Roberts, J. H., and Webb, M. J., Measurement of Droplet Size for Wide Range Particle Distributions, AIAA Journal 2 (3), 583-585 (1964).

105. Guyton, A. C., Electronic Counting and Size Determination of Particles in Aerosols, Journal Ind. Hyg. Toxicol, 28, 133 (1946).

106. Gucker, F. T., Jr., and O'Konski, C. T., Electronic Methods of Counting Aerosol Particles, Chem. Rev., 44, 373 (1949).

107. Geist, J. M., An Electronic Spray Analyzer for Electrically Conducting Particles, Ph.D. Thesis, University of Michigan 1950.

108. Geist, J. M., York, J. L., and Brown, G. G., Electronic Spray Analyzer for Electrically Conducting Particles, Ind. Eng. Chem., 43, 1371 (1951).

109. Fisher, M. A., Katz, S., Lieberman, A., and Alexander, N. E., The Aerosoloscope; An Instrument for the Automatic Counting and Sizing of Aerosol Particles, Proc. 3rd Nat. Air Pollution Symp., Pasadena, California, pp. 120-130 (1955).

110. Gucker, F. T., Jr., Sensitive Photoelectronic Photometer Electronics, 20, 106-111 (1947).

111. Gucker, F. T., Jr., and Rose, D. G., A Photoelectric Instrument for Counting and Sizing Aerosol Particles, Brit. J. Appl. Phys., Suppl. 3, S138-43 (1954).

112. Morgan, B. B., Automatic Particle Counting and Sizing, Research (London), 10, 271-280 (1957).

113. Turley, S. G., Brooks, W. D., and Barton, J. B., Size Distribution by Settling Method, Final Technical Report by W. G. Cutter and W. E. Meyer, A Basic Study of the Physics of Aerosol Formation, Penn. State University, 72 (1953).

114. May, K. R., The Cascade Impactor, An Instrument for Sampling Coarse Aerosols, J. Sci. Instr., 22, 187-195 (1945).

115. Pilcher, J. M., Approaches to Aerosol Problems, Battelle Tech. Rev., pp. 3-8, April 1956.

116. Wilcox, J. D., Design of a New Five Stage Cascade Impactor, A.M.A. Arch. Ind. Hyg. 7, 376-382 (1953).

117. Mozzon, D., An Information Search and an Evaluation of Factors Affecting Particle Size Determinations with Particular Emphasis on Cascade Impactors, M.S. Thesis, University of Windsor, 1972.

118. Ranz, W. E., Hofelt, C. Jr., Determining Drop Size Distribution of a Nozzle Spray, Ind. Eng. Chem., 49, 288-293 (1957).

119. Levine, J. and Kleinknecht, K. S., Adaptation of a Cascade Impactor to Flight Measurement of Droplet Size in Clouds, NACA Research Memorandum E51G05, September 18, 1951.

120. Chemical Engineers Handbook, J. H. Perry, 3rd Ed. p. 1170, New York, McGraw Hill Book Company, 1950.

V. LIQUID DROP SIZE ANALYSIS

A. Drop Size Characterization

The ultimate spray from any nozzle or atomizer consists of a large number of polydisperse non-spherical droplets. Analysis of drop size spectra is usually performed by first selecting a relevant length (diameter) parameter for the droplets, dividing the drop size range into class intervals, counting the number of drops in each class interval and then attempting to mathematically describe the spray in terms of a distribution function. This distribution function normally has two parameters. One is a relevant estimate of a mean diameter while the other is a measure of the dispersion of the spray, or deviation from the mean. A graphical display of the size distribution is usually achieved by plotting.

i. the cumulative relative number of droplets, $(\Sigma\Delta N)/N$, less than a given diameter, X

ii. the cumulative relative volume (or mass) of droplets, $(\Sigma\Delta V)/V$, less than a given diameter X versus the class mid-point diameters.

From elementary considerations, it can be shown that the following relation must exist between the number of droplets ΔN_i, the volume ΔV_i in a class interval ΔX_i and the ith class mid-point diameter $\overline{X}_i$:

$$\left(\frac{\Delta N_i}{\Delta X_i}\right) = \left\{\frac{6}{\pi \left(\bar{X}_i\right)^3}\right\} \left(\frac{\Delta V_i}{\Delta X_i}\right) \qquad 5.1$$

When the class interval is reduced to dX, then

$$\left(\frac{dN}{dX}\right) = \left(\frac{6}{\pi X^3}\right) \left(\frac{dV}{dX}\right) \qquad 5.2$$

If the drops are not spherical, X is an effective diameter so defined that the same effect is produced in the phenomenon under consideration as a spherical droplet of actual diameter, X.

1. Mean Diameters

A relevant mean diameter is required for effective correlation of drop size spectra in a distribution function. For predicting wet scrubber particulate collection efficiency, mean diameters are employed to facilitate analyses. The actual polydisperse, non-spherical, droplet spray is modelled by a fictitious monodisperse spray with every drop having a hypothetical mean diameter.

Various mean diameters, with different physical significance and application, have been reported [1]. Mugele and Evans [2] generalized and standardized the notation for various types of mean diameters by the expression

$$(\bar{X}_{qp})^{q-p} = \frac{\int_{X_o}^{X_m} X^q \, (dN/dX) \, dX}{\int_{X_o}^{X_m} X^p \, (dN/dX) \, dX} = \frac{\int_{X_o}^{X_m} X^{q-3} \, (dV/dX) \, dX}{\int_{X_o}^{X_m} X^{p-3} \, (dV/dX) \, dX} \qquad 5.3$$

where

X_o = the minimum drop diameter occurring in the spray, microns

X_m = the maximum drop diameter occurring in the spray, microns

q = dimensionless constant (normally integer), with a value between 0 and 4 depending upon the effect investigated

p = dimensionless constant (normally integer), with a value between 1 and 3 depending upon the effect investigated

$p+q$ = order of the mean diameter.

The generalized mean diameter, $\bar{X}_{qp}$, can be expressed in the following form applicable to count data:

$$(\bar{X}_{qp})^{q-p} = \frac{\sum_{i=1}^{h} (\bar{X}_i)^q \Delta N_i}{\sum_{i=1}^{h} (\bar{X}_i)^p \Delta N_i} \qquad 5.4$$

where

$\bar{X}_i$ = ith class interval mid-point diameter

h = total number of class intervals into which the drops size range ($X_o \leq X \leq X_m$) has been divided

ΔN_i = number of drops in the ith class interval.

There are various mean diameters encountered in drop size analysis. In Table 5.1 the more important mean diameters are summarized along with their physical significance, field of application and corresponding "p" and "q" values.

Table 5.2 provides a summary of a comparison of the length mean, surface mean, surface-diameter mean, volume mean and Sauter (volume-surface mean) diameters for the data reported by Houghton [3]. It must be emphasized that the significance of the bigger drops increases with the power to which $\bar{X}_i$ is raised.

2. Median Diameters

Sometimes median diameters are also used to discuss spray distributions. The median diameter of a spray is that

Name of Mean Diameter	Definition	q	p	order (p+q)	Significance and Field of Application
Geometric	$\ln \bar{X}_{oo} = \frac{\sum_{i=1}^{h} (\ln \bar{X}_i)\ \Delta N_i}{\sum_{i=1}^{h} (\Delta N_i)}$	0	0	0	Suitable for Characterizing Log Normal Distributions
Linear or Arithmetic	$\bar{X}_{10} = \frac{\sum_{i=1}^{h} \bar{X}_i\ (\Delta N_i)}{\sum_{i=1}^{h} (\Delta N_i)}$	1	0	1	Suitable for evaporation studies
Surface	$\bar{X}_{20} = \left[\frac{\sum_{i=1}^{h} (\bar{X}_i)^2\ \Delta N_i}{\sum_{i-1}^{h} (\Delta N_i)}\right]^{\frac{1}{2}}$	2	0	2	Suitable for surface behavior ie absorption
Volume	$\bar{X}_{30} = \left[\frac{\sum_{i=1}^{h} (\bar{X}_i)^3\ \Delta N_i}{\sum_{i=1}^{h} \Delta N_i}\right]^{\frac{1}{3}}$	3	0	3	Suitable for volume distribution studies
Surface Diameter	$\bar{X}_{21} = \frac{\sum_{i=1}^{h} (\bar{X}_i)^2\ \Delta N_i}{\sum_{i=1}^{h} (\bar{X}_i)\ \Delta N_i} = \frac{(\bar{X}_{20})^2}{\bar{X}_{10}}$	2	1	3	Useful where two functions, which depend upon surface and length, as in adsorption are compared
Volume diameter	$\bar{X}_{31} = \left[\frac{\sum_{i=1}^{h} (\bar{X}_i)^3\ \Delta N_i}{\sum_{i=1}^{h} (\bar{X}_i)\ \Delta N_i}\right]^{\frac{1}{2}} = \left[\frac{(\bar{X}_{30})^3}{\bar{X}_{10}}\right]^{\frac{1}{2}}$	3	1	4	Used for evaporation, molecular diffusion studies
Volume surface or Sauter	$\bar{X}_{32} = \frac{\sum_{i=1}^{h} (\bar{X}_i)^3\ \Delta N_i}{\sum_{i=1}^{h} (\bar{X}_i)^2\ \Delta N_i} = \frac{(\bar{X}_{30})^3}{(\bar{X}_{20})^2}$	3	2	5	Suitable for efficiency studies, mass transfer, reaction, wet scrubber performance
De Brouckere	$\bar{X}_{43} = \frac{\sum_{i=1}^{h} (\bar{X}_i)^4\ \Delta N_i}{\sum_{i=1}^{h} (\bar{X}_i)^3\ \Delta N_i}$	4	3	7	Combustion equilibrium

TABLE 5.1: Summary of Important Mean Diameters

Class Interval Microns ΔX_i	Class Mid-Point Diameter $\bar{X}_i$	Frequency ΔN_i	$(\bar{X}_i)(\Delta N_i)$	$(\bar{X}_i)^2 \Delta N_i$	$(X_i)^3 \Delta N_i$
1.5 - 2.5	2	390,000	780,000	1,560,000	3,120,000
2.5 - 7.5	5	340,000	1,700,000	8,500,000	42,500,000
7.5 - 12.5	10	165,000	1,650,000	16,500,000	165,000,000
12.5 - 17.5	15	40,200	603,000	9,045,000	135,675,000
17.5 - 22.5	20	11,680	233,600	4,672,000	93,440,000
22.5 - 27.5	25	4,970	124,250	3,106,250	77,656,250
27.5 - 32.5	30	2,160	64,800	1,944,000	58,320,000
32.5 - 37.5	35	1,730	60,550	2,119,250	74,173,750
37.5 - 42.5	40	1,080	43,200	1,728,000	69,120,000
42.5 - 47.5	45	650	29,250	1,316,250	59,231,250
47.5 - 55.0	50	430	21,500	1,075,000	53,750,000
55.0 - 65.0	60	350	21,000	1,260,000	75,600,000
65.0 - 75.0	70	220	15,400	1,078,000	75,460,000
Totals	--	958,470	5,346,550	53,903,750	983,046,250

Mean diameters are calculated according to

(Arithmetic Mean) $$\bar{X}_{10} = \frac{\sum_{i=1}^{h} (\bar{X}_i)\,\Delta N_i}{\sum_{i=1}^{h} \Delta N_i} = \frac{5,346,550}{958,470} = 5.58\mu$$

(Surface Mean) $$\bar{X}_{20} = \left[\frac{\sum_{i=1}^{h} (\bar{X}_i)^2\,\Delta N_i}{\sum_{i=1}^{h} \Delta N_i}\right]^{\frac{1}{2}} = \left(\frac{53,903,750}{958,470}\right)^{\frac{1}{2}} = 7.50\mu$$

Surface (Diameter) Mean $$\bar{X}_{21} = \frac{\sum_{i=1}^{h} (\bar{X}_i)^2\,\Delta N_i}{\sum_{i=1}^{h} (\bar{X}_i)\,\Delta N_i} = \left(\frac{53,903,750}{5,346,550}\right) = 10.08\mu$$

(Volume Mean) $$\bar{X}_{30} = \left[\frac{\sum_{i=1}^{h} (\bar{X}_i)^3\,\Delta N_i}{\sum_{i=1}^{h} \Delta N_i}\right]^{\frac{1}{3}} = \left(\frac{983,046,250}{958,470}\right)^{\frac{1}{3}} = 10.08\mu$$

(Sauter Mean) $$\bar{X}_{32} = \frac{\sum_{i=1}^{h} (\bar{X}_i)^3\,\Delta N_i}{\sum_{i=1}^{h} (X_i)^2\,\Delta N_i} = \frac{983,046,250}{53,903,750} = 18.24\mu$$

TABLE 5.2: Comparison of Mean Diameters for Houghton's [3] Data

diameter which divides the spray into two equal portions on a number, surface, volume or mass basis. Median diameters are usually obtained from the 50% point on the cumulative curve, although they can be calculated if the frequency function of the sample spray is known. The commonly used median diameters have been defined and then compared to the mean diameters of interest.

a. Number Median Diameter, X_{NM}

This is the diameter which divides the entire spray into two equal halves on a number basis. Houghton's [3] data when plotted in Figure 5.1 on a cumulative number basis gives a number median diameter of 2.9μ.

b. Mass Median Diameter, X_{MM}

The diameter that separates half of the spray mass into droplets of smaller diameter, and half into those of greater diameter is termed the mass median diameter.

c. Volume Median Diameter X_{VM}

This is a diameter for which half the spray volume is to be found in droplets of smaller diameter, and half in those of greater diameter. The value for Houghton's [3] data as shown in Figure 5.1 is 23.2μ.

Unless the liquid density changes with droplet size, the mass and volume medians will be identical.

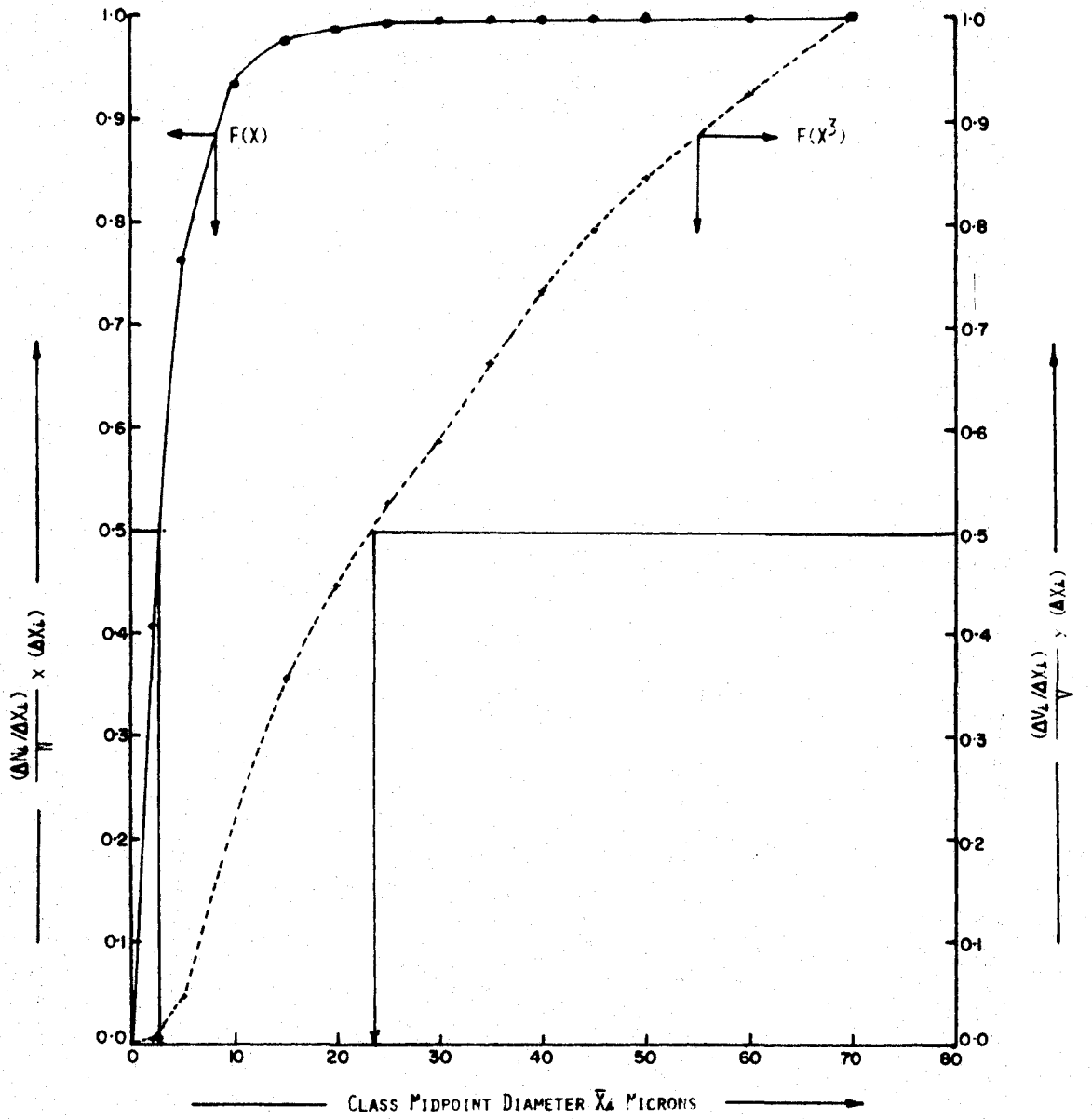

FIGURE 5.1 CUMULATIVE DROP SIZE DISTRIBUTION ON NUMBER AND VOLUME BASIS FOR HOUGHTON'S [3] DATA

d. Surface Median Diameters, X_{SM}

A diameter that locates half the spray droplet surface area in terms of droplets of smaller area and half with droplets of larger area is termed the surface median diameter.

Table 5.3 summarizes the comparison of mean to median diameters (on both mass and count bases) for various degrees of uniformity, expressed in terms of standard geometric deviation, assuming that droplets follow a log-probability distribution. Significant differences between the various means and median sizes occur for variations in the standard geometric deviation.

3. Dispersion Parameter

The measure of spray dispersion or deviation from the mean diameter is accounted for in distribution functions by the standard deviation σ. The standard deviation is the positive square root of the variance, σ^2, which is defined by

$$\sigma^2 = \frac{1}{(N-1)} \sum_{i=1}^{h} (\bar{X}_i - \bar{X}_{qp})^2 \, (N) \, f(X_i) \, \Delta X_i \qquad 5.5$$

for a discrete distribution with equal size class intervals, where

$\bar{X}_i$ = ith class mid-point drop diameter

$\bar{X}_{qp}$ = mean drop diameter of order (q+p) for the entire spray

Definition of Mean Diameter Name $\bar{X}_{qp}$	q	p	Standard Geometric Deviation σ	Mass Median/ Mean $X_{MM}/\bar{X}_{qp}$	Mean/ Number Median $\bar{X}_{qp}/X_{NM}$
Geometric Mean	0	0	2 3 4	4.23 37.37 319.1	1.00 1.00 1.00
Linear Mean (number mean)	1	0	2 3 4	3.32 20.4 122.1	1.272 1.829 2.614
Surface Mean (surface to number mean)	2	0	2 3 4	2.61 11.18 46.69	1.617 3.343 6.833
Volume Mean (volume to number mean)	3	0	2 3 4	2.06 6.11 17.86	2.06 6.11 17.86
Surface to Diameter	2	1	2 3 4	2.06 6.11 17.86	2.06 6.11 17.86
Volume to Diameter	3	1	2 3 4	1.62 3.34 6.83	2.61 11.18 46.69
Volume to Surface Mean	3	2	2 3 4	1.27 1.83 2.61	3.32 20.44 122.1
Mass Mean	4	3	2 3	.786 .547	5.38 68.2

TABLE 5.3: Comparison of Mean and Median Diameters [4]

$f(X_i)$ = normalized probability density curve of the drop size spectrum, equal to $(\Delta N_i/N)/\Delta X_i$

N = total number of droplets.

B. Drop Size Distribution Functions

Mean and median diameters are useful in characterizing the fineness of a spray but do not by themselves give information on the size distribution of the drop spectrum. It is quite conceivable, for example, that two sprays with identical mean-volume diameters, $\bar{X}_{30}$, could contain vastly different numbers of small droplets. This difference in the drop size distribution is usually quantified in terms of a dispersion parameter, or standard deviation, which would be different for each spray. It follows that drop size spectra can be completely characterized in a concise and accurate manner by distribution functions which employ at least the two parameters

i. mean drop size and

ii. standard deviation.

There have been many expressions proposed as mathematical representations of drop-size distributions for sprays. A suitable expression should [5]

i. fit the data adequately

ii. allow for extrapolation

iii. permit easy calculation of mean diameters and other relevant parameters

iv. provide for consolidation of large amounts of data

v. give some insight into the fundamental mechanisms of droplet production.

Drop size distribution functions in present use have been developed on the basis of purely empirical or probability arguments, since almost all conjectural models of droplet formation were too simplistic in that secondary atomization of the larger drops formed in the original spray was not considered. Brief descriptions and discussions of commonly employed distribution functions follow.

1. Normal Distribution

If a frequency histogram is plotted for a sample of a droplet spray and the density curve, f(X), is similar to that illustrated in Figure 5.2, it might be possible to represent the drop size spectrum by a normal distribution.

The density of a normal Gaussian distribution is described by the relationship

$$\frac{dN}{dX} = f(X) = \frac{1}{\sqrt{2\pi}\,\sigma_N} \exp\left[-\frac{1}{2}\left(\frac{X - \bar{X}_{qp}}{\sigma_N}\right)^2\right] \qquad 5.6$$

where

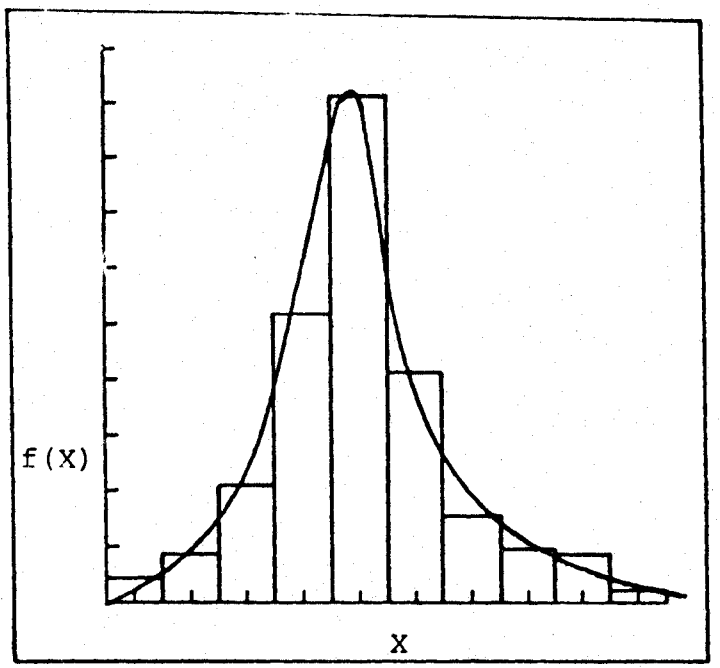

FIGURE 5.2: Typical Frequency Histogram

$f(X)$ = frequency function of the sample

σ_N = standard deviation of the normal distribution

X = drop diameter

$\bar{X}_{qp}$ = mean drop diameter of order (q+p)

The curve of $f(X)$ is symmetrical with respect to the mean drop diameter. The smaller the value of σ^2 the higher the peak at $X = \bar{X}_{qp}$, and the steeper are the descents on both

sides. The normal distribution law does not usually fit drop size distributions since it asserts that deviations in excess of the mean are counterbalanced by deficiencies of equal magnitude. This means that if droplets whose diameter are more than twice the magnitude of the mean are present in the drop spectrum, then droplets of negative size would exist, which is impossible for real systems.

For a normally distributed drop size spectrum, the distribution function

$$F(X) = \frac{1}{\sqrt{2\pi}\,\sigma_N} \int_{-\infty}^{X} \exp\left[-\frac{1}{2}\left(\frac{X - \bar{X}_{qp}}{\sigma_N}\right)^2\right] dX \qquad 5.7$$

gives the total fraction of the drop size spectrum having diameters less than or equal to X. For a discrete distribution

$$\frac{dN}{dX} = f(X) = \frac{\Delta(N_i/N)}{\Delta X_i} = \left(\frac{1}{2\sqrt{\pi}\,\sigma_N}\right) \exp\left[-\frac{1}{2}\left(\frac{X - \bar{X}_{qp}}{\sigma_N}\right)^2\right] \qquad 5.8$$

where

$\frac{\Delta(N_i/N)}{\Delta X_i}$ = normalized fraction of the total number of drops contained in the ith class interval

X_i = mid-point of the class interval.

The mean diameter, $\bar{X}_{qp}$, in equation 5.8 depends upon the quantity measured. For example if droplet diameters were measured, then the mean diameter would be termed the length mean $\bar{X}_{10}$. If volumes were measured, then the volume mean-diameter $\bar{X}_{30}$, is obtained. If the length mean diameter follows a normal distribution, then volume, mass or other geometric functions will not give a normal distribution. Conversely, if droplet mass data give a normal curve, then diameters based upon measures of length and surface area will not.

Substitution of $t^2 = \left(\frac{X - \bar{X}_{qp}}{\sigma_N}\right)^2$ into equation 5.7 yields

$$F(Z) = \frac{1}{2\pi} \int_{-\infty}^{Z} \exp\ [-t^2/2]\ dt$$

$$= \frac{1}{2} + \frac{1}{2\pi} \int_{0}^{Z} \exp\ [-t^2/2]\ dt \qquad 5.9$$

an expression that has been tabulated in many references [6, 7] for various values of Z. When $Z \to \infty$, $F(Z) \to 1.0$. Some typical values of F(Z) for selected values of Z are illustrated below.

Z	-3.0	-2.0	-1.0	-0.5	0	0.5	1.0	2.0
F(Z)	0.0013	0.0228	0.1587	0.3085	0.50	0.6915	0.8413	0.9772

Equation 5.9 is the basis for construction of arithmetic probability graph paper. On this paper a so-called probability scale is measured on the X-axis and an arithmetic scale on the Y-axis, as shown in Figure 5.3, The probability scale is constructed by measuring specific

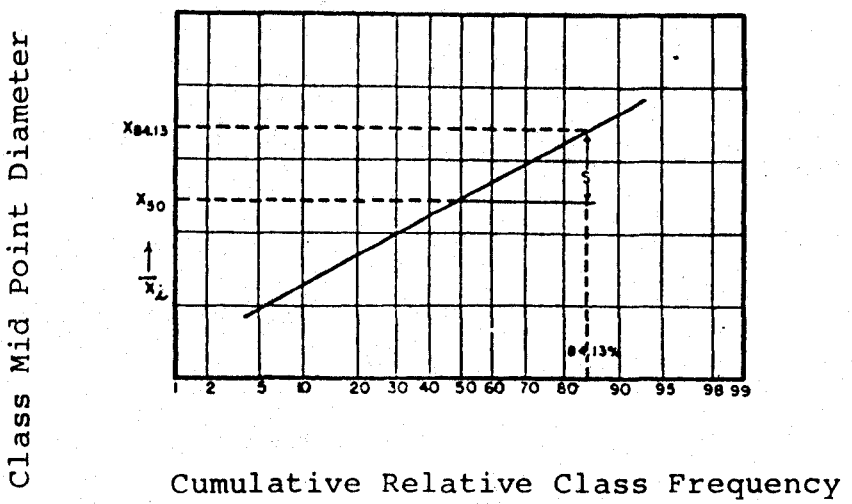

FIGURE 5.3: Normal Probability Paper [1]

distances from a mid line, which is designated as 50%. This 50% line corresponds to Z = 0 in equation 5.9. The lines corresponding to 40 and 60% would each be measured a distance 0.26 units (Z = 0.26) from the 50% line in both directions. In like manner, lines corresponding to 30 and 70% or 20 and 80% would be located in relation to the 50% line at distances corresponding to appropriate values of Z in equation 5.9

which make the integral equal to these percentages. For $Z = 1$, $F(Z) = 0,8413$ or 84.13% and for $Z = -1$, $F(Z) = 0.1587$ or 15.87%.

According to the basic statistical definition, the standard deviation, σ_N, is determined by subtracting $X_{84.13}$ from $X_{50.0}$ on Figure 5.3.

If the distribtuion function for the sample data obtained by Houghton [3] is plotted on normal probability paper according to Figure 5.4, a straight line is not obtained on a number nor on a volume basis. This shows that the drop size spectrum obtained by Houghton cannot be represented by a normal distribution function. As a result another distribution relationship must be sought.

2. Log-Normal Distribution

If a frequency histogram is plotted for a sample of a droplet spray and the resulting density curve is not symmetrical as illustrated in Figure 5.5, then a normal distribution function will fail to correlate the data. However a log-normal distribution function (sometimes referred to as a logarithmic distribution) has been found to be effective in describing non-symmetrical size distributions for both crushed solids and spray droplets [8, 9, 10].

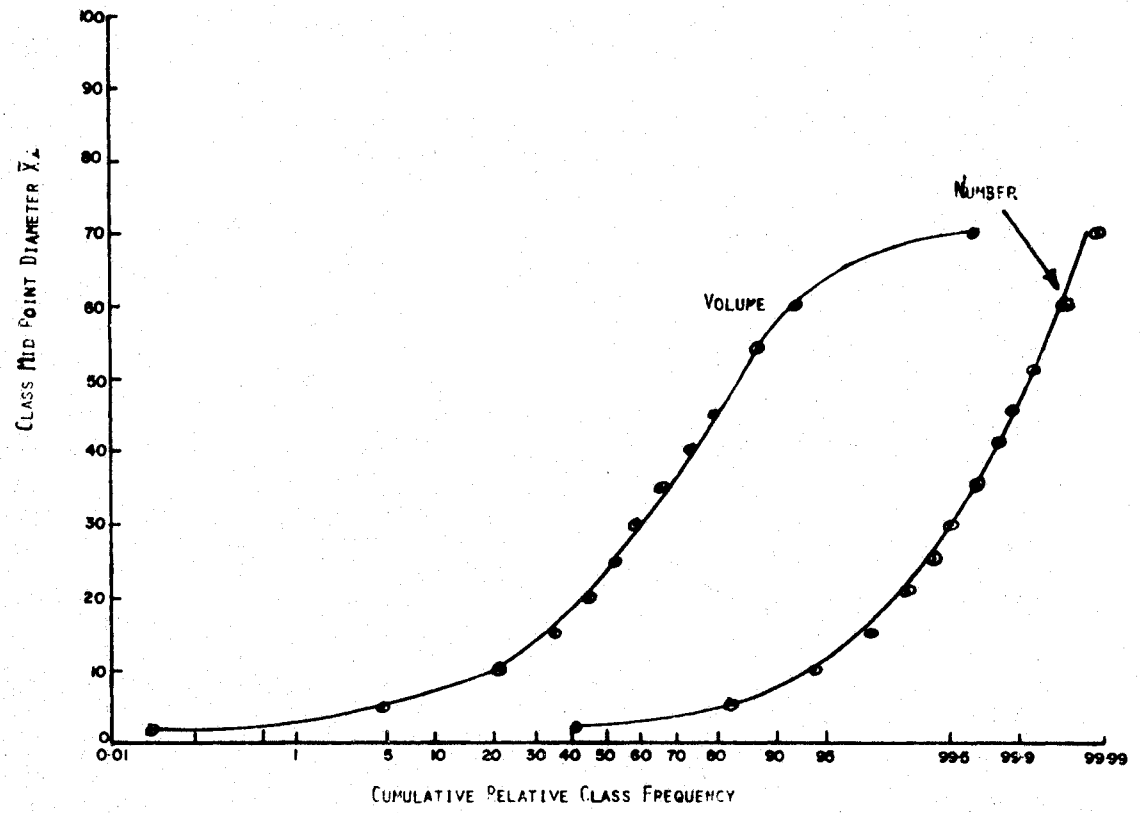

FIGURE 5.4: NORMAL DISTRIBUTION FOR HOUGHTON'S [3] DATA

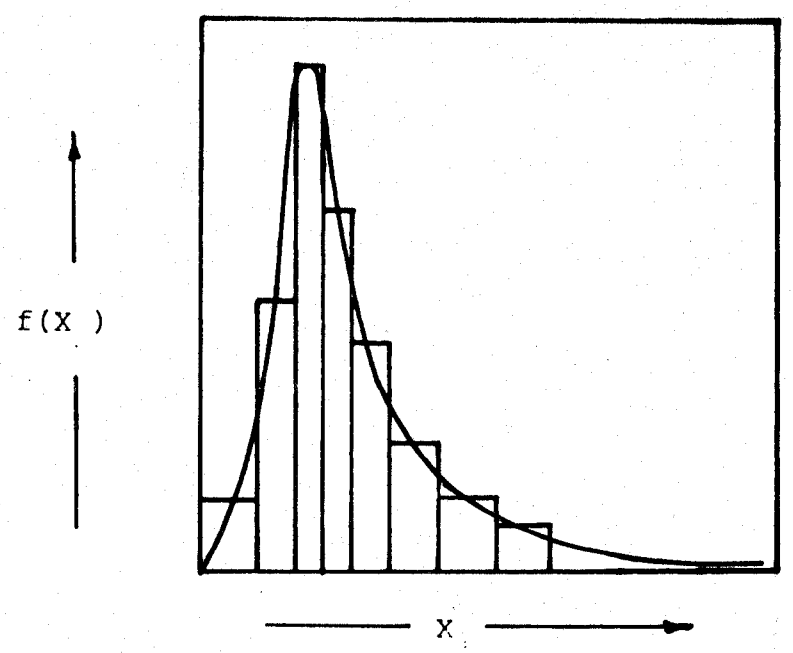

FIGURE 5.5: Typical Frequency Histogram for Droplet Spray Approximating a Log-Normal Density Function

The density curve for a log normal distribution function is expressed by the relation

$$\frac{dN}{dX} = f(X) = \frac{1}{X\,\sigma_g\,\sqrt{2\pi}} \exp\left[\frac{-(\ln X - \ln \bar{X}_{ng})^2}{2(\sigma_g)^2}\right] \qquad 5.10$$

where

$\bar{X}_{ng}$ = number geometric mean drop size

σ_g = geometric standard deviation.

It is apparent from this expression that when drop size data fit this type of function the logarithm of the diameter is distributed normally. The substitution

$$y = \frac{1}{(\sigma_g)\sqrt{2}} \ln \frac{X}{\overline{X}_{ng}} \qquad 5.11$$

reduces equation 5.10 to the normal distribution form of equation 5.6.

The log-normal function is a more realistic expression than the normal one for the distribution of a physical dimension such as drop diameter. It has been derived theoretically [5, 10] on the basis of a statistical approach and a consideration of the exponential law of decay.

The density curve for the log-normal distribution function can be readily written for number, surface, or volume distributions as shown in Table 5.4

For a log-normally distributed drop size spectrum, the distribution function based on volume is given by

$$F(X^3) = \frac{1}{\sqrt{2\pi}} \int_{-\infty}^{X} \frac{1}{(\sigma_g)(X)} \exp\left[-\frac{1}{2(\sigma_g)^2}\left(\ln \frac{X}{\overline{X}_{oo}}\right)^2\right] dX \qquad 5.17$$

This relationship gives the total volume fraction of the drop size spectrum having diameters less than or equal to X.

Figure 5.6 is a log-normal plot of Houghton's [3] data on a volume and number basis, as taken directly from

Length distribution

$$f(X) = \frac{1}{X\,\sigma_g\,\sqrt{2\pi}} \exp\left[\frac{-(\ln X - \ln \bar{X}_{ng})^2}{2\,(\sigma_g)^2}\right] \qquad 5.12$$

where $\bar{X}_{ng}$ = geometric number mean diameter

Surface distribution

$$f(X^2) = \frac{1}{X(\sigma_g\ \sqrt{2\pi}} \exp\left[\frac{-(\ln X - \ln \bar{X}_{gs})^2}{2\,(\sigma_g)^2}\right] \qquad 5.13$$

where $\bar{X}_{gs}$ = geometric surface mean diameter

Volume distribution

$$f(X^3) = \frac{1}{X(\sigma_g)\sqrt{2\pi}} \exp\left[\frac{-(\ln X - \ln \bar{X}_{oo})^2}{2(\sigma_g)^2}\right] \qquad 5.14$$

where $\bar{X}_{oo}$ = geometric mass or volume mean diameter

Relationships between geometric mean diameters

$$\ln \bar{X}_{ng} = \ln \bar{X}_{oo} - 3\,(\sigma_g)^2 \qquad 5.15$$

$$\ln \bar{X}_{ng} = \ln \bar{X}_{gs} - 2\,(\sigma_g)^2 \qquad 5.16$$

TABLE 5.4: Log-Normal Frequency Distribution Functions [1]

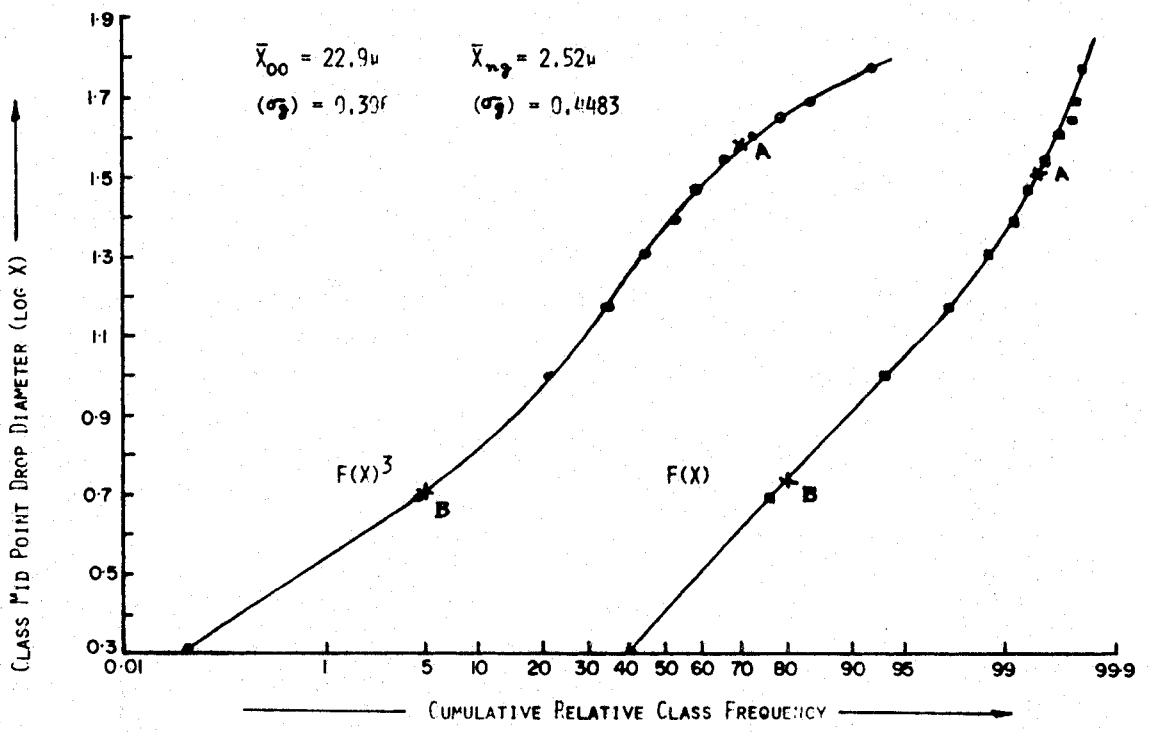

FIGURE 5.6: Log Normal Distribution of Houghton's [3] Data on Volume and Number Basis

columns 6 and 7 of Table 4.1. The value of $\bar{X}_{oo}$ can be determined by inspection of Figure 5.6 as the value of X for which $F(X^3) = 0.5$. Similarly the value of $\bar{X}_{nq}$ can be determined by inspection as the value of X for which $F(X) = 0.5$. The value of σ_g needs some mathematical simplification which depends on substitution of equation 5.11 into equation 5.17 to give

$$F(X^3) = \frac{1}{\sqrt{\pi}} \int_{-\infty}^{y} \exp\,[-y^2]\,dy$$

$$= \frac{1}{\sqrt{\pi}} \left[\int_{-\infty}^{0} \exp\,[-y^2]\,dy + \int_{0}^{v} \exp\,[-y^2]\,dy \right]$$

$$= \frac{1}{\sqrt{\pi}} \left[\frac{\sqrt{\pi}}{2} + \frac{\sqrt{\pi}}{2} \operatorname{erf}\,(y) \right]$$

$$= \frac{1}{2} \left[1 + \operatorname{erf}\,(y) \right]$$

from which

$$\operatorname{erf}\,(y) = 2\,\{F(X^3)\} - 1$$

or $$(y) = \operatorname{erf}^{-1}\,[2\,\{F(X^3)\} - 1] \qquad 5.18$$

For any two points X_a and X_b on the cumulative volume plot of Figure 5.6,

$$y_a = \text{erf}^{-1} [2\{F(X_a{}^3)\}-1] \qquad 5.19$$

and $$y_b = \text{erf}^{-1} [2\{F(X_b)^3\} -1] \qquad 5.20$$

Also from equation 5.11

$$y_a = \frac{1}{(\sigma_g)\sqrt{2}} \ln \frac{X_a}{\bar{X}_{oo}} \qquad 5.21$$

$$y_b = \frac{1}{(\sigma_g)\sqrt{2}} \ln \frac{X_b}{\bar{X}_{oo}} \qquad 5.22$$

From equations 5.19, 5.20, 5.21 and 5.22 it follows that

$$y_a - y_b = \text{erf}^{-1} [2\{F(X_a{}^3)\}-1]-\text{erf}^{-1}[2\{F(X_b{}^3)\}-1] = \frac{1}{(\sigma_g)\sqrt{2}} [\ln \frac{X_a}{X_b}]$$

and

$$(\sigma_g)\sqrt{2} = \frac{\ln (X_a/X_b)}{\text{erf}^{-1} [2\{F(X^3{}_a)\} -1]-\text{erf}^{-1} [2\{F(X^3{}_b)\} -1]} \qquad 5.23$$

Substitution for the values of X_a and X_b shown in Figure 5.6 yields

$$(\sigma_g)\sqrt{2} = \frac{1.58 - 0.71}{\text{erf}^{-1}\,[2\{0.7\} - 1] - \text{erf}^{-1}\,[2\{0.05\} - 1]}$$

$$= \frac{.87}{\text{erf}^{-1}\,[0.40] - \text{erf}^{-1}\,[0.9]}$$

$$= \frac{0.87}{\text{erf}^{-1}\,[0.40] + \text{erf}^{-1}\,[0.9]}$$

$$= \frac{0.87}{0.38 + 1.17} = \frac{0.87}{1.55}$$

$$= 0.561$$

from which

$$(\sigma_g) = \frac{0.561}{\sqrt{2}} = 0.396$$

For a cumulative number distribution, a similar treatment yields

$$\sqrt{2}\ (\sigma_g) = \frac{\ln\,(X_a/X_b)}{\text{erf}^{-1}\,[2\,F(X_a) - 1] - \text{erf}^{-1}\,[2\,F(X_b) - 1]} \qquad 5.24$$

From the number cumulative plot of Figure 5.6 any two arbitrary points give

$$\sqrt{2}\ (\sigma_g) = \frac{1.51 - 0.73}{\text{erf}^{-1}\ [2(.995)\ -1]\ -\text{erf}^{-1}\ [2(.80)-1]}$$

$$= \frac{0.78}{\text{erf}^{-1}\ [0.99]\ -\text{erf}^{-1}\ [0.6]}$$

$$= \frac{0.78}{1.83 - 0.60} = .6341$$

Therefore $(\sigma_g) = \frac{0.6341}{\sqrt{2}} = 0.4483$

The general expression for mean diameters based on log-normal distribution is obtained by substituting equation 5.10 into equation 5.3. When rewritten for a volume or mass distribution, Marshall [1] reported the general form to be

$$\bar{X}_{qp} = (X_{MM})\ \exp\ (p + q - 6)\ (\sigma_g)^2/2 \qquad 5.25$$

Although the plot of an exact log-normal distribution will be a straight line on log probability co-ordinates, any deviation of real experimental data from the exact log-normal distribution will be greatly distorted by the log-probability co-ordinates. Hence, in order to judge the goodness of fit of a particular log-normal distribution function to a given set

of experimental data, it is necessary to compare the experimental deviation, δ, with some standard error, S, associated with the particular log-normal function. Putnam et al [5] state that the log-normal function which best fits a given set of data will be that function for which the sum of the squares of experimental deviations, δ^2, divided by the squares of the standard errors, S^2, is a minimum.

Since the size range for real drop data is always finite, whereas the log-normal equation assumes an infinite range of sizes, it appears advisable to give consideration to the effect of upper and lower size limits. This is done by introducing the concept of "inner percentages" which was first defined by Landry [11]. The inner percentage, p_i, of droplets whose diameters are less than a given value of X_i is defined as the volume (or weight) of droplets whose sizes are less than X_i divided by the total volume (or weight) of droplets in the sample. Thus, the inner percentage of droplets whose diameters are less than X_i is expressed by

$$p_i = \frac{V_i - V^*}{V_m - V^*} \qquad 5.26$$

where

V_i = volume of droplets of diameters less than X_i

V_m = volume of droplets of diameter less than the upper limit X_m

V^* = volume of droplets whose diameter is less than the lower limit, X_o

Another method of making allowance for X_o and X_m, the minimum and maximum sizes respectively, is to modify the log-normal equation itself by redefining the y of equation 5.11 such that

$$y\ (X_o) = -\infty$$
$$y\ (X_m) = \infty \qquad 5.27$$

The use of these methods has been illustrated by Putnam et al [2, 5].

3. The Square Root-Normal Function

This mathematical expression was proposed by Tate and Marshall [12] who showed that the square root of the drop diameter appeared to be distributed normally for the case of swirl spray nozzles. The distribution may be written as

$$\frac{dN}{dX} = f(X) = \frac{1}{2\sqrt{2s\pi X}} \exp\left[-(\sqrt{X} - \sqrt{X_{10}}^{\,2}/2s\right] \qquad 5.28$$

where

s = standard deviation of the square root-normal distribution

$\bar{X}_{10}$ = arithmetic mean diameter.

Letting $y = \sqrt{X}$ in equation 5.28, yields

$$\frac{dN}{dy} = f(Y) = \frac{1}{2\sqrt{2s\pi}} \exp\left[-(y - \sqrt{\bar{X}_{10}})^2/2s\right] \qquad 5.29$$

an expression of the normal Gaussian form, illustrated by Equation 5.6, that can be plotted exactly as a normal distribution.

The value of the standard deviation, s, is given by

$$s = \sqrt{X_{84.13}} - \sqrt{X_{15.87}} \qquad 5.30$$

where

$X_{84.13}$ = fraction of drops less than 84.13% on a cumulative number plot

$X_{15.87}$ = fraction of drops less than 15.87% on a cumulative number plot

4. The Nukiyama-Tanasawa Distribution

Nukiyama and Tanasawa [13], who obtained extensive data on drop sizes in sprays formed by air atomization, attempted to correlate their data by the general probability density function

$$\frac{dN}{dX} = f(X) = aX^2 \exp\,[-bX^n] \qquad 5.31$$

where

a and b = empirical constants

n = measure of the spray uniformity

The exponent, n, did not deviate significantly from unity for the Nukiyama-Tanasawa data.

Dividing equation 5.31 by X^2 and taking logarithms of both sides gives

$$\log \frac{1}{X^2}\frac{dN}{dX} = \log a - bX^n \log e \qquad 5.32$$

If a value of, n, is assumed for a given set of data, it is apparent that, a, and, b, may be determined by plotting $\log (\frac{1}{X^2}\frac{dN}{dX})$ against X^n.

The value of, n, is a constant for a given nozzle over a wide range of operating conditions. Its magnitude is very sensitive to nozzle size and nozzle type. This means that, n, must be determined experimentally for each nozzle. Nukiyama and Tanasawa collected drop samples from several different locations in a spray and established an average value of, n, which satisified their distribution function.

In practice the applicability of the Nukiyama-Tanasawa relationship may be established from an accurate count of the droplets at any two distinctly different locations in a spray. The value of, n, thus found for any nozzle can be used to predict the distribution of drop sizes for that nozzle spray under any other set of conditions.

Figure 5.7 is a plot of log $(\frac{1}{X^2}\frac{\Delta N}{\Delta X})$ versus $X^{\frac{1}{4}}$ for Houghton's [3] data, as given by Putnam et al [5]. In order to better approximate the values of, a, b, and, n, the value of, n, obtained by the graphical trial-and-error method, was substituted into equation 5.32, which was then used to find solutions for, a, and, b, by the method of least squares. Substitution of the value of, a, thus obtained into the logarithm of equation 5.32, according to

$$\log \log \left(\frac{aX^2}{\frac{dN}{dX}}\right) = \log (b \log e) + n \log X \qquad 5.33$$

produced an equation which could be solved readily for, b, and, n, by the method of least squares. Putnam et al [5] recommended alternate use of equations 5.32 and 5.33 until a set of values of the parameters, a, b, and, n, differed from the previous set by less than a preassigned percentage (for example one percent). Using this graphical trial-and-error procedure they found the following values of, a, b, and, n, for Houghton's data:

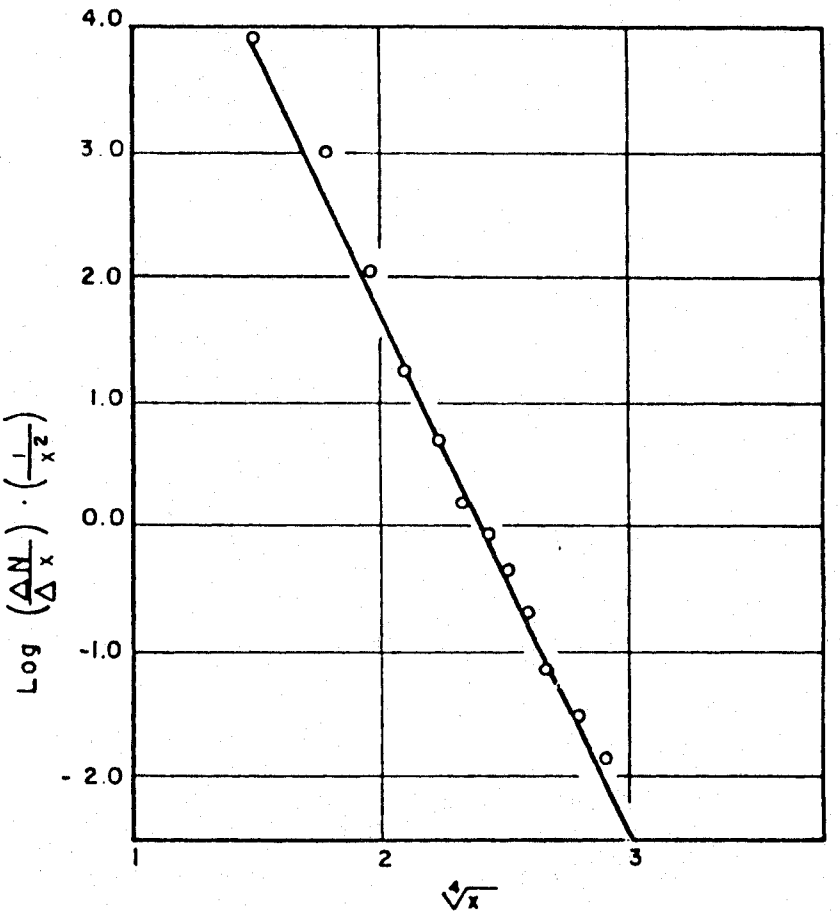

FIGURE 5.7: Fitting of Houghton's Data to the Nukiyama-Tanasawa Distribution [5]

$$n = 0.17$$

$$a = 1.39 \quad 10^{14}$$

$$b = 18.38$$

Accordingly the distribution equation for Houghton's data has the form

$$\frac{dN}{dX} = (1.39 \quad 10^{14}) \ (X^2) \ \exp \ [-18.38 \ (X^{0.17})] \qquad 5.34$$

The general equation for mean drop diameters corresponding to the Nukiyama-Tanasawa distribution function is obtained by substituting equation 5.31 into equation 5.3. This substitution yields

$$(\bar{X}_{qp})^{q-p} = \frac{\int_{X_o}^{X_m} (X)^q \ aX^2 \ \exp \ [-bx^n] \ dx}{\int_{X_o}^{X_m} (X)^p \ ax^2 \ \exp \ [-bx^n] \ dx} \qquad 5.35$$

which reduces to

$$(\bar{X}_{qp})^{q-p} = \frac{b^{\frac{-(q-p)}{n}} \left[\Gamma_{b(X_m)^n} \left(\frac{q+3}{n}\right) - \Gamma_{b(X_o)^n} \left(\frac{q+3}{n}\right) \right]}{\left[\Gamma_{b(X_m)^n} \left(\frac{p+3}{n}\right) - \Gamma_{b(X_o)^n} \left(\frac{q+3}{n}\right) \right]}$$

as discussed in Appendix I. Γ_α is the incomplete gamma function, as defined by

$$\Gamma_\alpha (c) = \int_0^\alpha U^{c-1} \exp [-U] \, dU \qquad 5.38$$

where

U = variable of integration

c = argument

Assuming that $X_o = o$, $X_m \to \infty$ and, n, is small, equation 5.38 can be integrated and simplified to

$$\frac{q+3}{p+3} (X_{qp})^{q-p} = \left[\frac{q+3}{bne} \right] \left(\frac{q+3}{p+3} \right)^{p+3/q-p} \Bigg]^{(q-p)/n} \qquad 5.39$$

The value of the Sauter mean diameter, $(\bar{X}_{32})$, for Houghton's [3] data, as determined by equation 5.39, and the constants, a, b, and, n, determined by Putnam et al [5] is

$$\bar{X}_{32} = 23.01 \text{ microns.}$$

It is interesting to note the discrepancies in the values of $\bar{X}_{32}$ obtained by different investigators, using the same data of Houghton [3] and the Nukiyama-Tanasawa distribution function. Table 5.4 summarizes these Sauter Mean Diameter evaluations.

n	$\bar{X}_{32}$	Reference
1/3	20.3μ	Mugele and Evans [2]
1/4	26.9μ	Mugele and Evans [2]
0.17	23.01μ	Putnam et al [5]
1/3	19.46μ	Lewis et al [14]
Actual value from experimental data is 18.237		

TABLE 5.5: Sauter Mean Diameters Evaluated for Houghton's [3] Data Using the Nukiyama-Tanasawa Distribution Function

In certain cases, the values of $\bar{X}_{32}$, obtained by using equation 5.31, are larger than any experimentally observed drop diameters. Lewis et al [14] explain such discrepancies by assuming that some large drops existed but were not counted. To maintain the validity of the Nukiyama-Tanasawa equation, it becomes necessary to discredit the counting techniques used in obtaining the data [2].

5. Rosin-Rammler Distribution

After many unsuccessful attempts Rosin and Rammler [15] were able to find a general expression which was flexible enough to give adequate representation of the size distribution of all samples of pulverized materials that they investigated. Their distribution function is a special version of the general three-constant probability density expression

$$f(X) = \frac{dN}{dX} = aX^p \exp\ [-bx^n] \qquad 5.40$$

The Rosin-Rammler function, often used for droplet systems, has the form

$$1-V = \exp\ [-(X/X_{RR})^n] \qquad 5.41$$

where

$1-V$ = volume fraction of drop material occurring in drops of diameter greater than X

X_{RR} = Rosin-Rammler mean, defined as the drop diameter above which 36.8% of the total spray volume should exist

n = empirical constant.

Taking logarithms of both sides of equation 5.41 gives

$$\log (1-V) = - \left(\frac{X}{X_{RR}}\right)^{n} \log e \qquad 5.42$$

or

$$\log (1-V)^{-1} = \left(\frac{X}{X_{RR}}\right)^{n} (0.4343) \qquad 5.43$$

Taking logarithms of both sides, once again, yields

$$\log \log (1-V)^{-1} = n \log X - n \log X_{RR} + \log 0.4343 \qquad 5.44$$

or

$$\log \log \left(\frac{1}{1-V}\right) = n \log X + (\log 0.4343 - n \log X_{RR}) \qquad 5.45$$

If this equation is applicable to the actual drop size distribution in a spray, a plot of $\log \left(\frac{1}{1-V}\right)$ versus X on log-log paper should give a straight line, the slope of which is, n. The value of, n, should be between 2 and 4, with the higher values indicating a more uniform distribution [16].

Mugele and Evans [2] analyzed Lees' [17] data using this function. A similar analysis was done by Fraser and Eisenklam [16] for their spray data. Figure 5.8 illustrates

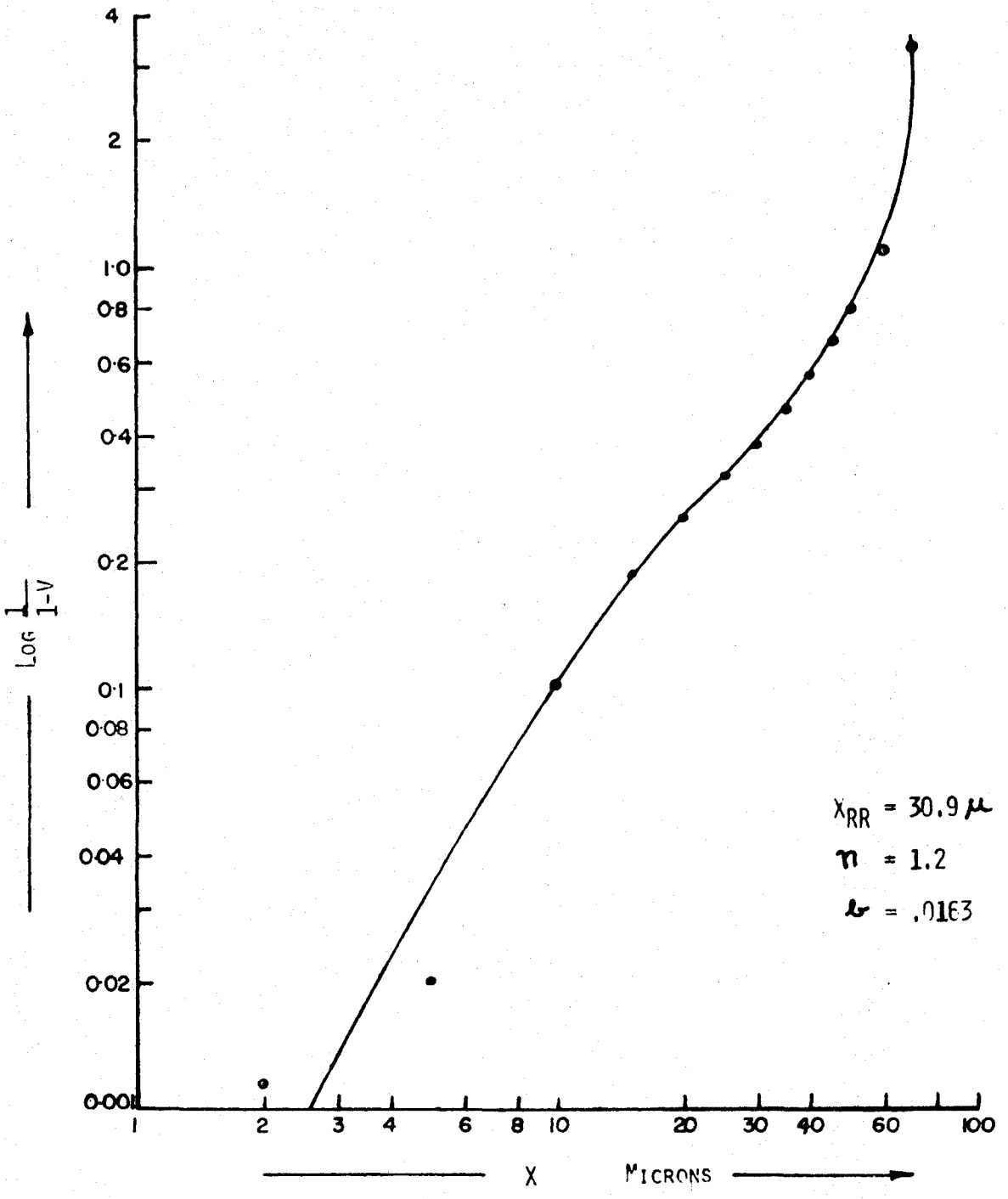

FIGURE 5.8: Rosin Rammler Analysis of Houghton's Data

the application of the Rosin-Rammler function to Houghton's data [3]. It can be seen that the curve is relatively straight for only a short portion of its length. It curves sharply in the vertical direction at the upper and lower size limits. This curvature precludes a direct evaluation of the parameters, X_{RR}, and, n, for subsequent use. The reason for this sharp change in slope at either size limit can be appreciated immediately from a consideration of equation 5.45. Since the percent of the finite droplets larger than the upper size limit X_m is zero, the log log $(\frac{1}{1-V})$ term becomes infinite. As a result the curve will turn sharply upward as X approaches X_m. Similarly, at the lower limit X_o, the percent oversize is one hundred. The corresponding log log $(\frac{1}{1-V})$ value becomes negatively infinite, which accounts for the sharp downward curvature as X approaches X_o [5].

Equation 5.41 can be written in the form

$$V = 1 - \exp\,[-bx^n] \qquad 5.46$$

where

$$b = \frac{1}{(X_{RR})^n}$$

Examination of equation 5.46 shows that V can be equal to unity, when the size X is equal to zero, and that volume fraction V of drop material oversize can be zero only for

infinite values of the size X. This implies that the size range of a sample extends from zero to infinity. In actual practice, this is never the case with spray samples. As a result a means must be found whereby a finite experimental system can be represented by an equation which implies an infinite spectrum of sizes. This is done by introducing the concept of "inner percentages", as discussed earlier.

Differentiation of Equation 5.46 yields

$$\frac{dV}{dX} = bnX^{n-1} \exp\ [-(bX)^n] \qquad 5.47$$

Substitution of equation 5.47 into equation 5.3 yields the following general equation for the various mean sizes of the droplets, as determined by the Rosin-Rammler distribution function

$$(\overline{X}_{qp})^{q-p} = \frac{\int_{X_o}^{X_m} (X^{q-3})(b)(n)(X^{n-1})(\exp\ [-(bX)^n])dX}{\int_{X_o}^{X_m} (X^{p-3})(b)(n)(X^{n-1})(\exp\ [-(bX)^n])dX} \qquad 5.48$$

Putnam et al [5] have simplified equation 5.48 to

$$(\overline{X}_{qp})^{q-p} = (b^{-\frac{q-p}{n}}) \frac{[\Gamma(\frac{q-3}{n}) + 1]}{[\Gamma(\frac{p-3}{n}) + 1]} \qquad 5.49$$

by assuming $X_o = o$ and $X_m \rightarrow \infty$. Using the concept of inner percentages and an iteration method Putnam et al [5] obtained the values b = 0.09282 and n = 0.65861. An approximate curve fit of Houghton's data [3] as shown in Figure 5.8 gives b = .0163 and n = 1.2. The value of the Rosin-Rammler mean, $X_{RR'}$ was found to be approximately 30.9μ, using the distribution function, and about 16μ using the basic definition. The discrepancies in the values arise from the fact that Houghton's data [3] give a bimodal curve, whereas the Rosin-Rammler function is valid only for unimodal distributions.

6. The Weibull Equation

By identifying the density distribution function, f(X), which determines the quantity of items of dimension $\leq$ X, with the probability, P(X), of choosing at random an item of dimension $\leq$ X, Weibull [18] deduced the general statistical distribution function

$$F(X) = 1 - \exp [-\phi(X)] \qquad 5.51$$

The function $\phi(X)$ is to be subject only to the following conditions:

i. $\phi(X_o) = o$; where X_o is the smallest value of X;

ii. $\phi(X) > o$, for $X > X_o$; 5.52

iii. $\frac{d\,\phi(X)}{dX} > o$

Weibull then chose a simple function, $\overline{\phi}\ (X)$, which would satisfy the conditions of equations 5.51 in the form

$$\overline{\phi}\ (X) = \left(\frac{X - X_o}{X_w}\right)^n \qquad 5.53$$

where

X_w = Weibull's mean diameter, microns

He made no claims regarding the theoretical basis of either equation 5.51 or equation 5.53. The only merit for F(X) and $\phi(X)$ of equation 5.51 and 5.53 is that these are the simplest mathematical expressions which satisfy the conditions of 5.52.

If Weibull's function is identified with the cumulative volume distribution, V, then

$$V = 1 - \exp\left[-\left(\frac{X - X_o}{X_w}\right)^n\right] \qquad 5.54$$

This relationship represents a modification of the Rosin-Rammler expression given by equation 5.46. The basic difference is that equation 5.54 allows for the existence of a lower size limit X_o.

Taking logarithms of both sides twice yields

$$\log \log \left(\frac{1}{1-V}\right) = n \log (X - X_o) - n \log X_w + \log \log e \qquad 5.55$$

Houghton's data [3] have been plotted in Figure 5.9 according to equation 5.55, with Weibull's cut-off method being incorporated. Figure 5.9 shows that all the data points, except those for 0 and 1 fraction oversize, fall close to the predicted straight line. This indicates that, at least in some instances, correlation can be obtained by plotting the experimental data directly on a graph for which the horizontal co-ordinate is $(X - X_o)$. The upper limit at $(X - X_o) = 67.5$ is certainly out of line.

For the two arbitrarily selected points A and B on the curve of Figure 5.9 equation 5.5 gives

$$\log (0.5) = n \log 31.5 - n \log X_w + \log \log e \qquad 5.56$$

for point A

and

$$\log (0.15) = n \log 10.0 - n \log X_w + \log \log e \qquad 5.57$$

for point B

Subtraction of 5.57 from 5.56 yields

$$\log \left(\frac{0.5}{0.15}\right) = n \log \frac{31.5}{10.0}$$

from which $n = 1.0492$

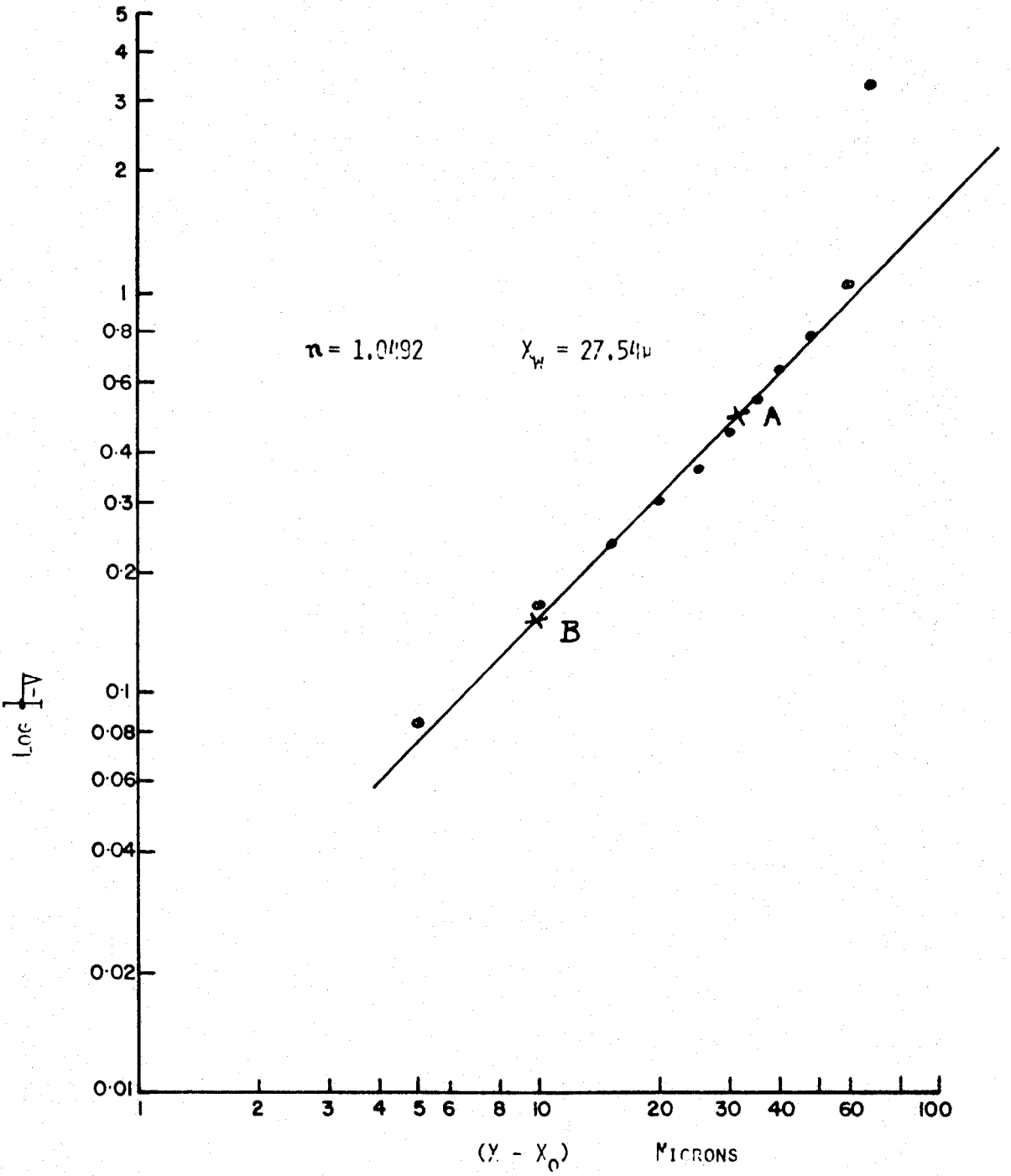

FIGURE 5.9: Weibull's Function for Houghton's Distribution Data Using X_0 = 7.5μ

Substitution of this value of n into equation 5.56 yields

$$\log (0.5) = 1.0432 \log 31.5 - \log (X_w)^{1.0492} + \log 2.7182$$

from which $X_w = 27.54$.

For Houghton's data, Weibull's function becomes

$$V = 1 - \exp \left[-\left(\frac{X-X_o}{27.54}\right)^{1.0492}\right] \qquad 5.58$$

7. Roller's Size Distribution Function

From empirical considerations, Roller [19] deduced the following expression for the cumulative volume distribution, V:

$$V = a(X^{\frac{1}{2}}) \exp [-b/X] \qquad 5.59$$

By rearranging and taking logs of both sides, it follows that

$$\log \left(\frac{V}{X^{\frac{1}{2}}}\right) = \log a - \frac{b}{X} \log e \qquad 5.60$$

or

$$\log \left(\frac{V}{X^{\frac{1}{2}}}\right) = \log a - (0.4343) \frac{b}{X} \qquad 5.61$$

If log $(\frac{V}{X^{\frac{1}{2}}})$ is plotted vs $(\frac{1}{X})$, the slope of the best straight line through these points will be equal to -0.4343b.

Figure 5.10 shows the plot of log $(\frac{V}{X^{\frac{1}{2}}})$ vs $(\frac{1}{X})$ for Houghton's data [3]. For any two points A and B on the straight line of Figure 5.10, equation 5.61 gives

$$\log 10 = \log a - .4343\ b\ (0.044) \qquad 5.62$$

for point A

and

$$\log 7 = \log a - .4343\ b\ (0.094) \qquad 5.63$$

for point B

Subtraction of 5.63 from 5.62 gives b = -7.1334. Substitution into equation 5.62 gives a = 7.3063. For Houghton's data [3], the Roller Distribution Function becomes

$$V = 7.3063\ (X)^{\frac{1}{2}}\ \exp\ (7.1334/X) \qquad 5.64$$

Differentiation of equation 5.59 yields

$$\frac{dV}{dX} = a\ \{(\frac{X}{2})^{\frac{-1}{2}} + b(X)^{-3/2}\}\ \exp\ [-b/X] \qquad 5.65$$

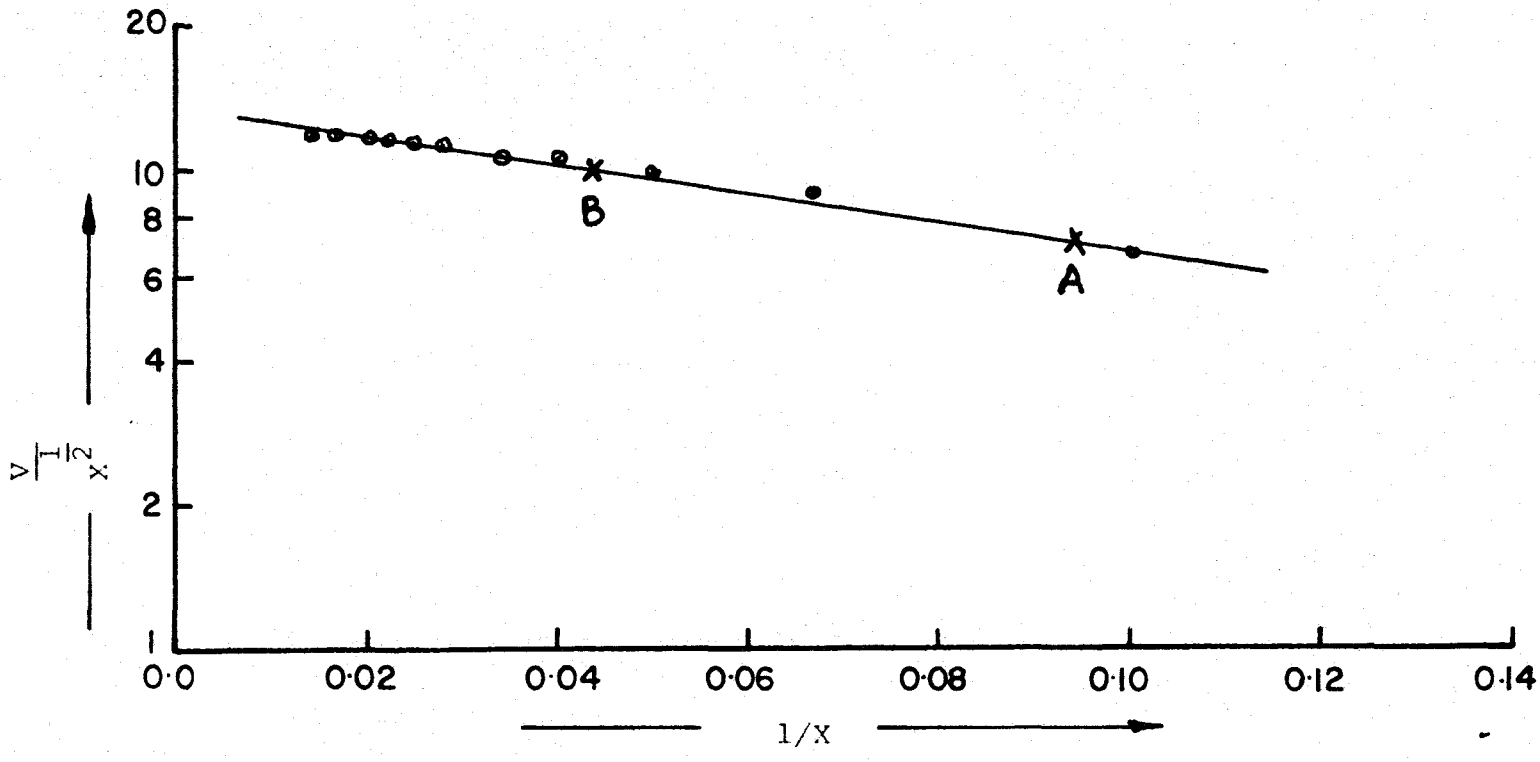

FIGURE 5.10: Correlation of Houghton's Cumulative Volume Distribution by Means of Roller's Function

Substitution of equation 5.2 into equation 5.59 gives

$$\frac{dN}{dX} = \frac{3a}{\pi} (X^{-7/2} + 2bX^{-9/2}) \exp [-b/X] \qquad 5.66$$

Substitution of equation 5.66 into equation 5.3 leads to the complex expression

$$(\bar{X}_{qp})^{q-p} = b^{q-p} \left[\frac{\Gamma_{b/X_o}(5/2-q) + \Gamma_{b/X_o}(7/2-q) - \{\Gamma_{b/X_m}(5/2-q) + \Gamma_{b/X_m}(7/2-q)\}}{\Gamma_{b/X_o}(5/2-p) + \Gamma_{b/X_o}(7/2-p) - \{\Gamma_{b/X_m}(5/2-p) + \Gamma_{b/X_m}(7/2-p)\}} \right] \qquad 5.67$$

given by Putnam et al [5] for mean diameters.

In addition to the size distribution functions discussed, several other relationships have been used for the analysis of drop size data. These include

i. the Griffith Comminution Function [20]

ii. Multimodal Size Distribution [21, 22]

iii. Persistence of Form [5]

For more detailed analyses of spray data and the use of these functions, reference should be made to the work of Putnam et al [5].

C. Conclusions

From the preceding discussion and a consideration of other general factors, it may be concluded that

i. none of the distribution curves have a theoretical basis with respect to droplet statistics

ii. two types of cut-off, natural and artificial, are inherent in all the data. Some examples of natural cut-off are an upper size of the order of magnitude of the spray nozzle diameter and a lower size below which the collection of molecules ceases to act as a drop. Artificial cut-offs are given by such factors as limits of observation on one hand and the size of the sampling instrument on the other.

iii. in order to verify the equation of best fit, a comparison should be made of the deviations of actual spray data (obtained experimentally) from potentially applicable functions

iv. extrapolation beyond the range of observed data should also be made to verify the validity of the distribution function

v. sometimes the cut-offs of the experimental data are so insignificant relative to the mean size and distribution that, for many practical purposes, an infinite sample may be assumed for the determination of mean sizes, standard deviations or median diameters

vi. since none of the curves has a theoretical basis, the important criteria are ease of use, goodness of fit, and, if used for extrapolation, acceptability of extrapolated values

vii. many distributions are multimodal, either because of inaccuracies in the data, (in which case the problem is one of statistical judgement), or because of natural factors in the method of producing the spray, (in which case methods of combining the appropriate unimodal distribution equations must be devised).

It appears that there is still a real need for the development of distribution equations based on plausible

assumptions of mechanisms responsible for the creation of a spray. Further work on improvement of data fitting or correlating by existing functions seems fruitles. As soon as a new theoretical background is developed for any particular type of spray, the emphasis will shift from curve fitting data to a more realistic approach in which variations in each parameter would be related to the physical conditions associated with the process of atomization.

REFERENCES

1. Marshall, W. R., Atomization and Spray Drying, Chemical Engineering Progress Monograph Series No. 2, Vol. 50 (1954).

2. Mugele, R. A. and Evans, H. D., Droplet Size Distribution in Sprays, Ind. Eng. Chem. 43, 1317-1324 (1951).

3. Chemical Engineers Handbook, Ed. by J. H. Perry, Third Edition, p. 1170, New York, McGraw-Hill Book Co., 1950.

4. Lapple, C. E., Particle Size Analysis and Analyzers, Chemical Engineering, 75 (11), 149-155 (1968).

5. Putnam, A. A., Benington, F., Einbinder, H., Hazard, H. R., Kettelle, J. D., Levy, A., Miesse, C. C., Pilcher, J. M., Thomas, R. E., Weller, A. E., Landry, B. A., Injection and Combustion of Liquid Fuels, p. 4-54, Wright Air Development Center, Tech. Rept. 56-344 (1957).

6. Dixon, W. J., and Massey, F. J., Jr., Introduction to Statistical Analysis, McGraw-Hill Book Co., Inc., New York (1951).

7. Hoel, P. G., Introduction to Mathematical Statistics, John Wiley and Sons, Inc., New York (1947).

8. Epstein, B., The Mathematical Description of Certain Breakage Mechanisms Leading to the Log-Normal Distribution, Jour. Franklin Institute, 244, 471 (1947).

9. Kottler, F., The Goodness of Fit and the Distribution of Particle Sizes, Jour. Franklin Institute, 251, 499 and 617 (1951).

10. Kottler, F., The Distribution of Particle Sizes, Jour. Franklin Institute, 250, 339 and 419 (1950).

11. Landry, B. A., Fundamentals of Coal Sampling, Bureau of Mines Bulletin, No. 454, 1944, 127 pp.

12. Tate, R. W., and Marshall, W. R., Atomization by Centrifugal Pressure Nozzles, Chemical Engineering Progress 49, 169-174, (1953)

13. Nukiyama, S., and Tanasawa, Y., Experiments on the Atomization of Liquids in an Air Stream, Reports 1-6, Transactions of the Society of Mechanical Engineers, Japan, Vol. 4, No. 14, pp. 86-93 (1938); Vol. 4, pp. 138-143 (1938); Vol. 5, No. 18, pp. 62-67 (1939); Vol. 5, No. 18, pp. 68-75 (1939); Vol. 6, No. 22, pp. II-7 and II-15 (1939); Vol. 6, No. 23, pp. II-18 to II-28 (1940). English Translation by E. Hope, Defense Research Board, Department of National Defense, Canada, March 18, 1950, Translation No. EO/28220.

14. Lewis, H. C., Edwards, D. G., Goglia, M. J., Rice, R. I., and Smith, L. W., Atomization of Liquids in High Velocity Gas Streams, Ind. Eng. Chem. 40 (1), 67-74 (1948).

15. Rosin, P., and Rammler, E., The Laws Governing the Fineness of Powdered Coal, J. Inst. Fuel, 7, 29-36 (1933).

16. Fraser, R. P., and Eisenklam P., Liquid Atomization and the Drop Size of Sprays, Trans. Instn. Chem. Engrs., 34, 294-319 (1956).

17. Lee. D. W., Effect of Nozzle Design and Operating Condition on Atomization of Fuel Sprays, Natl. Adivsory Comm. Aeronaut., Tech. Report 425 (1932).

18. Weibull, W., A Statistical Distribution Function of Wide Applicability, Jour. Appl. Mechanics 293 (1951).

19. Roller, P. S., Law of Size Distribution and Statistical Description of Particulate Materials, Jour. Franklin Institute, 223, 609 (1937).

20. Griffith, L., A Theory of the Size Distribution of Particles in a Comminuted System, Canadian Jour. of Research, 21, 57-64 (1943).

21. O'Toole, A. L., On the System of Curves of which the Method of Moments is the Best Method of Fitting, Annals of Math. Statistics, 4, 1-29 (1933).

22. Dallavalle, J. M., Orr, C., Jr., and Blocker, H. G., Fitting Bimodal Particle Size Distribution Curves, Ind. Eng. Chem. 43, (6), 1377, 1951.

VI. DROP SIZE PREDICTION

A. Introduction

The performance of wet scrubbers, especially of the Venturi type, is affected by the characteristics of the liquid injection system. In such units, a water stream is usually introduced at right angles [1] into a fast moving air stream to produce a distribution of liquid droplets. If complete scrubbing fluid atomization details were known, it would be possible to design an atomization system, for optimum scrubber performance, on a more scientific basis.

One of the most important variables which appears to affect the performance of a wet scrubber is the drop size of the scrubbing fluid. Several correlations [2-17] have been reported for the prediction of mean drop sizes resulting from liquid films, filaments or sheets [2, 5, 14, 18-23] and jets [3, 4, 6-13, 15, 16, 17] subjected to the disruptive action of high velocity air streams. Mean drop sizes are empirically related to such operating variables as nozzle dimensions, fluid properties and ambient conditions. It is only recently that theoretical analyses [2, 3, 4, 5, 18] have been made in an attempt to elucidate the atomization processes.

In this chapter emphasis is focussed on pneumatic or two fluid atomization. Drop size prediction equations for atomization considered to be of secondary importance to wet scrubber applications are summarized in Appendix II.

B. Pneumatic or Two Fluid Atomizers

1. Theoretical Relations

A realistic theoretical analysis of atomization requires an appreciation of the physical processes involved before a mathematical treatment can be considered.

Numerous theories have been postulated to explain the mechanism by which a liquid jet breaks up, disintegrates and is finally atomized. In many instances the various investigators do not agree on the type, number and order of the physical processes involved because

i. the mechanism by which atomization is accomplished is quite different for different conditions

ii. atomization may, and usually does, take place in successive stages involving more than one single mechanism.

There is general agreement, however, on one point that the atomization of a liquid is an extremely complicated process.

The physical mechanism of drop formation has been dealt with by several workers [24-49]. Notable amongst them are the studies of Rayleigh [24], Haenlein [25], Lee and Spencer [29], Siestrunck [34], Littaye [35, 36, 37], Lane [46], York [47], Dombrowski and co-workers [5, 18, 48, 49]. Since it is beyond the scope of the present study to discuss, in detail, the mechanism suggested by each of these investigators, an attempt has been made to summarize the existing knowledge of the physical process of atomization.

The mechanisms of atomization are complex and varied. They depend upon numerous factors, principally, the properties of the liquid being atomized, the atomizing device and the conditions of atomization. In general, however, the process of atomization may be considered to take place in three steps.

The first step involves the development of a disturbance on the liquid surface as a result of an instability. This initial disturbance may relate to one or more of the following factors:

i. surface tension
ii. inertial forces
iii. imperfections of the atomizing device

iv. vibrations of the atomizing device

v. turbulence of the liquid, and

vi. effervescence of a dissolved gas.

Disturbances may occur simultaneously at different locations on the liquid surface and may even overlap one another.

The second step is the formation of ligaments, threads or films of fluid by the action of air on these initial disturbances. These ligaments can break into fragments according to the Rayleigh [24] theory. Under the influence of surface tension, the fragments form spherical drops.

The third step involves fragmentation of these drops into smaller droplets. Drop disintegration will continue as long as the relative velocity of the drop with respect to the gas stream is sufficiently high. The mechanism by which drops breakup as they pass through the gas stream may involve one or more of the following processes in which

i. at low velocities, the drops may be formed into hollow bags which then break up into fragments

ii. at higher velocities, shatter of drops may occur following deformation in a direction opposite to that associated with low velocities

iii. centrifugal forces, resulting from rotation of the drops, may cause them to disrupt

iv. at extremely high velocities, a thin layer of liquid may be stripped from larger drops to produce almost instantaneous atomization.

The transition among the three basic steps is usually gradual but not readily recognizable because at high velocities the first may be over-shadowed by the second or third steps following in rapid succession.

Other mechanisms that may be involved in drop disintegration include

i. the formation of hollow tubes as a result of the flag-waving effect of a fluid sheet

ii. recombination of drops due to eddy diffusivity as well as different axial velocities

iii. formation of holes in thin sheets of liquid.

A discussion of analytical and empirical models is presented chronologically to show how various investigators approached this problem.

a. Mayer [2]

Mayer's theoretical approach to the problem of atomization was based on the qualitative conclusions of

Weiss and Worsham [11] who studied gas-liquid interface behaviour in the high velocity regime.

From a consideration of the development of capillary waves (ripples) produced by a high velocity gas flow along a liquid surface, Mayer stated that

i. waves of very small wave length cannot be developed readily because of viscous dissipation

ii. waves of very long wave length are slow to develop because of inertial effects.

Between the extremely short and long (capillary) wave lengths there exists a spectrum of wavelengths which can be excited to appreciable amplitudes during the time of interaction of the high velocity gas stream with the liquid surface.

It was postulated by Mayer [2] that, if a wave of length, λ, with a characteristic excitation time, $\tau(\lambda)$, has developed an amplitude comparable to λ, the gas stream will erode the wave-crest as a ligament from which droplets proportional, in size to λ will be formed, according to

$$X = (F_1)(\lambda) \qquad 6.1$$

where x is the diameter of droplets and

where F_1 is a dimensionless configuration factor stated to be independent of λ, but possibly dependent on fluid parameters.

The value of λ was found, from the analysis of Jeffreys (quoted in reference [50]), to be

$$\lambda \geq \lambda \text{ min} = 2\pi \sqrt[3]{16} \left[\frac{\mu \sqrt{\sigma_L / \rho_L}}{\beta \rho_G V_a^2}\right]^{2/3} \qquad 6.2$$

where

λ min = minimum wave length, cm

μ = viscosity of liquid, $\frac{gm}{(cm\text{-}sec)}$

σ_L = surface tension of liquid, dyne/cm

ρ_L = density of liquid, gm/cm^3

β = sheltering parameter (defined by Jeffrey) of value ≤ 1, dimensionless

ρ_G = density of gas, gm/cm^3

V_a = relative gas velocity, $(V_A - V_L)$, cm/sec

V_A = mean gas velocity, cm/sec

V_L = mean liquid velocity, cm/sec

Equation 6.1 was modified to give an average droplet size according to

$$X_{av} = F_1 \bar{\lambda} \qquad 6.3$$

with $\bar{\lambda}$ defined as

$$\bar{\lambda} = \frac{\int_{\lambda min}^{\infty} \frac{d\lambda}{\lambda \tau (\lambda)}}{\int_{\lambda min}^{\infty} \frac{d\lambda}{\lambda^2 \tau (\lambda)}} \qquad 6.4$$

from which $\bar{\lambda}$ was shown to equal $(\frac{9}{2})$ λmin. From equations 6.2, 6.3 and 6.4 the expression for an average droplet diameter in terms of fluid parameters was obtained in the form

$$X_{av} = 9\pi \sqrt[3]{16}\, B \left[\frac{(\mu)\sqrt{(\sigma_L)(\rho_L)}}{(\rho_G)(V_a^2)}\right]^{2/3} \qquad 6.5$$

where

$$B = F_1/(\beta)^{2/3}$$

If B is taken to be of the order of 0.3, equation 6.5 reduces to

$$X_{av} = 9\pi \sqrt[3]{16}\, (0.3) \left[\frac{(\mu)\sqrt{(\sigma_L)(\rho_L)}}{(\rho_G)(V_a^2)}\right]^{2/3} \qquad 6.6$$

This theoretical relationship was compared to the equation proposed by Weiss and Worsham [11]. Although agreement was limited to only specific parameters, Mayer [2]

nevertheless concluded that the capillary mechanism accounted for spray formation produced by high velocity atomization of liquid jets. Although his model was for an infinite flat surface, (very large compared to the wave-length), Mayer suggested that the work could be extended to jets of finite size by considering the deformation and erosion of the finite liquid element under external aerodynamic forces and internal wave interference effects.

b. Adelberg [3, 4]

The model proposed by Mayer [2, 51] was used by Adelberg to estimate the mean drop size resulting from the injection of a liquid jet into a high speed gas stream. He assumed that waves, formed on the liquid surface, were amplified and shed ligaments which rapidly collapsed to form drops as shown in Figure 6.1.

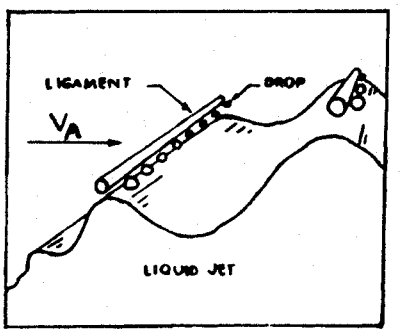

FIGURE 6.1: Schematic of Liquid Jet Cross Section Illustrating Breakup Mechanism [3]

The approach was to estimate the local mass shedding rate [4] and to correlate the mass loss rate expression to the mean drop size.

Adelberg defined four regimes of interest which were separated according to the relative dynamic pressure. The first region was defined as the "Rayleigh Regime". Here a low velocity jet breaks up in stagnant air, primarily due to surface tension instabilities. Rayleigh [24] had shown that in such situations a liquid jet would break into sections of lengths of about 4.5 times the jet diameter.

The second region, defined as the "Weber Regime", involves a high velocity jet breaking up primarily due to aerodynamic forces. When a jet is deformed from a constant cylindrical cross-section, the external pressure varies over the surface due to variations in gas velocity. As a result the pressure jet has a smaller diameter. This tends to accelerate the breakup process. Liquid viscosity on the other hand tends to slow it down. When the ratio of aerodynamic forces to surface tension forces, called the Weber Number, exceeds unity, breakup occurs in the Weber regime.

For any relative jet to gas velocity causing waves on the jet surface to grow, different mechanisms of breakup

occur. Because the waves on the jet surface may be either capillary or acceleration waves, it is common to refer to "capillary wave" and "acceleration wave" regions respectively. Acceleration waves dominate when the wave-length λ exceeds a critical magnitude given by

$$\lambda_{cv} = [(\pi^3)(\sigma_L)(d)/(C_{Do})(\sin^2\phi)(\tfrac{1}{2})(\rho_G)(V_A^2)]^{\frac{1}{2}} \qquad 6.7$$

where

d = diameter of jet, cm

C_{Do} = drag coefficient for cross flow of gas with a cylindrical surface, dimensionless

ϕ = angle that jet axis makes with free stream velocity vector, degrees

V_A = mean gas velocity, cm/sec.

Capillary waves dominate when λ is less than this critical value.

Adelberg investigated the mean drop size in the capillary and acceleration wave regimes. He reported the equations

$$X_{av} = 2.4(d_{max})^{\frac{1}{2}} \left[\frac{(\mu)(\sigma_L/\rho_L)^{\frac{1}{2}}}{(\beta)(\rho_G)(V_A^2)}\right]^{\frac{1}{3}} \left[1 - \frac{(K_1)(\beta)(\pi/2)^{\frac{1}{2}}(e^{\frac{3}{2}})}{5(j)}\right] \qquad 6.8$$

for the capillary wave regime, and

$$X_{av} = 65.3 \left[\frac{(\mu)(\sigma_L/\rho_L)^{\frac{1}{2}}}{(\beta)(\rho_G)(V_A^2)} \right]^{2/3} \qquad 6.9$$

for the acceleration wave regime, where

d_{max} = maximum jet diameter, cm

j = modified sheltering parameter
$= \frac{2}{5} (K_4)(\beta)(\pi/2)^{1/2} (e)^{3/2}$

e = 0.06

K, β & K_4 = constants whose values have been stated to be close to unity

A comparison of the exponents of several independent variables, as summarized in Table 6.1, shows reasonable consistency with the data of other investigators.

c. Fraser, Dombrowski & Routley [5, 18]

Investigations were carried out to study the mechanism of disintegration of liquid sheets by cross-current air streams blasted at approximately right angles. Symmetrical and uniform liquid sheets were produced by spinning cups. Drop sizes, resulting from the air blast, were correlated to the thickness of the sheets and other operating variables.

Independent Variable	Experimental Data for Capillary Regime				Adelberg Analysis	
	Weiss & Worsham [11]		Ingebo & Foster [52]	Kurzius & Raab [53]	Cap. Waves	Accel. Waves
	Low Velocity	High Velocity				
Velocity	-1.3	-1.3	-3/4	-3/4	-2/3	-4/3
Orifice diameter	1/2 to 0	0.15	1/2	3/8	1/2	0
Surface Tension			1/4	3/8	1/6	1/3
Fluid Viscosity	1/3	1/3	1/4	1/4	1/3	2/3
Liquid Velocity	0.1	0.07	0	0	0	0
Gas Density	-1	-0.7	-1/4	-1/4	-1/3	-2/3
Liquid Density			-1/4	-3/8	-1/3	0

TABLE 6.1: Summary of Effective Exponents on Various Terms as Obtained from Experiments and Adelberg's Analysis [3]

The developed equation is, however, semi-theoretical.

The background for the development of the semi-theoretical equation was a systematic series of investigations carried out by Dombrowski and co-workers [19-23] who analyzed the complex process of drop formation from a sheet subjected to aerodynamic sinuous waves. The process of drop formation, as illustrated in Figure 6.2, shows that the waves on the

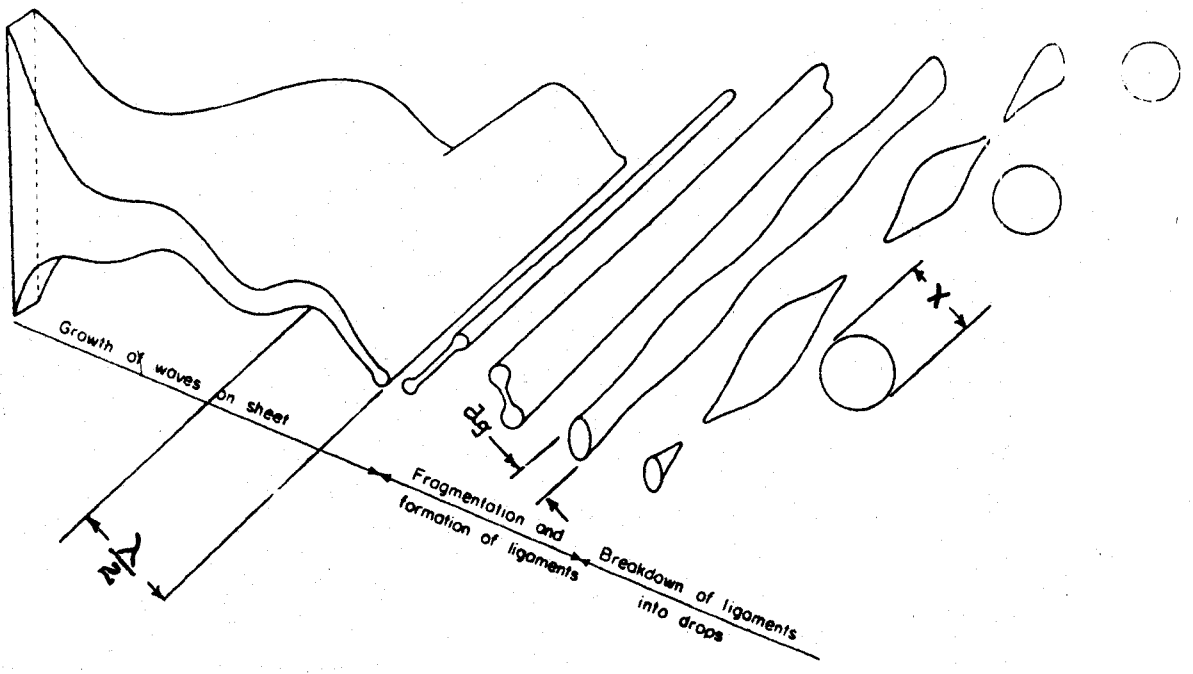

FIGURE 6.2: Idealized Process of Drop Formation From a Sheet Subjected to Aerodynamic Sinuous Waves [19]

sheet continue to grow until the crests are blown out. The sheet is thus broken up into half wave lengths which rapidly contract into ligaments. The ligaments, in turn, break up into drops. In the Fraser et al studies [5], experiments indicated detachment of full wave lengths, as shown in Figure 6.3.

The diameter of a ligament, dg, is given by

$$\frac{\pi (dg)^2}{4} = (\lambda)(m)$$

or

$$dg = \sqrt{\frac{(4)(\lambda)(m)}{(\pi)}} \qquad 6.10$$

where

m = sheet thickness, cm

In order to find the value of λ, Dombrowski and Johns [19] related the pressure and surface tension forces on each side of a viscous sheet subject to sinusoidal wave motion presuming that waves in the Fraser et al [5] system were also sinusoidal in character. The wave length of a disintegrating sheet under these conditions is given by

$$\lambda = \frac{\text{const } (\nu_r)^{k_5} (\sigma_L)}{(\rho_G)(V_L^2 - V_L V_A + \frac{V_A^2}{2})} \qquad 6.11$$

where

ν_r = kinematic viscosity ratio relative to water, dimensionless

V_L = liquid velocity, cm/sec

V_A = gas velocity, cm/sec

k_5 = constant

From Rayleigh's analysis [24] the collapse of a ligament

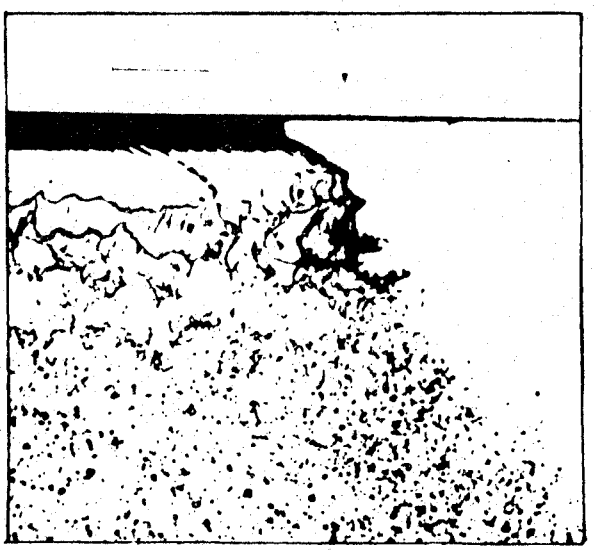

FIGURE 6.3: Disintegration of Sheet in Air Stream (a = 0.2 in). Rotary Speed 1500 rpm, Liquid Flow rate 250 lbs/hr, Liquid Viscosity 40 cs, Air Velocity 100 ft/sec, Air Flow rate 72 lbs/hr [5]

of an inviscid liquid produces drops of diameter X = 1.89 dg. Assuming this to be applicable to the present case, substitution for λ from equation 6.11 into 6.10 yields

$$X = \text{Const.} \left[\frac{(\nu_r^{k_5})\ (\sigma_L)\,(m)}{(\rho_G)\,(V_L^2 - V_L V_A + V_A^2/2)} \right]^{\frac{1}{2}} \qquad 6.12$$

The sheet thickness, m, has been given by earlier investigators [22, 23] as

$$m = \frac{Q_L}{2\pi\ V_P\ (d_L a + a^2)^{\frac{1}{2}}} \qquad 6.13$$

where

Q_L = volumetric liquid flow rate, cm^3/sec

V_P = cup peripheral velocity, cm/sec

d_L = diameter of cup at lip, cm

a = radial distance from cup lip, cm

Substitution of equation 6.13 in 6.12 gives

$$X = \text{Const.} \left[\frac{(\nu_r)^{k_5}\ (Q_L)\ (\sigma_L)}{(\rho_G)\ \{V_P^3 - V_P^2 V_A + V_P V_A^2\}(a d_L + a^2)^{1/2}} \right]^{\frac{1}{2}} \qquad 6.14$$

Fraser et al [5], who conducted experiments with oils of different viscosities, used equation 6.14 to correlate their results. They found that for each viscosity satisfactory agreement with theory was obtained, except that below air-liquid mass ratios of approximately 2, the results were segregated according to the value of mass ratio. This relation was therefore empirically corrected for air-liquid mass ratios below 2 according to

$$\bar{X}_{32} = 6 \times 10^{-4} + \left[\frac{0.59\ (\sigma_L)^{\frac{1}{2}}\ (\nu_r)^{0.21}}{(\rho_G)^{\frac{1}{2}}\ (ad_L + a^2)^{\frac{1}{4}}}\right]\left[1 + \frac{0.065}{(W_G/W_L)^{1.5}}\right]\left[\frac{\rho_L}{V_P^{\,3}\ (0.5\ V_R^{\,2} - V_R + 1)}\right]^{\frac{1}{2}} \qquad 6.15$$

where

$\bar{X}_{32}$ = Sauter mean diameter, microns

σ_L = surface tension of liquid, dynes/cm

ρ_G = density of gas, gm/cm^3

a = radial distance from cup lip, cm

W_G = mass flow rate of air, gm/sec

W_L = mass flow rate of liquid, gm/sec

V_R = gas to liquid velocity ratio, V_A/V_P, dimensionless

d_L = diameter of cup at lip, cm

V_p = cup peripheral velocity, cm/sec

V_A = air velocity, cm/sec .

Fraser et al [5] used microsecond flash photography to determine the processes of sheet disintegration while a photometric technique was used to measure the drop size. Extensive data were reported for three oils of different viscosities. A series of photographs was taken to show the spray patterns at various air velocities, liquid flow rates, rotary speeds of the cup and liquid viscosities. The drop size distribution was curve fitted by the Rosin-Rammler function. The calculated values of Sauter mean diameter closely matched the experimental values for the range of conditions investigated, as shown in Appendix III.

A plot of equation 6.15 in Figure 6.4 shows the effect of air velocity on drop size at constant cup speed, liquid viscosity and air/liquid ratio. It can be seen that as the air velocity is increased from low values the drop size, for a wide range of liquid flow rates, rapidly decreases until an air velocity of approximately 300-400 ft/sec is attained. The spray patterns observed over the range of operating conditions are illustrated in Figure 6.5. The photographs show the reduction in drop size and the

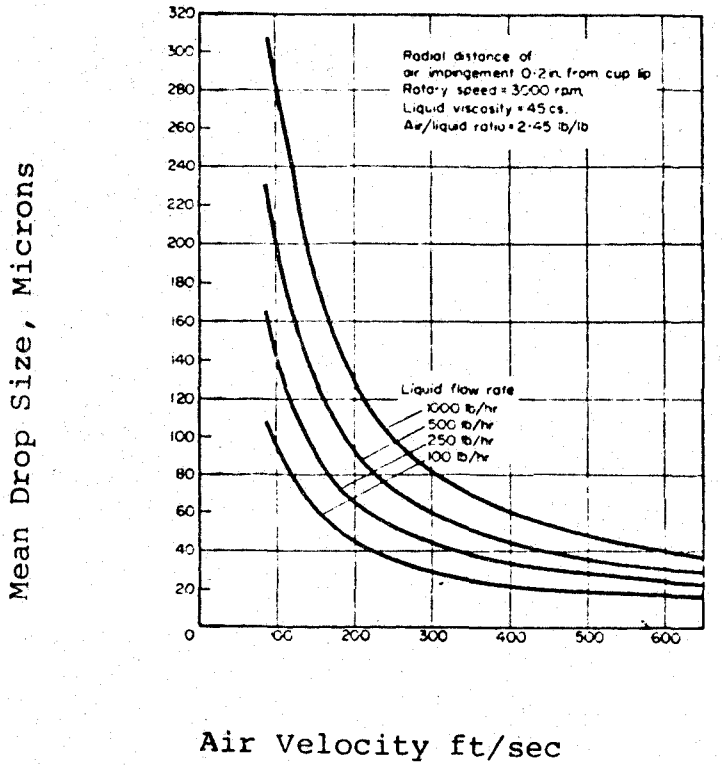

FIGURE 6.4: Variation of Mean Drop Size With Air Velocity at Different Liquid Flow Rates [5]

corresponding reduction of sheet extent and cone angle as the air velocity is increased from 100 to 600 ft/sec.

Figure 6.6 illustrates the effect of liquid flow rate on drop size at various air velocities. It can be seen that the effect diminishes with increasing air velocities. For air velocities of 95 ft/sec the drop size increases from 96 to 340μ as the liquid flow rate is raised from 100 to 1400 lb/hr. However for air velocities of 650 ft/sec the

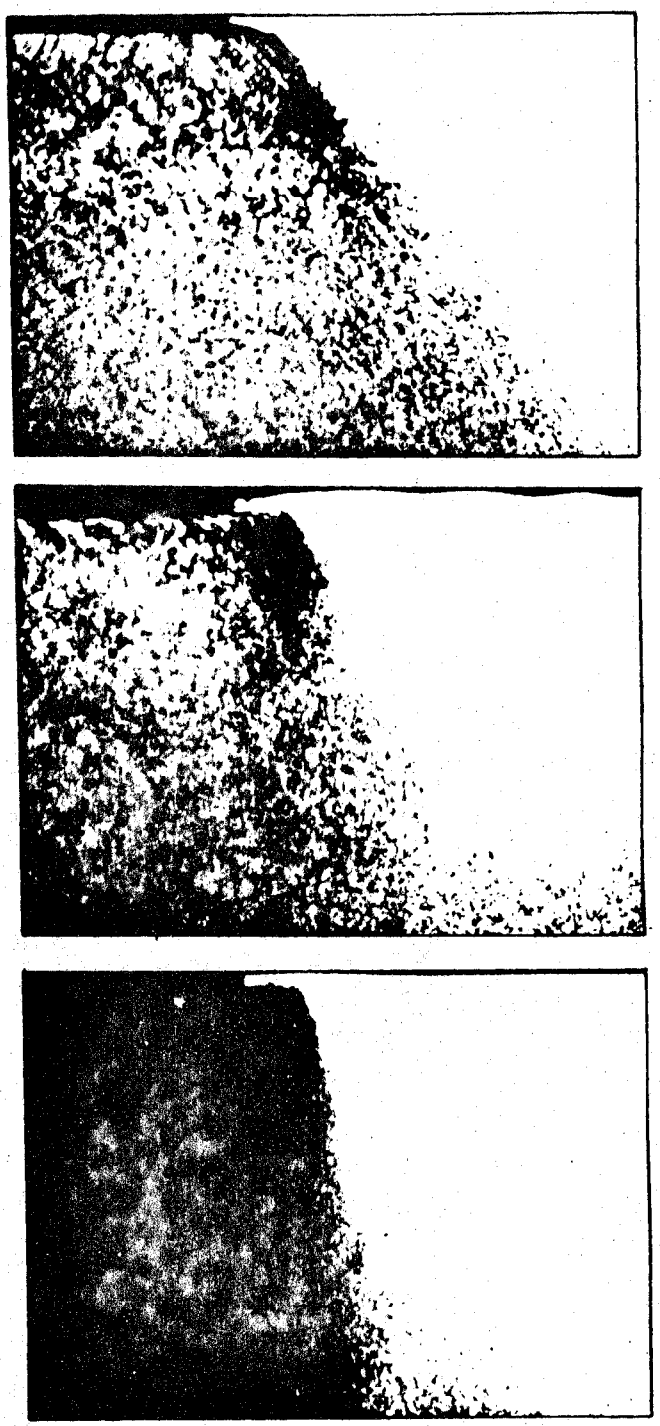

FIGURE 6.5: Spray Patterns at Various Air Velocities (a = 0.2 inches). Rotary speed 4500 rpm; Liquid flow rates 500 lbs/hr; Liquid viscosity 45 cs; Air flow rate 216 lbs/hr; Magnification x1.2 [5]

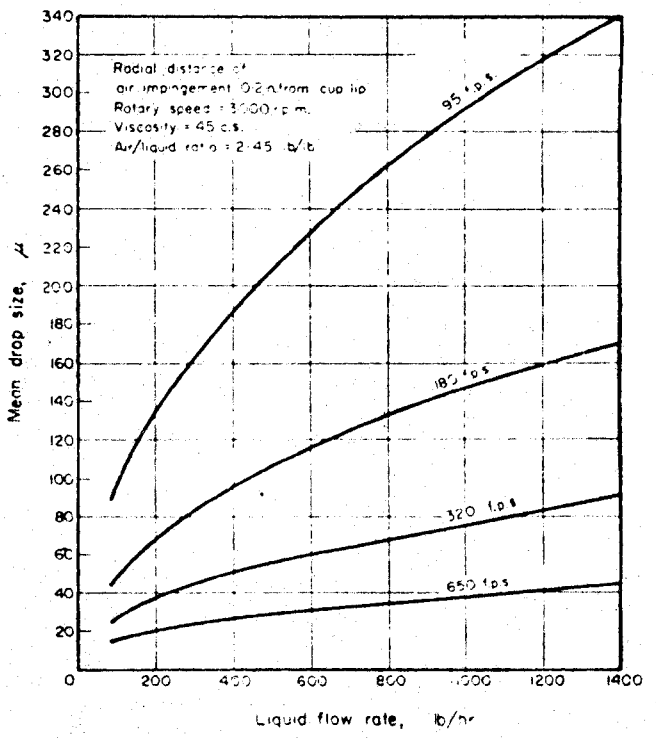

FIGURE 6.6: Variations of Mean Drop Size With Liquid Flowrate at Different Air Velocities [5]

drop size increases only from 18 to 44μ. The corresponding spray patterns are shown in Figure 6.7. There is little effect on the sheet disintegration with the exception that sheet extent and spray angle increase with increase of liquid flow rate.

Fraser et al [5] concluded that prefilming atomizers produced smaller drops than jet atomizers and that controlled production of thin sheets is an essential prerequisite for fine atomization.

In another investigation, carried out primarily to study the mechanism of disintegration of liquid sheets in air streams flowing normal to the liquid sheet, Fraser et al [18] observed some interesting results, which seem to be directly relevant to atomization in wet collectors. Their work indicated that

i. two principal mechanisms of disintegration seem to occur (continuous and vibratory). Continuous atomization proceeds through the formation of circumferential waves with fragments of the sheet being subsequently torn off and atomized. When a vibratory system is set up between the two fluids the sheet breaks up into periodic clusters of drops through resonance between the fluids.

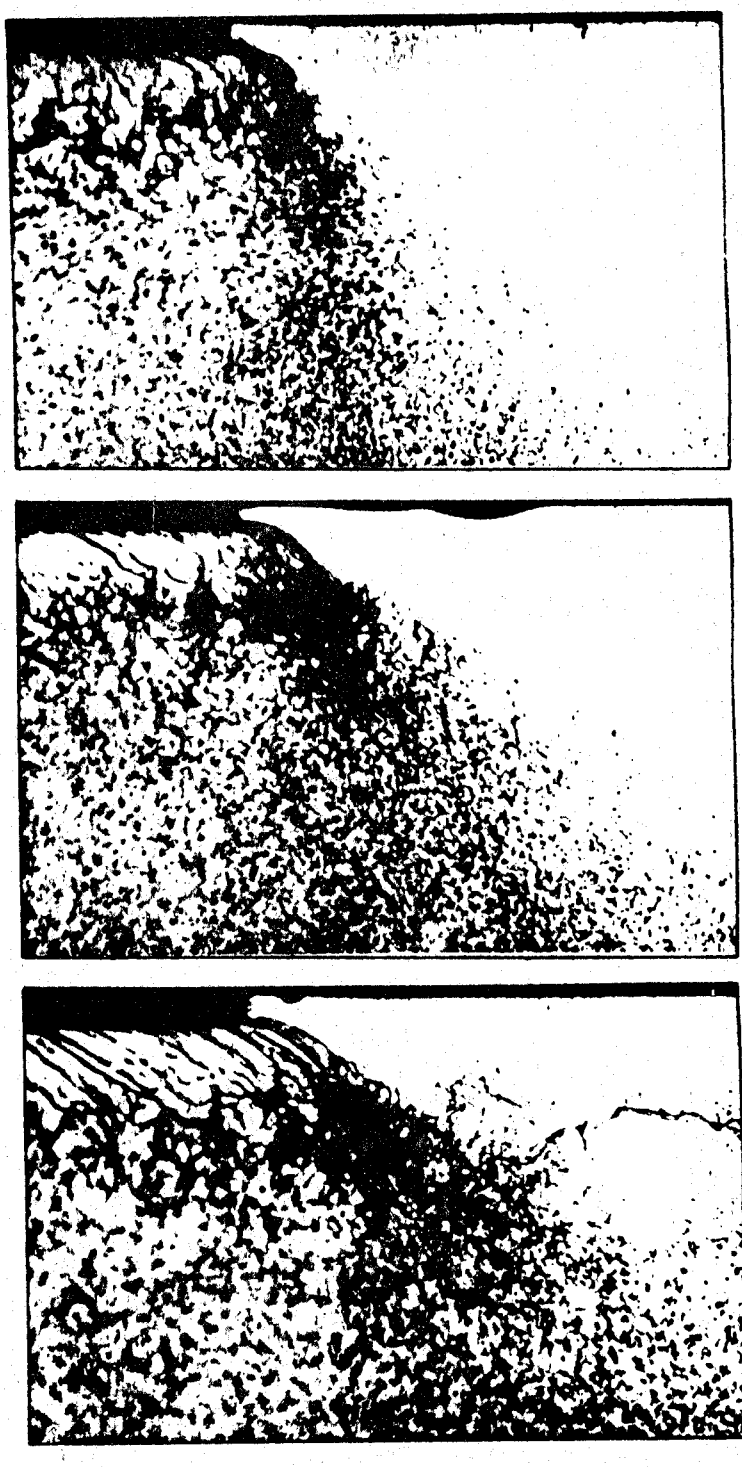

FIGURE 6.7: Spray Patterns at Various Liquid Flow Rates (a = 0.2 in). Rotary Speed 3000 rpm; Liquid viscosity 45 cs; Air velocity 100 ft/sec; Air flow rate 216 lbs/hr; Magnification x1.2 [5]

ii. the occurrence of each mechanism is markedly affected by the operating conditions.

iii. a sheet undergoing wave disintegration produces smaller drops than a vibrating sheet. Since for given air flow conditions the air/liquid momentum ratio can be reduced by increasing the liquid flow rate, these phenomena demonstrate the surprising result that smaller drop sizes can be achieved by an increase in liquid flow rate, or, a decrease in air/liquid mass ratio under the range of experimental conditions encountered by Fraser et al [18].

iv. at any level of air energy, atomization is improved when the air is distributed from a narrower annular gap.

v. when the sheet is atomized by a wide air stream close to the orifice, an increase of 50% in sheet thickness produces a coarser spray. Normally a sheet thickness of 58 microns was produced [18] at point-of-impingement. When the sheet is atomized by a narrow air stream at a greater distance from the orifice, the effect of sheet thickness is less marked.

vi. spatial drop dispersion in the atmosphere is affected by the mechanism of disintegration. Wave disintegration results in a relatively well dispersed spray while the vibratory mechanism produces a dense core of drops along the nozzle axis.

2. Empirical Relations

a. Nukiyama and Tanasawa [6]

In studies on the atomization of mixtures of alcohol and glycerine by compressed air jets, Nukiyama and Tanasawa [6] developed an expression for the mean drop size to be expected from small air atomizing nozzles. The drop size distribution was determined for a range of liquid viscosities, surface tensions, and relative air velocities. Drop size data were correlated by the following empirical equation for the Sauter mean diameter:

$$\bar{X}_{32} = \frac{5.85\sqrt{\sigma_L}}{(V_a)\sqrt{\rho_L}} + 597\left[\frac{\mu}{\sqrt{(\sigma_L)(\rho_L)}}\right]^{0.45}\left[\frac{1000\,Q_L}{Q_G}\right]^{1.5} \qquad 6.16$$

where

$\bar{X}_{32}$ = Sauter mean drop diameter, microns

V_a = relative velocity between air and liquid, cm/sec

Q_L = volumetric flow rate of the liquid, cm^3/sec

Q_G = volumetric flow rate of the air, cm^3/sec

μ = liquid viscosity, poise

ρ_L = liquid density, gm/cm^3

σ_L = surface tension of liquid, dynes/cm

The experimental apparatus and atomizing nozzle used by Nukiyama and Tanasawa [6] are shown in Figures 6.8 and 6.9 respectively.

The atomized liquid droplets were sampled by means of a tubular micro-shutter shown in Figure 6.9. A glass slide, previously coated with oil, served as a collector for the atomized liquid droplets. The shutter was opened for 0.002 to 0.01 seconds to allow the jet of atomized liquid to enter the sampling device. After photographing the glass slide the drops were counted from the exposures obtained and then normalized according to Figure 6.10. On a mass basis, the number of hypothetical drops corresponding to a class mid-point diameter X_i was evaluated from the total mass of drops in a particular class interval. A droplet size distribution function was then developed empirically by taking a series of micro-photographs for various radial positions at an arbitrarily selected point on the axis of the jet.

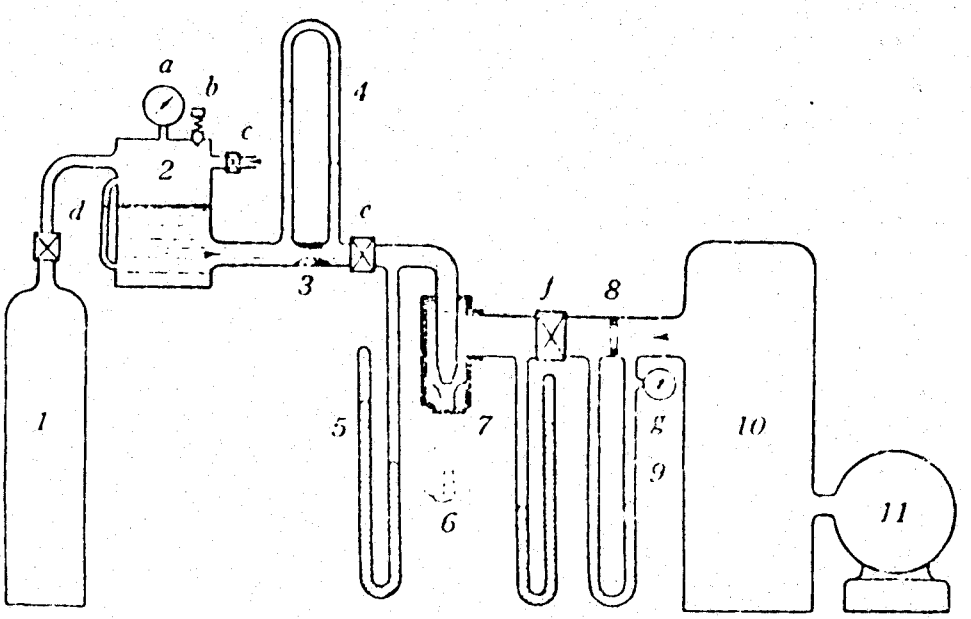

1. air supply, 2. water reservoir, 3. venturi, 4. water flow gauge, 5. mercury manometer, 6. atomizing nozzle, 7. mercury manometer, 8. orifice, 9. air flow gauge, 10. air tank, 11. compressor; a. pressure gauge, b. safety valve, c. water inlet pipe, d. water level gauge, e.f. metering valves, g. pressure gauge

FIGURE 6.8: Experimental Apparatus Used by Nukiyama and Tanasawa [6]

This density function, previously discussed in Chapter V, is given by

$$\frac{dN}{dx} = ax^2 \, e^{-bx^n} \qquad 6.17$$

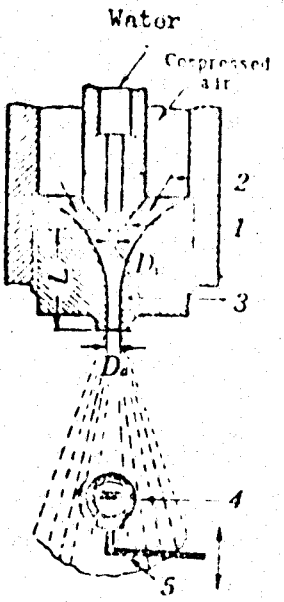

1. water nozzle
2. air nozzle
3. convergent air-orifice
4. tubular shutter
5. micro-traveller

FIGURE 6.9: Atomizing Nozzle Used by Nukiyama and Tanasawa [6]

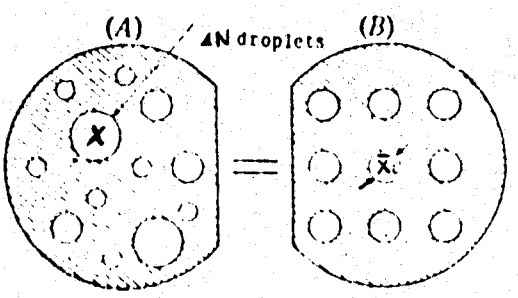

FIGURE 6.10: Normalizing Droplets According to Nukiyama and Tanasawa [6]

where

N = cumulative number of drops of diameter less than x

x = diameter of drops, microns

a,b,n = constants

Nukiyama and Tanasawa [6] correlated their experimental data using this density distribution function. Later they tested the validity of the function by taking samples at various points across the diameter of the jet. After establishing a size distribution function, liquids of different surface tension, viscosity, and density were atomized. Results, obtained using ethyl alcohol-water and glycerine-ethyl alcohol-water solutions, were extrapolated to predict the mean drop diameter for gasoline, alcohol and heavy oil atomized in a continuous jet of air.

Equation 6.16 has been extensively used [54, 55 56] to describe atomization data. Figure 6.11 graphically illustrates equation 6.16, in terms of $\bar{X}_{32}$ and $\frac{1}{V_a}$, for an air-water system for several Q_L/Q_G ratios. In order to obtain an average drop diameter of less than 20μ, the Nukiyama-Tanasawa (N-T) correlation indicates that relative air velocities of 750 ft/sec and air to liquid volumetric ratios of about 10,000 are required. If the air to liquid ratio is

great enough, the second term in equation 6.16 becomes negligible, thus eliminating the effect of viscosity.

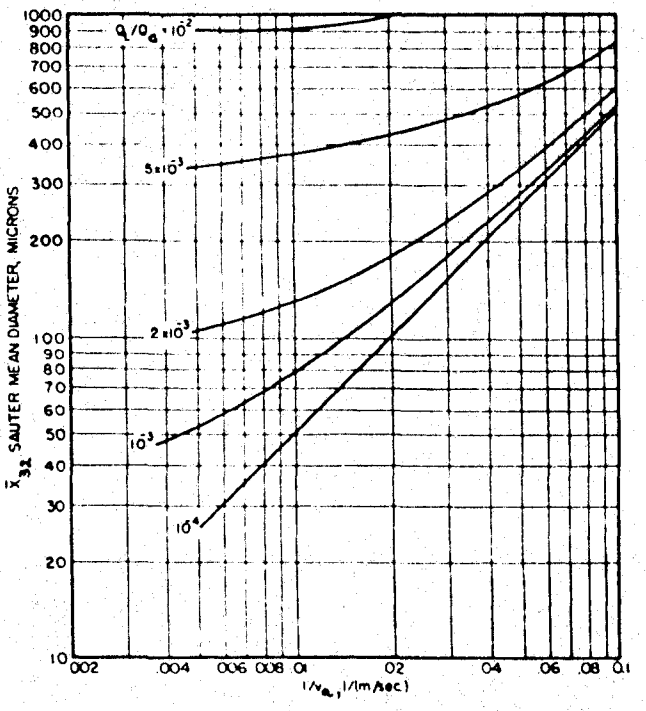

FIGURE 6.11: Graphical Representation of the Nukiyama Tanasawa Equation According to Marshall [57]

According to Gretzinger and Marshall [14], analysis of the N-T equation shows that for ratios of Q_G to Q_L greater than 5000, the second term on the right hand side of equation 6.16 contributes very little to the predicted drop size for most low viscosity liquids. Since the relative velocity of the gas to the liquid generally approaches sonic velocity at a Q_G/Q_L ratio of 5000 for most nozzles, the value of the predicted drop size approaches a constant which depends primarily on liquid density and surface tension. On the

basis of these observations and the descriptions of the experimental techniques used by Nukiyama and Tanasawa [6] it would appear that application of this equation to prediction of drop sizes in the range 5 to 30μ is of doubtful value.

Procedures for applying the N-T equation to experimental data in order to establish values of the various constants were presented by Lewis and co-workers [54]. The N-T equation was used to reinterpret experimental data published by Sauter [55], Houghton [56] and Houghton and Radford [58]. As values of Sauter mean diameter computed using the N-T equation were not always in agreement with the reported experimental results, a variety of explanations were offered. Lewis et al doubted the validity of applying the N-T equation, which was obtained for pneumatic atomization, to the data of Lee [59] and Pierce [60] derived from hydraulic pressure nozzles. With such nozzles, atomization, although caused by a number of different factors, is due predominantly to liquid turbulence rather than to relative air velocity.

One of the most important findings of Nukiyama and Tanasawa was that the final diameter of droplets was independent of the size of the water and air nozzles but was determined by the liquid to air ratio and the relative velocity of air and water.

b. Wetzel and Marshall [7, 8]

In a study of the atomization of liquid jets injected cocurrently along the axis into high velocity gas streams flowing through a Venturi throat, Wetzel and Marshall [7, 57] correlated their data according to Figure 6.12. The geometric mean drop diameter obtained during the spray cooling

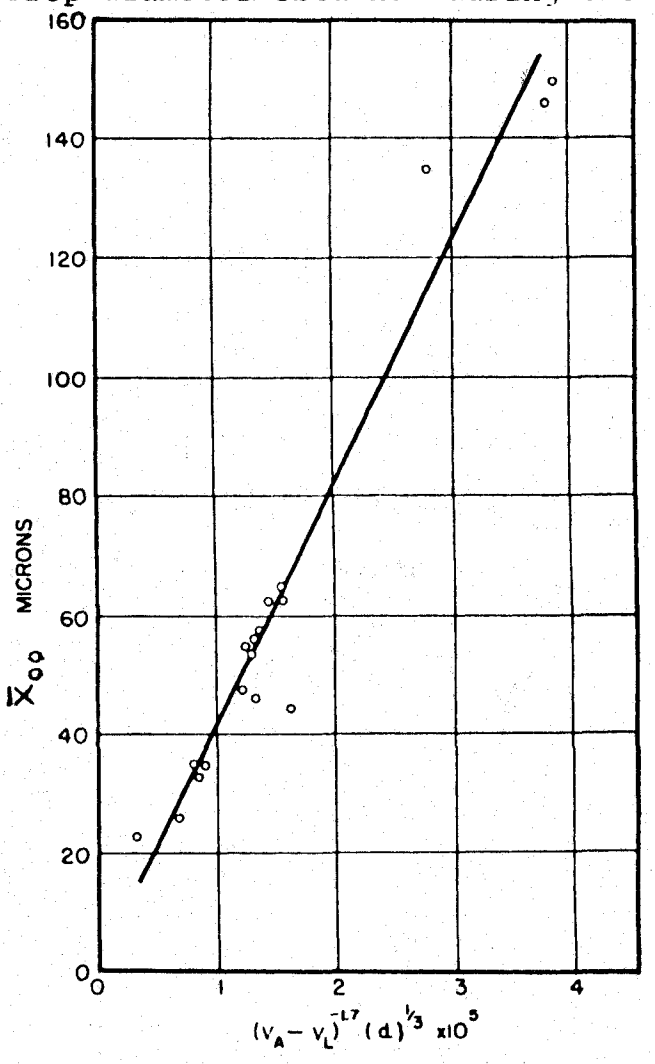

FIGURE 6.12: Correlation for Venturi Atomization of Molten Wax [57]

of a molten wax was expressed by

$$\bar{X}_{oo} = \frac{4.2 \times 10^6 \, (d)^{0.35}}{(V_A - V_L)^{1.68}} \qquad 6.18$$

where

$\bar{X}_{oo}$ = geometric mean diameter, microns

d = diameter of injection orifice, inches

V_A = velocity of air stream, ft/sec

V_L = velocity of liquid stream, ft/sec.

The drop size distribution data were found to follow a log-normal pattern in all instances as illustrated by Figure 6.13.

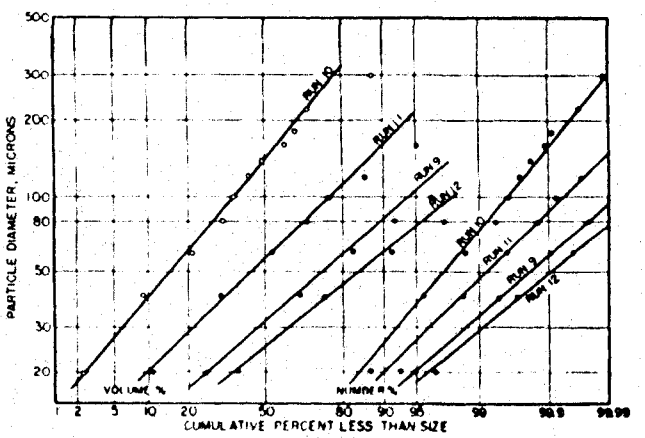

Figure 6.13: Typical Drop Size Distribution Plots Obtained by Wetzel and Marshall for Venturi Atomization of Molten Wax [57]

Equation 6.18 shows that the relative gas to liquid velocity has a large effect on the geometric mean drop diameter and also that, as the jet diameter increases, the geometric mean drop diameter increases for a constant relative velocity. Wetzel and Marshall [57] stated that this latter effect had not received extensive investigation, but it was important for scale-up purposes in designs for high atomization capacities.

For the atomization of a low melting alloy, Wetzel and Marshall [7] obtained the empirical relationship

$$\bar{X}_{oo} = 10^5/(V_A-V_L)^{1.11} \qquad 6.19$$

The spray cooling of the alloy produced the irregular particles shown in Figure 6.14.

FIGURE 6.14: Photomicrographs of Spray Cooled Alloy Atomized in a Venturi [8]

The Wetzel and Marshall equation differs from the N-T drop size expression most significantly in terms of the relative velocity dependency. Comparison of these two correlations reveals that the Sauter mean diameter $\bar{X}_{32}$ varies inversely with the relative velocity raised to the 1.5 power for the Wetzel and Marshall equation and the 1.0 power for the N-T relationship.

One explanation for this discrepancy relies on the great difference between the experimental equipment. Whereas Nukiyama and Tanasawa [6] used small nozzles with small air and liquid rates, Wetzel and Marshall [57] employed pilot size equipment with volumetric air rates of about 500 ft^3/min. A comparison of the two correlations is given in Table 6.2.

Wetzel-Marshall run	Relative Velocity, ft/sec	Material	$\bar{X}_{32}$ from N-T equation μ	$\bar{X}_{32}$ from exp. data μ
10	187	Wax	62.4	94.5
11	349	Wax	33.2	41.5
9	453	Wax	25.4	25.1
12	522	Wax	22.0	21.1
26	385	Alloy	33.2	108
27	482	Alloy	26.7	94
28	561	Alloy	23.1	95

TABLE 6.2: Comparison of Nukiyama-Tanasawa and Wetzel-Marshall Correlations [57]

This table illustrates good agreement for those runs with wax when the air velocity was above 400 ft/sec. Poor agreement was obtained for the high density, high surface tension molten alloy. This suggests that the Nukiyama-Tanasawa equation should be used only within the range of variables for which it was established.

c. Ingebo and Foster [9]

Ingebo and Foster obtained drop size distribution data for liquid jets atomized by cross-stream injection from simple orifices into high velocity air streams. The volume mean drop diameter, $\bar{X}_{30}$, was calculated using the Rosin-Rammler, the log-probability, and the Nukiyama-Tanasawa distribution functions. Dimensional analysis yielded an empirical correlation for the ratio of the volume mean drop diameter to the orifice diameter, $\bar{X}_{30}/d$, in the form

$$\frac{\bar{X}_{30}}{d} = 3.9 \left[\frac{1}{(N_{We})(N_{Re})}\right]^{0.25} \qquad 6.20$$

where

N_{We} = Weber number, $(\rho_G)(d)(V_a^2)/(\sigma_L)$, dimensionless

N_{Re} = Reynolds number, $(d)(V_a)/(\nu)$, dimensionless

σ_L = surface tension of liquid, dynes/cm

ν = kinematic viscosity of liquid, μ/ρ_L, cm^2/sec

V_a = relative velocity of air, cm/sec

ρ_G = density of air, gm/cm^3

$\overline{X}_{30}$ = volume mean drop diameter, cm

d = nozzle diameter, cm

The expression

$$\frac{X_m}{d} = 22.3 \left[\frac{1}{(N_{We})(N_{Re})}\right]^{0.29} \qquad 6.21$$

was similarly obtained for the maximum drop diameter, X_m, in each spray. From equations 6.20 and 6.21, the following relationship was derived for drop size distribution:

$$\frac{dV}{dX} = 10^6 \left[\frac{1}{(N_{We})(N_{Re})}\right]^{0.24} \left[\frac{X^5}{(X_m)^6}\right] \exp\left[-22.3 \left[\frac{1}{(N_{We})(N_{Re})}\right]^{0.4} \frac{(X)}{(X_m)}\right] 6.$$

The experimental data were obtained from a combination of high speed photography of microscopic drops travelling at high velocities in airstreams [61] and a sampling probe technique [52]. Analysis of the photographs gave droplet size distribution data while analyses of the probe samples provided data on liquid concentrations in the

spray profile. The experimental equipment is schematically illustrated in Figures 6.15 and 6.16. Figures 6.17 and 6.18 provide typical spray distribution curves for various air-stream velocities atomizing iso-octane (2, 2, 4-trimethyl-pentane), JP-5 fuel, water, benzene, and carbon tetrachloride. The N-T distribution function was selected as most appropriate for the correlation of the experimental data after testing proved the log-probability and Rosin-Rammler functions to be less satisfactory. The droplet mean diameter, $\bar{X}_{30}$, as calculated by this distribution function, was correlated with nozzle dimensions and fluid properties through dimensional analysis.

Ingebo and Foster found that injection conditions (liquid jet-velocity, V_L, orifice discharge coefficient, C_Q, and the length to diameter ratio for the orifice, Lo/d), had little effect on the mean drop diameter, $\bar{X}_{30}$. The only remaining injector variable to be considered was, d, the orifice diameter. Considering the mean drop diameter to be a function of the variables according to

$$\bar{X}_{30} = f_1 (d, \rho_L, V_A, \sigma_L, \mu \quad \rho_G, \mu_G) \qquad 6.23$$

and rewriting according to the π theorm,

$$\bar{X}_{30} = f_2 (d)^a (\rho_L)^b (V_A)^c (\sigma_L)^d (\mu)^e (\rho_G)^f (\mu_G)^g \qquad 6.24$$

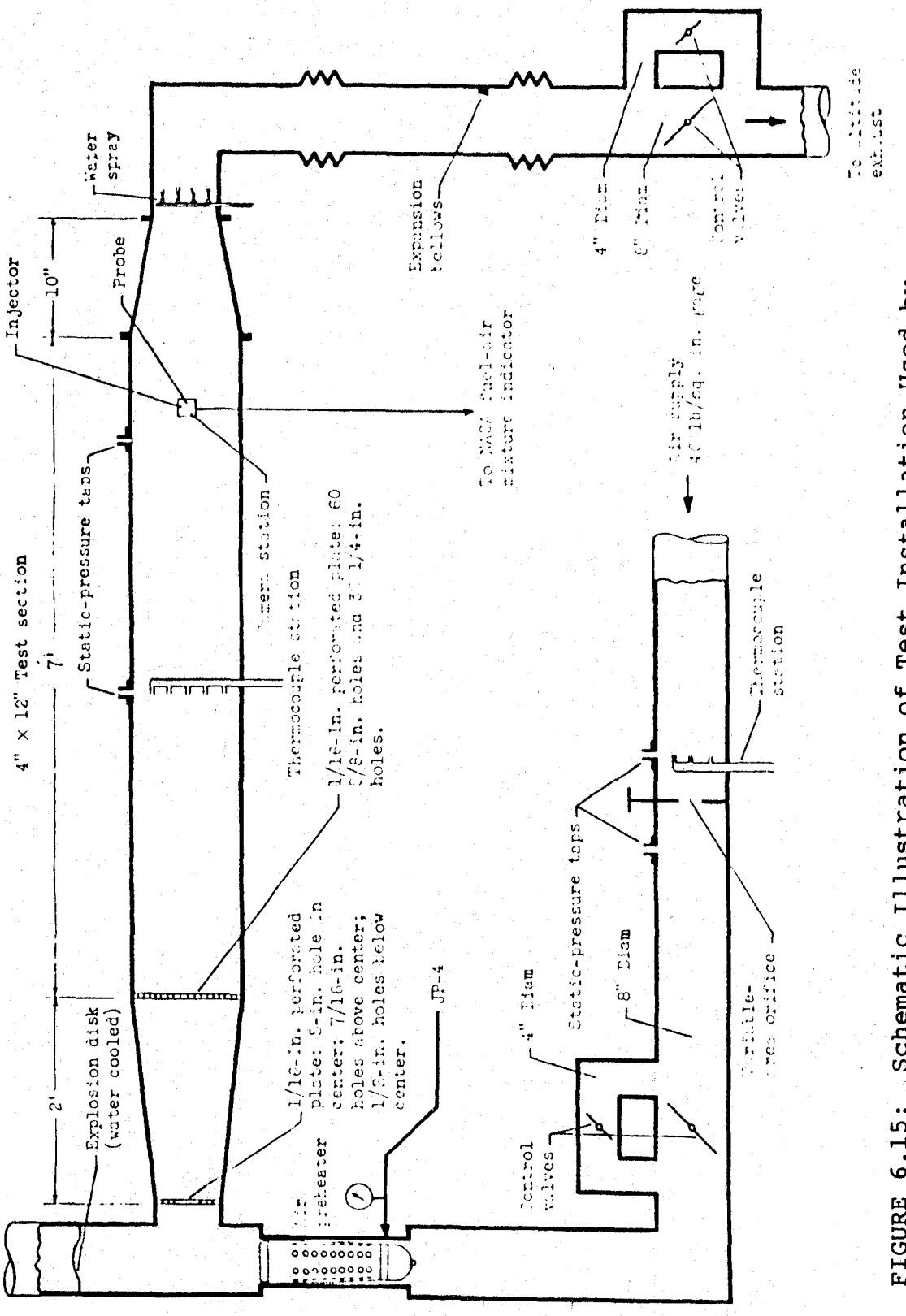

FIGURE 6.15: Schematic Illustration of Test Installation Used by Ingebo and Foster [9]

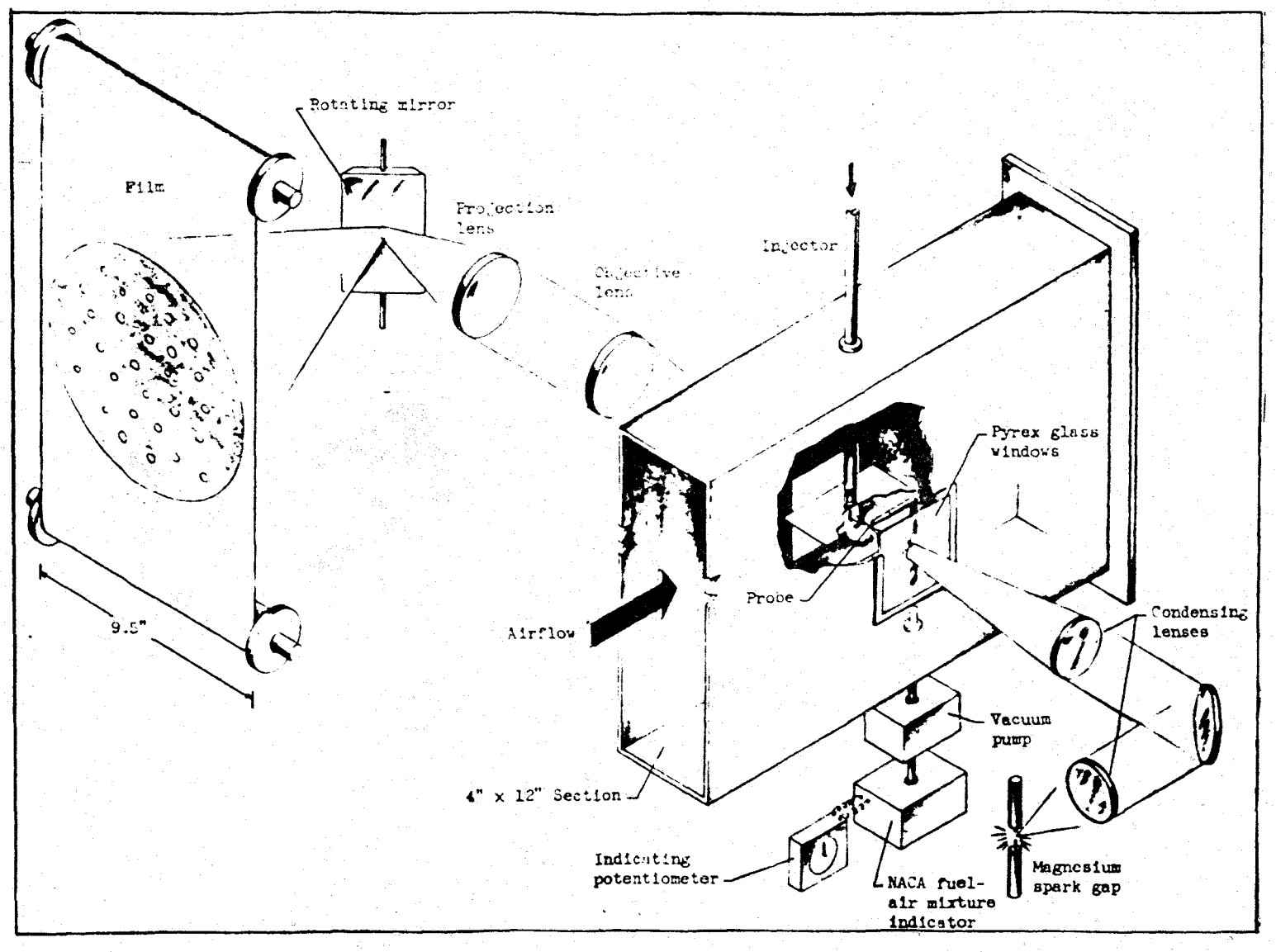

FIGURE 6.16: Diagram of Test Section Equipment and Camera Unit Used by Ingebo and Foster [9]

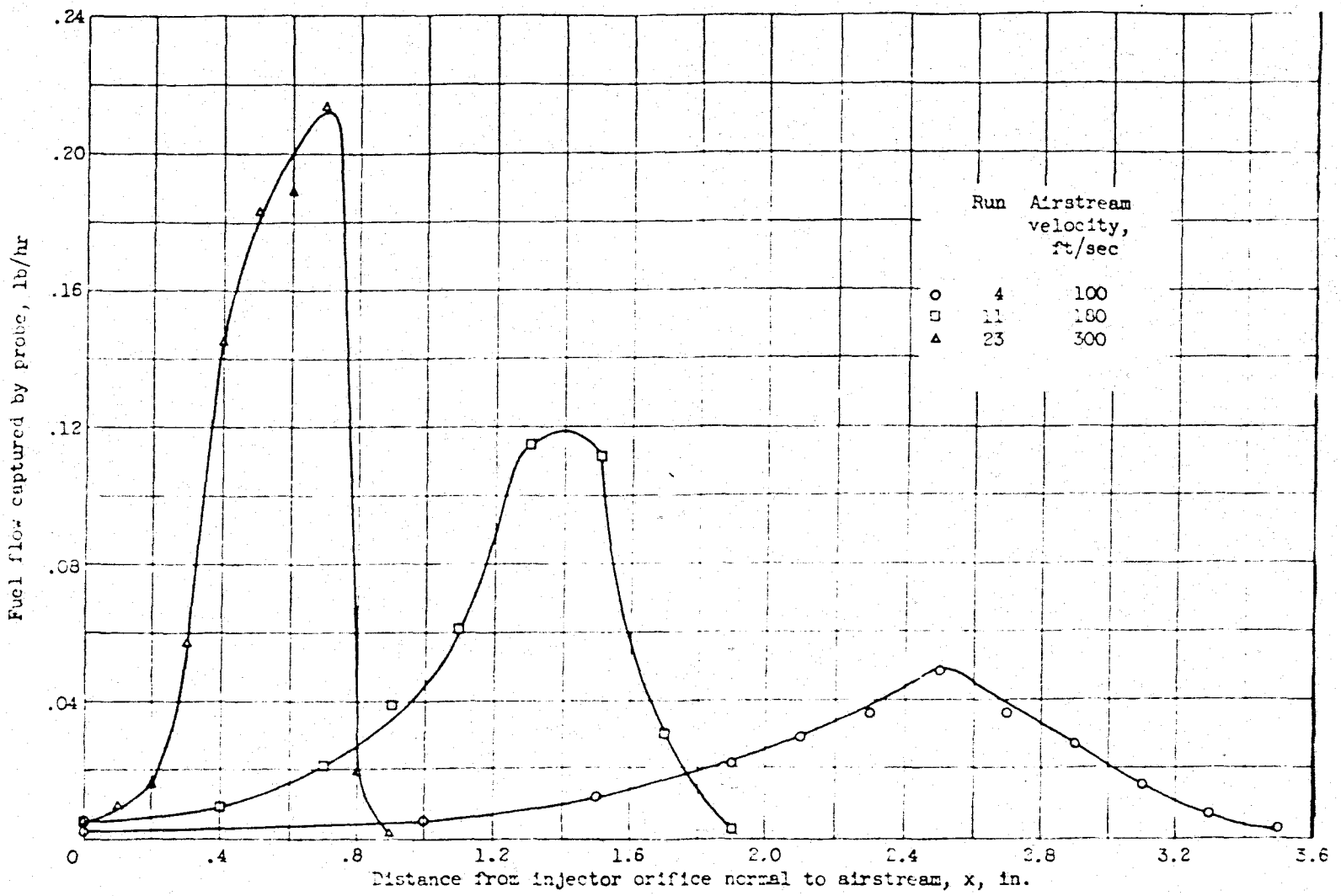

FIGURE 6.17: Distribution of Iso-octane Sprays Normal to Airflow and 1 Inch Downstream from the Injector. Orifice Diameter 0.030 inch; Fuel Jet Velocity 51 ft/sec; Fuel Density 42.6 lbs/ft^3; Air Temp. 86°F; Air Pressure 29.3 in-Hg. [9]

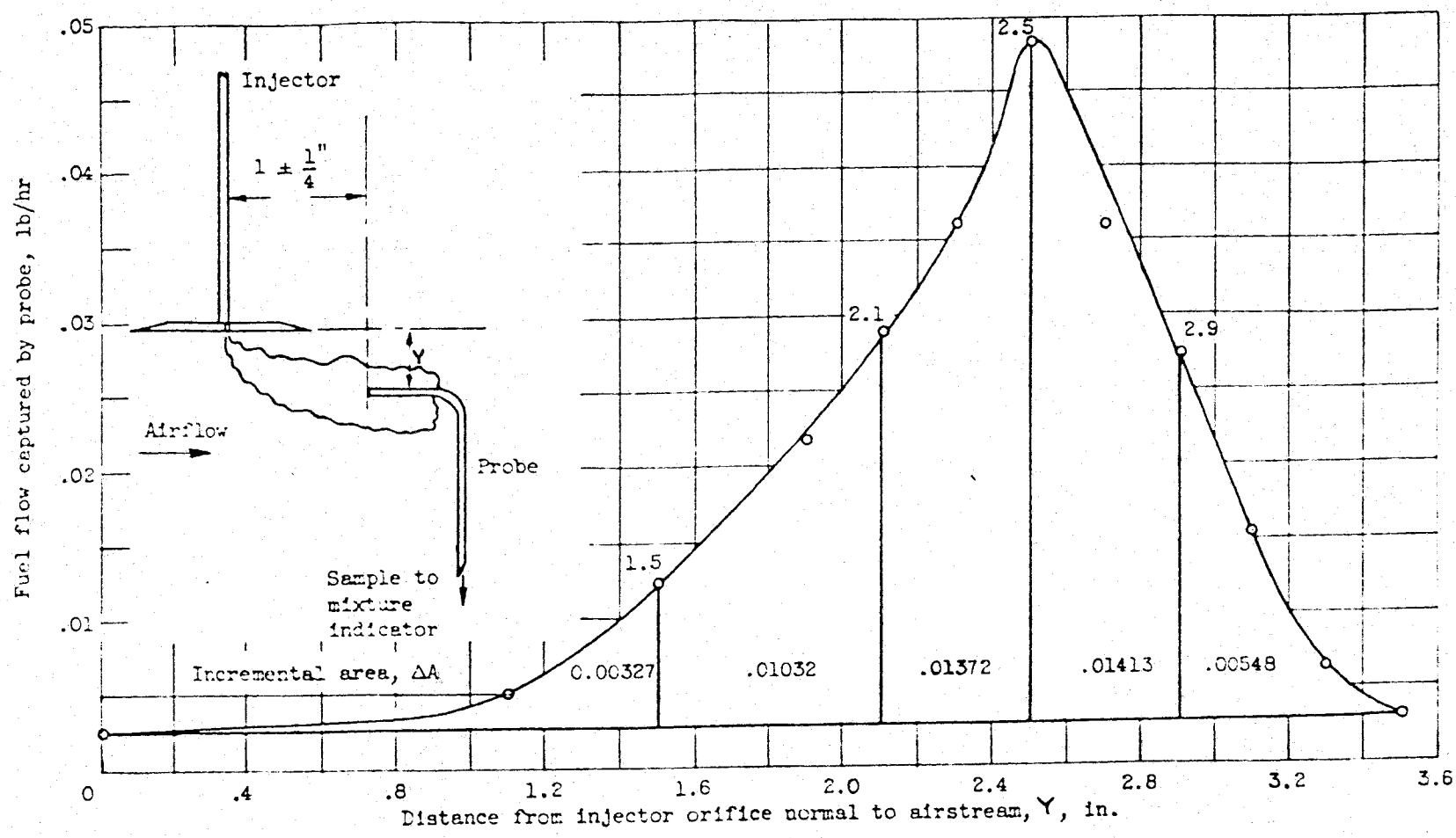

FIGURE 6.18: Typical Distribution Curve Showing Nominal Areas Used to Calculate Total Drop Size Distribution for Sprays [9]

dimensional analysis yielded

$$\frac{\bar{X}_{30}}{d} = f_2 \left[\frac{(\sigma_L)}{(d)(\rho_L)(V_A^2)}\right]^d \left[\frac{\mu_L}{(d)(\rho_L)(V_A)}\right]^{g+e} \left[\frac{(\rho_G)}{(\rho_L)}\right]^f \left[\frac{(\mu_L}{(\mu)}\right]^g \qquad 6.25$$

This relationship combines the seven variables assumed to influence $\bar{X}_{30}$ into four dimensionless groups. The magnitudes of the exponents d, g, e, f, and constant of proportionality, f_2, were experimentally found, to be $\frac{1}{4}$, 0, $\frac{1}{4}$, $\frac{-1}{4}$ and 3.9 respectively. Substitution of these values into equation 6.25 gave

$$\frac{\bar{X}_{30}}{d} = 3.9 \left[\frac{1}{(N_{We})(N_{Re})}\right]^{0.25} \qquad 6.20$$

the expression described earlier.

Substitution of X_m for $\bar{X}_{30}$ in equation 6.23 and a similar dimensional analysis approach leads to equation 6.21. Equations 6.21 and 6.22 produce

$$\frac{X_m}{\bar{X}_{30}} = 5.7 \left[\frac{1}{(N_{We})(N_{Re})}\right]^{0.04} \qquad 6.26$$

Substitution of $\bar{X}_{30}$ into the N-T distribution function gave the modified Nukiyama-Tanasawa equation described by equation 6.22.

d. Ingebo [10]

Ingebo [10] obtained drop size distribution data for heptane sprays produced by pairs of jets impinging at right angles in air streams. He attempted to fit the experimental results by log-probability, Rosin-Rammler, and N-T distribution functions. Because the best fit was obtained with the Nukiyama-Tanasawa function, Ingebo used this expression to determine the volume mean diameter, $\bar{X}_{30}$.

The experiments of Ingebo [10] were conducted over a range of orifice diameters, liquid jet velocities, and air-liquid relative velocities. These variables were empirically correlated according to

$$\frac{d}{\bar{X}_{30}} = 2.64\ \sqrt{(d)\,(V_L)} + 0.97\ (d)\ (V_a) \qquad 6.27$$

where

d = injector orifice diameter, cm

$\bar{X}_{30}$ = volume mean diameter, cm

V_L = injection velocity, cm/sec

V_a = velocity difference between airstream and liquid jets, cm/sec

The experimental approach was similar to that of Ingebo and Foster [9]. Typical jet injectors used in the study are shown in Figure 6.19 a,b. Photomicrographs of the

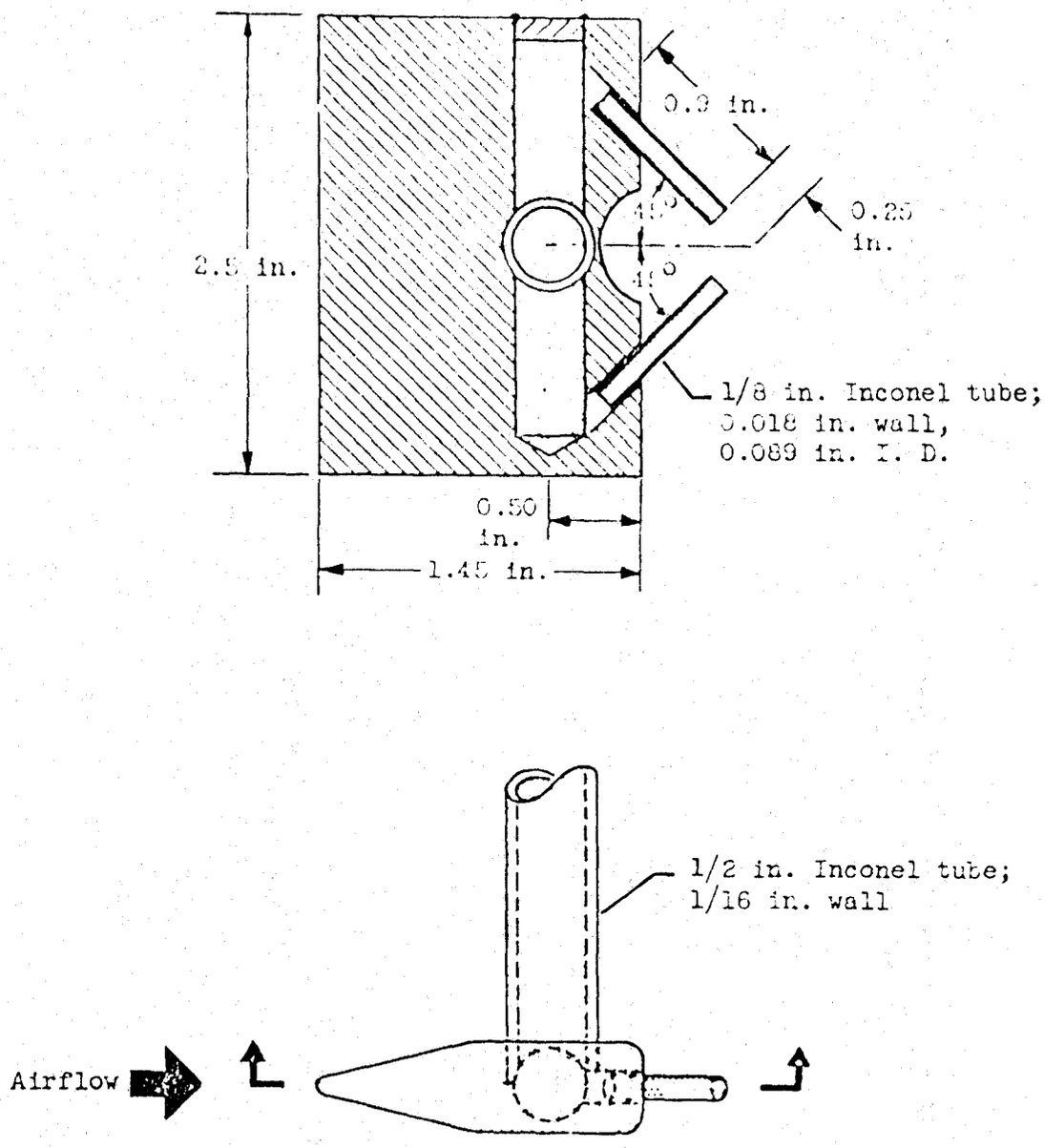

(a) Large injector.

FIGURE 6.19a: Impinging Jet Injectors Used by Ingebo [10]

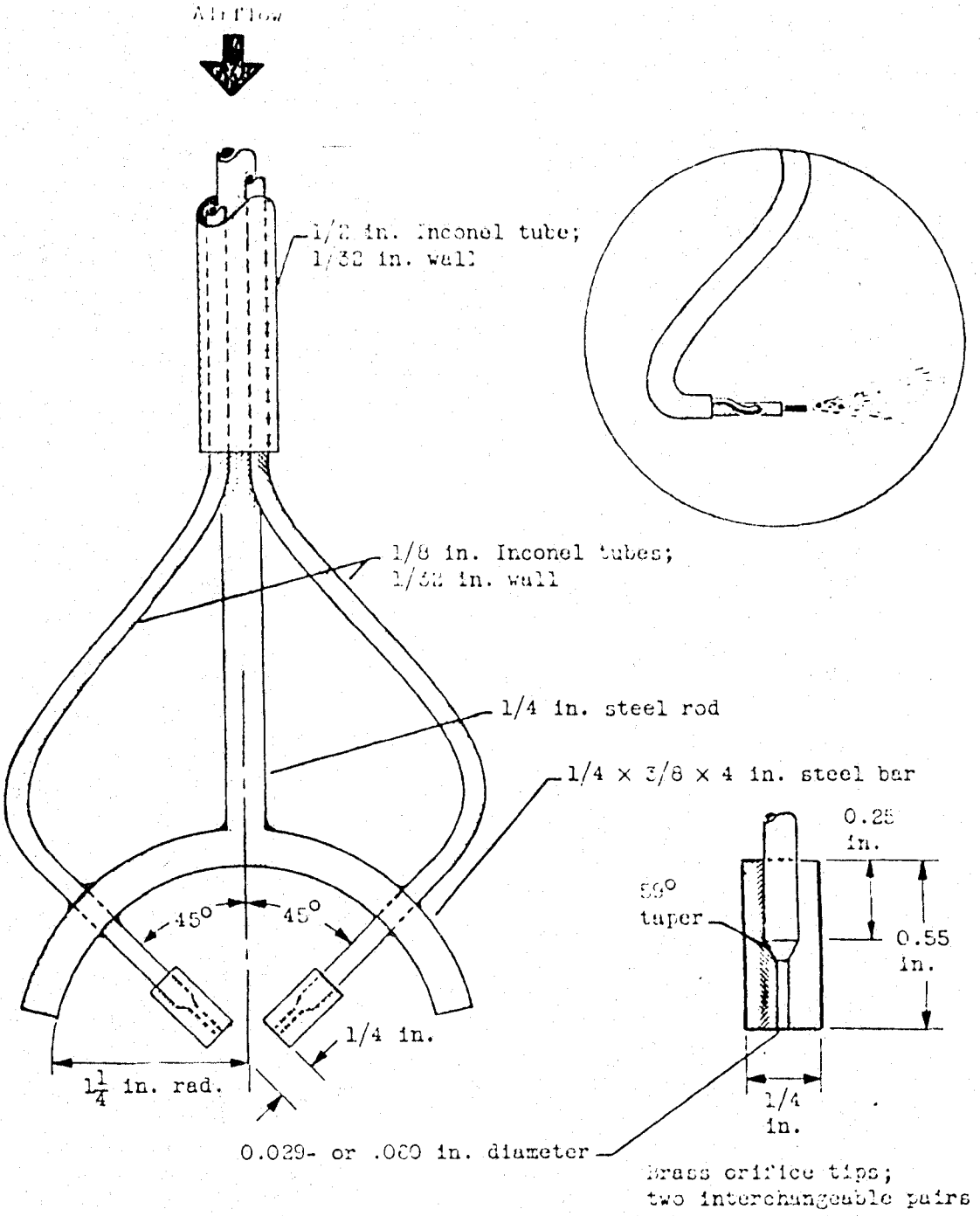

(b) Medium and small injectors.

FIGURE 6.19b: Impinging Jet Injectors Used by Ingebo [10]

breakup of n-heptane jets were taken by means of a high speed camera at distances of 1, 3, 5 and 8 inches downstream from the point of impingement as shown in Figure 6.20a. Typical results are given in Figure 6.20b,c,d,e.

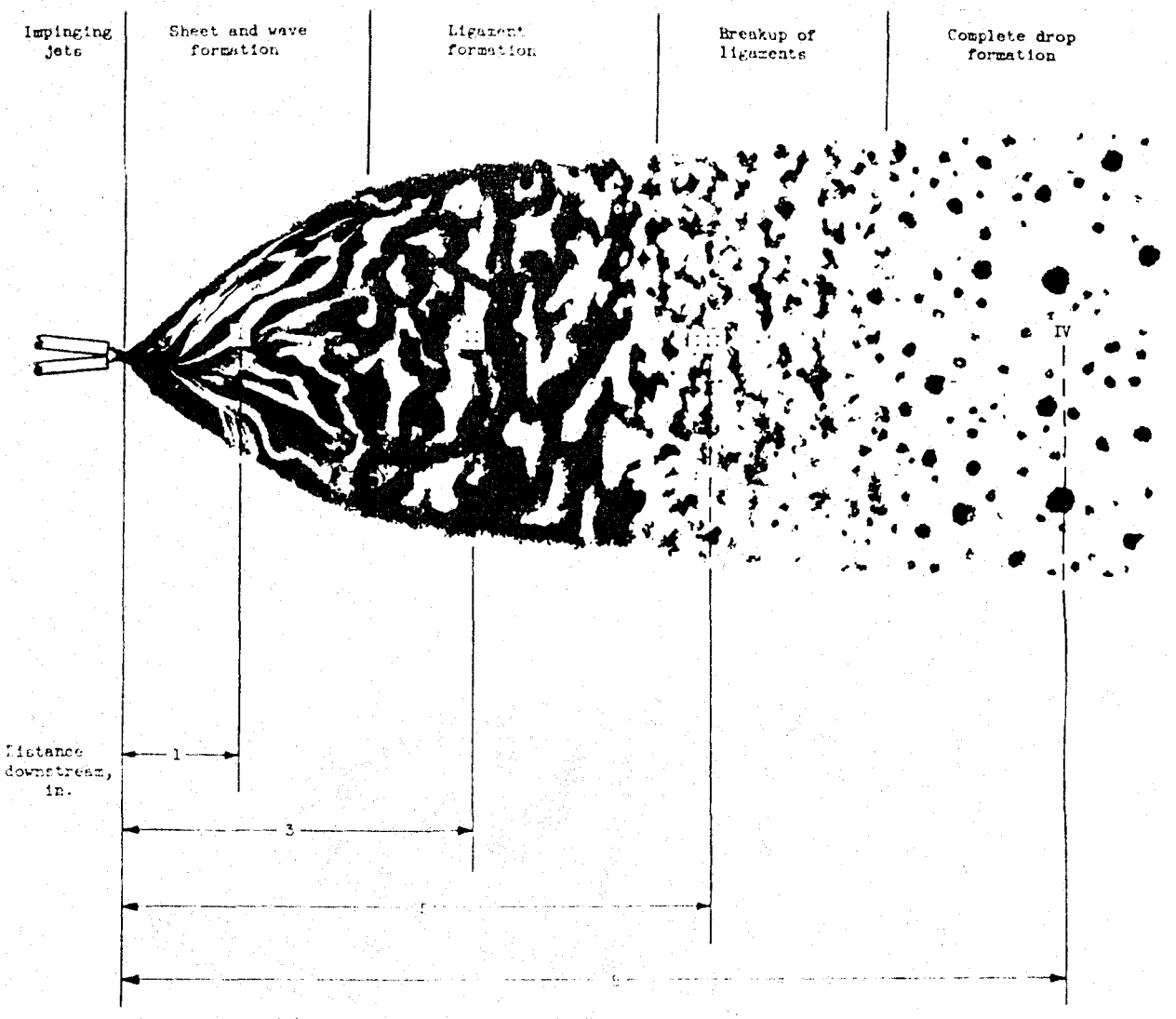

(a) Schematic representation of atomization using impinging jets.

FIGURE 6.20a: Atomization Process for Impinging Jets [10]

(b) Sheet and wave formation, 1 inch from point of impingement (zone I); x21.

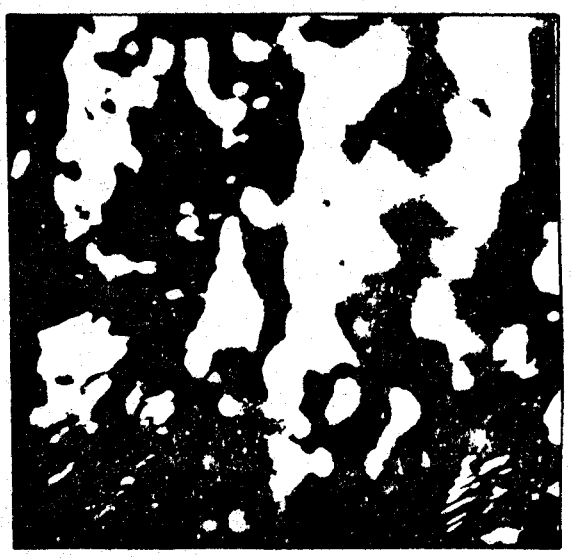

(c) Ligament formation, 3 inches from point of impingement (zone II); x21.

(d) Breakup of ligaments, 5 inches from point of impingement (zone III); x21.

(e) Complete drop formation, 8 inches from point of impingement (zone IV); x21.

FIGURE 6.20b,c,d,e: Atomization for Impinging Jets [10]

Ingebo [10] concluded that impinging jet injectors produced relatively coarse sprays and that the velocity difference between air and liquid had a pronounced effect on the atomization over the range of conditions used in his investigations.

e. Weiss and Worsham [11]

Weiss and Worsham [11] studied the atomization of molten synthetic wax injected into large hot airstreams moving at velocities as high as 1000 ft/sec. The injectors used in this investigation are shown in Figure 6.21. These devices were located in the duct to provide countercurrent or co-current operation. The traversing probe, depicted in Figure 6.22 was located downstream. It was used to withdraw a representative sample which was cooled to freeze the drops. Figure 6.23 illustrates the path of the sampling probe traverse during the collection of solid particles which were analyzed later by sedimentation and sieving. The results, correlated as shown in Figure 6.24, were summarized by the dimensionless equation

$$\left[\frac{(X_{MM})(\rho_G)(V_a^2)}{(\sigma_L)}\right] = 0.61\left[\frac{(V_a)(\mu)}{(\sigma_L)}\right]^{2/3}\left[1 + \frac{1000\ (\rho_G)}{(\rho_L)}\right]\left[\frac{(W_L)(\rho_L)(\mu_G)(\sigma_L)}{(\mu^4)}\right]^{\frac{1}{12}} \qquad 6.28$$

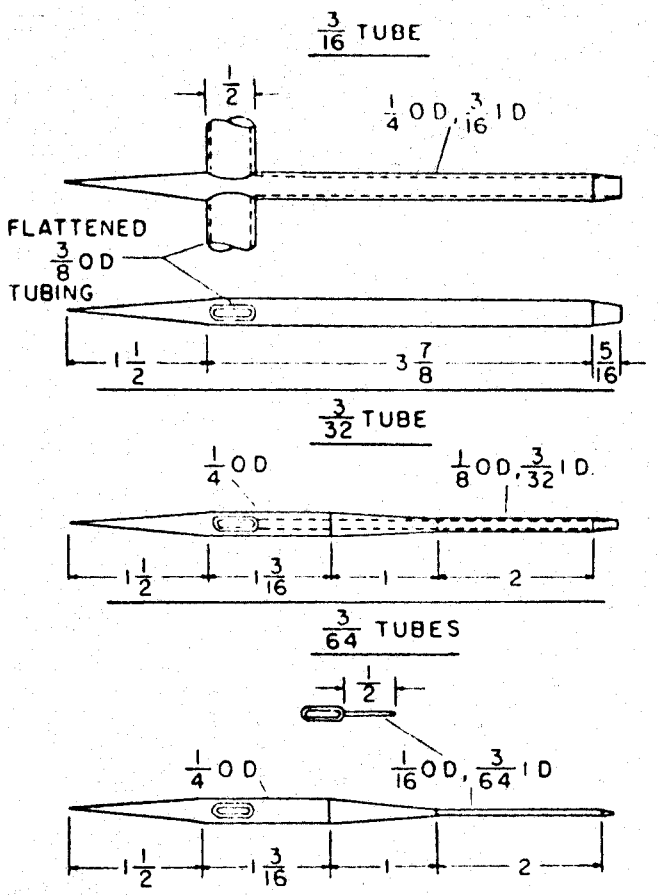

FIGURE 6.21: Geometry of Cylindrical Injectors Used by Weiss and Worsham [11]

Weiss and Worsham [11] concluded that atomization of liquids by high velocity air streams occurred by direct action of the airstream on the exposed liquid surface.

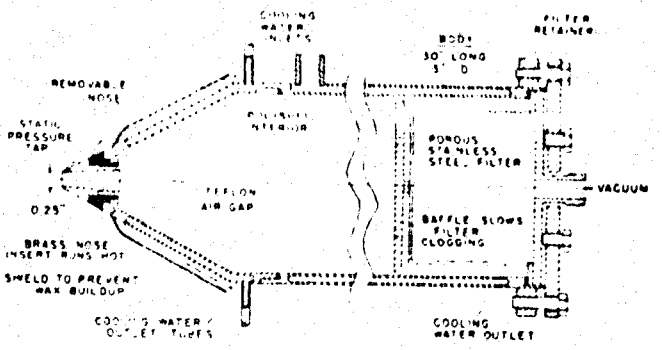

FIGURE 6.22: Droplet Sampling Probe Used by Weiss and Worsham [11]

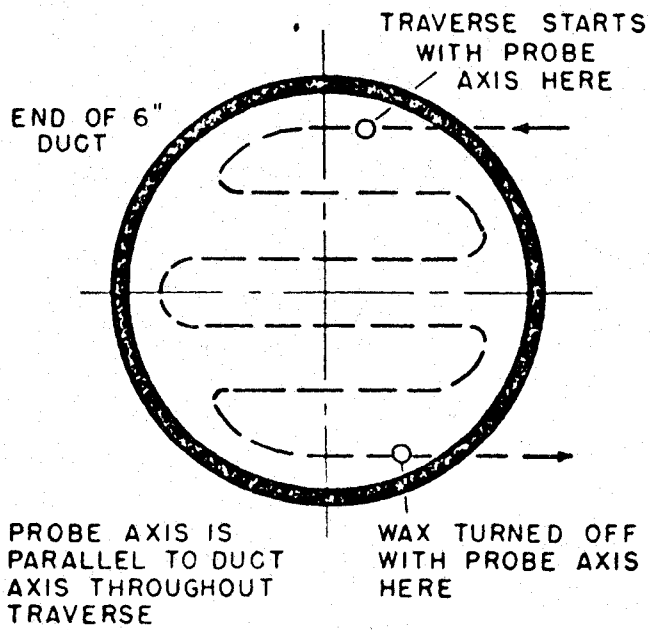

FIGURE 6.23: Path of Sampling Probe Traverse at Duct Exit [11]

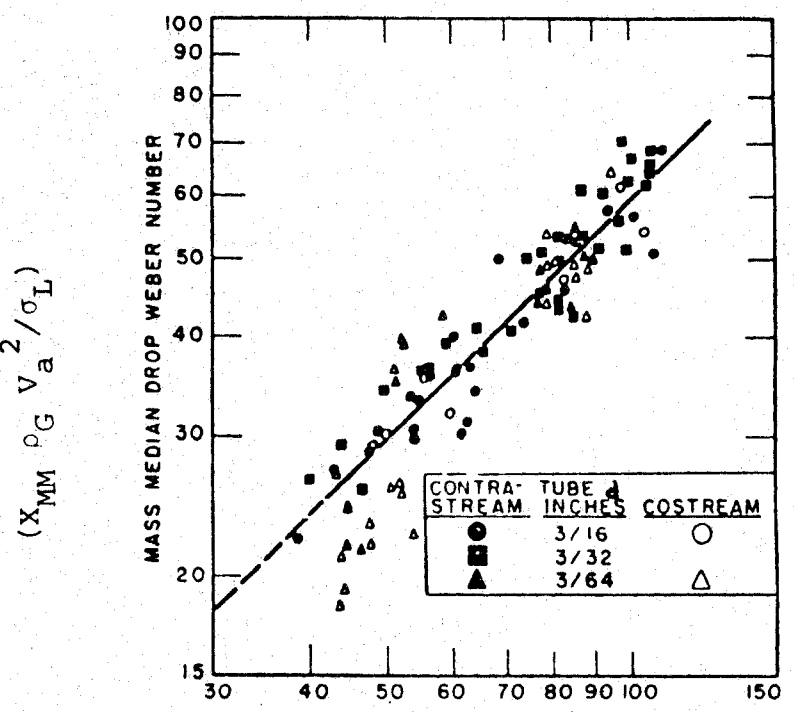

FIGURE 6.24: Correlation of Mass Median Drop Diameters from Tube Injectors [11]

Furthermore it appeared that the mode of liquid introduction into the air, (i.e. the geometry and operation of the injector) was of least importance, particularly at high air velocities

(presumably of the order of 750 ft/sec). The relative velocity between the air and liquid was of prime importance. Spray fineness did depend on the physical properties of the fluid, but, the net influence of these physical properties was less significant than the effect of relative velocity.

f. Mugele [12]

Mugele [12] obtained correlations for the Sauter mean drop diameter and the maximum stable drop diameter in a spray. General correlative equations were developed employing a dimensional analysis approach. The relationship

$$\frac{\bar{X}_{32}}{d} = A \left[\frac{(d)(\rho_L)(V_a)}{(\mu)}\right]^B \left[\frac{(\mu_G)(V_a)}{(\sigma_L)}\right]^C \qquad 6.29$$

was derived and the constants A, B and C, which were specific for each type of atomizer, were evaluated from experimental data for a number of nozzles.

In order to facilitate prediction of maximum drop diameters, X_m, corresponding values of the constants Am, Bm and Cm, to be used in Mugele's equation, were evaluated (as given in Table 6.3) for each atomizer tested.

Type of Atomizer	Calculation of $\bar{X}_{32}$			Standard Deviation %	Calculation of X_m		
	A	B	C		Am	Bm	Cm
Straight pressure or tangential nozzle	5.0	-0.35	-0.20	22	57	-0.48	-0.18
Venturi atomizer	1140	-0.82	-0.45	30			
Modified pressure nozzles (printle, lip, impinging jet etc.)	5.0	-0.35	-0.20	30	57	-0.48	-0.18
Spinning disks or cups					1.73	-0.50	-0.45
Whirl chambers	5.0	-0.35	-0.20	26	57	-0.48	-0.18

TABLE 6.3: Summary of Constants to be Used for Estimating Drop Size as Reported by Mugele [12]

For atomizer types other than those discussed in Table 6.3, V_L was calculated from the equation

$$V_L = C_Q \sqrt{2(\Delta P)/(\rho_L)} \qquad 6.30$$

where (ΔP) is the pressure drop corresponding to the energy required for the breakup of the bulk liquid. A value of 0.7 was recommended for the effective discharge coefficient, C_Q, in cases where its magnitude was unknown. For spinning atomizers the representative diameter, d, to be used in equation 6.29 is the outer diameter of the spinning component, while for pressure or Venturi atomizers it is the orifice diameter or the hydraulic diameter of the liquid disperser. If the geometry of the spray generator is complicated by interior grooves, vanes, multiple inlets, or pintles (or for swirl type of atomizers which have an air core), the following equation was recommended for calculating the effective diameter d:

$$d = \sqrt{4\ Q_L/\pi(V_L)} \qquad 6.31$$

where

Q_L = volumetric flow rate of liquid cm^3/sec

V_L = velocity of liquid, cm/sec.

Using equations 6.29, 6.30 and 6.31, the values of $\bar{X}_{32}$ and X_m were calculated and compared with experimental data of several other investigators. For rapid estimates of X_m and $\bar{X}_{32}$ as functions of the interfacial tension and Reynolds number groups for straight or modified pressure nozzles and whirl chambers, the nomograph shown in Figure 6.25 was developed.

Mugele's investigations showed that the relative air to liquid velocity was the important parameter controlling drop diameter. Therefore in accordance with the approach of Nukiyama-Tanasawa [6] relative velocity was used as the basis for correlating data for all types of atomizers.

g. Eisenklam [13]

Eisenklam [13], who reviewed the existing work on atomization, modified the Nukiyama-Tanasawa equation slightly to the form

$$\bar{X}_{20} = \frac{5.85}{(V_a)}\sqrt{\frac{(\sigma_L)}{(\rho_L)}} + \frac{725}{(\rho_L)^{1.72}}\left[\frac{(\mu)}{\sqrt{(\sigma_L)}}\right]^{0.45}\frac{1}{(MR)^{1.5}} \qquad 6.32$$

where

$\bar{X}_{20}$ = surface mean diameter, microns

V_a = relative velocity of gas, cm/sec

σ_L = surface tension of liquid, dynes/cm

ρ_L = liquid density, gm/cm^3

μ = absolute viscosity of liquid, poise

MR = mass ratio of air to liquid with air at 100°F

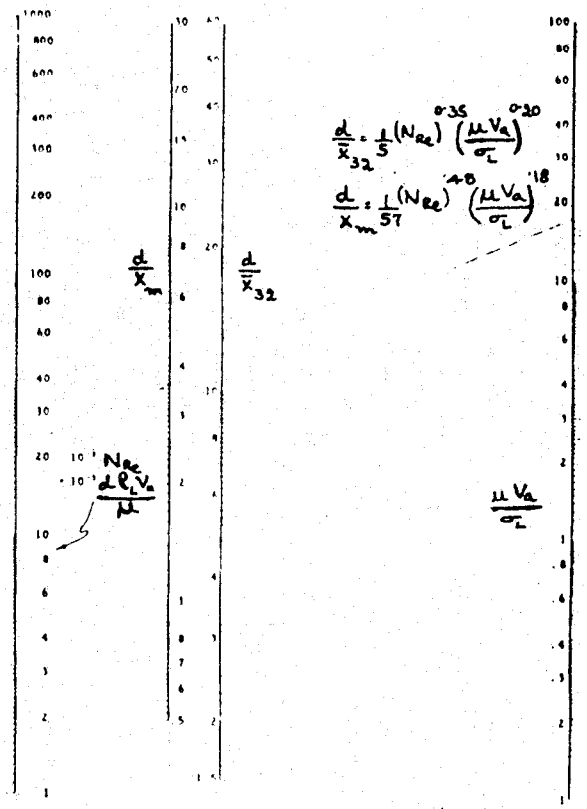

FIGURE 6.25: Nomograph for Droplet Sizes From Atomization Via Pressure Nozzles into Gases Similar to Air [12]

for prediction of drop diameters from the Venturi type internal mixer illustrated in Figure 6.26.

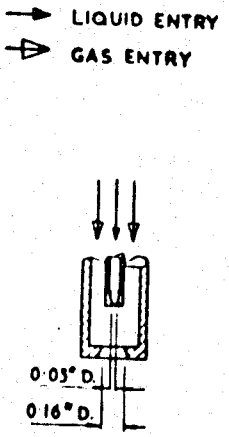

FIGURE 6.26: Internal Mixer Type Venturi Nozzle Reported by Eisenklam [13]

The mass ratio of air to liquid was found to be a significant variable for liquids whose viscosities ranged from 0.01 to 0.3 poise at 100°F and a pressure differential of 10 psi. The Sauter mean diameter was found to be below 100μ for the nozzle used.

h. Gretzinger and Marshall [14]

Converging pneumatic and pneumatic impingement nozzles were studied by Gretzinger and Marshall [14]. The disruptive

action of a high velocity air stream on thin liquid films or filaments provided the mechanism of atomization. Typical nozzles used in this investigation are shown in Figures 6.27 and 6.28.

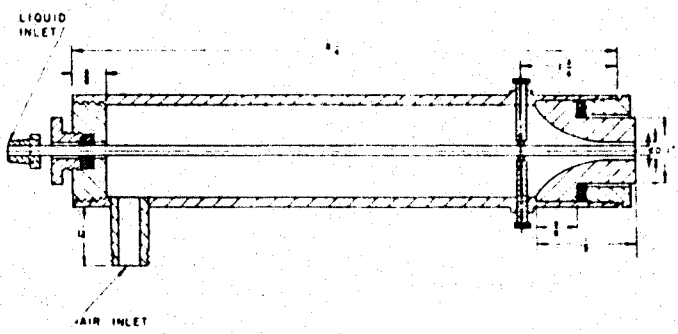

FIGURE 6.27: Converging Pneumatic Nozzle Used by Gretzinger and Marshall [14]

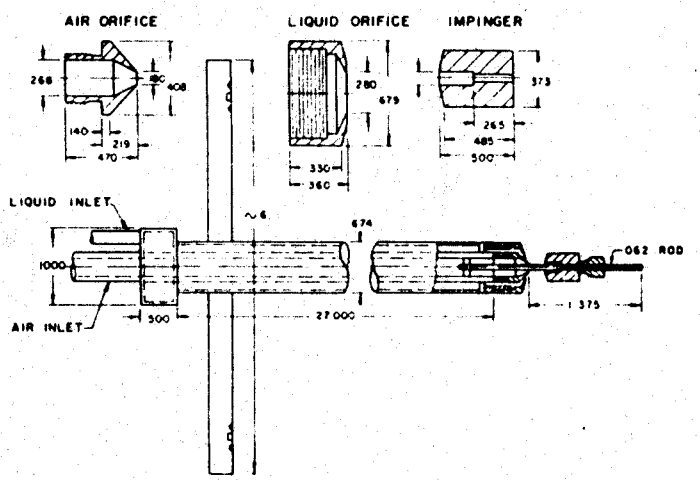

FIGURE 6.28: Pneumatic Impingement Nozzle Used by Gretzinger and Marshall [14]

For the converging pneumatic nozzle, the liquid was drawn from the central tube, in the form of a thin cylindrical shell, and broken up by the surrounding high velocity air stream emerging as an exterior annulus from the converging section of the nozzle.

In the pneumatic impingement device, the innermost tube was the air conduit. The annular space between the tubes carried the liquid. Each tube was fitted with converging outlet pieces. The outer converging piece brought the liquid to the surface of the outlet of the air tube nozzle. An impinger, mounted on a rod centered in the air tube, permitted adjustment of the air flow pattern and produced corresponding changes in the spray cone angle. Air flow patterns from the two nozzles were observed by a shadowgraph technique described by Dvorak [62] and Foley [63].

A new technique for drop size measurement was developed. This consisted of

i. forming a fine spray from an aqueous solution of a black dye
ii. evaporating the water from the droplets
iii. collecting a sample of the resultant dye aerosol in mineral oil

iv. counting the dye particles with the aid of a light microscope

v. plotting the number frequency distribution of the dye particles

vi. calculating the mass distribution of the original spray droplets from the dye particle number distribution, the density of the dye particles and the original concentration of dye in the liquid sprayed.

Some of the observations made by Gretzinger and Marshall [14] during shadowgraph studies are particularly noteworthy. The air flow from the pneumatic impingement nozzle suggested that liquid or spray travelled along the outside of the air pattern and followed a rapidly diverging conical path. This condition, varying with the position of the impinger and the applied air pressure, resulted in very effective use of the energy of the expanding air stream to break the liquid film into small and relatively uniform drops.

In the case of the converging nozzle, it was observed that the liquid flow, which was interior to the air stream, closely followed the inside of the air flow pattern which had a definite scalloped effect on the interior. The wavelength of the air flow pattern was constant at 0.08" for

liquid feed rates from 0.5 to 4.5 gal/hr and air pressures from 80 to 100 lbs/in^2 gauge. Thus it was concluded that liquid flow rate in the range studied had relatively little effect on air flow patterns in the vicinity of the nozzle outlet at a given air supply pressure.

In another study, when flat sheets of liquid were introduced co-currently into high velocity air, it was noticed that the smallest drops in a given spray were formed on the side of the liquid sheet in intimate contact with the gas stream. Large drops were formed on the opposite side of the liquid sheet and moved away from the air stream slowly in a stable condition. These observations served to emphasize the need for uniformly contacting a liquid sheet on both sides if uniform breakup was to be achieved.

The drop size data for each nozzle were correlated as functions of the mass ratio of the air and liquid streams and the product of the air mass velocity at the nozzle outlet and the diameter of the contact periphery of the air and gas streams. The relationship for mass median diameter

$$X_{MM} = 2600 \left[\left(\frac{W_L}{W_G}\right) \left(\frac{\mu_G}{GL}\right) \right]^{0.4} \qquad 6.33$$

where

W_L = mass flow rate of liquid, gm/sec

W_G = mass flow rate of air, gm/sec

G = mass velocity of gas at nozzle outlet, $\frac{gm}{sec\text{-}cm^2}$

L = diameter of wetted periphery between gas and liquid, cm

was dervied for converging pneumatic nozzles, while

$$X_{MM} = 122 \left(\frac{W_L}{W_G}\right)^{0.6} \left(\frac{\mu_G}{GL}\right)^{0.15} \qquad 6.34$$

was recommended for pneumatic impinging nozzles.

The spread of the drop size distributions formed by the nozzles was expressed in terms of the geometric standard deviation, σ_g. Figure 6.29 illustrates curves of log σ_g as functions of mass median drop size for each nozzle.

Log-log coordinate plotting yielded

$$\sigma_g = (1.77) \left(X_{MM}\right)^{0.14} \qquad 6.35$$

for converging nozzles, and

$$\sigma_g = (1.735) \left(X_{MM}\right)^{0.16} \qquad 6.36$$

for pneumatic impingement nozzles.

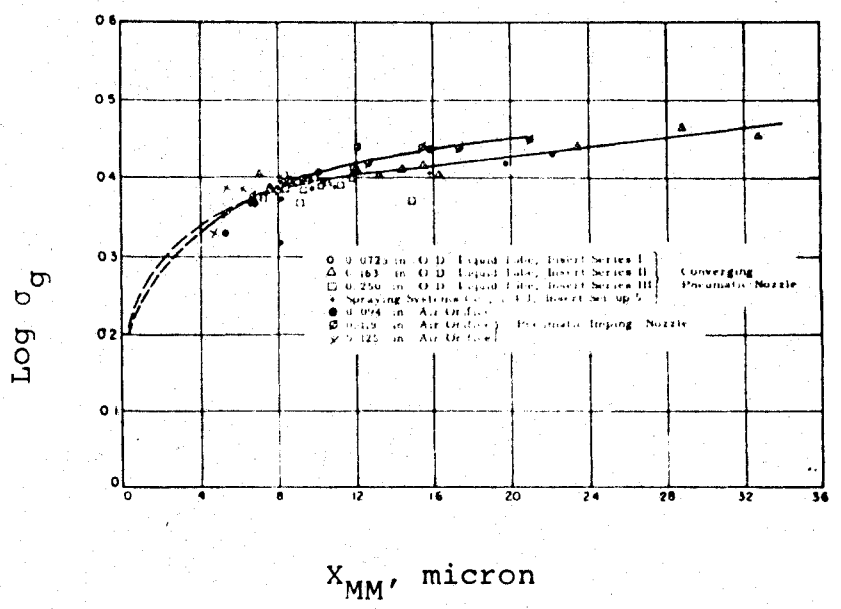

FIGURE 6.29: Variation of Standard Deviation with Mass Median Diameter [14]

Gretzinger and Marshall [14] specified that the following conditions must be satisifed for equations 6.33, 6.34, 6.35 and 6.36 to be valid:

i. mass median drop diameters ranging between 5 to 29μ

ii. liquid rates from 0.5 to 5 gal/hr.

iii. liquid viscosity close to 1 centipoise

iv. surface tension in the range of 50 dynes/cm

v. mass ratios of air to liquid between 1 to 15

vi. liquid film thickness between 0.3 and 0.6 mm, as calculated by the method of Friedman and Miller [64]

vii. gas at sonic velocity in the nozzle discharge port

viii. gas densities in the nozzle discharge port ranging between 2×10^{-3} to 5×10^{-3} gm/cm^3

i. Wigg [15]

Using experimental data and predictions of several previous investigators [6, 9, 65, 66, 67, 68], Wigg [15] correlated the drop mass median diameter, X_{MM}, of several wax sprays according to

$$X_{MM} = 2.0 \left[\frac{(\nu)^{0.5} \ (W_L)^{0.1} \ \left(1 + \frac{W_L}{W_G} \right)^{0.5} \ (h)^{0.1} \ (\sigma_L)^{0.2}}{(\rho_G)^{0.3} \ (V_A - V_L)} \right] \qquad 6.37$$

where

ν = kinematic viscosity of liquid, centistokes

W_L = liquid mass flow rate, gm/sec

W_G = air mass flow rate, gm/sec

h = height of air annulus, cm

σ_L = surface tension of liquid, dynes/cm

ρ_G = density of air, gm/cm^3

$(V_A - V_L)$ = relative velocity, cm/sec

For conditions where recombination and coalescence of drops were significant, Wigg [15] suggested that a correction term be incorporated into equation 6.37 to account for the coalescence phenomena. This new correction parameter was obtained using data [6, 9, 65, 66, 67, 68, 69] for several high pressure air atomizers, operating at velocities not less than 300 metres/sec. The modification to equation 6.37 yielded

$$X_{MM} = 2.0 \left[\frac{(\nu)^{0.5} (W_L)^{0.1} (1 + \frac{W_L}{W_G})^{0.5} (h)^{0.1} (\sigma_L)^{0.2}}{(\rho_G)^{0.3} (V_A - V_L)} \right] \left[1 + 2.5 (\frac{W_L}{W_G})^{0.6} (W_L)^{0.1} \right] \quad 6.38$$

j. Kim and Marshall [16]

This study was made with the purpose of correlating mass median diameters of drops produced by convergent

pneumatic atomizers of the type shown in Figure 6.30. The atomizers, consisting of five major parts (nozzle fastener, air nozzle, main body, liquid nozzle and secondary air nozzle) generated drops in the size range 6 to 350 microns. Assembly of the first four parts produced an atomizer with a single gas nozzle, while five part assembly generated an atomizer with two gas nozzles. In the latter arrangement, the secondary gas nozzle was inserted axially into the liquid nozzle. Thus an annular liquid sheet could be produced between two air streams. The dimensions and flow areas of the atomizers formed from the various combinations of air and liquid nozzles are given in Table 6.4. Variations in viscosity of the liquids atomized were achieved by using molten wax and melts of wax-polyethylene mixtures of various compositions. The generated sprays were solidified and solid particles collected for subsequent size analysis. Microscopic counting and sieving were used for determinations of particle size. The distributions obtained by these two techniques are shown in Figure 6.31.

The drop size distribution data were curve fitted by a Pearl-Reed or logistic equation [70] because the usual functions (discussed earlier in Chapter V) could not approximate the experimental results. The so-called logistic equation is given by

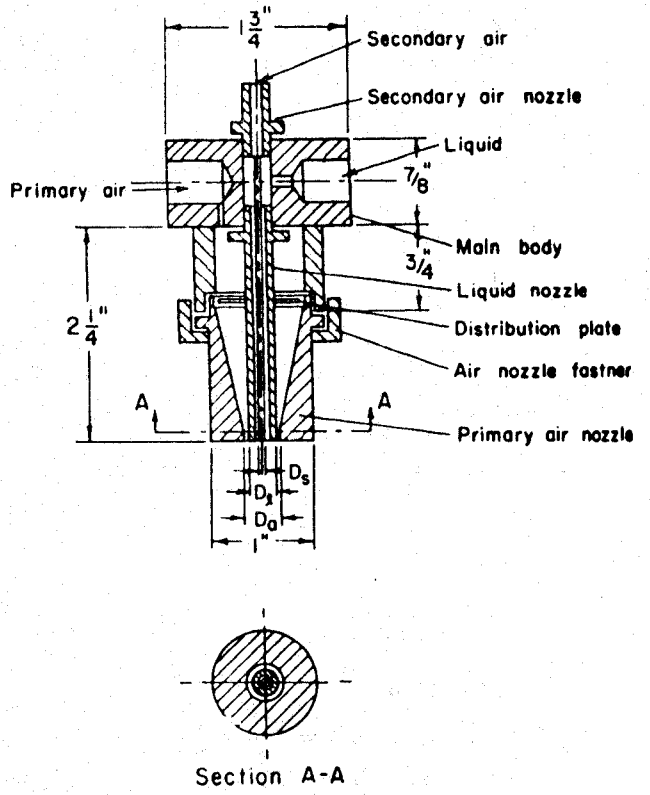

FIGURE 6.30: Experimental Pneumatic Atomizer Used by Kim and Marshall [16]

$$Q_v - b = \frac{b(1-b)}{b-\exp(arx)} \qquad 6.39$$

1. Dimensions of nozzles

Air nozzle Symbol	Diam. in.	Area, sq. in.	Liquid nozzle Symbol	O.D. in.	I.D., in.	Area for liquid, sq. in.
A-1	0.1285	0.01131	L-1	0.072	0.054	0.002290
A-2	0.166	0.02164	L-2	0.125	0.105	0.008659
A-3	0.272	0.05811	L-3	0.250	0.222	0.03871
S.S.N.†	0.120	0.01297	S.S.N.†	0.100	0.060	0.00283

2. Area and clearance of air annulus with various combinations

Insert series	I		II		III					
Nozzle combination	A-1	L-1	A-2	L-2	A-3	L-3	A-2	L-1	A-3	L-1	A-3	L-2
Clearance, in.	0.0283		0.0205		0.011		0.047		0.100		0.0735	
Area, sq. in.	0.00890		0.00937		0.00902		0.0176		0.0540		0.0458	

3. Dimensions of concentric double air nozzle atomizer

Primary air nozzle diam., in.	Secondary air nozzle O.D., in.	I.D. in.	Liquid nozzle O.D., in.	I.D., in.	Areas of flow Primary air, sq. in.	Secondary air, sq. in.	Liquid sq. in.
0.272	0.095	0.073	0.250	0.222	0.00902	0.00418	0.0316

† Fluid nozzle 60100, air nozzle 120, Spraying Systems Company.

TABLE 6.4: Details of Pneumatic Atomizers Studied by Kim and Marshall [16]

where

Q_v = cumulative volume distribution

b,r,a = constants

$a = \frac{1}{X_{MM}}$.

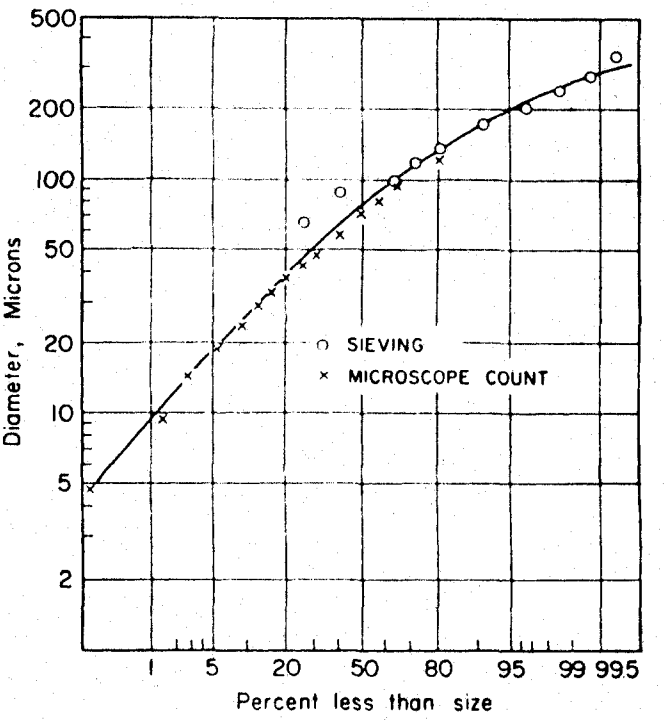

FIGURE 6.31: Comparison of Drop Size Distributions Obtained by Different Analytical Techniques Employed by Kim and Marshall [16]

The constants b and r were obtained graphically. It was found that the mass median diameter for this distribution was given by

$$X_{MM} = \frac{\overline{X}_{32}}{0.83} \qquad 6.40$$

Kim and Marshall [16] correlated the results of their investigations on single air nozzles by the equation

$$X_{MM} = \frac{249\ (\sigma_L)^{0.41}\ (\mu)^{0.32}}{[(V_A - V_L)^2\ \rho_G]^{0.57}\ (A)^{0.36}\ (\rho_L)^{0.16}} + 1260\ \left(\frac{\mu^2}{\rho_L \sigma_L}\right)^{0.17} \times \frac{1}{(V_A - V_L)^{0.54}} \left[\frac{W_G}{W_L}\right]^C \qquad 6.41$$

where

X_{MM} = mass median diameter, microns

σ_L = liquid surface tension, dynes/cm

μ = viscosity of liquid, centipoises

$(V_A - V_L)$ = relative velocity, ft/sec

ρ_G = gas density, gm/cm^3

ρ_L = liquid density, gm/cm^3

A = flow area for atomizing air, in^2

W_G = mass flow rate of atomizing air, gm/sec

W_L = mass flow rate of liquid, gm/sec

c = -1, if $W_G/W_L < 3$

= 0.5, if $W_G/W_L > 3$

For the concentric double air nozzle atomizer, a similar treatment of drop size data was made. The mass median diameter of a spray was correlated by an analogous equation written in the form

$$X_{MM} = \frac{8140}{[(V_A - V_L)^2 \rho_G]_{av}^{0.72}} \left[\frac{(\sigma_L)^{0.41} (\mu_L)^{0.32}}{(\rho_L)^{0.16}}\right] + 1240 \left(\frac{\mu}{\rho_L \sigma_L}\right)^{0.17} \frac{1}{[(V_A - V_L)_{av}]^{0.54}} \left(\frac{W_G}{W_L}\right)^{c}$$

where

$$c = -1, \text{ if } W_G/W_L < 3$$

$$= 0.5 \text{ if } W_G/W_L > 3$$

The value of $(V_A - V_L)_{av}$ is expressed in terms of f, the weight fraction of total air flowing in the primary nozzle according to

$$[(V_A - V_L)^2 \rho_G]_{av} = f[(V_A - V_L)^2 \rho_G]_{primary} + (1-f)[(V_A - V_L)^2 \rho_G]_{secondary} \qquad 6.43$$

Kim and Marshall [16] concluded that the most important operating variables affecting pneumatic atomization were the dynamic force of the atomizing gas, $[(V_A - V_L)^2(\rho_G)]$, and the mass flow ratio of air to liquid. Increasing the

the mass ratio or the air dynamic force, or both simultaneously decreases the drop size of the sprays. When an atomizer is operated at very large mass ratios the mass median drop size of the spray approaches an asymptote which is a function of the air dynamic force and liquid properties. Kim and Marshall [16] called this the limiting mass median diameter. It was recommended that the operating range of the mass ratio should be limited from 0.1 to 10. Below the lower limit atomization deteriorates. Above the upper limit atomization requires excessive energy expenditure.

k. Kumar and Prasad [17]

The external mixing type of pneumatic atomizer shown in Figure 6.32 was used by Kumar and Prasad [17] to study the effects of liquid viscosity, liquid surface tension, liquid flow rate, air velocity and nozzle angle on drop size.

Investigations were conducted with glycerine-water, glycerine-alcohol and pure water as the spray liquids in the experimental arrangement illustrated in Figure 6.33. The generated drops were sampled on vaseline-coated cells by means of a shutter arrangement. Drop sizes were measured under

a microscope. In order to avoid excessive impaction of droplets which made differentiation between drop boundaries

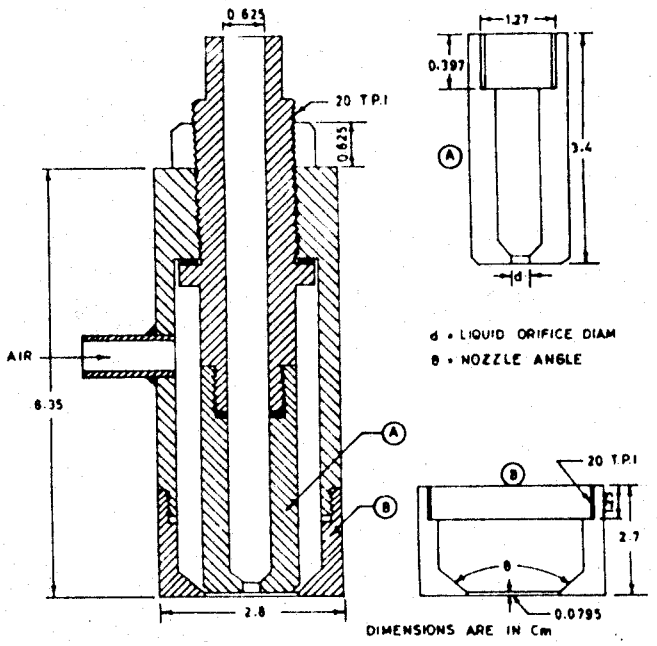

FIGURE 6.32: Atomizer used by Kumar and Prasad [17]

impossible, the sampling point was located 9 inches below the atomizer where coalescence was assumed to be negligible and secondary atomization effects could be ignored. Since the drops flattened on hitting the vaseline coating, a

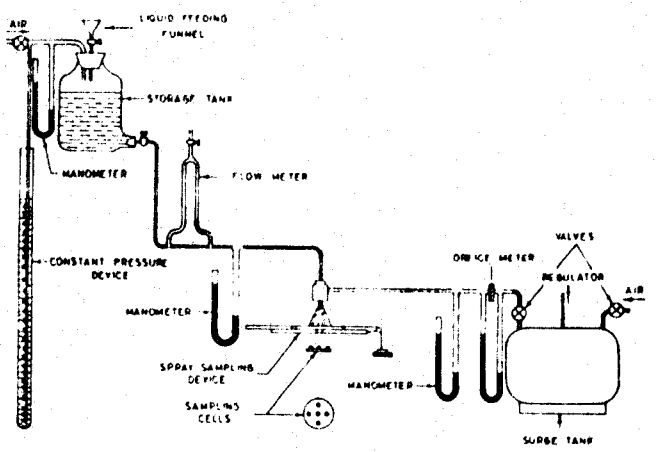

FIGURE 6.33: Experimental Equipment Used by Kumar and Prasad [17]

relationship had to be found between the true sizes of the drops in the spray and those collected. This relationship was used for drop sizes above 100μ.

The theoretical model used to describe the atomization phenomenon was based on the typical drop formation mechanism illustrated in Figure 6.34. The detachment of the drop from the nozzle was analyzed in terms of forces assisting and resisting separation. A force balance on a drop shows that

F_I		F_{II}		F_{III}		F_{IV}		F_V		F_{VI}		F_{VII}
Surface Tension Force	+	Expansion Force	+	Drag Force	+	Force Due to Tensile Velocity	=	Net Drop Weight	+	Force Due to K.E. of Liquid	+	Force Due to K. E. of Gas

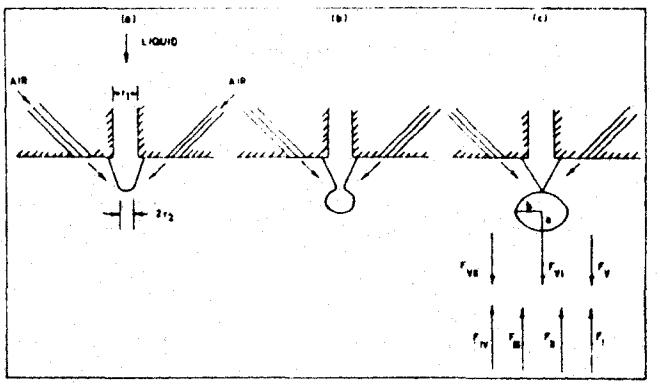

FIGURE 6.34 : Mechanism of Drop Formation [17]

Kumar and Prasad [17] evaluated the magnitude of each force. They correlated their experimental data for the special case of an atomizer discharging spray into still air at normal pressure and room temperature. Their simplified equation is given by

$$\frac{\pi}{6}\left[(r_2)^2(\mu)(Q_L)(V_s)^{-1}\right]+\frac{(Q_L)^2(\rho_L)(V_s)^{-2/3}}{14.5\left[\frac{(Q_L)(\rho_L)(V_A)}{2.5\times 10^4}\right]^{\frac{2}{3}}}=\left[(Q_G)(\rho_G)(V_A)\right] \quad 6.44$$

where

r_2 = radius of the constriction caused in the liquid jet, cm

μ = viscosity of liquid, gm/(cm-sec)

Q_L = volumetric flow rate of liquid, cm^3/sec

V_s = volume of a single drop, cm^3

ρ_L = density of liquid, gm/cm^3

V_A = velocity of air, cm/sec

Q_G = volumetric flow rate of air, cm^3/sec

Equation 6.44 was used to verify the theoretical model. Kumar and Prasad [17] employed a series of graphs to show that their experimental data matched the values

predicted by equation 6.44 quite closely. The comparison of predictions of data by the Kumar-Prasad model and the Nukiyama-Tanasawa [6] approach is shown in Figure 6.35.

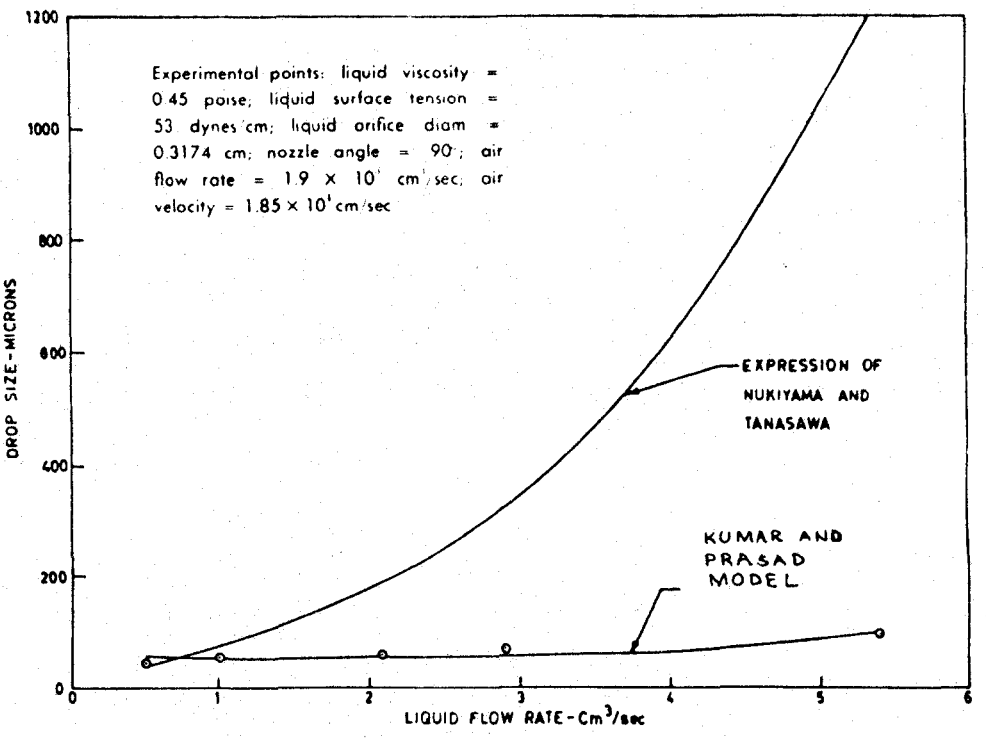

FIGURE 6.35: Comparison of Kumar-Prasad Model and Empirical Expression of Nukiyama-Tanasawa [17]

This diagram clearly shows that very large differences are to be expected between the two models at high liquid flow rates (low air-to-liquid flow ratios). The agreement is quite good at low liquid flow rates (high air-to-liquid flow ratios).

C. Conclusions

The equations to be used for predicting diameters of drops generated by two-fluid atomization are summarized in Table 6.5 along with their range of applicability, the system employed and method of analysis. Most of the important parameters for these equations have been included in Table 6.5. Lapple, Henry and Blake [71] have shown that if these equations are used for conditions outside of the variable range for which they were developed then large deviations are to be expected among the predicted mean diameter values.

One method of comparing the applicability of the published equations would be to predict mean drop diameters for each model at a selected set of standard conditions for which reliable experimental data are available. Lapple et al [71], in a general survey of atomization literature, have shown that predicted mean diameters may differ by factors of two to ten.

Investigator	Atomizer	Mathematical Treatment	Applicable Range				
			Relative Velocity	Liquid Viscosity	Liquid Density	Liquid Surface Tension	System Used
Mayer [2]	Air induced atomization from a flat liquid surface	Theoretical treatment based on air induced capillary waves					
$X_{av.} = 9\pi \sqrt[3]{16}\ (0.3) \left[\frac{(u)\sqrt{(\sigma_L)(\rho_L)}}{(\rho_G)(V_a^2)}\right]^{2/3}$							
Adelberg [3, 4]	Simple jet	Theoretical treatment based on wave and ligament formation, which collapse into drops					
i. capillary wave regime $X_{av.} = 2.4(dmax.)^{\frac{1}{2}} \left[\frac{(u)(\sigma_L/\rho_L)^{\frac{1}{2}}}{(\rho_G)(V_A^2)}\right]^{\frac{1}{3}} \left[\frac{1-(K_1)(8)(\pi/2)^{1/2}(e^{3/2})}{5(1)}\right]$							
ii. acceleration wave regime $X_{av.} = 65.3 \left[\frac{(u)(\sigma_L/\rho_L)^{\frac{1}{2}}}{(\rho_G)(V_A^2)}\right]^{2/3}$							
Fraser, Dombrowski and Routley [5]	Spinning cup	Sheet break up related to drop size using Rayleigh's analysis	Up to 650 ft/sec	5-165 centistokes	0.81- .83 gm/cc	29-35 dyne/cm	Air/Oil
$\bar{X}_{32} = (6 \times 10^{-4}) + \left[\frac{0.59(\sigma_L)^{\frac{1}{2}}(v_r)^{0.21}}{(\rho_G)^{\frac{1}{2}}(a\,d_L + a^2)^{\frac{1}{4}}}\right]\left[1 + 0.065\left(\frac{w_a}{w_L}\right)^{1.5}\right]\left[\frac{\sigma_L}{v_p^3(0.5v_R^2 - v_R + 1)}\right]^{\frac{1}{2}}$							

TABLE 6.5: Summary of Pneumatic Atomization Investigations

Investigator	Atomizer	Mathematical Treatment	Applicable Range: Relative Velocity	Liquid Viscosity	Liquid Density	Liquid Surface Tension	System Used
Nukiyama and Tanasawa [6]	Pneumatic	Empirical Equation	Up to sonic	0.3 to 50 centipoises	43.7 to 75 lb/ft^3	19 to 73 dyne/cm	Air/Mixtures of ethyl alcohol-water, and glycerine-etyl alcohol-water solutions
		$\bar{x}_{32} = \frac{5.85\sqrt{\sigma_L}}{(v_a)\sqrt{\rho_L}} + 597\left(\frac{\mu}{\sqrt{\sigma_L \rho_L}}\right)^{0.45}(1000\frac{Q_L}{Q_a})^{1.5}$					
Wetzel and Marshall [7, 8]	Pneumatic	Empirical Equation i) ii)	Up to 400 ft/sec	9 cp 5.5 cp	0.83 gm/cc 9.75 gm/cc	29.5 dyne/cm 470 dyne per cm	Air/Molten wax Air/low melting alloy
		i) $x_{oo} = \frac{10^6(4.2)(d)^{0.35}}{(v_A - v_L)^{0.68}}$ ii) $x_{oo} = \frac{10^5}{(v_A - v_L)^{1.11}}$					
Ingebo and Foster [9]	Cross current break up of single jet in air stream	Empirical Equation	Up to 620 ft/sec	.285 cp to 1.58 cp	40.0 to 99.5 lb/ft^3	16.0 to 71.0 dyne/cm	Air/Iso-Octane, JP-5 fuel, H_2O, benzene, Carbon Tetrachloride
		$\frac{\bar{x}_{30}}{d} = (3.9)(N_{We}\, N_{Re}^{-1})^{-0.25}$ $N_{We} = (\sigma_L)/(\rho_a)(d)(v_a^2)$ $N_{Re} = (d)(v_a)/(\nu)$					
Ingebo [10]	Two impinging jets in crosscurrent air stream	Empirical Equation	Up to 235 ft/sec				Air/n-heptane
		$\frac{d}{\bar{x}_{30}} = 2.64\sqrt{(d)(v_L)} + (0.97)(d)(v_a)$					

TABLE 6.5: Summary of Pneumatic Atomization Investigations

Continued ...

Investigator	Atomizer	Mathematical Treatment	Applicable Range				
			Relative Velocity	Liquid Viscosity	Liquid Density	Liquid Surface Tension	System Used
Weiss and Worsham [11]	Cylindrical injectors	Empirical Equation	200 to 1000 ft/sec	3.2 to 11.3 cp	0.806 to 0.828 gm/cc	18.2 to 22.0 dyne/cm	Air/Synthetic Wax + 4% alcohol soluble nigrosine dye
$\left[\frac{(X_{MMD})(\rho_G)(V_a^2)}{(\sigma_L)}\right] = 0.61\left[\frac{(V_a)(\mu)}{(\sigma_L)}\right]^{2/3}\left[1+\frac{1000(\rho_G)}{(\rho_L)}\right]\left[\frac{(W_L)(\rho_L)(\sigma_L)(\mu_G)}{(\mu)^4}\right]^{\frac{1}{12}}$							
Nuqele [12]	General equation for i. straight pressure nozzle, ii. Impinging jet nozzle iii. Spinning Cups or disks iv. Swirl or Whirl chambers v. Venturi Atomizers	Experimental data of other investigators correlated by dimensional analysis	300 to sonic Velocity ft/sec				
$\frac{\bar{X}_{32}}{d} = A\left[\frac{d\,\rho_L\,V_a}{\mu}\right]^B\left[\frac{\mu_G\,V_a}{\sigma_L}\right]^C$ where A = 1140, B = -0.82 and C = -0.45 for Venturi Atomizer.							
Fisenklam [13]	Venturi type internal mixer	Experimental data of other investigators correlated by dimensional analysis	Up to sonic velocity	0.01 to 0.3 poise	0.89 gm/cc	21 dyne/cm	Air/Fuel Oil
$\bar{X}_{20} = \frac{5.85\sqrt{\sigma_L}}{V_a\sqrt{\rho_L}} + \frac{725}{(\rho_L)^{1.25}}\left(\frac{\mu}{\sqrt{\sigma_L}}\right)^{0.4}\frac{1}{(W_R)^{1.5}}$							
Gretzinger and Marshall [14]	i. Converging Pneumatic Nozzle ii. Pneumatic Impingement Nozzle	Experimental data fitted on a log-log plot after forming dimensionless groups	300 to sonic velocity in ft/sec	1 to 30 centipoise	In the region of 1 gm/cc	50 dyne per cm	Air/Water
i. $X_{MMD} = 2600\left[\left(\frac{W_L}{W_G}\right)\left(\frac{(\mu_G)}{(\sigma)(L)}\right)\right]^{0.4}$							
ii. $X_{MMD} = 122\left[\frac{W_L}{W_G}\right]^{0.6}\left[\frac{(\mu_G)}{(\sigma)(L)}\right]^{0.15}$							

TABLE 6.5: Summary of Pneumatic Atomization Investigations

Continued ...

Investigator	Atomizer	Mathematical Treatment	Applicable Range				
			Relative Velocity	Liquid Viscosity	Liquid Density	Liquid Surface Tension	System Used
Wigg [15]	Twin fluid atomizer	Correlation of experimental data of other investigations for i. without coalescence ii. with coalescence or recombination of droplets	100 to 1100 ft/sec	0.45 to 40 centistokes		18 to 71 dynes per cm.	Air/Wax, Water, Iso-Octane, JFS Fuel, Benzene,
		i. $X_{MM} = 2.0 \left[\frac{(\sigma_L)^{0.5} (\mu_L)^{0.1} (1 + \frac{W_L}{W_G})^{0.5} (h)^{0.1} (\rho_L)^{0.2}}{(\rho_G)^{0.3} (V_A - V_L)}\right]$ ii. $X_{MM} = 2.0 \left[\frac{(\sigma_L)^{0.5} (\mu_L)^{0.1} (1 + \frac{W_L}{W_G})^{0.5} (h)^{0.1} (\rho_L)^{0.2}}{(\rho_G)^{0.3} (V_A - V_L)}\right] \times \left[1 + 2.5 \left(\frac{W_L}{W_G}\right)^{0.6} (\mu_L)^{0.1}\right]$					
Kim and Marshall [16]	i. single air nozzle atomizer ii. concentric double air nozzle atomizer	Empirical correlation of experimental data	250 ft/sec to sonic velocity	1 to 50 cp	0.782 to 0.834 gm/cc	31.2 dyne/cm	Air/Molten wax, melts of wax-polyethylene mixture
		i. $X_{MM} = \left[\frac{345 (\mu_L)^{.41} (\sigma_L)^{.32}}{\left[(V_A - V_L)^2 \rho_G\right]^{0.44} (h)^{0.16} (\rho_L)^{0.16}}\right] + 1260 \left[\frac{\mu_L^2}{\sigma_L \rho_L}\right]^{0.17} \left[\frac{1}{(V_A - V_L)^{0.54}}\right] \left[\frac{W_G}{W_L}\right]^C$ ii. $X_{MM} = \frac{8140}{\left[(V_A - V_L)^2 (\rho_G)\right]^{0.72}_{av.}} \left[\frac{(\mu_L)^{0.41} (\sigma_L)^{0.32}}{(\rho_L)^{0.16}}\right] \cdot 1240 \left[\frac{\mu_L}{\rho_L \sigma_L}\right]^{0.17} \frac{1}{\left[(V_A - V_L)_{av}\right]^{0.54}} \left[\frac{W_G}{W_L}\right]^C$ $[(V_A - V_L)^2 (\rho_G)]_{av.} = f [(V_A - V_L)^2 (\rho_G)]_{pri} + (1-f) [(V_A - V_L)^2 (\rho_G)]_{sec}$ $C = -1$, if $W_G/W_L < 3$ $= 0.5$, if $W_G/W_L > 3$					
Kumar and Prasad [17]	Pneumatic atomizer	Theoretical model proposed based on the forces acting on the drop		0.01 to 2.3 poise		37 to 64 dyne per cm	Air/Glycerine-water, Glycerine alcohol mixtures, water
		$\bar{K} \left[(r_2)^2 (\mu) (\rho_L)^{-1} (V_s)^{-1}\right] + \left[\frac{(\sigma_L)^2 (\rho_L) (V_s)^{-2/3}}{14.5 \left[\frac{\rho_L \sigma_L V_A}{2.5 \times 10^4}\right]^{\frac{2}{3}}}\right] = \rho_G \rho_G V_A$					

TABLE 6.5: Summary of Pneumatic Atomization Investigations

An alternate approach would be to compare the exponents of important parameters in each of the equations. Table 6.6 compares powers of selected parameters in the equations discussed previously. Except for the work of Gretzinger and Marshall [14] this crude comparison shows that there is rather good agreement (-0.5 to -1.7) for the exponent to which the relative velocity is raised. Relative velocity has generally been accepted as one of the most important variables controlling drop size.

Although extensive work has been done in the field of atomization, reliable equations for scrubber design seem to be scarce. Considering the theoretical models, it appears that the equations proposed by Mayer and Adelberg could be used to predict mean drop diameter for a wet scrubber, fairly accurately. The constants reported for these equations have been arbitrarily set at values close to unity, even though their actual values may be far less than that. It is difficult, if not impossible, to make a fair estimate of these constants, since they are expected to change with the conditions of atomization. Therefore if the constants used in these equations could be predicted, it is expected that the theoretical equations might give close predictions.

	Nozzle Diameter (d)	$(V_A - V_L)$	ρ_L	ρ_G	μ	μ_G	σ_L
Mayer [2]		-1.333	-0.333	-0.667	0.667		0.333
Adelberg [3]							
i. capilliary wave	0.5	-0.666	-0.16666	-0.333	0.333		0.17
ii. acceleration wave regime		-1.333	-0.333	-0.666	0.666		0.333
Fraser, Dombrowski & Routley [5]			-0.21	-0.5	0.21		0.50
Nukiyama and Tanasawa [6]		-1.00	-0.50		0.45		0.50
Wetzel and Marshall [7, 8]							
- wax	0.35	-1.68					
- alloy		-1.11					
Ingebo and Foster [9]	0.5		-0.25	-0.25	0.25		0.25
Ingebo [10]	0.5	-1.00					
Weiss and Worsham [11]		-1.334	-0.916		0.333	0.08333	0.41
Mugele [12]	0.18	-1.27	-0.82		0.82	-0.45	0.45
Eisenklam [13]		-1.00	-0.50		0.45		0.50
Gretzinger and Marshall [14]							
- convergent	-0.4	-0.4	0.4	-0.8		0.4	
- impingement	-0.15	-0.15	0.6	-0.75		0.15	
Wigg [15]		-1.00	-0.5	-0.3	0.5		0.2
Kim and Marshall [16]	-.72	-0.54 to -1.14	-0.16	-0.57	0.32		0.41
-single							
-double		-0.54 to -1.44	-0.16	-0.72	0.32		0.41

TABLE 6.6: Comparison of Exponent Values in Equations Predicting Mean Drop Sizes for Pneumatic Atomization

The semi-theoretical equation proposed by Fraser, Dombrowski, and Routley [5] for the atomization of liquid sheets seems to be the most reliable for prediction of drop diameters. As long as the mechanism of drop formation in a wet scrubber is not different from conditions for which their relationship was developed, reliable estimates of drop size can be made using this equation.

The empirical equations with direct application to wet collector design appear to be those of Ingebo and Foster [9], Ingebo [10] and Nukiyama-Tanasawa [6].

Differences between predicted and experimental mean drop diameter values are due to

i. limitations in drop size analysis techniques, including sampling methods

ii. changes in the mechanism of drop formation within the applicable range of operating conditions

iii. the narrow range for which each equation was developed

iv. the arbitrary manner in which some investigators introduced the effects of specific variables into their correlations.

REFERENCES

1. Behie, S. W., and Beckmans, J. M., Trajectory and Dispersion of Transverse Jets of Water in a Turbulent Air Stream, Personal Communication, July 29, 1974, University of Western Ontario, London, Ontario.

2. Mayer, E., Theory of Liquid Atomization in High Velocity Gas Streams, American Rocket Society Journal, 31 (12), 1783-1785 (1961).

3. Adelberg, M., Mean Drop Size Resulting from the Injection Of A Liquid Jet into a High Speed Gas Stream, Amer. Inst. of Aeronautics and Astronautics Jour., 6(6), 1143-1147 (1968).

4. Adelberg, M., Break up Rate and Penetration of a Liquid Jet in a Gas Stream, American Inst. of Aeronautics and Astronautics Jour., 5(8), 1408-1415 (1967).

5. Fraser, R. P., Dombrowski, N., and Routley, J. H., The Atomization of a Liquid Sheet by an Impinging Air Stream, Chemical Engineering Science, 18, 339-353 (1963).

6. Nukiyama, S., and Tanasawa, Y., Experiments on the Atomization of Liquids in an Air Stream, Reports 1-6, Transaction of Society for Mechanical Engineers (Japan), Volume 4, 5 and 6 (1938-40). English Translation by E. Hope, Defence Research Board, Department of National Defence, Canada, March 18, 1950, Translation No. E0/28220.

7. Wetzel, R. H., and Marshall, W. R., Paper Presented at Washington, D. C., National Meeting, American Institute of Chemical Engineers, March 1954.

8. Wetzel, R. H., Venturi Atomization, Ph.D. Thesis, University of Wisconsin (1952).

9. Ingebo, R. D., and Foster, H. H., Drop Size Distribution for Crosscurrent Break-up of Liquid Jets in Airstreams, N.A.C.A. Technical Note 4087, (1957).

10. Ingebo, R. D., Drop Size Distributions for Impinging Jet Break-up in Airstreams Simulating the Velocity Conditions in Rocket Combustors, N.A.C.A. Technical Note 4222, (1958).

11. Weiss, M. A., and Worsham, C. H., Atomization in High Velocity Airstreams, American Rocket Society Journal, 29 (4), 252-259 (1959).

12. Mugele, R. A., Maximum Stable Droplets in Dispersoids, American Institute of Chemical Engineers Journal, 6 (1), 3-8 (1960).

13. Eisenklam, P., Atomization of Liquid Fuel for Combustion, Journal of Institute of Fuel, 34, 130-143 (1961).

14. Gretzinger, J., and Marshall, W. R., Characteristics of Pneumatic Atomization, American Institute of Chemical Engineers Journal, 7 (2), 312-318 (1961).

15. Wigg, L. D., Drop Size Predictions for Twin-Fluid Atomizers, Journal Institute of Fuel, 37, 500-505 (1964).

16. Kim, K. Y., and Marshall, W. R., Drop Size Distributions from Pneumatic Atomizers, American Institute of Chemical Engineers Journal, 17 (3), 575-584 (1971).

17. Kumar, R., and Prasad, K. S. L., Studies on Pneumatic Atomization, Industrial Engineering Chemistry, Process Design and Development, 10 (3), 357-365 (1971).

18. Fraser, R. P., Dombrowski, N., and Routley, J. H., The Mechanism of Disintegration of Liquid Sheets in Cross-Current Air Streams, Appl. Sci. Res., Sec. A, 12, 143-150 (1963).

19. Dombrowski, N., and Johns, W. R., The Aerodynamic Instability and Disintegration of Viscous Liquid Sheets, Chemical Engineering Science, 18, 203 (1963).

20. Dombrowski, N., and Hooper, P. C., The Effect of Ambient Density on Drop Formation in Sprays, Chemical Engineering Science, 17, 291-305 (1962).

21. Fraser, R. P., Eisenklam, P., Dombrowski, N., and Hasson, D., Drop Formation from Rapidly Moving Liquid Sheets, American Institute of Chemical Engineers Journal, 8 (5), 672-680 (1962).

22. Fraser, R. P., Dombrowski, N., and Routley, J. H., The Production of Uniform Liquid Sheets from Spinning Cups, Chemical Engineering Science, 18, 315-321 (1963).

23. Fraser, R. P., Dombrowski, N., and Routley, J. H., The Filming of Liquids by Spinning Cups, Chemical Engineering Science, 18, 323-337 (1963).

24. Rayleigh, Lord, On the Instability of Jets, Proceedings of London Mathematics Society, 10, 4, 1878.

25. Haenlein, A., Ueber den Zerfall eines Flussigkeitsstrahles, Forschung auf dem Gebiete des Ingenieurwesens, 2, (4), 139, (1931). English Translation: Disintegration of a Liquid Jet; N.A.C.A. Tech. Memo N-. 659, February 1932.

26. Weber, C., Zum Zerfall eines Fluessigkeitsstrahles; Zeitschrift fuer angewandte Mathematik und Mechanik, 11, 136 (1931). (English Translation: On the Breakdown of a Fluid Jet; Ninth Progress Report, Project MX-833, Sect. II, University of Colorado, Boulder, Colorado).

27. Castleman, R. A., Jr., The Mechanism of the Atomization Accompanying Solid Injection; N.A.C.A. Report No. 440, 12 pp. (1932).

28. Castleman, R. A., Jr., The Mechanism of the Atomization of Liquids, Bur. Std. Jour. of Research, 6, (3), 369 (1931).

29. Lee, Dana, W., and Spencer, Robert C., Photo-micrographic Studies of Fuel Sprays, N.A.C.A. Report No. 454, 27 pp. (1933).

30. De Juhasz, Kalman, J., Zahn, O. F., and Schweitzer, P. H., On the Formation and Dispersion of Oil Sprays, Pennsylvania State College, Engr. Expt. Sta. Bulletin No. 40, 1932, 94 pp.

31. Schweitzer, P. H., Mechanism of Disintegration of Liquid Jets; Journal of Applied Physics, 8, 513 (1937).

32. Tyler, E., Instability of Liquid Jets, Phil. Magazine (London), 16, 504 (1933).

33. Fogler, B. B., and Kleinschmidt, R. V., Spray Drving, Ind. Eng. Chem., 30, 1372 (1938).

34. Siestrunck, Raymond, Sur les Regimes de Resolution des Jets Liquides sous L' Influence d'un Soufflage Axial, Comptes Rendus, 215, 404 (1942).

35. Littaye, Guy, Sur une Theorie de la Pulverisation des Jets Liquides, Comptes Rendus, 217, 99 (1943).

36. Littaye, Guy. Sur L'Atomisation d'un Jet Liquide, Comptes Rendus, 217, 340 (1943).

37. Littaye, Guy. Influence de la Vitesse de l'air sur le Diametre des plus Petites Gouttes Obtenues par Atomisation Pneumatique, Comptes Rendus, 218, 440 (1944).

38. Hinze, J. O., On the Mechanism of Disintegration of High Speed Jets, Intern de la Mechanique Appliquee, Paris, 2, 8 (1946).

39. Merrington, A. C., and Richardson, E. G., The Break-up of Liquid Jets, Proc. of the Physical Soc., 59, Part I, No. 331, 1, (1947).

40. Larcombe, H. L. M., Principles of Pressure Spray Nozzles, Chemical Age (London), 57, Part I, 563-566; Part II, 597-598; Part III, 621-623, (1947).

41. Baron, Thomas, Atomization of Liquid Jets and Droplets, University of Illinois Technical Report No. 4, February 15, 1949, 24 pp. (Prepared Under Contract N6-ori-71, Task Order No. XI, Office of Naval Research, Navy Department).

42. Joyce, J. R., The Atomization of Liquid Fuels for Combustion, Jour. of Inst. of Fuel, 22 (124), 150-156 (1949).

43. Borodin, V. A., and Dityakin, Y. F., Neustoichivye Kapillyarnye Volny na Poverkhnosti Razdela Dvukh Vyazkikh Zhidkostei, Prikladnaya Matematika i Mekhanika, Vol. XIII, No. 3, 1949, 19 pp. (Translation: Unstable Capillary Waves on Surface of Separation of Two Viscous Fluids; N.A.C.A. Tech. Memo, No. 1281, April 1951.)

44. Balje, O. E., and Larson, L. V., The Mechanism of Jet Disintegration, A.A.F. Air Material Command, Engineering Division Memorandum Report No. MCREXE - 664 - 531 B, GS-USAF - Wright Patterson No. 179, August 29, 1949, 48 pp.

45. Donnelly, J. J., and Wohl, K., Progress on Spray Research, Chemical Engineering Project, No. 62, University of Delaware Report No. 106, August 23, 1950, 18 pp. and 25 Fig.

46. Lane, W. R., Shatter of Drops in Streams of Air, Ind. Eng. Chem. 43, 1312 (1951).

47. York, J. Louis, Stubbs, H. E., and Tek, M. R., The Mechanism of Disintegration of Liquid Sheets, ASME Paper No. 53-S-40 presented Apr. 30, 1953 at Columbus, Ohio, Trans. ASME, 1279-1286 (1953).

48. Fraser, R. P., Dombrowski, N., Eisenklam, P., Vibrations as a Cause of Disintegration in Liquid Sheets, Nature, 4402, 495, March 13 (1954).

49. Dombrowski, N., and Munday, G., Spray Drying, Biochemical and Biological Engineering Science, Ed. N. Blakebrough Academic Press, (1968).

50. Lamb, H., Hydrodynamics, 6th ed., p. 625, Dover Publications, New York, 1945.

51. Mayer, E., Capillary Mechanisms of Liquid Atomization in High Velocity Gas Streams, Proceedings of the 12th International Astronautical Congress, Academic, New York, 1963, p. 731.

52. Ingebo, R. D., and Foster, H. H., Evaporation of JP-5 Fuel Sprays in Air Streams, N.A.C.A. RM E55 K02, 1956.

53. Kurzius, S. C., and Raab, F. H., Measurement of Droplet Sizes in Liquid Jets Atomized in Low-Density Supersonic Streams, Rept. TP 152, March 1967, Aerochem. Research Laboratories, Princeton, N.J.

54. Lewis, H. C., Edwards, D. G., Goglia, M. J., Rise, R. I. and Smith, L. W., Atomization of Liquids in High Velocity Gas Streams, Ind. Eng. Chem., 40, 67-74 (1948).

55. Sauter, J., Determining the Efficiency of Atomization by its Fineness and Uniformity, N.A.C.A. Tech. Memorandum No. 3960. Translated from Forsch. Gebiete Ingenieurw, No. 279 (1926).

56. Houghton, H. G., Chemical Engineers Handbook, 2nd Edition, Edited by J. H. Perry, pp 1984-1993, New York, McGraw-Hill Book Co., 1941.

57. Marshall, W. R., Atomization and Spray Drying, American Institute of Chemical Engineers Monograph No. 2, Vol. 50, p. 77, (1954).

58. Houghton, H. G., and Radford, W. H., Papers in Physical Oceanography and Meteorology, 6(3), (1938).

59. Lee, D. W., The Effect of Nozzle Design and Operating Conditions on the Atomization and Distribution of Fuel Sprays, National Advisory Committee on Aerodynamics, Technical Report No. 425 (1932).

60. Pierce, N. C., M. S. Thesis, University of Illinois (1947).

61. Ingebo, R. D., Vaporization Rates and Drag Coefficients for Iso-Octane Sprays in Turbulent Air Streams, N.A.C.A. Technical Note 3265, (1954).

62. Dvorak, D., Ann. Phys. 9, 502, (1880).

63. Foley, J., Phy. Rev. 16, 449 (1920).

64. Friedman, S. J., and Miller, C. O., Liquid Films in the Viscous Flow Regime, Ind. Eng. Chem., 33, 885-897 (1941).

65. Wigg, L. D., Unpublished Work at National Gas Turbine Establishment, July 1959. Quoted from Journal of Institute of Fuel, 37, 500-505 (1964).

66. Golitzine, N., Sharp, R., and Bacham, L. G., Spray Nozzles for the Simulation of Cloud Conditions in Icing Tests of Jet Engines, National Aeronautical Establishment, Canada, Report 14, (1951).

67. Clare, H., and Radcliff, A., An Air-Blast Atomizer for Use with Viscous Fuel, Journal of Institute of Fuel, 27, 510 (1954).

68. Fraser, R. P., and Eisenklam, P., Liquid Atomization and the Drop Size of Sprays, Transactions Institution of Chemical Engineers (London), 34, 294-319 (1956).

69. Wood, R., Unpublished Work at Thornton Research Centre, (U.K.), July 1954).

70. Pearl, R., Medical Biometry and Statistics, 2nd Edition, p. 417, W. B. Saunders Co., Philadelphia (1930).

71. Lapple, C. E., Henry, J. P., and Blake, D. E., Atomization - A Survey and Critique of the Literature, Stanford Research Institute, Technical Report No. 6, April 1967.

72. Tate, R. W., and Marshall, W. R., Atomization by Centrifugal Pressure Nozzles, Chemical Engineering Progress, 49, 169-174 (1953), Part I.

73. Tate, R. W., and Marshall, W. R., Atomization by Centrifugal Pressure Nozzles, Chemical Engineering Progress, 49, 226-234 (1953), Part II.

74. Longwell, J. P., Fuel Oil Atomization, Doctoral Dissertation Massachussets Institute of Technology (1943).

75. Turner, G. H., and Moulton, R. W., Drop Size Distribution From Spray Nozzles, Chemical Engineering Progress, 49, 185-190 (1953).

76. Orr, C., Spraying and Atomizing, Particulate Technology. The MacMillan Co., New York, p. 19 (1966).

77. Friedman, S. J., Gluckart, F. A., and Marshall, W. R., Centrifugal Disk Atomization, Chemical Engineering Progress, 48, 181-191 (1952).

78. Walton, W. H., and Prewett, W. C., The Production of Sprays and Mists of Uniform Drop Size by Means of Spinning Disc Type Sprayers, Proc. Physical Soc. 62 (354B), 341-350 (1949).

79. Fraser, R. P., Eisenklam, P., and Dombrowski, N., Liquid Atomization in Chemical Engineering, British Chemical Engineering, 2, 414-417 (1957).

80. Ryan, N. W., Mixing and Atomization by Impingement of Unconfined Liquid Jets, D.Sc. Thesis, Massachussetts Institute of Technology (1948).

81. Lang, R. J., Ultrasonic Atomization of Liquids, Journal of Acoustic Society of America, 34, 6-8 (1962).

82. Putnam, A. A., Benington, F., Einbinder, H., Hazard, H. R., Kettelle, J. D., Levy, A., Miesse, C. C., Pilcher, J. M., Thomas, R. E., Weller, A. E., and Landry, B. A., Injection and Combustion of Liquid Fuels, Wright Air Development Centre Tech. Rept, 56, 344, 2-6 (1957).

83. Fraser, R. P., Liquid Fuel Atomization, Sixth (International) Symposium on Combustion, Yale University, New Haven, Connecticut, August 19-24, 687-701 (1956).

84. Dorman, R. G., The Atomization of Liquid in a Flat Spray, British Journal of Applied Physics 3, 189-192 (1952).

85. Nelson, P. A., and Stevens, W. F., Size Distribution of Droplets from Centrifugal Spray Nozzles, AIChE Journal, 7 (1), 80-86 (1961).

86. Mizutani, Y., Uga, Y., and Nishimoto, T., An Investigation on Ultrasonic Atomization, Bulletin of Japan Society of Mechanical Engineers, 15 (83), 620-627 (1972).

87. Harmon, D. B., An Equation for Predicting a Mean Drop Size in a High Speed Spray, University of California, Berkeley, Publications in Engineering, 5(5), 145-158 (1953).

88. Takahashi, T., and Kitamura, Y., Break-up Length of a Liquid Jet in Atmosphere and Diameter of Drops Formed by Disintegration of a Jet, Kagaku Kogaku, 36(5), 527-533 (1972).

89. Dunskiy, V. F., Nikitin, N. V., and Tonkacheyeva, N. F., Satellite Droplets Forming During Atomization of Liquids by Rotating Disk, Fluid Mechanics-Soviet-Research, 1 (1), 110-113 (1972).

90. Baryshev, Yu, N., Vachagin, K. D., Nikolaev, V. S., Atomization of Liquids by Rapidly Rotating Discs with Gas Stream Interaction (Cocurrent), International Chem. Eng., 9 (4), 579-580 (1969).

91. Chechik, O. S., and Lyuminarskii, B. M., Calculations of the Diameter of Drops Formed During Centrifugal Spraying of Liquids. Zhurnal Prikladnoi Khimi, 45 (4), 895-897 (1972), English Translation by Consultants Bureau.

92. Clark, C. J., and Dombrowski, N., On the Formation of Drops From the Rims of Fan Spray Sheets, Aerosol Sci. 3, 173-183 (1972).

93. Dombrowski, N., and Johns, W. R., The Aerodynamic Instability and Disintegration of Viscous Liquid Sheets, Chem. Eng. Sci., 18, 203-214 (1963).

94. Hasson, D., and Mizrahi, J., The Drop Size of Fan Spray Nozzles: Measurements by the Solidifying Wax Methods Compared with those Obtained by Other Sizing Techniques, Trans. Instn. Chem. Engr., 39, 415-422 (1961)..

95. Wissema, J. G., and Davies, G. A., The Formation of Uniformly Sized Drops by Vibration-Atomization, Can. Journal Chem. Eng. 47, 530-535 (1969).

96. Eisenklam, P., Dombrowski, N., and Hasson, D., Ministry of Supply Rept. No. D.G.G.W./E.M.R./59/3.

97. Rajagopalan, R., Tien, Chi, and Subramanian, G., Production of Mono-Dispersed Drops by Vibration-Atomization, Can. J. Chem. Eng., 50, 410-411 (1972).

98. Straus, R., The Mechanism of Formation of Liquid Droplets in Sprays, Ph.D. Thesis, University of London (1949).

99. Kuchn, R., Uber die Zerstaubung Flussiger Brennstoffe; English Translation N.A.C.A. Technical Memorandum, No. 329 (1925).

100. Kuchn, R., Uber die Zerstaubung Flussiger Brennstoffe; English Translation N.A.C.A. Technical Memorandum No. 330 (1925).

101. Hodkinson, T. G., Control of Surface Tension of a Conical Fluid Sheet Jet, May 1950, Porton Technical Paper, Unpublished.

102. Wang, K. H., and Tien, Chi., Atomization and Drop Size of Polymer Solution, Ind. Eng. Chem., Process Des. Develop, 11 (2), 169-178 (1972).

103. Baranaev, M. K., and Tenyakov, V. I., Centrifugal Injector Droplet Size Over a Wide Range of Dispersant Properties, Izv. ANSSSR, Mekhanika Zhidkosti i Gaza, 5 (3), 155-162 (1970); (English Translation from Consultants Bureau).

104. Holroyd, H. B., On the Atomization of Liquid Jets, Journ. Franklin Inst. 215, 93-97 (1933).

VII. APPLICATION TO VENTURI SCRUBBER DESIGN

The equations reported in the previous chapter can be used to predict mean drop diameters. In the past, mean drop sizes provided the basic variable for collection efficiency studies involving inertial impaction type scrubbers. The purpose of this chapter is to apply the drop size distribution data to the interpretation of Venturi scrubber performance. A determination of the penetration of a single air-atomized liquid jet before it disintegrates and a subsequent evaluation of the droplet distribution in the throat of the Venturi provides a simple model. Recent studies [1] show that the distribution of drops in the throat is far less uniform than expected from visual observation. The maldistribution of drop sizes may be primarily responsible for theoretical assessments of particle collection overestimating actual performance.

The experimental data obtained by Ingebo and Foster [2] have been used as a basis for the comparison of mean drop sizes predicted by the presently available correlations.

A. Comparison of Existing Equations

The predictions of mean drop diameters, by equations 6.6, 6.8, 6.9, 6.16, 6.18-6.20, 6.27-6.29, 6.32-6.34, 6.37, 6.38, 6.41 and 6.44 have been compared with the data of Ingebo and Foster [2] in Table 7.1.

Ingebo and Foster [2] provide drop size distribution data for iso-octane jets injected in the downward (y) direction into a turbulent air stream. Their experimental conditions which have been used for the preparation of Table 7.1 are summarized in Table 7.2.

The Ingebo and Foster [2] study involved measurement of drop size distributions at various distances, y, from the point of injection. From an analysis of the data given in Table 7.3, values of $\bar{X}_{20}$, $\bar{X}_{30}$ and $\bar{X}_{32}$ have been calculated for y = 0-1.5, 1.5-2.1, 2.1-2.5, 2.5-2.9 and 2.9-3.5 inches. The results are summarized in Tables 7.4, 7.5 and 7.6 respectively. The extent of drop size maldistribution is illustrated by the variations in surface, $\bar{X}_{20}$, volume, $\bar{X}_{30}$, and Sauter mean, $\bar{X}_{32}$, diameters at various regions across the flow area of the duct. For example the surface mean diameter, $\bar{X}_{20}$, varies from 33.55 microns at y = 0-1.5 inches to 135.15 microns at y = 2.9-3.5 inches. Similarly the volume mean diameter, $\bar{X}_{30}$, varies from 35.08 microns at y = 0-1.5 inches to 143.38 microns at y = 2.9-3.5 inches.

Investigator	Mean Drop Diameter Correlated	Predicted Diameter μ	Experimentally Obtained Diameter μ
Mayer [3]	$\bar{X}_{10}$	101.28	55.24
Adelberg [4,5]			
i. Capillary wave regime	i. $\bar{X}_{10}$	44.81	55.24
ii. Acceleration wave regime	ii. $\bar{X}_{10}$	119.53	55.24
Nukiyama-Tanasawa [6]	$\bar{X}_{32}$	298.48	114.18
Wetzel & Marshall [7,8]			
i. Molten wax	$\bar{X}_{oo}$	1781.20	44.83
ii. Molten alloy	$\bar{X}_{oo}$	1330.10	44.83
Ingebo & Foster [2]	$\bar{X}_{30}$	150.35	80.83
Ingebo [10]	$\bar{X}_{30}$	5.48	80.83
Weiss & Worsham [11]	X_{MM}	43.90	132
Mugele [12]	$\bar{X}_{32}$	2173.16	1141.18
Eisenklam [13]	$\bar{X}_{20}$	408.45	68.00
Kim & Marshall [14]	X_{MM}	581.34	132
Gretzinger & Marshall [15]			
i. Converging pneumatic nozzle	i. X_{MM}	16.07	132
ii. Pneumatic impinging nozzle	ii. X_{MM}	1.59	132
Wigg [16]			
i. With coalescence	i. X_{MM}	240.65	132
ii. Without coalescence	ii. X_{MM}	215.93	132
Kumar & Prasad [17]	$\bar{X}_{10}$	6.59	55.24

TABLE 7.1: Comparison of Predicted and Experimentally Determined Drop Diameters Using Data of Ingebo and Foster [2].

Liquid injected	=	Iso-octane
Injector orifice diameter	=	0.030 in
	=	0.0762 cm
Air stream velocity, V_A	=	100 ft/sec
	=	3048 cm/sec
Air temperature	=	88°F
Air pressure	=	29.3 inches of mercury absolute
Air density, ρ_G	=	0.071 lb /ft^3
	=	0.001137 gm/cm^3
Liquid jet velocity, V_L	=	51 ft/sec
	=	1554.48 cm/sec
Liquid temperature	=	93°F
Liquid density, ρ_L	=	42.6 lb /ft^3
	=	0.6824 gm/cm^3
Liquid viscosity, μ	=	4.75 millipoise
	=	.00475 poise
Liquid surface tension, σ_L	=	20.7 dynes/cm
Air viscosity, μ_G, at 88°F and 29.3 inches of pressure	=	0.000176 poise
Density of water at 88°F	=	0.9995 gm/cm^3

TABLE 7.2: Experimental Conditions of Ingebo and Foster [2] Used for Comparison of Predictive Equations

continued ..

Viscosity of water at 88°F = 0.0084 poise

$W_G = (100)\frac{(4x12)}{(144)} x\ (0.071)(453.5923) = 1073.5017$ gm/sec

$W_L = (51)(\pi)\frac{(0.015)^2}{144}(42.6)(453.5923) = 4.8374$ gm/sec

$Q_G = \frac{1073.5017}{0.001137} = 944152.77\ cm^3/sec$

$Q_L = \frac{4.8374}{0.6824} = 7.089\ cm^3/sec$

$A = 6" \times 4" = 24\ in^2$

$G = \frac{1073.5017}{(12)(4)(2.54)(2.54)} = 3.4665\ \frac{gm}{sec\text{-}cm^2}$

$L = .0762$ cm

$j = \frac{(2)}{(5)}(\pi/2)^{1/2}(e)^{3/2}(K_4)(\beta)$

$K_4 = 1,\ \beta = 1,\ K_1 = 1$

$d_{max} = 0.0762$ cm

$h = (2.00) - \frac{(0.030)}{(2)} = 5.0419$ cm

$\nu = \frac{(.00475)}{(0.6824)} = 6.9607 \times 10^{-3}$ stokes

$V_a = 3048 - 1554.48 = 1493.52$ cm/sec

$N_{Re} = (d)(V_a)/(\nu) = (.0762)(1493.52)/(.0069)$

$= 16349$

TABLE 7.2: Experimental Conditions of Ingebo and Foster [2] Used for Comparison of Predictive Equations

continued ..

$$N_{We} = (\rho_G)\ (d)\ (V_a^2)/(\sigma_L)$$

$$= (0.001137)(0.0762)(1493.52)^2/(20.7)$$

$$= 9.3$$

TABLE 7.2: Experimental Conditions of Ingebo and Foster [2] Used for Comparison of Predictive Equations

Distance from Orifice, y, in Class Interval ΔR_i	$\bar{R}_i$	0-1.5 in $(\Delta N_i)_{0-1.5}$	1.5-2.1 in $(\Delta N_i)_{1.5-2.1}$	2.1-2.5 in $(\Delta N_i)_{2.1-2.5}$	2.5-2.9 in $(\Delta N_i)_{2.5-2.9}$	2.9-3.5 in $(\Delta N_i)_{2.9-3.5}$
7.5-20	15	0	60	0	0	0
20-32.5	25	120	575	22	0	0
32.5-45	40	81	193	45	0	0
45-57.5	50	0	193	83	13	0
57.5-70	65	7	66	49	4	3
70-82.5	75	0	23	40	7	6
82.5-95	90		36	52	11	7
95-107.5	100		13	38	10	6
107.5-120	115		10	19	20	3
120-132.5	125		5	36	21	6
132.5-145	140		3	18	18	3
145-157	150		1	10	0	0
157.5-170	165		0	6	10	3
170-182.5	175		1	9	7	3
182.5-195	190		0	5	7	3
195-207.5	200			0	3	3
207.5-220	215			0	0	4
220-232.5	225			2	1	0
		208	1174	414	142	46

Class Interval ΔR_i	$(\bar{R}_i)^2 (\Delta N_i)_{0-1.5}$	$(\bar{R}_i)^3 (\Delta N_i)_{0-1.5}$	$(\bar{R}_i)^2 \Delta N_i)_{1.5-2.1}$	$(\bar{R}_i)^3 \Delta N_i)_{1.5-2.1}$	$(\bar{R}_i)^2 \Delta N_i)_{2.1-2.5}$	$(\bar{R}_i)^3 \Delta N_i)_{2.1-2.5}$	$(\bar{R}_i)^2 \Delta N_i)_{2.5-2.9}$	$(\bar{R}_i)^3 \Delta N_i)_{2.5-2.9}$	$(\bar{R}_i)^2 \Delta N_i)_{2.9-3.5}$	$(\bar{R}_i)^3 \Delta N_i)_{2.9-3.5}$
7.5-20										
20-32.5	0	0	13,500	202,500	0	0	0	0	0	
32.5-45	73,000	1,875,000	159,375	5,906,375	11,250	443,750	0	0	0	
45-57.5	129,600	5,184,000	108,000	12,150,000	22,500	2,880,000	0	0	0	
57.5-70	0	0	402,500	24,125,000	207,900	18,375,000	37,500	1,875,000	0	
70-82.5	28,575	1,823,375	270,400	17,576,000	207,025	13,456,625	10,000	1,000,500	12,675	823,875
82.5-95			129,375	9,703,125	225,000	16,875,000	30,375	2,953,125	11,750	2,531,250
95-107.5			275,400	26,706,000	421,200	37,900,000	99,100	9,819,000	56,700	5,103,000
107.5-120			170,000	13,000,000	300,000	30,000,000	100,000	10,000,000	60,000	6,000,000
120-132.5			132,250	15,200,750	251,275	30,034,625	364,500	30,617,500	35,625	3,562,625
132.5-145			78,125	9,765,625	962,500	76,312,500	390,625	48,828,125	62,500	7,812,500
145-157			30,300	5,400,000	352,800	49,392,000	294,000	41,160,000	6,000	8,232,000
157.5-170			22,500	3,375,000	225,000	33,750,000	100,000	37,000,000	0	0
170-182.5			0	0	163,350	26,052,750	272,250	40,021,250	61,875	11,876,175
182.5-195			30,625	5,359,375	275,625	48,234,375	210,375	37,515,625	61,250	10,718,750
195-207.5			0	0	180,500	34,295,000	252,700	48,013,000	100,100	20,577,000
207.5-220					0	0	90,000	16,000,000	80,000	16,000,000
220-232.5					0	0	0	0	144,400	39,753,500
					101,250	23,791,250	56,925	11,190,625	0	0
	258,175	9,883,375	2,272,050	148,025,750	5,830,375	414,452,875	2,281,995	349,491,750	840,225	135,590,875

TABLE 7.3: Analysis of Ingebo and Foster [2] Data for Drop Diameters Measured at Various Distances in the Downward y Direction From the Point of Liquid Injection

$$\bar{X}_{20} = \left[\frac{\sum_{i=1}^{h} (\bar{X}_i)^2 \, \Delta N_i}{\sum_{i=1}^{h} \Delta N_i} \right]^{\frac{1}{2}}$$

$$[\bar{X}_{20}]_{0-1.5} = \left[\frac{234,175}{208}\right]^{\frac{1}{2}} = 33.55\mu$$

$$[\bar{X}_{20}]_{1.5-2.1} \left[\frac{2,272,050}{1174}\right]^{\frac{1}{2}} = 43.99\mu$$

$$[\bar{X}_{20}]_{2.1-2.5} \left[\frac{3,638,775}{434}\right]^{\frac{1}{2}} = 91.57\mu$$

$$[\bar{X}_{20}]_{2.5-2.9} = \left[\frac{2,281,950}{142}\right]^{\frac{1}{2}} = 126.77\mu$$

$$[\bar{X}_{20}]_{2.9-3.5} = \left[\frac{840,225}{46}\right]^{\frac{1}{2}} = 135.15\mu$$

TABLE 7.4: Surface Mean Diameters Calculated at Various Distances in the Downward y Direction From the Point of Liquid Injection for Data of Ingebo and Foster [2]

$$\bar{X}_{30} = \left[\frac{\sum_{i=1}^{h} (\bar{X}_i)^3 \, \Delta N_i}{\sum_{i=1}^{h} \Delta N_i} \right]^{\frac{1}{3}}$$

$$[\bar{X}_{30}]_{0\text{-}1.5} \left[\frac{8,981,375}{208}\right]^{\frac{1}{3}} = 35.08\mu$$

$$[\bar{X}_{30}]_{1.5\text{-}2.1} = \left[\frac{149,925,750}{1174}\right]^{\frac{1}{3}} = 50.36\mu$$

$$[\bar{X}_{30}]_{2.1\text{-}2.5} = \left[\frac{434,452,875}{434}\right]^{\frac{1}{3}} = 100.03\mu$$

$$[\bar{X}_{30}]_{2.5\text{-}2.9} = \left[\frac{329,191,750}{142}\right]^{\frac{1}{3}} = 132.35\mu$$

$$[\bar{X}_{30}]_{2.9\text{-}3.5} = \left[\frac{135,590,875}{46}\right]^{\frac{1}{3}} = 143.38\mu$$

TABLE 7.5: Volume Mean Diameters Calculated at Various Distances in the Downward y Direction From the Point of Liquid Injection for Data of Ingebo and Foster [2]

$$\bar{X}_{32} = \frac{\sum_{i=1}^{h} (X_i)^3 \Delta N_i}{\sum_{i=1}^{h} (X_i)^2 \Delta N_i}$$

$$[\bar{X}_{32}]_{0-1.5} = [\frac{8,981,375}{234,175}] = 38.35\mu$$

$$[\bar{X}_{32}]_{1.5-2.1} = [\frac{149,925,750}{2,272,050}] = 65.99\mu$$

$$[\bar{X}_{32}]_{2.1-2.5} = [\frac{434,452,875}{3,638,775}] = 119.40\mu$$

$$[\bar{X}_{32}]_{2.5-2.9} = [\frac{329,191,750}{2,281,950}] = 144.26\mu$$

$$[\bar{X}_{32}]_{2.9-3.5} = [\frac{135,590,875}{840,225}] = 161.37\mu$$

TABLE 7.6: Sauter Mean Diameters Calculated at Various Distances in the Downward y Direction From the Point of Liquid Injection for Data of Ingebo and Foster [2]

In order to obtain an averaged value for the drop distribution over the entire cross-section of the duct, the number of drops, ΔN_i, for a particular class mid point diameter, $\bar{X}_i$, was summed with the process repeated for the entire range of drop sizes. The results of this summing process are shown in Table 7.7. Averaged values of geometric, length, surface, volume and Sauter mean diameters were estimated as shown in Table 7.8. In order to obtain the value of, X_{MM}, the mass median diameter, $F(X^3)$ was plotted against X, according to Figure 7.1, to yield X_{MM} = 132 microns.

The comparisons of predicted and experimentally determined drop diameters in Table 7.1 show poor agreement. Only the Adelberg [4,5] capillary wave regime treatment approximates the test data. Unfortunately the analysis of Adelberg [4,5] does not provide any theoretical background for estimation of drop diameter in the intermediate region (between the capillary wave and acceleration wave regimes). In terms of the Adelberg analysis, the data of Ingebo and Foster [2] appear to be in the intermediate region, but closer to the capillary wave regime. It must be emphasized that Adelberg [4,5] did not clearly define the average diameter that he used for his correlation. It appears that the length mean diameter, $\bar{X}_{10}$, is the most appropriate average dimension for his relationship.

Class Interval	$\bar{X}_i$	ΔN_i	$(\ln \bar{X}_i)\ \Delta N_i$	$(\bar{X}_i^2)\ \Delta N_i$	$(\bar{X}_i^3)\ \Delta N_i$	$F(X^3)$	$(\bar{X}_i)\ \Delta N_i$
7.5 - 20	15	60	162.48	13,500	202,500	.000191	900
20 - 32.5	25	717	2307.93	448,125	11,203,125	.01078	17,925
32.5 - 45	40	319	1176.75	510,400	20,416,000	.0300	12,760
45 - 57.5	50	291	1138.40	727,500	36,375,000	.0644	14,550
57.5 - 70	65	127	530.15	536,575	34,877,375	.0974	8,255
70 - 82.5	75	76	328.1	427,500	32,062,500	.1277	5,700
82.5 - 95	90	104	467.98	842,400	75,816,000	.1994	9,360
95 - 107.5	100	67	308.55	670,000	67,000,000	.2627	6,700
107.5 - 120	115	52	246.74	687,700	79,085,500	.3374	5,980
120 - 132.5	125	70	337.98	1,093,750	136,718,750	.4666	8,750
132.5 - 145	140	38	187.78	744,800	104,272,000	.5652	5,320
145 - 157.5	150	19	95.20	427,500	64,125,000	.6258	2,850
157.5 - 170	165	19	97.01	517,275	85,350,375	.7064	3,135
170 - 182.5	175	19	98.13	581,875	101,828,125	.8027	3,325
182.5 - 195	190	15	78.7	541,500	102,885,000	.8999	2,850
195 - 207.5	200	4	21.19	160,000	32,000,000	.9301	800
207.5 - 220	215	4	21.48	184,900	39,753,500	.9677	860
220 - 232.5	225	3	16.25	151,875	34,171,875	1.000	675
		2004	7620.85	9,267,175	1,058,142,625		110,695

TABLE 7.7: Analysis of Ingebo and Foster [2] Data for Drop Diameters Averaged Across the Flow Area

$$\bar{X}_{oo} = \frac{7620.8476}{2004} = 3.8028$$

Therefore $\bar{X}_{oo} = 44.83\mu$

$$\bar{X}_{20} = \left[\frac{9,267,175}{2004}\right]^{\frac{1}{2}} = 68.00\mu$$

$$\bar{X}_{30} = \left[\frac{1,058,142,625}{2004}\right]^{\frac{1}{3}} = 80.83\mu$$

$$\bar{X}_{32} = \left[\frac{1,058,142,625}{9,267,175}\right] = 114.18\mu$$

$$\bar{X}_{10} = \frac{110695}{2004} = 55.24\mu$$

$X_{MM} = 132\mu$ (From Figure 7.1)

TABLE 7.8: Averaged Mean Drop Diameter Calculated for Duct Cross-Section Using Data of Ingebo and Foster [2]

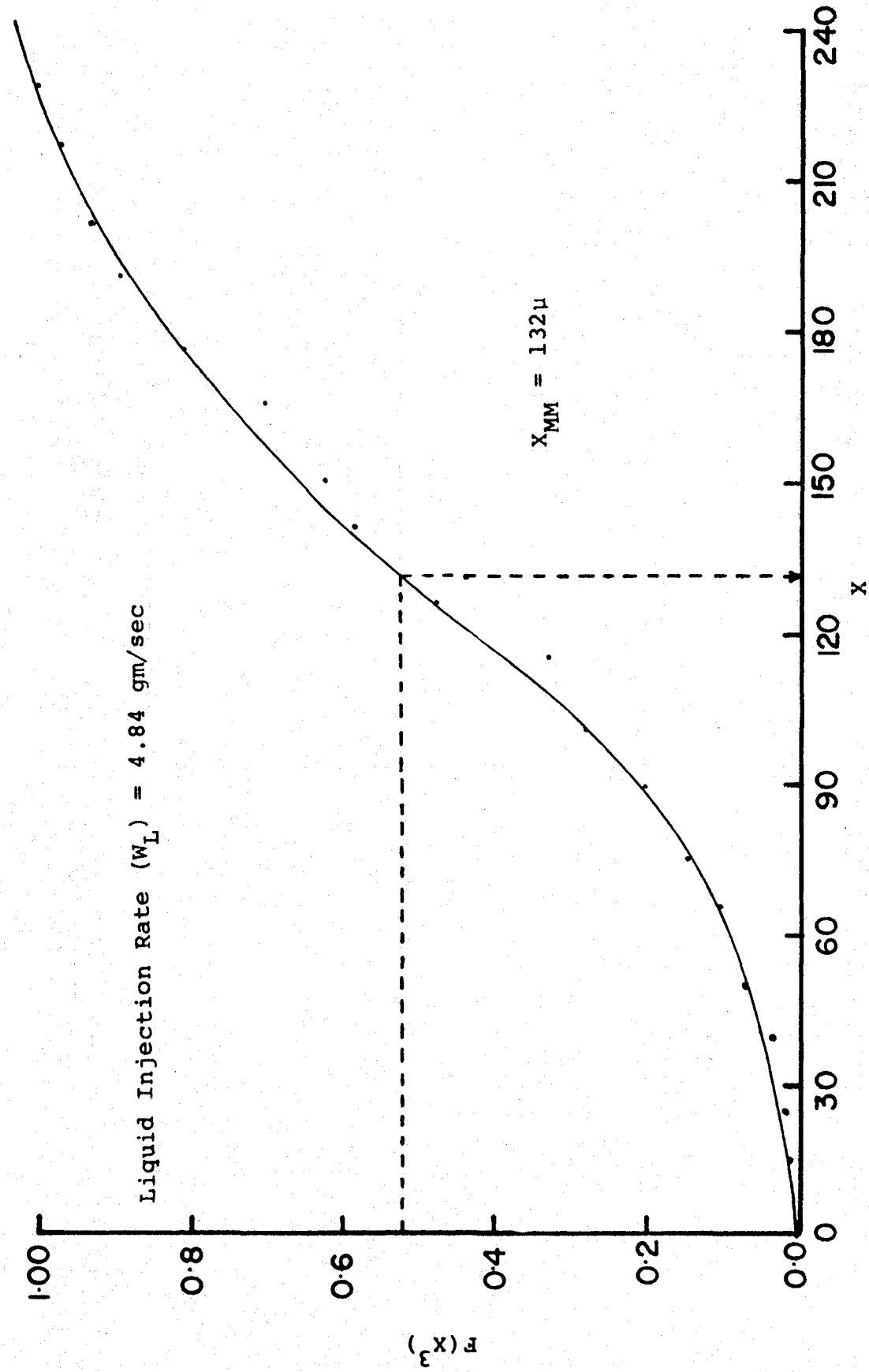

FIGURE 7.1; Cumulative Volume Distribution for Data of Ingebo and Foster [2]

Generally, predicted drop sizes are 2 to 40 times greater than experimentally found values, but the equation proposed by Gretzinger and Marshall [15] predicts much lower values.

Although the theoretical equations proposed by Mayer [3] and Adelberg [4,5] appear to approximate experimentally found mean drop diameters, the Adelberg [4,5] analysis is handicapped by the evaluation of the constants β, K, K_4 and e, whose actual values are not known.

Empirical equations tend to provide poorer agreement with experimentally found mean drop diameters, especially when the location and position of the injector with respect to gas flow, the type of injector system used, or the range of variables are changed significantly from the conditions for which any equation was developed. Another approach would be to compare the entire drop size spectrum (predicted by distribution functions), with the experimental data. It is possible that the predicted drop size distribution may not vary substantially from the experimental values contrary to what the comparisons of mean values show. This might be a good exercise for future work.

B. Penetration of a Single Jet

The estimation of the distance that a liquid jet will travel before disintegrating when injected into a high velocity gas stream is based on the analysis of Adelberg [5]. He suggested that the penetration length, ℓ^*, in the acceleration wave regime can be expressed by the relationship

$$\ell^* = (d_{max}/b)\,[L(\theta_o)\ I\ \{\theta,\ J/2b\}] \qquad 7.1$$

where

ℓ^* = penetration length of jet, cm

d_{max} = maximum jet diameter, cm

b = dynamic pressure ratio parameter, dimensionless

θ_o = maximum angle jet axis makes with free stream velocity vector, degrees

$$J = \left[\frac{(\sqrt{2})\,(j)\,\sqrt{n}}{(\pi)\,(\sqrt{C_{Do}})}\right]\left[\frac{(\frac{1}{2})\,(\rho_G)\,(V_A)^2}{(\frac{1}{2})\,(\rho_L)\,(V_L)^2}\right]^{1/2} \qquad 7.2$$

j = modified sheltering parameter, dimensionless

n = shock dynamic pressure ratio

$= [\bar{\rho}_G(\bar{V}_A)^2/(\rho_G\ V_A^2)]$, dimensionless

C_{Do} = drag coefficient for a cylinder in cross flow, dimensionless

The dimensionless functions $L(\theta_o)$ and $I(\theta, J/2b)$ are given by

$$L(\theta_o) = \left[\frac{1 + \text{Cos}\ \theta_o}{1 - \text{Cos}\ \theta_o}\right]^{J/2b} \exp\left[(J/2b)\left(\frac{\text{Cos}\ \theta_o}{\text{Sin}^2\ \theta_o}\right)\right] \qquad 7.3$$

and

$$I(\theta, J/2b) = \int_{\theta_o}^{\theta} \left[\frac{1 + \cos\theta}{1 - \cos\theta}\right]^{-(J/2b)} \left[\frac{\exp-[(J/2b)(\cos\theta/\sin^2\theta)]}{\sin\theta}\right] d\theta \qquad 7.4$$

where

θ = angle jet axis makes with free stream velocity vector at any point, degrees

and

$$b = \left(\frac{2\ C_{Do}}{\pi}\right)\left(\frac{\rho_G\ V_A^{\ 2}}{\rho_L\ V_L^{\ 2}}\right) \qquad 7.5$$

For a jet disintegrating in the capillary wave regime, Adelberg [5] suggested an equation for the penetration length in the form

$$\frac{s}{d_{max}} = \left[\frac{b}{\cot\theta - \cot\theta_o} + \frac{\sqrt{d_{max}}}{\pi}\left[\frac{(\frac{1}{2})(\rho_G\ V_A^{\ 2})}{(\frac{1}{2})(\rho_L\ V_L^{\ 2})}\right]\left[\frac{L\ V_L^{\ 2}}{\sigma_L}\right]^{\frac{1}{2}} j_\sigma\right]^{-1} \qquad 7.6$$

where

s = arc length measured along liquid jet axis, cm

j_σ = modified sheltering parameter for the capillary wave regime, dimensionless

The procedure for applying these equations is illustrated using experimental data of Ingebo and Foster [2]

Step I: Find C_{Do}

The Reynolds number based on free stream properties and jet diameter is given by

$$N_{Re} = (d_{max})\ (V_A)(\rho_L)/(\mu)$$

$$= (0.0762)(3048)(0.6824)/(0.00475)$$

$$= 3.34 \times 10^4$$

For $10^4 < N_{Re} < 5 \times 10^5$, $C_{Do} = 1.2$

$N_{Re} > 6 \times 10^5$, . $C_{Do} \approx 0.4$

$1 < N_{Re} < 10^3$, C_{Do} is given by

$$C_{Do} = \frac{(10.9)/N_{Re}}{0.87 - \log N_{Re}} \qquad 7.7$$

For the Ingebo and Foster [2] experimental conditions

$$C_{Do} = 1.2$$

Step II: Find the regime in which breakup occurs by calculating critical λ.

$$\lambda_{cr} = [(\pi)^3 (\sigma_L)(d)/\{(C_{Do})(\sin^2\phi)(\tfrac{1}{2})(\rho_G)(V_A^2)\}]^{\frac{1}{2}}$$

$$= \left[\frac{(\pi)^3 (20.7)(0.0762)}{(1.2)(1)(\frac{1}{2})(0.001137)(3048)^2}\right]^{\frac{1}{2}}$$

$$= 7.7162 \times 10^{-3} \text{ cm}$$

$$\lambda_{max} = 0.06 \times .0762 = 4.572 \times 10^{-3} \text{ cm}$$

Although the value of λ_{max} is less than λ_{cr}, it is comparable to λ_{cr}. This indicates that breakup occurs in the intermediate region, but close to the capillary wave regime. However, Adelberg [5] also states "For jets of the order of 0.02 to 0.1 inches in diameter, typical of those reported in the literature, injected into high-speed gas streams the critical free stream dynamic pressure above which acceleration waves are more important than capillary waves is somewhere in the range of 300 psf". If this is true then Ingebo and Foster [2] breakup falls outside the capillary wave regime.

Based on the arguments of a critical wave length, λ_{cr}, and a free stream dynamic pressure, it appears that the data of Ingebo and Foster [2] fall in the intermediate region. Since theoretical treatments for the intermediate

region are not available, jet penetrations for both capillary and acceleration wave regimes will be estimated.

Step III: Find the value of b from

$$b = \frac{(2\ C_{Do})}{(\pi)} \frac{(\rho_G\ V_A^{\ 2})}{(\rho_L\ V_L^{\ 2})}$$

$$= \frac{(2\ x\ 1.2)}{(\pi)} \frac{(0.00137)(3048)^2}{(0.6824)(1554.48)}^2$$

$$= 0.0049$$

Step IV: Find the penetration length in the capillary wave regime according to

$$\frac{s}{d_{max}} = \left[\frac{b}{(Cot\theta - Cot\theta_o)} + \frac{\sqrt{d_{max}}}{(\pi)} \left[\frac{\frac{1}{2}\rho_G\ V_A^{\ 2}}{\frac{1}{2}\ \rho_L\ V_L^{\ 2}} \right] \left[\frac{(\rho_L)\ (V_L^{\ 2})}{(\sigma_L)} \right]^{\frac{1}{2}} j_\sigma \right]^{-1}$$

Since the jet ultimately aligns itself with the X-axis centreline, $\theta=0$. Adelberg [5] recommends a value of $j_\sigma = 3.2 \times 10^{-3}$.

Accordingly

$$\frac{s}{(.0762)} = \left\{\frac{.0049}{\text{Cot}0-\text{Cot}90} + \frac{\sqrt{.0762}}{\pi}\left[\frac{(.001137)(3048)^2}{(.6824)(1554.48)^2}\right] \times \left[\frac{(.6824)(1554.48)^2}{20.7}\right] \times (3.29 \times 10^{-3})\right\}^{-1}$$

or $s = (.0762)\ \{0.000523\}^{-1}$

$= 145.6979$ cm.

Since practical considerations do not justify this high value, it is rejected. Jet penetration for the acceleration wave regime is therefore estimated.

Step V: Estimate J

$$J = \left[\frac{(\sqrt{2})(j)(\sqrt{n})}{(\pi)\ (C_{Do})^{\frac{1}{2}}}\right]\left[\frac{(\frac{1}{2})(\rho_G)(V_A)^2}{(\frac{1}{2})(\rho_L)(V_1)^2}\right]^{\frac{1}{2}}$$

The value of n from Figure 7.2 is 1.4, and j = 0.8 as given by Adelberg [5].

On this basis

$$n = \frac{\bar{\rho}_G \bar{V}_A^2}{\rho_G V_A^2}$$

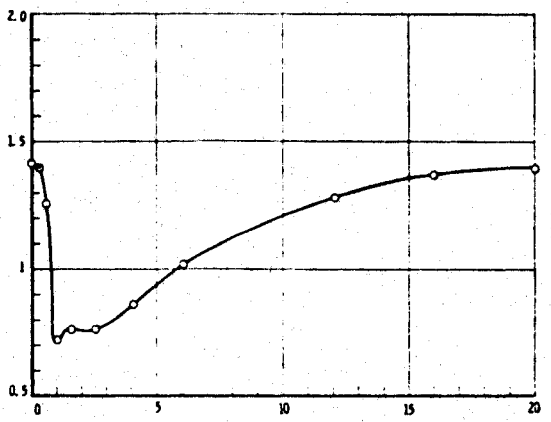

Mach Number

FIGURE 7.2: 'n' as a Function of Mach Number [5]

$$J = \left[\frac{(\sqrt{2})(0.8)(\sqrt{1.4})}{(\pi)(\sqrt{1.2})}\right]\left[\frac{(.001137)(3048)^2}{(0.6824)(1554.48)^2}\right]^{\frac{1}{2}}$$

$$= 0.0311$$

Step VI: Estimate $L(\theta_o)$

$$J/2b = \frac{.0311}{(2)(.0049)} = 3.1735$$

Therefore $$L(\theta_o) = \left[\frac{1+\cos\theta_o}{1-\cos\theta_o}\right]^{J/2b} \exp\left[\left(\frac{J}{2b}\right)\left(\frac{\cos\theta_o}{\sin^2\theta_o}\right)\right]$$

$$= \left[\frac{1+\cos 90}{1-\cos 90}\right]^{3.1735} \exp\left[\frac{(3.1735)(\cos 90)}{\sin^2 90}\right]$$

$$= 1$$

Step VII: Estimate $I(\theta, J/2b)$

In order to use the equation

$$I(\theta, J/2b) = \int_{\theta_o}^{\theta} \left[\frac{1+\cos\theta}{1-\cos\theta}\right]^{-(J/2b)} \times \frac{\exp-[(J/2b)(\cos\theta/\sin^2\theta)]}{\sin\theta}\, d\theta$$

more readily, Adelberg [5] employed numerical techniques and presented the solution in the form of Table 7.9.

a) Magnitude of I for cases A–Q

θ	A	B	C	D	E	F	G	H
0	1.7650	5.6383 − 1	6.8757 − 3	3.1537 − 16	2.6334	1.3294	3.0333 − 1	3.3527 − 2
15	1.0532	5.2875 − 1	6.8757 − 3	3.1298 − 16	1.9219	1.2943	3.0333 − 1	3.3430 − 2
30	0.4146	2.7887 − 1	6.6596 − 3	3.1203 − 16	1.2852	1.0445	3.0312 − 1	3.3361 − 2
45	0	0	0	0	0.8687	0.7656	2.9646 − 1	3.3317 − 2
60	...	...	...	...	0.5446	0.5651	2.6493 − 1	3.3294 − 2
75	...	...	...	...	0.2638	0.2545	1.8229 − 1	3.3276 − 2
90	...	...	...	...	0	0	0	0

θ	J	K	L	M	N	P	Q
0	3.5295	2.3523	5.8827	9.97 + 2	3.37 + 5	1.40 + 10	1.5245 + 14
15	2.8163	2.3173	5.8819	9.97 + 2	3.37 + 5	1.40 + 10	1.4675 + 1o
30	2.1795	2.0674	5.8810	9.97 + 2	3.37 + 5	1.40 + 10	1.4178 + 14
45	1.7630	1.7885	5.8738	9.97 + 2	3.37 + 5	1.40 + 10	1.3756 − 14
60	1.4389	1.5280	5.8420	9.97 + 2	3.37 + 5	1.40 + 10	1.3417 + 14
75	1.1581	1.2774	5.7591	9.97 + 2	3.37 + 5	1.40 + 10	1.3160 + 14
90	0.8943	1.0229	5.5766	9.97 + 2	3.37 + 5	1.40 + 10	1.2983 + 14
105	0.6284	0.7472	5.170	9.917 + 2	3.37 + 5	1.40 + 10	...
120	0.3403	0.440	4.115	9.774 + 2	3.37 + 5	1.40 + 10	...
135	0	0	0	0	0		0

b) Magnitude of L for cases A–Q

Case	θ_0, deg	$J/2b$	L
A	45	0.01	1.0323
B	45	0.1	1.3740
C	45	1.0	2.3974 + 1
D	45	10	6.2714 + 13
E	90	0.01	1.0
F	90	0.1	1.0
G	90	1.0	1.0
H	90	10	1.0
J	135	0.01	0.0687
K	135	0.1	0.7278
L	135	1.0	4.1712 − 1
M	135	3.0	7.258 − 5
N	135	5.0	1.263 − 7
P	135	7.0	2.197 − 10
Q	135	10	1.5945 − 14

TABLE 7.9: Numerical Values of I and L Over a Range of Variables as Given by Adelberg [5]

According to part b of this table, when θ_o = 90° and L = 1 (which already has been calculated and found to be 1 in step VI), J/2b varies from 0.01 to 10 for cases E, F, G and H. The values of I (θ, J/2b) corresponding to each case are given in Part a of Table 7.9. The value of J/2b =3.1735 falls between cases G and H. Therefore, in order to find the value of I(θ,J/2b) for J/2b = 3.1735, interpolation between the tabulated values was carried out as shown in Figure 7.2. The value of I(θ,J/2b), from Figure 7.2, corresponding to J/2b = 3.1735 is 0.12.

Step VIII: Estimate jet penetration.

For the acceleration wave regime, the jet penetration is

$$\ell^* = \frac{(d_{max})}{(b)} [L(\theta_o)\ I\ \{\theta,\ J/2b\}]$$

$$= \frac{(.0762)}{(.0049)}\ [1]\ [0.12]$$

$$= 1.8661 \text{ cm.}$$

This is accepted as the possible jet penetration for the experimental conditions of Ingebo and Foster [2].

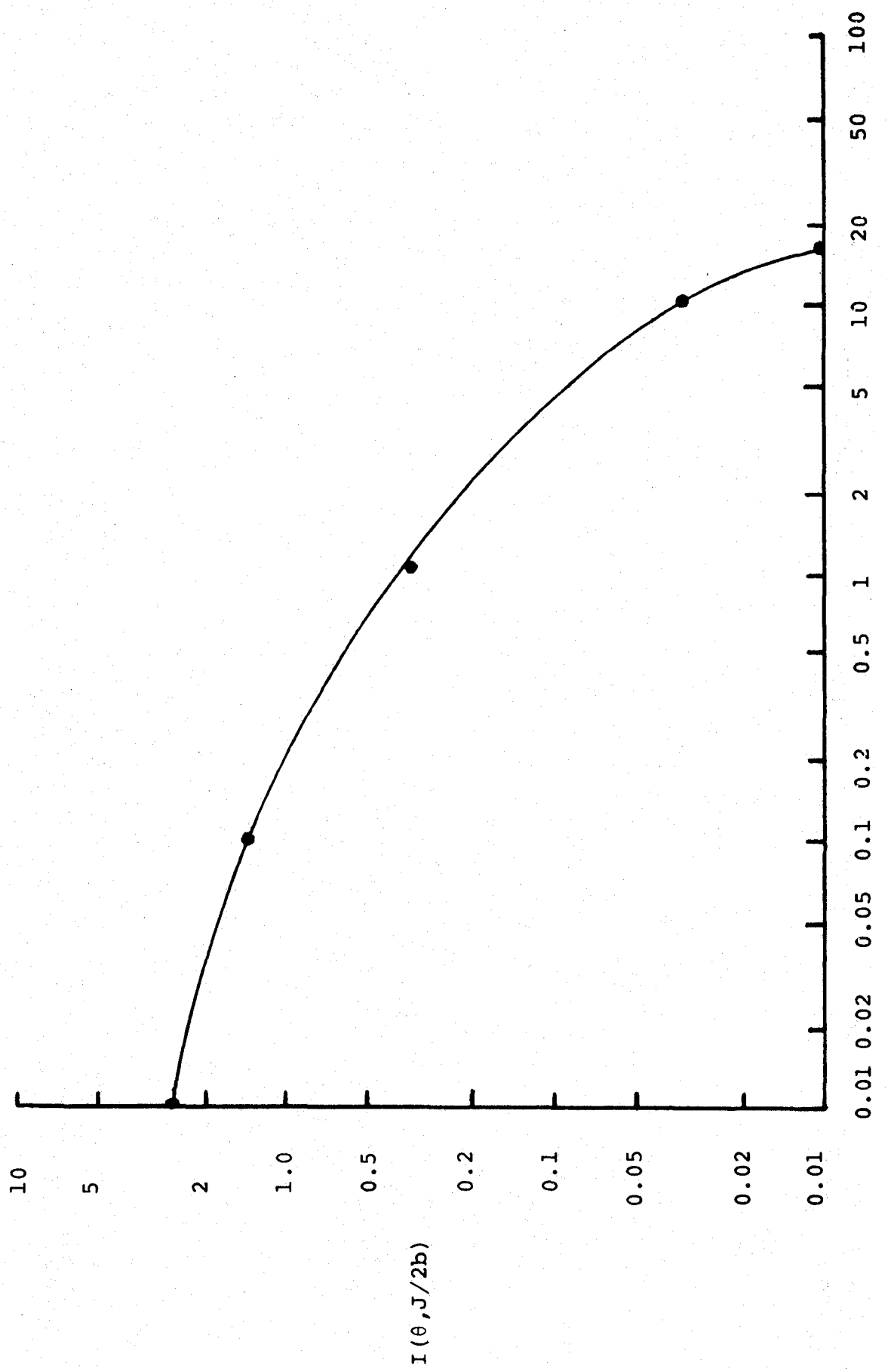

FIGURE 7.3: Graph of Function I(θ,J/2b) Vs (J/2b)

C. Trajectories and Dispersion of Liquid Jets

In wet gas scrubbers, the performance of the equipment is dependent, among other factors, on good coverage of the throat by the atomized drops. In this context the trajectories and spreading characteristics of the atomized liquid drops are important considerations when describing Venturi scrubber operation and determining theoretical scrubber efficiency. Clearly, in practice, the contacting between the aerosol and atomized liquid is not uniform across the scrubber. An appreciation of the spreading characteristics of the atomized liquid jets can provide a better insight into the conditions required to optimize the contacting between aerosol and liquid drops. A preliminary analysis of Venturi scrubber characteristics has been carried out using the data of Ingebo and Foster [2] for transverse jet injection of iso-octane into a turbulent air stream. The model proposed by Behie and Beeckmans [18] has been extended to dispersion of several drop sizes.

Consider a jet of liquid injected in the downward (y) direction into a turbulent air stream flowing in the horizontal (x) direction. The characterization of the spray distribution requires a determination of the centre line trajectory and a quantitative estimation of the

dispersion of the spray by turbulent diffusion. Behie and Beeckmans [18] obtained the spray centreline trajectory by considering the motion of a single drop which has remained undisturbed by the turbulence. Ingebo's [19] expression was used for the drag coefficient. The quantitative estimation of the dispersion of the spray was based on the approach followed for evaluating two dimensional diffusion from a point source.

1. Spray Centre Line Trajectory

Behie and Beeckmans [18], by assuming that the spray centre line corresponds to the trajectory which would be followed by a single drop injected under the same conditions as the spray, obtained the expressions

$$y_o = \frac{(1.19)}{(k')} \{(V_L)^{0.84} - [0.16\ k'\ t + (V_L)^{-0.16}]^{-5.25}\} \quad 7.8$$

and

$$x_o = (V_A)t - \frac{(V_A)}{(V_L)}\frac{(1.19)}{(k')} \{(V_L)^{0.84} - [0.16\ k't + (V_L)^{-0.16}]^{-5.25}\} \quad 7.9$$

where

$$k' = \frac{(81)(\rho_G)}{(4)(X_{av})(\rho_L)} \left[\frac{(\rho_G)(X_{av})}{(\mu_G)}\right]^{-0.84} \left[\sqrt{1 + \left(\frac{V_A}{V_L}\right)^2}\right]^{0.16} \qquad 7.10$$

The jet injection point was located at the origin. Behie and Beeckmans [18] presumed that the jet disintegrates at the origin. However, as discussed in the previous section, the jet penetration for the Ingebo and Foster [2] data was of the order of 1.87 cm (ie the y-co-ordinate is shifted 1.87 cm from point of injection). Consequently equation 7.8 was modified to account for the jet breakup length according to

$$y_o = 1.87 + \frac{(1.19)}{(k')} \left\{(V_L)^{0.84} - [0.16\, k'\, t + (V_L)^{-0.16}]^{-5.25}\right\} \qquad 7.11$$

Drop trajectories and computed values of y_o and x_o for 60, 150 and 202.5 micron drops are shown in Appendix IV for the Ingebo and Foster [2] experimental conditions. It is evident that smaller drops approach the gas velocity much more readily than the bigger drops.

b. Spray Dispersion

Behie and Beeckmans [18] considered the drop dispersion around the spray centre line to be equivalent to dispersion from an infinite line source, initially at t = 0, located in an infinite medium. The solution to this problem has the form

$$C = \frac{M}{(4)(\pi)(\mathcal{D})(t)}\, e^{-(r^2)/[(4)(\mathcal{D})(t)]} \qquad 7.12$$

where

C = concentration of material at a distance r, cm, from the centre line, gm/cm^3

M = quantity of material per unit length of line, gm/cm, at t = 0

$\mathcal{D}$ = diffusivity, cm^2/sec

Equation 7.12 represents a Gaussian curve in two dimensions with variance, σ^2, equal to $4(\mathcal{D})(t)$. An alternate physical system giving an identical solution to equation 7.12 is obtained by considering diffusion of a finite quantity of matter, originally located at r = 0, in a two dimensional plane. If dispersion of material from the centreline trajectory is assumed to take place in the y and z directions only, then these two problems are equivalent. Based on these arguments Behie and Beeckmans [18] proposed the following equation:

$$F(x,y,z) = \frac{W_L}{(2)(\pi)(\sigma_y)(\sigma_z)} \exp\left[-\frac{(y-y_o)}{(2)(\sigma_y)^2} - \frac{(z-z_o)^2}{(2)(\sigma_z)^2}\right] \qquad 7.13$$

where

$F(x,y,z)$ = flux of droplets per unit area at a point (x,y,z), $\frac{gm}{cm^2\text{-sec}}$

W_L = total mass of liquid passing plane x per unit time, $\frac{gm}{sec}$

σ_y = variance in the y-direction, cm

σ_z = variance in the z-direction, cm

z_o = z-co-ordinate of spray centre line

y_o = y-co-ordinate of spray centre line

The origin of the co-ordinate system in the y, z plane was displaced so as to coincide with the centre line trajectory at (y_o, z_o), and variances σ_y and σ_z were determined according to

$$\mathfrak{D}_z = (\sigma_z)^2/2t \qquad 7.14$$

$$\mathfrak{D}_y = (\sigma_y)^2/2t \qquad 7.15$$

In order to test the Ingebo and Foster [2] data in terms of this dispersion model, the following stepwise procedure was adopted:

i. A graph of X_{av} vs σ_y and X_{av} vs σ_z was plotted from the data of Behie and Beeckmans [18], in order to quantify the variances as functions of drop diameter. The data were inadequate to provide good relationships. For low values of drop diameter it was not possible to predict the variances from Figure 7.4. As a result the variances σ_y and σ_z were arbitrarily chosen for the average drop diameter (X_{av}) of 60 microns

ii. Since Figure 7.1 shows that the drop size distribution varies from 0 to 225 microns it was decided to arbitrarily split the drop size spectrum into three separate streams with drop sizes ranging from 0 to 120 microns, 120 to 180 microns and 180 to 225 microns. Accordingly the total amount of liquid injected, W_L, was split into three parts W_{L1}, W_{L2} and W_{L3}. On a mass basis

W_{L1} = liquid existing as drops ranging from 0 to 120 microns

W_{L2} = liquid existing as drops ranging from 120 to 180 microns

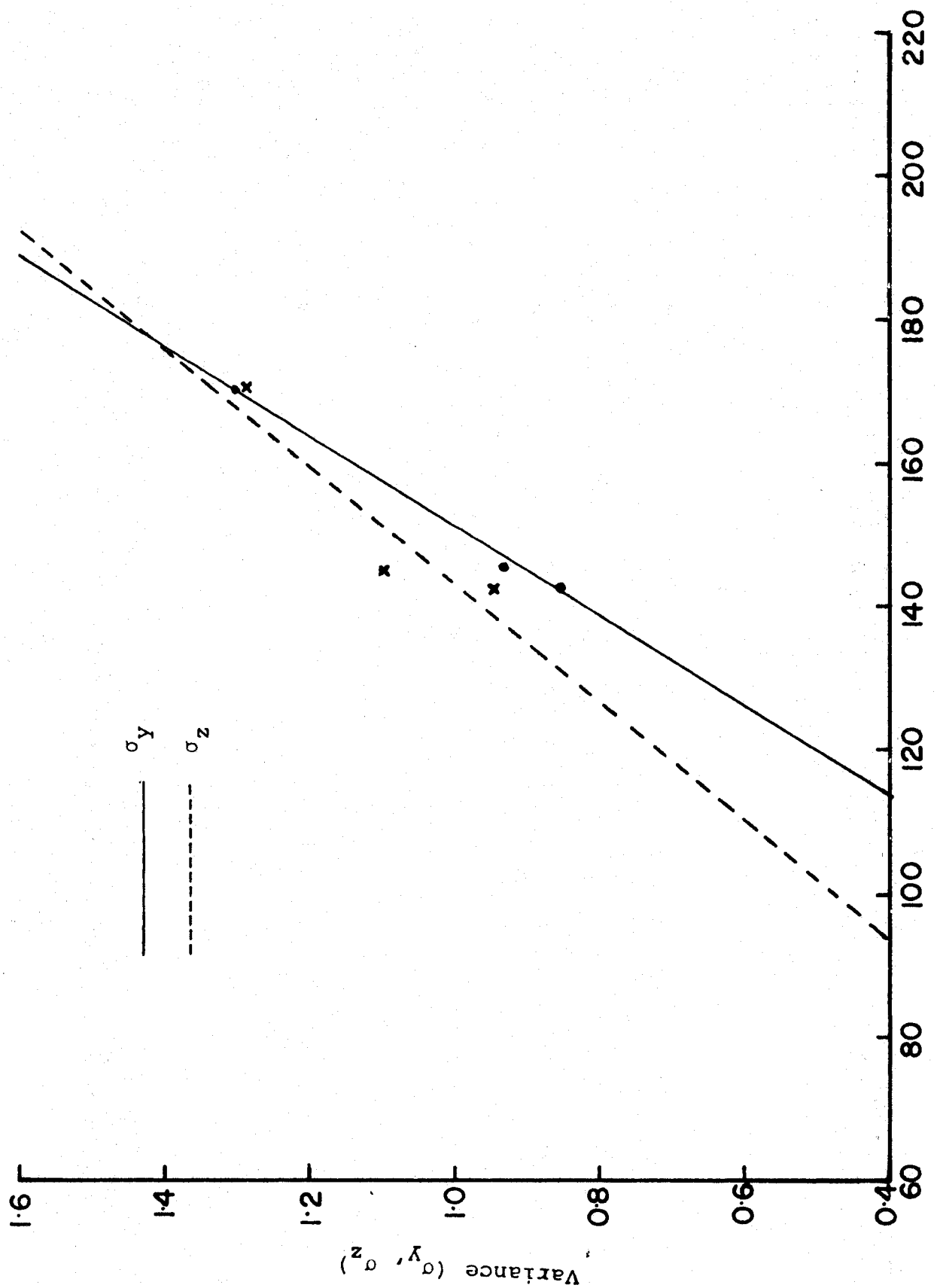

FIGURE 7.4: Variance σ_y, σ_z as a Function of Drop Diameter from Data of Behie and Beeckmans [18].

W_{L3} = liquid existing as drops ranging from 180 to 225 microns

W_{L1}, W_{L2} and W_{L3} represent 43%,(84-43)% and (100-84)% of the spray and are characterized by average diameters of 60, 150 and 202.5 microns respectively.

Table 7.10 summarizes the data needed for the estimation of drop flux.

W_L	σ_y	σ_z	X_{av}
W_{L1} = 4.84 x .43 = 2.0812	0.1	0.1	60μ
W_{L2} = 4.84 x(.84-.43) = 1.9844	0.98	1.09	150μ
W_{L3} = 4.84 x(1.0-.84) = 0.7744	1.82	1.73	202.5μ

Table 7.10: Parameters for Estimation of Drop Flux

iii. The drop trajectory relationships (equations 7.9 and 7.11) were used to estimate the values of y_o, for x_o = 1 cm for average drop diameters of 60, 150 and 202.5 microns. Since drop trajectories are in the x, y plane z_o = 0.

iv. The entire area in the y-z plane, downstream from the point of injection, was divided into squares of one centimeter each, extending from y=+15 to -15 cm and z = +5 to -5 cm to correspond to the Ingebo and Foster test section dimensions.

v. The flux F(x,y,z) at x = 1, 2 and 3 cm was estimated using W_{L1} as the amount of liquid injected. The sequence of finding F at x = 1,2 and 3 cm was repeated for W_{L2} and W_{L3}.

The net drop flux at any cross-section downstream from the point of injection would be the cumulative effect due to W_{L1}, W_{L2} and W_{L3}. The computer programme and the final results of the output are shown in Appendix IV. Better presentation of distribution of various fluxes could be by graphs showing variation of flux with distance.

REFERENCES

1. Boll, R. H., Flais, L. R., Maurer, P. W., and Thompson, W. L., Mean Drop Size in a Full Scale Venturi Scrubber via Transmissometer, Technical Paper presented at E.P.A. Fine Particle Scrubber Symposium, May 28-30, 1974, San Diego, California.

2. Ingebo, R. D., and Foster, H. H., Drop Size Distribution for Cross Current Breakup of Liquid Jets in Airstreams, Lewis Flight Propulsion Laboratory, Cleveland, Ohio, NACA Technical Note 4087 (1957).

3. Mayer, E., Theory of Liquid Atomization in High Velocity Gas Streams, American Rocket Society Journal, 31 (12), 1783-1785 (1961).

4. Adelberg, M., Mean Drop Size Resulting from the Injection of a Liquid Jet into a High-Speed Gas Stream, American Institute of Aeronautics and Astronautics Journal, 6 (6), 1143-1147 (1968).

5. Adelberg, M., Breakup Rate and Penetration of a Liquid Jet in a Gas Stream, American Institute of Aeronautics and Astronautics Journal 5 (8), 1408-1415 (1967).

6. Nukiyama, S., and Tanasawa, Y., Experiments on the Atomization of Liquids in an Air Stream, Reports 1-6, Transaction of Society for Mechanical Engineers (Japan), Volume 4, 5 and 6 (1938-40). English Translation by E. Hope, Defence Research Board, Department of National Defence, Canada, March 18, 1950, Translation No. EO/28220.

7. Wetzel, R. H., and Marshall, W. R., Paper Presented at Washington, D. C., National Meeting, American Institute of Chemical Engineers, March 1954.

8. Wetzel, R. H., Venturi Atomization, Ph.D., Thesis, University of Wisconsin (1952).

9. Ingebo, R. D., NASA Technical Note 3762 (1956).

10. Ingebo, R. D., Drop Size Distributions for Impinging Jet Breakup in Airstreams Simulating the Velocity Conditions in Rocket Combustors, NACA Technical Note 4222 (1958).

11. Weiss, M. A. and Worsham, C. H., Atomization in High Velocity Airstreams, American Rocket Society Journal, 29 (4), 252-259 (1959).

12. Mugele, R. A., Maximum Stable Droplets in Dispersoids, American Institute of Chemical Engineers Journal 6, (1), 3-8 (1960).

13. Eisenklam, P., Atomization of Liquid Fuel for Combustion, Journal of Institute of Fuel, 34, 130-143 (1961).

14. Kim, K. Y., and Marshall, W. R., Drop Size Distribution from Pneumatic Atomizers, American Institute of Chemical Engineers Journal, 17 (3), 575-584 (1971).

15. Gretzinger, J., and Marshall, W. R., Characteristics of Pneumatic Atomization, American Institute of Chemical Engineers Journal, 7 (2), 312-318 (1961).

16. Wigg, L. D., Drop Size Prediction for Twin-Fluid Atomizers, Journal Institute of Fuel, 37, 500-505 (1964).

17. Kumar, R., and Prasad, K. S. L., Studies on Pneumatic Atomization, Industrial Engineering Chemistry, Process Design and Development 10 (3), 357-365 (1971).

18. Behie, S. W., and Beeckmans, J. M., Faculty of Engineering Science, The University of Western Ontario, London, Canada, Personal Communication.

NOMENCLATURE

A	Orifice area, cm^2 Constant used in equation 6.29, dimensionless; Flow area for atomizing air, equation 6.41, in^2
A_s	Total area of swirl grooves, cm^2
A_m	Constant used in equation 6.29 to find maximum drop diameter, dimensionless Amplitude of vibration, micron
a	Empirical constant used in equation 5.31, $(micron)^{-3}$ Constant used in equation 5.59, $(micron)^{2.5}$ Constant used in equation 6.39 Radial extent of sheet measured from cup lip, inches
B	Parameter defined as $F_1/(\beta)^{2/3}$ in equation 6.5, dimensionless Constant used in equation 6.29, dimensionless
B_m	Constant used in equation 6.29 to find the maximum drop diameter, dimensionless
b	Empirical constant used in equations 5.31 and 5.46, $micron^{-n}$ Constant used in equations 5.59 and 6.39, Dynamic pressure ratio parameter, dimensionless, defined by equation 7.5
C	Constant used in equation 6.29, dimensionless
C_m	Constant used in equation 6.29 to find the maximum drop diameter, dimensionless
C_Q	Discharge coefficient, dimensionless
C_Q'	Discharge coefficient for orifice of finite length Lo, dimensionless
C_{Do}	Drag coefficient for cross flow of gas with a cylindrical surface, dimensionless

c	Argument for incomplete gamma function defined by equation 5.38 Constant used in equations 6.41 and 6.42, dimensionless Concentration, gm/cm^3
D	Distance between limiting streamlines, cm
D_2	Orifice diameter of swirl spray atomizer, cm
D_3	Swirl chamber diameter, cm
D_M	Mean diameter of swirl chamber, cm
d	Representative dimension of atomizer perpendicular to flow, cm Orifice diameter of nozzle, cm, inch Jet diameter, cm
dg	Diameter of a ligament, cm
d_L	Cup diameter at lip radius, cm, inch
d_{max}	Maximum jet diameter, cm
do	Diameter of swirl groove equivalent in area to total area of swirl groove, cm
e	Constant whose value varies between 0 and 1, used in equation 6.8, dimensionless
F	Frequency of vibration, kilo hertz (KHZ)
F_1	Dimensionless configuration factor, used in equation 6.1
FN	Flow number defined as $\left[\frac{\text{flow rate (gal/hr)}}{\sqrt{\text{pressure lbs/in}^2}} \times C_Q \times \text{Orifice area} \times \sqrt{\frac{2g}{2\rho_L}}\right]$
F(X)	Cumulative drop size frequency on number basis, $\sum_{i=1}^{h} \left(\frac{\Delta N_i/\Delta X_i}{N}\right) \times (\Delta X_i)$, dimensionless

$F(X^3)$	Cumulative drop size frequency on volume basis $\sum_{i=1}^{h} \left(\frac{\Delta V_i/\Delta X_i}{V}\right) \times (\Delta X_i)$, dimensionless
$F(Z)$	Probability integral, used in equation 5.9
f	Weight fraction of total air flowing in the primary nozzle, dimensionless
f^*	Exciting sound frequency, cycles/sec
$f(X)$	Drop size frequency function on number basis, dN/dX, micron^{-1}
$f(X_i)$	Normalized probability density function $(\Delta N_i/N)/\Delta X_i$, micron^{-1}
$f(X^2)$	Frequency function (surface), micron^{-1}
$f(X^3)$	Frequency function (volume), $\frac{(\Delta V_i/\Delta X_i)}{V}$, micron^{-1}
G	Mass velocity of gas at nozzle exit, gm/(sec-cm^2)
G_L	Mass velocity of liquid based on wetted perimeter of the atomizer disk, gm/(sec-cm)
h	Total number of class intervals in a given spray sample, dimensionless Height of air annulus, cm, used in equation 6.37
$I(\theta,J/2b)$	Function defined by Equation 7.4, dimensionless
j	Modified sheltering parameter $\frac{2}{5}(K_4)(\beta)(\pi/2)^{\frac{1}{2}}(e),^{3/2}$, dimensionless
j_σ	Modified sheltering parameter for capillary wave regime, dimensionless

J	Parameter, defined by equation 7.2, dimensionless
K_1, K_4, K_5	Dimensionless constants
k_L	Empirical constant (0.72 for fuel oil)
ko	Empirical constant for fan spray nozzle
k'	Parameter defined by equation 7.10, $(cm)^{-0.16}(sec)^{-0.84}$
L	Diameter of wetted periphery between gas and liquid, cm
Lω	Wetted perimeter of the atomizer disk, cm
Lo	Orifice length, cm
$L(\theta_o)$	Function defined by Equation 7.3, dimensionless
ℓ	Wave length of a disturbance, cm
ℓ*	Break up length of a liquid jet, cm
MR	Mass ratio of air to liquid with air at 100°F, dimensionless
m	sheet thickness, micron, cm
m*	sheet or film thickness at break up, micron, cm
M	quantity of material per unit length of line, gm/cm
N	Cumulative number of drops less than a given size
ΔN_i	Number of drops counted in the ith class interval
N_{Re}	Reynolds number, $(d)(V_a)/(\nu)$, dimensionless
N_{we}	Weber number $(\rho_G)(d)(V_a^2)/(\sigma_L)$, dimensionless

n	Empirical constant, dimensionless Rate of rotation of disk, revolutions/sec Constant whose value varies from +1 for free vortex to -1 for a forced vortex, dimensionless Shock dynamic pressure ratio $[\rho_G V_A^2/\rho_G V_A^2]$, dimensionless
dN	Number of drops in an infinitesimally small class interval
P	Nozzle pressure, lb /in^2
ΔP	Pressure drop across an atomizer, dyne/cm^2, lb/in^2
p	Constant (normally integer), with a value between 1 and 3, dimensionless
pi	Inner percentage of drops, whose diameters are less than X_i, equation 5.26, dimensionless
Q_G	Volumetric flow rate of gas cm^3/sec
Q_L	Volumetric flow rate of liquid, cm^3/sec
Q_m	Mass flow rate of liquid, lb_m/hr
q	Constant (normally integer), with a value between 0 and 4, dimensionless Time rate growth of the amplitude of disturbance, sec^{-1}
R	Initial jet radius, cm Radius of nozzle orifice, cm
R_o	Ratio of orifice diameters, smaller/larger, dimensionless
R_2	Orifice radius, cm
R_3	Swirl chamber radius, cm
R*	Radial distance measured from jet axis in a fan spray sheet, cm
r	Radius, cm Constant used in equation 6.39 Radius of spinning disk atomizer, cm

r_2	Radius of the constriction caused in the liquid jet, cm, (equation 6.44).
r_3	Air core radius, cm
S	Standard error, dimensionless
s	Standard deviation for the square root normal function, micron Arc length measured along liquid jet axis, cm
t	Time, seconds Variable of integration, equation 5.9
U	Variable of integration, equation 5.38
U_i	Liquid velocity at inlet to swirl chamber, cm/sec
U_m	Mean radial velocity of liquid along wall of cup, ft/sec
V	Cumulative volume of drops less than a given size, micron^3
V_A	Mean gas velocity, cm/sec
$\bar{V}_A$	Local gas velocity, cm/sec
V_a	Relative gas to liquid velocity, cm/sec
V_i	Volume of drops of diameter less than X_i, micron^3
V_L	Liquid velocity, cm/sec
V_m	Volume of drops of diameter less than X_o, micron^3
V_o	Initial liquid velocity, cm/sec
V_P	Cup peripheral velocity, cm/sec
V_R	Resultant sheet velocity, ft/sec, equation 4.12 Gas-liquid velocity ratio, V_A/V_P, dimensionless (equation 6.15)

V_s	Volume of a single drop, micron^3, cm^3, equation 6.44
V_T	Tangential component of sheet velocity, ft/sec
V*	Volume of drops of diameter less than Xo, micron^3
ΔV_i	Volume of drops in ith class interval, micron^3
dV	Volume of drops in an infinitesimally small class interval, micron^3
$(V_t)_i$	Average tangential velocity component of liquid as it enters nozzle swirl chamber, $4Q_L/(\pi(do)^2)$, ft/sec
$(V_v)_o$	Average axial velocity for orifice running full, $4Q_L/(\pi)(d)^2)$, ft/sec
W	Cumulative weight of drops less than a given size, gm
W_{L1}	Mass flow rate of liquid existing as drops ranging from 0 to 120 microns, gm/sec
W_{L2}	Mass flow rate of liquid existing as drops ranging from 120 to 180 microns, gm/sec
W_{L3}	Mass flow rate of liquid existing as drops ranging from 180 to 225 microns, gm/sec
W_G	Mass flow rate of gas, gm/sec
W_L	Mass flow rate of liquid, gm/sec
X	Diameter of drop, micron, cm
x_o	X co-ordinate of spray centre line trajectory, cm
x	Distance in direction of x-axis, cm
X_i	ith class mid-point diameter, micron

ΔX_i	Length of ith class interval, micron
X_m	Maximum drop diameter in a spray sample, micron
X_o	Minimum drop diameter in a spray sample, micron
X_W	Weibull mean diameter, micron
X_{av}	Arithmetic average drop diameter, micron
$\bar{X}_{gs}$	Geometric surface mean diameter, micron
$\bar{X}_{ng}$	Number geometric mean drop diameter, micron
X_{MM}	Mass median diameter, micron
X_{NM}	Number median diameter, micron
$\bar{X}_{qp}$	General mean diameter of the order (p+q), micron
X_{RR}	Rosin Rammler mean diameter, micron
X_{SM}	Surface median diameter, micron
X_{VM}	Volume median diameter, micron
X_{WM}	Weighted mean diameter, mm
$\bar{X}_{oo}$	Geometric mass or volume mean diameter, micron
$\bar{X}_{10}$	Length mean diameter, micron
$\bar{X}_{20}$	Surface mean diameter, micron
$\bar{X}_{30}$	Volume mean diameter, micron
$\bar{X}_{21}$	Surface diameter mean, micron
$\bar{X}_{31}$	Volume diameter mean, micron
$\bar{X}_{32}$	Volume surface or Sauter mean diameter, micron
$\bar{X}_{43}$	De Brouckere mean diameter, micron

$X_{84.13\%}$	Fraction of drops less than 84.13% on a cumulative number plot, dimensionless
$X_{15.87\%}$	Fraction of drops less than 15.87% on a cumulative number plot, dimensionless
y_o	y co-ordinate of spray centre line trajectory, cm
y	Variable expressed as a function of X, equation 5.11 and 5.28a: Distance in direction of y-axis, cm
z	Variable limit on probability integral, equation 5.9
z_o	z co-ordinate of spray centre line trajectory cm
z	Distance in direction of z-axis, cm

Greek Symbols

α	Amplitude of the disturbance at time t, cm
α_o	Initial amplitude of the disturbance, cm
β	Sheltering parameter, whose value is $\leq$ 1, dimensionless, (equation 6.2)
θ	Full spray angle, degree , radian Half angle between two colliding jets, degree, radian Angle jet axis makes with free stream velocity vector, degree
θ_o	Maximum angle jet axis makes with free stream velocity vector, degree
θ'	Full spray angle for orifice of finite length, Lo, degree
η	Boundary layer thickness (swirl nozzle), micron

ρ_G	Mean gas density, gm/cm^3
$\bar{\rho}_G$	Local gas density, gm/cm^3
ρ_L	Liquid density, gm/cm^3
μ	Liquid viscosity, poise, centipoise
μ_G	Gas viscosity, poise
σ	Standard deviation, micron Variance, cm
σ_g	Geometric standard deviation, micron
σ_g'	Geometric standard deviation based on drop weight, micron
σ_L	Liquid surface tension, dyne /cm
σ_N	Standard deviation of normal distribution, micron
σ_y	Variance in y-direction, cm
σ_z	Variance in z-direction, cm
ϕ	Angle that jet axis makes with free stream velocity vector, degree
ϕ_v	Pearl-Reed cumulative volume distribution function, dimensionless
$\phi(X)$	Function given by equation 5.51
$\bar{\phi}(X)$	Function defined by equation 5.53
λ	Length of a wave, cm
$\tau(\lambda)$	Excitation time for a wave of length, λ, sec
λ_{cr}	Critical wave length, cm
λ_{max}	Wave length corresponding to maximum instability, cm

λ_{min}	Minimum wavelength, cm
ν	Liquid kinematic viscosity, μ/ρ_L, cm^2/sec
ν_r	Kinematic viscosity ratio relative to water, dimensionless
$\Gamma_\alpha(c)$	Incomplete gamma function defined by equation 5.38
δ	Experimental deviation
Δ'	$As/(D_2D_M)$, dimensionless
Δ''	$As/(D_2D_3)$, dimensionless
ω	Angular speed of cup, rpm, cm/sec, radians/sec
ε	Angle between the radial velocity component and the resultant liquid velocity of the sheet at the cup lip, degree
ψ	Angle between the resultant sheet velocity and the sheet diameter at the free edge of the sheet, degree
$\mathscr{D}$	Diffusivity, cm^2/sec
$\mathscr{D}_y$	Diffusivity in y-direction, cm^2/sec
$\mathscr{D}_z$	Diffusivity in z-direction, cm^2/sec

APPENDIX I

Mean Drop Diameters from Nukiyama-Tanasawa Distribution

From

$$(\bar{X}_{qp})^{q-p} = \frac{\int_{X_o}^{X_m} (X)^q \, aX^2 \, e^{-bX^n} \, dX}{\int_{X_o}^{X_m} (X)^p \, aX^2 \, e^{-bX^n} \, dX}$$

it is possible to write

$$(\bar{X}_{qp})^{q-p} = \frac{\frac{1}{bn} \int_{X_m}^{X_m} \left(\frac{X^{q+2}}{X^{n-1}}\right) (a) \left(e^{-bX^n}\right) d\left[bX\left(X^{n-1}\right)\right]}{\frac{1}{bn} \int_{X_o}^{X_m} \left(\frac{X^{p+2}}{X^{n-1}}\right) (a) \left(e^{-bX^n}\right) d\left[bX\left(X^{n-1}\right)\right]}$$

$$= \frac{\int_{X_o}^{X_m} \left(\frac{X^{q+2}}{X^{n-1}}\right) \left(e^{-bX^n}\right) \, d\left(bX \; X^{n-1}\right)}{\int_{X_o}^{X_m} \left(\frac{X^{p+2}}{X^{n-1}}\right) \left(e^{-bX^n}\right) \, d\left(bX \; X^{n-1}\right)}$$

$$= \frac{\int_{X_o}^{X_m} (X^{q+3-n})\ (e^{-bX^n})\ d\ (bX\ X^{n-1})}{\int_{X_o}^{X_m} (X^{p+3-n})\ (e^{-bX^n})\ d\ (bX\ X^{n-1})}$$

The substitution $U = bX^n$ leads to

$$(\bar{X}_{qp})^{q-p} = \frac{\int_{X_o}^{X_m} (X^{q+3-n})\ e^{-U}\ dU}{\int_{X_o}^{X_m} (X^{p+3-n})\ e^{-U}\ dU} \qquad \text{I-1}$$

The incomplete gamma function, defined as

$$\Gamma_{\alpha}(C) = \int_{o}^{\alpha} (U^{C-1})\ (e^{-U})\ dU \qquad \text{I-2}$$

where

U = a variable of integration

C = the argument

provides a comparison between equations I-1 and I-2 which yields

$$U^{C-1} = X^{q+3-n}$$

Since $X = \left(\frac{U}{b}\right)^{\frac{1}{n}}$

it now follows that

$$U^{C-1} = \left(\frac{U}{b}\right)^{\frac{q+3-n}{n}} = U^{\left(\frac{q+3}{n}-1\right)} b^{-\left(\frac{q+3}{n}-1\right)} \qquad \text{I-3}$$

Substitution of equation I-3 into equation I-1 yields

$$\left(\bar{X}_{qp}\right)^{q-p} = \frac{\int_{X_o}^{X_m} U^{\frac{q+3}{n}-1} b^{-\left(\frac{q+3}{n}-1\right)} e^{-U}\, dU}{\int_{X_o}^{X_m} U^{\frac{p+3}{n}-1} b^{-\left(\frac{p+3}{n}-1\right)} e^{-U}\, dU}$$

or

$$= \frac{b^{-\left(\frac{q+3}{n}-1\right)} \int_{X_o}^{X_m} U^{\frac{q+3}{n}-1} e^{-U}\, dU}{b^{-\left(\frac{p+3}{n}-1\right)} \int_{X_o}^{X_m} U^{\frac{p+3}{n}-1} e^{-U}\, dU}$$

Changing the limits of integration yields

$$(\bar{X}_{qp})^{q-p} = \frac{b^{-(\frac{q+3}{n}-1)} \int_{b(X_o)^n}^{b(X_m)^n} U^{\frac{q+3}{n}-1} e^{-U}\, dU}{b^{-(\frac{p+3}{n}-1)} \int_{b(X_o)^n}^{b(X_m)^n} U^{\frac{p+3}{n}-1} e^{-U}\, dU}$$

or

$$= \frac{b^{-(\frac{q+3}{n}-1)} \left[\Gamma_{b(X_m)^n}(\frac{q+3}{n}) - \Gamma_{b(X_o)^n}(\frac{q+3}{n}) \right]}{b^{-(\frac{p+3}{n}-1)} \left[\Gamma_{b(X_m)^n}(\frac{p+3}{n}) - \Gamma_{b(X_o)^n}(\frac{q+3}{n}) \right]}$$

or

$$= \frac{b^{-\frac{(q-p)}{n}} \left[\Gamma_{b(X_m)^n}(\frac{q+3}{n}) - \Gamma_{b(X_o)^n}(\frac{q+3}{n}) \right]}{\left[\Gamma_{b(X_m)^n}(\frac{p+3}{n}) = \Gamma_{b(X_o)^n}(\frac{q+3}{n}) \right]}$$

Investigator	Atomizer	Mathematical Treatment	Applicable Range				
			Relative Velocity	Liquid Viscosity	Liquid Density	Liquid Surface Tension	System Used
York, Stubb and Tek [47]	Swirl type pressure nozzle	Critical wave length related to sheet thickness	1910 cm/sec	1cp	1 gm/cm^3	74 dyne/cm	Air/Water
$\frac{X}{r} = 1.06 \left[\frac{(2\pi)(N_{We})(\rho_L)}{(\rho_G)(V_r^2)}\right]^{\frac{1}{2}} = 1.06 \left[(2\pi)/(\lambda_{max})\right]^{\frac{1}{2}}$ λ_{max} = wave length corresponding to max. instability, cm							
Tate and Marshall [72, 73]	Centrifugal pressure nozzle	Empirical equation correlating in terms of axial and velocity components of jet		1.0 to 2.0 centistokes		62.5 dyne/cm	Air/2.5% Solution of Nigrosine dye in water
$\bar{x}_{32} = 286 (d + 0.17) \exp. [13(V_v)_o - 0.0094 (V_t)_i]$ $(V_t)_i$ = Average tangential velocity component of liquid as it enters nozzle swirl chamber, ft/sec $(V_v)_o$ = Average axial velocity for orifice running full, ft/sec							
Longwell [74]	Swirl chamber type pressure nozzle	Empirical correlation of experimental data					
$X_{MM} = \frac{(d)(k_L)\exp.[0.705]}{2(P)^{0.175}\sin(\theta/2)}$ k_L = constant (0.72 for fuel oil)							
Turner and Moulton [35]	i. Grooved core-nozzle ii. Swirl type nozzle	Empirical correlation of experimental data		.81 to 2.02 cp	1.016 to 1.075 gm/cm^3	26.9 to 37.2 dyne/cm	Air/Molten Beta Napthol and Benzoic Acid
i. $X_{MM} = 16.56 (d)^{1.62} (N_{We})^{-0.444} (\pi_L)^{0.713} (\pi_G)^{0.159}$ ii. $X_{MM} = 41.4 (d)^{1.589} (N_{We})^{-0.537} (\pi_L)^{0.594} (\pi_G)^{0.220}$							
Orr [76]	Pressure nozzle	Correlating experimental data	200-1000 ft/sec	1.4 to 11.1 cp			
$\left[\frac{(X_{MM})(\rho_G)(V_r)^2}{(\sigma_L)}\right] = 0.61 \left[\frac{(V_{rc})}{(V_r)}\right]^{2.1} \left[\frac{1000\ \rho_G}{\rho_L}\right] \left[\frac{d\ \rho_L \sqrt{\rho_L \rho_G}}{\mu_L^2}\right]$							

APPENDIX II: Summary of Atomization Investigations Excluding Pneumatic Techniques

Investigator	Atomizer	Mathematical Treatment	Applicable Range				
			Relative Velocity	Liquid Viscosity	Liquid Density	Liquid Surface Tension	System Used
Friedman, Gluckart and Marshall [77]	Spinning disk atomizer	Dimensional Analysis		1-9000 cp	62.4 to 88 lb/ft^3	74 to 100 dyne per cm	Air/Various liquid mixtures designated as A, B, C and D
$\frac{\overline{X}_{32}}{r} = 0.4 \left[\frac{(G_L)}{(\mu_L)(\omega)(r^2)}\right]^{0.6} \left[\frac{(\mu)}{(\sigma_L)}\right]^{0.2} \left[\frac{(\mu_L)(\sigma_L)(L_w)}{(G_L)^2}\right]^{0.1}$ r = Radius of spinning disk atomizer L_w = Wetted perimeter of the atomizer disk, cm G_L = Mass velocity of liquid based on wetted perimeter, gm/sec-cm n = revolutions/unit time							
Walton and Prewett [78]	Spinning disc type atomizer	Balancing surface tension forces with centrifugal forces on drop		0.01 to 15 poise	0.9 to 13.6 gm/cm^3	31 to 465 dyne/cm	Air/Methyl Salicylate, Mercury, Water, Dibutyl Phthalate + 10 Waxolinble, Glycerine, O-dichloro-benzene, Ethylene dibromide
$x = 1.8 \left(\frac{\sigma_L}{2\pi^2 r \rho_L \omega^2}\right)^{\frac{1}{3}} (\omega)$							
Fraser, Eisenklam and Dombrowski [79]	A. Fan Spray nozzle B. Impact nozzles			A. 1 cp B. 1 cp	A. 1. 1 gm/cm^3 ii. 0.8 to 1.0 gm/cm^3 B. 1 gm/cm^3	74 dyne per cm 28 to 71 dyne per cm 74 dyne/cm	A i. Air/Water ii. Air/liquids other than water B Air/water
A. i. $\ln \overline{X}_{20} = 1.823 + \frac{4.42}{\Delta P} + 2.03 \frac{Q_L}{\sqrt{\Delta P}}$ ii. $\overline{X}_{20} = 181 \left[\frac{Q_L \sigma_L}{(\Delta P)^{3/2} a}\right]^{\frac{1}{3}}$ B. $X_{MM} = 1480 \left[\frac{(Q_L)^{\frac{1}{3}}}{(\Delta P)^{\frac{1}{3}}}\right]$ $\overline{X}_{20}$ = microns; ΔP = psi; Q_L = British gallons/hr; a = Radius; σ_L = dynes/cm							
Ryan [80]	Two impinging jets	Empirical equation		1 to 40 cp		50 to 70 dyne/cm	Air/Aqueous solutions of carboxy methyl cellulose
$X_{MM} = \frac{1}{V_L}[11.16 + 38.7 (1 - R_o)/(\Delta P)]$ R_o = Ratio of orifice diameters, smaller/larger, dimensionless							

APPENDIX II: Summary of Atomization Investigations Excluding Pneumatic Techniques

Continued ...

Investigator	Atomizer	Mathematical Treatment	Applicable Range				
			Relative Velocity	Liquid Viscosity	Liquid Density	Liquid Surface Tension	System Used
Lang [81]	Ultrasonic atomizer	Rupture of capillary surface waves related empirically to drop size			.82 to .89 gm/cm^3	21.7 to 30 dyne/cm	Air/Synthetic wax, paraffin wax, oil
$X_{MM} = 0.34 \left(\frac{8 - \rho_L}{\rho_L f^*}\right)^{1/3}$ f^* = Exciting sound frequency, cycles/sec							
Putnam et al [82]	Spinning disc atomizer	Used data of Walton and Prewett [78] to obtain the equation by dimensional analysis		0.01 to 15 poise	0.9 to 11.6 gm/cm^3	31 to 468 dyne per cm	Air/Methyl Salicylate, Mercury Water, Dibutyl Phthalate, 1% Waxolin blue, Glycerine, O-Dichloro-benzene, Ethylene dibromide
$X = (6.855)\ (2r)^{\ } \left[\frac{(\ )^2}{(2r)(\rho_L)(\sigma_L)}\right]^{0.041} \left[\frac{(w)^2 (2r)^{\ } (\rho_L)}{(\sigma_L)}\right]^{-0.522}$							
Fraser [83]	Swirl atomizer	Correlation of experimental data of several other investigators		0.5 to 25 cp	0.75 to 1.6 gm/cm^3	24 dyne per cm	Air/kerosene, petrol, Mixtures of D.T.D. 44D and kerosene, Mixtures of kerosene and hydrogenated oil
$\bar{X}_{32} = 220\ (P)^{-0.458}\ (Q_m)^{0.209}\ (\nu)^{0.215}$							
Putnam et al [82]	Jet injection into still air	Equation proposed based on work of other investigators					
$\bar{X}_{10} = f \left[\frac{(d)^{0.5}\ (\ )^{0.2}}{(P)^{0.4}}\right]$							
Fraser et al [21]	Fan Spray nozzles	Drop size by Rayleigh's analysis from an unstable liquid sheet		1 cp	1 gm/cm^3	74 dyne/cm	Air Water
$X = \text{Const.} \left[\frac{(k_Q)(\ )}{(C_Q)^2 (\Delta P)}\right]^{\frac{1}{3}} \left[\frac{\rho_L}{\rho_G}\right]^{\frac{1}{6}}$							
Norman [84]	Flat spray nozzles	Empirical correlation of experimental results			0.8-1 gm/cm^3	28 dyne/cm	Air Water, Kerosene
$\bar{X}_{32} = 4.4\ (\ )_L^{(a)\frac{1}{7}}\ (\ )^{\frac{1}{7}}\ (\ )^{\frac{1}{6}}\ (\Delta P)^{\frac{1}{5}}$							

APPENDIX II: Summary of Atomization Investigations Excluding Pneumatic Techniques — Continued ...

Investigator	Atomizer	Mathematical Treatment	Applicable Range				System Used
			Relative Velocity	Liquid Viscosity	Liquid Density	Liquid Surface Tension	
Nelson and Stevens [85]	Grooved-core centrifugal spray nozzle	Empirical correlation of experimental data					Air/Cyclohexane, n-octyl alcohol, CCl_4, Water, Nitrobenzene, Aniline, 1, 1, 2, 2 Tetra Chloroethane. Also used N_2 atmosphere
		$\log_{10} \frac{\bar{X}_{10}}{d} = A^2 + B^2 + C$ $Z = \log_{10}\left[\left(N_{Re}\right)^{X}\left(N_{We}/N_{Re}\right)^{X}\right]\left[\frac{(V_t)_1}{(V_t)_0}\right]^{Y}$ $N_{Re} = (d)\,(V_t)_0\,(\rho_L)/\mu_L$ $N_{We} = (V_t)_0^2\,(d)\,(\rho_L)/\sigma_L$		For water A = -0.144, B = 0.702, C = -1.260, X = 0.200, Y = 1.2		For Organic Liquids A = -0.081, B = 0.124, C = -0.186, X = 0.55, Y = 1.2	
Dombrowski and Hooper [20]	Single hole fan spray nozzle	Theoretical constants proposed earlier [21, 84, 34], have been corrected experimentally		1 to 5.3 cp	0.79 to 1.12 gm/cm^3	24 to 71dyne per cm	Air/Water ethyl alcohol, 48% weight weight glycerine-water
		$\bar{X}_{32} = \frac{137\,(\mu_L)^{0.2}\,(ko)^{\frac{1}{2}}}{(C_D)^{0.6}\,(\Delta P)^{0.4}}\left(\frac{\sigma_L}{\rho_L}\right)^{\frac{1}{4}}$					
Mizutani, Uga and Nishimoto [86]	Ultrasonic atomizer	Empirical correlation of experimental data		1 to 6.05 cp	0.95 to 1.13 gm/cm^3	33 to 75 dyne per cm	Air/Water, Ethanol solutions and glycerol solution
		$\bar{X}_{32} = 4.16\left(\frac{\mu_L}{\rho_L}\right)^{\frac{1}{3}}\left(\sigma_L\right)^{\frac{1}{4}}\left[540(F)^{-2/3} + \frac{7000}{F(Am)}\left(\frac{Q_L}{\sigma_L}\right)^{120/F(Am)}\right]$ μ = centipoise, Q_L = cm^3/min, Am = Amplitude of vibration, micron F = Frequency of vibration, kilo hertz					
Harmon [87]	Cylindrical nozzle	Correlation of energy balance to dimension less ratios, using data of other investigators [59, 29, 99, 100]					Air/alcohol, gasoline, diesel, kerosene
		$\frac{(d)}{(\bar{X}_{32})(N_{We})} = 3.00 \times 10^{-4}\,\frac{\left[\frac{(\mu_G)^2\,(\rho_L)}{(\sigma)(\rho_L - (\rho))}\right]^{0.3}\left[\frac{(\rho_L)}{(\rho_G)}\right]^{1.38}}{\left[\frac{(V_t)_0\,(\rho_L)}{(\sigma)}\right]^{1.45}\left[\frac{(\rho_G)}{(\rho_L)}\right]^{0.062}}$					

APPENDIX II: Summary of Atomization Investigations Excluding Pneumatic Techniques

Continued ...

Investigator	Atomizer	Mathematical Treatment	Applicable Range				
			Relative Velocity	Liquid Viscosity	Liquid Density	Liquid Surface Tension	System Used
Takahashi and Kitamura [88]	Simple tubes	Drop diameter is related to frequency and amplitude of surface disturbance		0.800 to 122.7 cp	0.996 to 1.228 gm per cm^3	22.5 to 71.2 dyne/cm	Air/Water, methanol, glycerine solution of various concentrations
		$X = (0.5(Y)^{-4/3}[(4.5)(-2) + 2)]^{\frac{1}{4}}$					$\hat{l}$ = Break up length of a liquid jet, cm.
		$Y = [2(q)(l^*)/(V_v)_o^2 + 1]^{\frac{1}{8}}$, $X = 3(\mu)/\sqrt{(\sigma_L)(d)(\rho_L)}$					
Dunskiy, Nikitin, and Tonkacheyeva [89]	Rotating disk atomizer	Empirical correlation of experimental data			.89 to 1 gm/cm^3	29 to 73 gm/sec^2	
		$r_{MM} \propto \frac{1.1}{\omega}[\frac{(\sigma_L)}{(r)(\rho_L)}]^{\frac{1}{2}}$					
Baryshev, Vachagin, Nikolaev [90]	Rotating disk with co-current gas stream	Empirical correlation of experimental data	0.15 to 14.5 m/sec	--	1 gm/cc	74 dyne/cm	Air/Distilled Water
		$\frac{\bar{r}_{10}}{2r} = 1.10\left[\frac{(\sigma_L)(\rho_L)}{(2r)(\mu)}\right]^{0.1}\left[\frac{(V_A)(2r)(\rho_G)}{(\mu_G)}\right]^{-0.1}\left[\frac{(2r)^2(\omega)(\rho_G)}{(\mu_G)}\right]^{-0.35}\left[\frac{(\sigma_L)}{(2r)^3(\omega)^2(\rho_L)}\right]^{0.05}$					
		ω = radians/sec, $\rho_L = \frac{K_g - sec^2}{metre^4}$, $\mu = \frac{K_g\text{-}sec}{metre^2}$, $\sigma_L = \frac{metre^3}{sec^2}$, $\bar{r}_{10}$ = metre, r = metre					
Chechik and Lyuminarskii [91]	Centrifugal disk sprayer	Force balance on the liquid detached from the disk		0.10 to 1200 poise	1.02 to 1.25 gm/cm^3	68.3 to 74.3 dyne/cm	
		$X = \frac{30\sqrt{4}}{(\gamma)(n)}\sqrt{\frac{3(\sigma_L) - 4.5(\mu_G)(V_A) - 3\sqrt{(r)(n^2)(\mu)[\rho_L/(L\omega)]^2}}{100(\cdot)}}{(\sigma_L)(r)}$					
Clark and Dombrowski [92]	Analysis of fan spray sheet	Instability of the jet is analyzed by Lagrange's method					Air/Water, Carbon Tetrachloride, Mercury
		$\bar{x}_{1n} = 2.41 \times 10^6\left[\frac{(\sigma_L)}{(\rho_L)}\right]^{\frac{1}{2}}\left[\frac{(2)(m)(R^*)^2}{(V_R)}\right]^{2.0} \pm 1\%$					
		R^* = Radial distance measured from jet axis in a fan spray sheet, cm.					

APPENDIX II: Summary of Atomization Investigations Excluding Pneumatic Techniques

Continued ...

Investigator	Atomizer	Mathematical Treatment	Applicable Range				
			Relative Velocity	Liquid Viscosity	Liquid Density	Liquid Surface Tension	System Used
Dombrowski and Johns [93]	Fan Spray Nozzle	Aerodynamic instability of viscous liquid sheets is related to various forces acting on the sheet		1.12 to 2.15 cp	0.754 to 1.27 gm/cm^3	25 to 85 dyne per cm	Air/Paraffin Wax, Microcrystalline wax, Carnauba wax, $CaCl_2$ aq. solutions, Diethyl phthalate, water and kerosene
$X = \left(\frac{3}{\sqrt{2}}\right)^{1/3} (dq) \left[1 + \frac{3(\mu_L)}{\left[(\rho_L)(\sigma_L)(dq)\right]^{\frac{1}{2}}}\right]^{\frac{1}{6}}$ $(dq) = 0.961 \left[\frac{(mx)^2 (\sigma_L)^2}{(\rho_G)(\rho_L)(V_a)^4}\right]^{\frac{1}{6}} \left[1 + 2.69(u)\sqrt{\frac{(m)(x)(\rho_G)^4 (V_a)^7}{72(\rho_L)^2(\sigma_L)^3}}\right]^{\frac{1}{6}}$						
Hasson & Mizrahi [94]	Fan spray nozzles	Equation proposed earlier [96] is modified for viscosity and tested over a wide range		1.12 to 2.15 cp	0.754 to 1.27 gm/cm^3	25 to 85 dyne/cm	
$\bar{X}_{20} = 0.071 \left[\frac{(mx)^2 (\sigma_L)^2}{(\rho_L)(V_a)^4}\right]^{\frac{1}{6}} (\mu)^{\frac{1}{6}}$							
Wissema and Davies [95]	Vibration atomizer	Rayleigh's analysis is used to find the effect of forced vibrations		66 to 1408 cp	1.21 to 1.26 gm/cm^3	63.1 to 66.7 dyne per cm	Air/Various concentrations of Glycerol-water solution
$X \propto 0.98 (d)^{2/3} \left[\frac{(V_R)}{f}\right]^{\frac{1}{3}}$							
Rajagopalan, Tien, and Subramanian [97]	Vibration atomization	Equation proposed [98] is modified					
$\frac{X}{d} = 1.12 \left[\frac{(V_R)}{(f^4)(d)}\right]^{0.328}$							
Straus [98]	Single hole fan spray nozzle	Disintegration of flat sheet related to drop size					Air Water
$\bar{X}_{20} = 15400 \sqrt{\frac{(m^*)(\sigma_L)}{(V_R)^2}}$ m^* = Sheet or film thickness at break up, cm.							

APPENDIX II: Summary of Atomization Investigations Excluding Pneumatic Techniques

Continued ...

Investigator	Atomizer	Mathematical Treatment	Applicable Range				
			Relative Velocity	Liquid Viscosity	Liquid Density	Liquid Surface Tension	System Used
Fraser and Eisenklam [68]	Single hole fan spray nozzle	Revised version of equation by Strauss [9]		1 cp	1 gm/cm^3	74 dyne per cm	Air/Water
$\log_{10} \bar{X}_{20} = 1.823 + \frac{4.42}{P} + 0.203\ (FN)$ $FN = \frac{\text{flow rate (gal/hr)}}{\sqrt{\text{pressure lb/sq.in.}}} \times C_D \times \text{orifice area} \times \sqrt{\frac{2g}{\rho_L}}$ $= 293 \times C_D \times (\text{area in cm}^2)$ for water							
Fraser and Eisenklam [68]	Swirl spray Nozzle	Revised version of equation proposed [47, 101]		1 cp	1 gm/cm^3	74 dyne per cm	Air/water
$\log \bar{X}_{20} = 1.808 + \frac{6.94}{P} + 0.138\ (FN)$							
Wang and Tien [102]	Grooved core swirl nozzle	i. Empirical correlation of experimental data ii. mean drop size related to boundary layer thickness		0.89 to 31.0 cp	0.997 gm/cm^3 to 1.2 gm/cm^3	67.5 to 72.0 dyne/cm	Air/0.11 Wt. % Carbopol 934, 0.15 Wt. % Carbopol 934, CMC and Glycerine solution
i. $\log_{10} \left(\frac{X}{d}\right) = -0.60 \log_{10} \left[(N_{Re})^{0.40} (N_{We})^{0.52} (A/A_s)^{0.30}\right]$ ii. $\log_{10} (\eta) = 0.671 \log_{10} \left[(\bar{X}_{30})(N_{Re})^{-0.436} (N_{We})^{0.258} (A/A_s)^{-0.339}\right]$ η = Boundary layer thickness, microns							
Baranaev and Tenyakov [103]	Centrifugal atomizer	A semi-theoretical equation based on Isotropic theory of turbulence. Data fitting of other investigators is also done		0.0101 to 1.30 poise	89.2 to 1390 kg-sec^2/ metres^4	47 to 460 dynes/cm	Air/Mercury, Water, Mineral Oil
$X_{MN} = 0.28 \left[\left[\frac{(\sigma_L)}{(\rho_L)(V_R)^2}\right]^{\frac{1}{2}} + 1.07 \left[\frac{u}{(\rho_L)(V_R)}\right]^{\frac{1}{3}}\right] 4/(2\pi m)$							
X_{MN} = Weighted mean dia. mm; V_R = metre/sec; u = poises; m = mm; ρ_L = gm/cm^3; σ_L = dyne/cm							
Holroyd [104]	Simple orifice	Empirical equation tested on data of other investigators		0.0634 to 0.0187 gm/cm.sec.	.812 to .852 gm/cc	26.5 to 28 dyne/cm	Air/Gas Oil Kerosene
$x = f \left[\frac{(\sigma_L)(A)^2}{(\sigma_L)(V_L)^2}\right]^{\frac{1}{4}} \left[\frac{(d)(V_L)(\rho_L)}{(\mu)}\right]$							

APPENDIX II: Summary of Atomization Investigations Excluding Pneumatic Techniques

APPENDIX III

Experimental and Predicted Sauter Mean Diameter (SMD) as Reported by Fraser, Dombrowski and Routley [5]

(*a*). *Relative position of air impingement: a* = 0 in.
Oil viscosity 45 cS

Liquid flow rate (lb/hr)	*Air velocity* (ft/sec)	*Air flow rate* (lb/hr)	*Mass ratio air/liquid*	*Cup speed* (rev/min)	*Sheet thickness at point of disintegration* (μ)	*Axial drop velocity at* 1½ in. *from lip* (ft/sec)	*Calc.* SMD (μ)	*Measured* SMD (μ)	*Maximum drop size* (μ)
500	320	168	0·34	3000	44	200	80	78	360
500	320	162	0·33	4500	30	200	70	65	280
500	650	343	0·69	3000	44	280	30	33	250
500	650	342	0·69	4500	30	280	28	32	220
1000	320	168	0·17	3000	90	200	158	141	450
1000	320	162	0·17	4500	58	195	138	132	400
1000	650	341	0·34	3000	90	280	54	55	230
1000	650	339	0·34	4500	58	280	47	50	225

(*b*). *Relative position of air impingement: a* = 0·2 in.

Liquid flow rate (lb/hr)	*Air velocity* (ft/sec)	*Air flow rate* (lb/hr)	*Mass ratio air/liquid*	*Cup speed* (rev/min)	*Sheet thickness at impingement* (μ)	*Axial drop velocity at* 1½ in. *from lip* (ft/sec)	*Calc.* SMD (μ)	*Measured* SMD (μ)	*Maximum drop size* (μ)
				(i) *Oil viscosity* 5 cS					
500	95	960	1·92	3000	31	16·5	136	124	355
500	95	960	1·92	4500	22	16·5	95	90	300
500	320	398	0·80	3000	31	22·0	40	46	235
500	320	398	0·80	4500	22	21·5	36	32	230
				(ii) *Oil viscosity* 45 cS					
100	95	990	9·6	1500	12	16·2	123	120	365
100	95	960	9·6	3000	6	16·2	96	92	325
100	95	960	9·6	4500	45	16·2	68	55	290
100	95	960	9·6	6000	3	16·2	47	55	210
100	320	398	3·98	1500	12	22·0	34	35	—
100	320	398	3·98	3000	6	22·5	28	30	280
100	320	398	3·98	4500	4·5	22·5	25	29	265
100	320	398	3·98	6000	3	22·5	24	23	210
250	95	56·4	0·22	1500	32	14·5	305	280	570
250	95	56·4	0·22	3000	17	14·0	238	230	520
250	95	444	1·78	1500	32	14·8	195	200	425
250	95	441	1·75	3000	16	14·8	153	150	375
250	95	960	3·84	1500	32	16·2	191	200	330
250	95	960	3·84	3000	16	16·2	149	158	300
250	95	960	3·84	4500	11	16·2	102	95	310
250	95	960	3·84	6000	8	16·2	70	78	290
250	320	93·6	0·37	1500	32	19·5	64	64	305
250	320	93·6	0·37	3000	17	19·5	50	46	230
250	320	190	0·76	1500	32	21·5	57	60	305
250	320	190	0·76	3000	17	21·5	44	45	265
250	320	398	1·58	1500	32	22·0	54	54	305
250	320	398	1·58	3000	16	22·0	42	40	260
250	320	398	1·58	4500	11	22·0	37	33	240
250	320	398	1·58	6000	8	22·0	35	27	210

Liquid flow rate (lb/hr)	Air velocity (ft/sec)	Air flow rate (lb/hr)	Mass ratio air/liquid	Cup speed (rev/min)	Sheet thickness at impingement (μ)	Axial drop velocity at 1½ in. from lip (ft/sec)	Calc. SMD (μ)	Measured SMD (μ)	Maximum drop size (μ)
250	320	684	2·74	1500	32	21·5	53	54	300
250	320	684	2·74	3000	17	21·5	41	38	265
500	95	203	0·41	3000	32	14·0	200	198	510
500	95	203	0·41	4500	24	14·5	180	170	450
500	95	414	0·83	3000	32	14·8	221	195	425
500	95	401	0·80	4500	24	14·8	152	150	375
500	95	960	1·92	1500	64	16·2	265	250	630
500	95	960	1·92	3000	32	16·2	212	195	540
500	95	960	1·92	4500	24	16·2	147	160	430
500	95	960	1·92	6000	16	16·2	99	105	380
500	180	387	0·77	3000	32	20·0	114	115	370
500	180	387	0·77	4500	24	20·0	101	95	350
500	320	189	0.38	3000	34	21.5	69	75	265
500	320	189	0·38	4500	22	21·0	61	58	250
500	320	396	0·79	1500	64	22·0	77	78	320
500	320	396	0·79	3000	32	22·0	60	63	295
500	320	396	0·79	4500	24	21·0	53	59	265
500	320	396	0·79	6000	16	21·0	49	50	210
500	650	192	0·38	3000	32	27·5	35	39	250
500	650	192	0·38	4500	24	27·0	31	34	225
500	650	384	0·77	3000	34	30 0	27	28	230
500	650	384	0·77	4500	22	29·5	25	25	200
1000	95	396	0·40	4500	46	14·8	246	220	475
1000	95	960	0·96	3000	64	16·2	311	320	630
1000	95	960	0·96	4500	46	16·2	214	220	485
1000	95	960	0·96	6000	31	16·2	145	160	400
1000	180	384	0·38	3000	64	19·5	183	180	445
1000	180	384	0·38	4500	46	19·5	161	145	390
1000	320	188	0·19	3000	64	20·0	131	129	405
1000	320	188	0·19	4500	46	19·5	114	105	350
1000	320	396	0·40	1500	128	19·5	123	125	380
1000	320	396	0·40	3000	64	20·0	95	91	340
1000	320	396	0·40	4500	46	20·0	84	82	310
1000	320	396	0·40	6000	31	20·0	77	80	265
1000	650	192	0·19	3000	64	20·0	63	58	305
1000	650	192	0·19	4500	46	25·5	55	55	285
1000	650	381	0·38	3000	64	29·0	47	50	225
1000	650	381	0·38	4500	46	28·5	41	42	220
				(iii) *Oil viscosity* 165 cS					
500	95	960	1·92	3000	32	16·5	278	290	485
500	95	960	1·92	4500	24	16·5	192	170	405
500	320	398	0·80	3000	32	22·0	78	74	300
500	320	398	0·80	4500	24	22·0	68	65	285
1000	320	398	0·40	3000	44	21·5	122	120	405
1000	320	398	0·40	4500	31	21·5	107	110	315

(c). *Relative position of air impingement: a* = 0·55 in.
Oil viscosity 45 cS

Liquid flow rate (lb/hr)	Air velocity (ft/sec)	Air flow rate (lb/hr)	Mass ratio air/liquid	Cup speed (rev/min)	Sheet thickness at impingement (μ)	Axial drop velocity at 1½ in. from lip (ft/sec)	Calc. SMD (μ)	Measured SMD (μ)	Maximum drop size (μ)
500	320	198	0·38	3000	19	21·5	56	60	285
500	320	198	0·38	4500	13	21·5	50	51	260
500	650	387	0·77	3000	19	30·6	23	25	235
500	650	387	0·77	4500	13	29·5	21	23	220
1000	320	380	0·38	3000	38	20·5	105	110	385
1000	320	380	0·38	4500	26	20·0	92	95	340
1000	650	792	0·79	3000	38	29·0	39	41	245
1000	650	792	0·79	4500	26	28·5	34	36	225

APPENDIX IV

Trajectories and Dispersion of Liquid Jets

Appendix IV provides the computer program which was written for the calculation of drop trajectories and droplet flux at various locations downstream from the point of injection. It includes subroutine CALCOM used to plot Figure AIV.1. Approximately 37 seconds of computer time was required.

```
C     CHEMICAL ENGINEERING DEPARTMENT
C     UNIVERSITY OF WINDSOR, WINDSOR, ONTARIO
C     M.S. THESIS
C     TRAJECTORIES AND DISPERSION OF LIQUID JETS
C     PROGRAM VINOD
C     NOMENCLATURE
C     XO = X COORDINATE OF SPRAY
      CENTRELINE TRAJECTORY, CM
C     YO = Y COORDINATE OF SPRAY CENTRE LINE TRAJECTORY, CM
C     XOO = VALUE OF X COORDINATE FOR 1 CM, 2 CM AND 3 CM
C     YOO = CORRESPONDING VALUES OF Y COORDINATE WHEN XOO = 1, 2
      AND 3, CM
C     F = FLUX OF DROPLETS PER UNIT AREA AT A POINT (X, Y, Z),
      GM/CM2-SEC
C     F TOT = TOTAL DROPLET FLUX AT ANY POINT DUE TO W1, W2 and W3
C     W1 = LIQUID EXISTING AS DROPS RANGING FROM 0 TO 120 MICRONS
C     W2 = LIQUID EXISTING AS DROPS RANGING FROM 120 TO 180 MICRONS
C     W3 = LIQUID EXISTING AS DROPS RANGING FROM 180 TO 225 MICRONS
C     SIGY = VARIANCE IN Y DIRECTION, CM
C     SIGZ = VARIANCE IN Z DIRECTION, CM
C     X AVG = AVERAGE DROP DIAMETERS, 60, 150 AND 202.5 MICRONS
C     MUAIR = VISCOSITY OF AIR, POISE
C     VA = VELOCITY OF AIR, CM/SEC
C     VL = VELOCITY OF LIQUID, CM/SEC
C     RHOG = DENSITY OF AIR, GM/CM3
C     RHOL = DENSITY OF LIQUID, GM/CM3
```

```
0001              DIMENSION XO(3,30),YO(3,30),XOO(3),F(3,3),10,3),FTOT(3,30,10)
0002               DIMENSION PLOTXO(32),PLOTYO(32)
0003               DIMENSION W(3),SIGY(3),SIGZ(3),XAVG(3)
0004               REAL MUAIR,KPRIME
0005               PLOTXO(31)=0.0
0006               PLOTYO(31)=0.0
0007               PLOTXO(32)=2.0
0008               PLOTYO(32)=2.0
0009               DO 10 II=1,3
0010               READ 11,W(II),SIGY(II),SIGZ(II),XAVG(II)
0011               PRINT 11,W(II),SIGY(II),SIGZ(II),XAVG(II)
0012          10   CONTINUE
0013           11  FORMAT(2X,F6.4,2X,F4.2,2X,F4.2,2X,F7.5)
0014               CALL PLOTID(' VINOD K MARMAHA','R122000341')
0015               CALL PLOT(0.0,0.5,-3)
0016               CALL AXIS(0.0,0.0,18HX COORDINATE  (CM),-18,10.0,0.0,PLOTXO(31),
                  1 PLOTXO(32))
0017               CALL AXIS(0.0,0.0,18HY COORDINATE  (CM),18,8.0,90.0, PLOTYO(31),
                  1 PLOTYO(32))
0018               MUAIR=0.000176
0019               VA=3048.0
0020               VL=1554.48
0021               RHOG=0.001137
0022               RHOL=0.6824
0023               DO 1 J=1,3
0024               KPRIME=81.0*RHOG/4.0/XAVG(J)/RHOL*((RHOG*XAVG(J)/MUAIR)**(-0.84))
                  1 *((SQRT(1.0+((VA/VL)**2)))**(0.16))
0025               AA=1.0
0026               DO2I=1,30
0027               T=AA/3048.0
0028               YO(J,I)=1.87+(1.19/KPRIME)*(((VL)**0.84)-(0.16*KPRIME*T+((VL)**(-
                  1 0.16)))**(-5.25))
0029               XO(J,I)=VA*T-VA*(YO(J,I)-1.87)/VL
0030               PRINT3,XAVG(J),XO(J,I),YO(J,I),T
0031               AA=AA+1.0
0032               PLOTXO(I)=XO(J,I)
0033               PLOTYO(I)=YO(J,I)
0034             2 CONTINUE
0035               CALL LINE(PLOTXO,PLOTYO,30,1,0,0)
0036             1 CONTINUE
0037               DO9L=1,3
0038               DO4I=1,3
0039               XOO(I)=I
0040               T=0.0001
0041               KPRIME=81.0*RHOG/4.0/XAVG(L)/RHOL*((RHOG*XAVG(L)/MUAIR)**(-0.84))
                  1 *((SQRT(1.0+((VA/VL)**2)))**(0.16))
0042          6    IF(T.GT.0.010) GO TO 999
0043               DUMX=-XOO(I)+VA*T-(VA/VL)*((1.19/KPRIME)*(((VL)**0.84)-(0.16*
                  1 KPRIME*T+((VL)**(-0.16)))**(-5.25)))
```

```
0044                    IF(ABS(DUMX).LE.0.001) GO TO 5
0045                    T=T+0.000001
0046                    GO TO 6
0047                5   YOO=1.87+(1.19/KPRIME)*(((VL)**0.84)-(0.15*KPRIME*T+((VL)**(-0.16
                     1  )))**(-5.25))
0048                    Y=-14.5
0049                    DO 7 J=1,30
0050                    Z=-4.5
0051                    DO 8 K=1,10
0052                    ETC=(-((Y-YOO)**2)/2.0/(SIGY(L)**2)-(Z**2)/2.0/(SIGZ(L)**2))
0053                    IF(ETC.LT.-30.0) GO TO 55
0054                    IF(ETC.GT.30.0) GO TO 55
0055                    F(I,J,K,L)=(W(L)/2.0/3.14159/SIGY(L)/SIGZ(L))*(EXP(ETC))
0056                    GO TO 66
0057           55       F(I,J,K,L)=0.0
0058           66       CONTINUE
0059                    Z=Z+1.0
0060           8        CONTINUE
0061                    Y=Y+1.0
0062           7        CONTINUE
0063           4        CONTINUE
0064           9        CONTINUE
0065                   DO 13 I=1,3
0066                   DO14 J=1,30
0067                   DO 15 K=1,10
0068                   FTOT(I,J,K)=F(I,J,K,1)+F(I,J,K,2)+F(I,J,K,3)
0069           15       CONTINUE
0070           14       CONTINUE
0071           13       CONTINUE
0072                   X=1.0
0073                    DO 16 I=1,3
0074                   Y=-14.5
0075                    DO 17 J=1,30
0076                   Z=-4.5
0077                    DO 18 K=1,10
0078                    PRINT 19,X,Y,Z,F(I,J,K,1),F(I,J,K,2),F(I,J,K,3),FTOT(I,J,K)
0079           19       FORMAT(3X,'F(',F3.1,',',F5.1,',',F4.1,')',9X,'F1=',F9.7,4X,'F2=',
                     1  F9.7,4X,'F3=',F9.7,4X,'FTOT=',F9.7)
0080             18    Z=Z+1.
0081             17    Y=Y+1.
0082             16    X=X+1.
0083           3        FORMAT(' ',4(5X,F14.7))
0084           999      PRINT 998
0085           998      FORMAT(' ','TOLERANCE TOO HIGH')
0086                    CALL PLTEND(15.0)
0087                    STOP
0088                    END
```

		σ_y	σ_z	x_{av} (cm)
WL_1	2.0812	0.40	0.40	0.00600
WL_2	1.9844	0.98	1.09	0.01500
WL_3	0.7744	1.82	1.73	0.02025

x_{av} (cm)	x_o	Y_o	t
0.0060000	0.0503817	2.3543053	0.0003281
0.0060000	0.1931067	2.7915154	0.0006562
0.0060000	0.4180012	3.1868191	0.0009843
0.0060000	0.7160406	3.5448189	0.0013123
0.0060000	1.0793152	3.8695498	0.0016404
0.0060000	1.5009270	4.1645279	0.0019685
0.0060000	1.9747381	4.4328842	0.0022966
0.0060000	2.4953651	4.6773643	0.0026247
0.0060000	3.0580454	4.9003973	0.0029528
0.0060000	3.6585999	5.1041136	0.0032808
0.0060000	4.2931976	5.2904592	0.0036089
0.0060000	4.9585924	5.4611158	0.0039370
0.0060000	5.6517725	5.6175909	0.0042651
0.0060000	6.3701115	5.7612419	0.0045932
0.0060000	7.1112366	5.8932657	0.0049213
0.0060000	7.8730450	6.0147476	0.0052493
0.0060000	8.6535379	6.1266384	0.0055774
0.0060000	9.4513245	6.2298174	0.0059055
0.0060000	10.2645807	6.3250570	0.0062336
0.0060000	11.0920277	6.4130592	0.0065617
0.0060000	11.9324360	6.4944506	0.0068898
0.0060000	12.7846851	6.5698042	0.0072178
0.0060000	13.6477671	6.6396313	0.0075459
0.0060000	14.5207729	6.7043991	0.0078740
0.0060000	15.4028797	6.7645235	0.0082021
0.0060000	16.2933350	6.8203907	0.0085302
0.0060000	17.1914673	6.8723440	0.0088583
0.0060000	18.0966492	6.9206991	0.0091863
0.0060000	19.0083313	6.9657402	0.0095144
0.0060000	19.9259949	7.0077295	0.0098425
0.0150000	0.0097907	2.3750067	0.0003281
0.0150000	0.0386229	2.8703022	0.0006562
0.0150000	0.0858393	3.3562222	0.0009843
0.0150000	0.1511869	3.8328953	0.0013123
0.0150000	0.2339115	4.3007059	0.0016404
0.0150000	0.3340149	4.7596531	0.0019685
0.0150000	0.4511175	5.2099304	0.0022966
0.0150000	0.5844669	5.6519222	0.0026247
0.0150000	0.7342205	6.0855484	0.0029528
0.0150000	0.8998423	6.5110807	0.0032808
0.0150000	1.0805779	6.9289055	0.0036089
0.0150000	1.2766132	7.3389244	0.0039370
0.0150000	1.4876413	7.7412987	0.0042651
0.0150000	1.7128792	8.1364298	0.0045932
0.0150000	1.9524727	8.5242357	0.0049213
0.0150000	2.2056808	8.9051027	0.0052493

TABLE IV.1: LIQUID DROP TRAJECTORIES FOR INJECTION CONDITIONS OF INGEBO AND FOSTER; USING BEHIE AND BEECKMAN'S MODEL

continued ..

x_{av} (cm)	x_o	Y_o	t
0.0150000	2.4727268	9.2783021	0.0055774
0.0150000	2.7530479	9.6459389	0.0059055
0.0150000	3.0464106	10.0063239	0.0062336
0.0150000	3.3523865	10.3602829	0.0065617
0.0150000	3.6710052	10.7077827	0.0068898
0.0150000	4.0017242	11.0491133	0.0072178
0.0150000	4.3444672	11.3843212	0.0075459
0.0150000	4.6989746	11.7135191	0.0078740
0.0150000	5.0648651	12.0369158	0.0082021
0.0150000	5.4422607	12.3544464	0.0085302
0.0150000	5.8303528	12.6655125	0.0088583
0.0150000	6.2293701	12.9730167	0.0091863
0.0150000	6.6390381	13.2740889	0.0095144
0.0150000	7.0587616	13.5700321	0.0098425
0.0202500	0.0058300	2.3770266	0.0003281
0.0202500	0.0224676	2.8785410	0.0006562
0.0202500	0.0504045	3.3742943	0.0009843
0.0202500	0.0888767	3.8646736	0.0013123
0.0202500	0.1376648	4.3497915	0.0016404
0.0202500	0.1967697	4.8296480	0.0019685
0.0202500	0.2665730	5.3040476	0.0022966
0.0202500	0.3458195	5.7736320	0.0026247
0.0202500	0.4360399	6.2375204	0.0029528
0.0202500	0.5355377	6.6968756	0.0032808
0.0202500	0.6446981	7.1512041	0.0036089
0.0202500	0.7638969	7.6004105	0.0039370
0.0202500	0.8925400	8.0447998	0.0042651
0.0202500	1.0305824	8.4844017	0.0045932
0.0202500	1.1777306	8.9193544	0.0049213
0.0202500	1.3340044	9.3496580	0.0052493
0.0202500	1.4993181	9.7753401	0.0055774
0.0202500	1.6738739	10.1963177	0.0059055
0.0202500	1.8568878	10.6129799	0.0062336
0.0202500	2.0489655	11.0250216	0.0065617
0.0202500	2.2496796	11.4326639	0.0068898
0.0202500	2.4582825	11.8362703	0.0072178
0.0202500	2.6753575	12.2353106	0.0075459
0.0202500	2.9016113	12.6301756	0.0078740
0.0202500	3.1356049	13.0208368	0.0082021
0.0202500	3.3776855	13.4073772	0.0085302
0.0202500	3.6276703	13.7898817	0.0088583
0.0202500	3.8856964	14.1682940	0.0091863
0.0202500	4.1513977	14.5427809	0.0095144
0.0202500	4.4248047	14.9133425	0.0098425

TABLE AIV.1: LIQUID DROP TRAJECTORIES FOR INJECTION CONDITIONS OF INGEBO AND FOSTER; USING BEHIE AND BEECKMAN'S MODEL

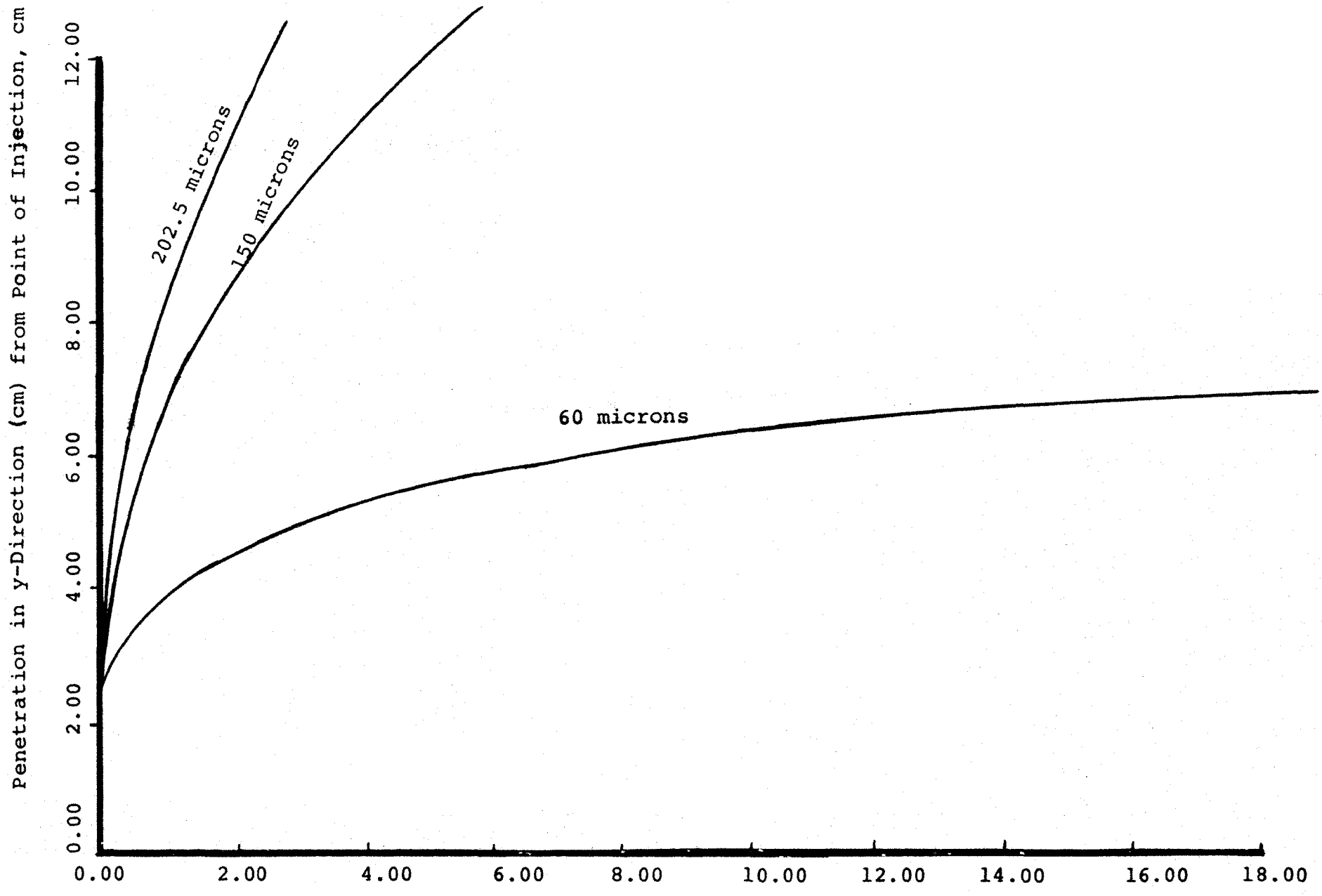

FIGURE AIV.1: Trajectories of Liquid Drops

Flux at Any Point	Flux due to WL1	Flux due to WL2	Flux due to WL3	Total Flux
F(1.0,-14.5,-4.5)	F1=0.0	F2=0.0	F3=0.0	FTOT=0.0
F(1.0,-14.5,-3.5)	F1=0.0	F2=0.0	F3=0.0	FTOT=0.0
F(1.0,-14.5,-2.5)	F1=0.0	F2=0.0	F3=0.0	FTOT=0.0
F(1.0,-14.5,-1.5)	F1=0.0	F2=0.0	F3=0.0	FTOT=0.0
F(1.0,-14.5,-0.5)	F1=0.0	F2=0.0	F3=0.0	FTOT=0.0
F(1.0,-14.5, 0.5)	F1=0.0	F2=0.0	F3=0.0	FTOT=0.0
F(1.0,-14.5, 1.5)	F1=0.0	F2=0.0	F3=0.0	FTOT=0.0
F(1.0,-14.5, 2.5)	F1=0.0	F2=0.0	F3=0.0	FTOT=0.0
F(1.0,-14.5, 3.5)	F1=0.0	F2=0.0	F3=0.0	FTOT=0.0
F(1.0,-14.5, 4.5)	F1=0.0	F2=0.0	F3=0.0	FTOT=0.0
F(1.0,-13.5,-4.5)	F1=0.0	F2=0.0	F3=0.0	FTOT=0.0
F(1.0,-13.5,-3.5)	F1=0.0	F2=0.0	F3=0.0	FTOT=0.0
F(1.0,-13.5,-2.5)	F1=0.0	F2=0.0	F3=0.0	FTOT=0.0
F(1.0,-13.5,-1.5)	F1=0.0	F2=0.0	F3=0.0	FTOT=0.0
F(1.0,-13.5,-0.5)	F1=0.0	F2=0.0	F3=0.0	FTOT=0.0
F(1.0,-13.5, 0.5)	F1=0.0	F2=0.0	F3=0.0	FTOT=0.0
F(1.0,-13.5, 1.5)	F1=0.0	F2=0.0	F3=0.0	FTOT=0.0
F(1.0,-13.5, 2.5)	F1=0.0	F2=0.0	F3=0.0	FTOT=0.0
F(1.0,-13.5, 3.5)	F1=0.0	F2=0.0	F3=0.0	FTOT=0.0
F(1.0,-13.5, 4.5)	F1=0.0	F2=0.0	F3=0.0	FTOT=0.0
F(1.0,-12.5,-4.5)	F1=0.0	F2=0.0	F3=0.0	FTOT=0.0
F(1.0,-12.5,-3.5)	F1=0.0	F2=0.0	F3=0.0	FTOT=0.0
F(1.0,-12.5,-2.5)	F1=0.0	F2=0.0	F3=0.0	FTOT=0.0
F(1.0,-12.5,-1.5)	F1=0.0	F2=0.0	F3=0.0	FTOT=0.0
F(1.0,-12.5,-0.5)	F1=0.0	F2=0.0	F3=0.0	FTOT=0.0
F(1.0,-12.5, 0.5)	F1=0.0	F2=0.0	F3=0.0	FTOT=0.0
F(1.0,-12.5, 1.5)	F1=0.0	F2=0.0	F3=0.0	FTOT=0.0
F(1.0,-12.5, 2.5)	F1=0.0	F2=0.0	F3=0.0	FTOT=0.0
F(1.0,-12.5, 3.5)	F1=0.0	F2=0.0	F3=0.0	FTOT=0.0
F(1.0,-12.5, 4.5)	F1=0.0	F2=0.0	F3=0.0	FTOT=0.0
F(1.0,-11.5,-4.5)	F1=0.0	F2=0.0	F3=0.0	FTOT=0.0
F(1.0,-11.5,-3.5)	F1=0.0	F2=0.0	F3=0.0	FTOT=0.0
F(1.0,-11.5,-2.5)	F1=0.0	F2=0.0	F3=0.0	FTOT=0.0
F(1.0,-11.5,-1.5)	F1=0.0	F2=0.0	F3=0.0	FTOT=0.0
F(1.0,-11.5,-0.5)	F1=0.0	F2=0.0	F3=0.0	FTOT=0.0
F(1.0,-11.5, 0.5)	F1=0.0	F2=0.0	F3=0.0	FTOT=0.0
F(1.0,-11.5, 1.5)	F1=0.0	F2=0.0	F3=0.0	FTOT=0.0
F(1.0,-11.5, 2.5)	F1=0.0	F2=0.0	F3=0.0	FTOT=0.0
F(1.0,-11.5, 3.5)	F1=0.0	F2=0.0	F3=0.0	FTOT=0.0
F(1.0,-11.5, 4.5)	F1=0.0	F2=0.0	F3=0.0	FTOT=0.0
F(1.0,-10.5,-4.5)	F1=0.0	F2=0.0	F3=0.0	FTOT=0.0
F(1.0,-10.5,-3.5)	F1=0.0	F2=0.0	F3=0.0	FTOT=0.0
F(1.0,-10.5,-2.5)	F1=0.0	F2=0.0	F3=0.0	FTOT=0.0
F(1.0,-10.5,-1.5)	F1=0.0	F2=0.0	F3=0.0	FTOT=0.0
F(1.0,-10.5,-0.5)	F1=0.0	F2=0.0	F3=0.0	FTOT=0.0
F(1.0,-10.5, 0.5)	F1=0.0	F2=0.0	F3=0.0	FTOT=0.0
F(1.0,-10.5, 1.5)	F1=0.0	F2=0.0	F3=0.0	FTOT=0.0
F(1.0,-10.5, 2.5)	F1=0.0	F2=0.0	F3=0.0	FTOT=0.0
F(1.0,-10.5, 3.5)	F1=0.0	F2=0.0	F3=0.0	FTOT=0.0

TABLE AIV.2: LIQUID DROP FLUX AT VARIOUS POSITIONS DOWNSTREAM FROM POINT OF INJECTION

Flux at Any Point	Flux due to WL1	Flux due to WL2	Flux due to WL3	Total Flux
F(1.0,-10.5, 4.5)	F1=0.0	F2=0.0	F3=0.0	FTOT=0.0
F(1.0, -9.5,-4.5)	F1=0.0	F2=0.0	F3=0.0	FTOT=0.0
F(1.0, -9.5,-3.5)	F1=0.0	F2=0.0	F3=0.0	FTOT=0.0
F(1.0, -9.5,-2.5)	F1=0.0	F2=0.0	F3=0.0	FTOT=0.0
F(1.0, -9.5,-1.5)	F1=0.0	F2=0.0	F3=0.0	FTOT=0.0
F(1.0, -9.5,-0.5)	F1=0.0	F2=0.0	F3=0.0	FTOT=0.0
F(1.0, -9.5, 0.5)	F1=0.0	F2=0.0	F3=0.0	FTOT=0.0
F(1.0, -9.5, 1.5)	F1=0.0	F2=0.0	F3=0.0	FTOT=0.0
F(1.0, -9.5, 2.5)	F1=0.0	F2=0.0	F3=0.0	FTOT=0.0
F(1.0, -9.5, 3.5)	F1=0.0	F2=0.0	F3=0.0	FTOT=0.0
F(1.0, -9.5, 4.5)	F1=0.0	F2=0.0	F3=0.0	FTOT=0.0
F(1.0, -8.5,-4.5)	F1=0.0	F2=0.0	F3=0.0	FTOT=0.0
F(1.0, -8.5,-3.5)	F1=0.0	F2=0.0	F3=0.0	FTOT=0.0
F(1.0, -8.5,-2.5)	F1=0.0	F2=0.0	F3=0.0	FTOT=0.0
F(1.0, -8.5,-1.5)	F1=0.0	F2=0.0	F3=0.0	FTOT=0.0
F(1.0, -8.5,-0.5)	F1=0.0	F2=0.0	F3=0.0	FTOT=0.0
F(1.0, -8.5, 0.5)	F1=0.0	F2=0.0	F3=0.0	FTOT=0.0
F(1.0, -8.5, 1.5)	F1=0.0	F2=0.0	F3=0.0	FTOT=0.0
F(1.0, -8.5, 2.5)	F1=0.0	F2=0.0	F3=0.0	FTOT=0.0
F(1.0, -8.5, 3.5)	F1=0.0	F2=0.0	F3=0.0	FTOT=0.0
F(1.0, -8.5, 4.5)	F1=0.0	F2=0.0	F3=0.0	FTOT=0.0
F(1.0, -7.5,-4.5)	F1=0.0	F2=0.0	F3=0.0	FTOT=0.0
F(1.0, -7.5,-3.5)	F1=0.0	F2=0.0	F3=0.0	FTOT=0.0
F(1.0, -7.5,-2.5)	F1=0.0	F2=0.0	F3=0.0	FTOT=0.0
F(1.0, -7.5,-1.5)	F1=0.0	F2=0.0	F3=0.0	FTOT=0.0
F(1.0, -7.5,-0.5)	F1=0.0	F2=0.0	F3=0.0	FTOT=0.0
F(1.0, -7.5, 0.5)	F1=0.0	F2=0.0	F3=0.0	FTOT=0.0
F(1.0, -7.5, 1.5)	F1=0.0	F2=0.0	F3=0.0	FTOT=0.0
F(1.0, -7.5, 2.5)	F1=0.0	F2=0.0	F3=0.0	FTOT=0.0
F(1.0, -7.5, 3.5)	F1=0.0	F2=0.0	F3=0.0	FTOT=0.0
F(1.0, -7.5, 4.5)	F1=0.0	F2=0.0	F3=0.0	FTOT=0.0
F(1.0, -6.5,-4.5)	F1=0.0	F2=0.0	F3=0.0	FTOT=0.0
F(1.0, -6.5,-3.5)	F1=0.0	F2=0.0	F3=0.0	FTOT=0.0
F(1.0, -6.5,-2.5)	F1=0.0	F2=0.0	F3=0.0	FTOT=0.0
F(1.0, -6.5,-1.5)	F1=0.0	F2=0.0	F3=0.0	FTOT=0.0
F(1.0, -6.5,-0.5)	F1=0.0	F2=0.0	F3=0.0	FTOT=0.0
F(1.0, -6.5, 0.5)	F1=0.0	F2=0.0	F3=0.0	FTOT=0.0
F(1.0, -6.5, 1.5)	F1=0.0	F2=0.0	F3=0.0	FTOT=0.0
F(1.0, -6.5, 2.5)	F1=0.0	F2=0.0	F3=0.0	FTOT=0.0
F(1.0, -6.5, 3.5)	F1=0.0	F2=0.0	F3=0.0	FTOT=0.0
F(1.0, -6.5, 4.5)	F1=0.0	F2=0.0	F3=0.0	FTOT=0.0
F(1.0, -5.5,-4.5)	F1=0.0	F2=0.0	F3=0.0	FTOT=0.0
F(1.0, -5.5,-3.5)	F1=0.0	F2=0.0	F3=0.0	FTOT=0.0
F(1.0, -5.5,-2.5)	F1=0.0	F2=0.0	F3=0.0	FTOT=0.0
F(1.0, -5.5,-1.5)	F1=0.0	F2=0.0	F3=0.0000000	FTOT=0.0000000
F(1.0, -5.5,-0.5)	F1=0.0	F2=0.0	F3=0.0000000	FTOT=0.0000000
F(1.0, -5.5, 0.5)	F1=0.0	F2=0.0	F3=0.0000000	FTOT=0.0000000
F(1.0, -5.5, 1.5)	F1=0.0	F2=0.0	F3=0.0000000	FTOT=0.0000000

TABLE AIV.2 LIQUID DROP FLUX AT VARIOUS POSITIONS DOWNSTREAM FROM POINT OF INJECTION

continued ..

Flux at Any Point	Flux due to WL1	Flux due to WL2	Flux due to WL3	Total Flux
F(1.0, -5.5, 2.5)	F1=0.0	F2=0.0	F3=0.0	FTOT=0.0
F(1.0, -5.5, 3.5)	F1=0.0	F2=0.0	F3=0.0	FTOT=0.0
F(1.0, -5.5, 4.5)	F1=0.0	F2=0.0	F3=0.0	FTOT=0.0
F(1.0, -4.5,-4.5)	F1=0.0	F2=0.0	F3=0.0000000	FTOT=0.0000000
F(1.0, -4.5,-3.5)	F1=0.0	F2=0.0	F3=0.0000000	FTOT=0.0000000
F(1.0, -4.5,-2.5)	F1=0.0	F2=0.0	F3=0.0000000	FTOT=0.0000000
F(1.0, -4.5,-1.5)	F1=0.0	F2=0.0	F3=0.0000000	FTOT=0.0000000
F(1.0, -4.5,-0.5)	F1=0.0	F2=0.0	F3=0.0000000	FTOT=0.0000000
F(1.0, -4.5, 0.5)	F1=0.0	F2=0.0	F3=0.0000000	FTOT=0.0000000
F(1.0, -4.5, 1.5)	F1=0.0	F2=0.0	F3=0.0000000	FTOT=0.0000000
F(1.0, -4.5, 2.5)	F1=0.0	F2=0.0	F3=0.0000000	FTOT=0.0000000
F(1.0, -4.5, 3.5)	F1=0.0	F2=0.0	F3=0.0000000	FTOT=0.0000000
F(1.0, -4.5, 4.5)	F1=0.0	F2=0.0	F3=0.0000000	FTOT=0.0000000
F(1.0, -3.5,-4.5)	F1=0.0	F2=0.0	F3=0.0000000	FTOT=0.0000000
F(1.0, -3.5,-3.5)	F1=0.0	F2=0.0	F3=0.0000000	FTOT=0.0000000
F(1.0, -3.5,-2.5)	F1=0.0	F2=0.0	F3=0.0000000	FTOT=0.0000000
F(1.0, -3.5,-1.5)	F1=0.0	F2=0.0	F3=0.0000000	FTOT=0.0000000
F(1.0, -3.5,-0.5)	F1=0.0	F2=0.0	F3=0.0000000	FTOT=0.0000000
F(1.0, -3.5, 0.5)	F1=0.0	F2=0.0	F3=0.0000000	FTOT=0.0000000
F(1.0, -3.5, 1.5)	F1=0.0	F2=0.0	F3=0.0000000	FTOT=0.0000000
F(1.0, -3.5, 2.5)	F1=0.0	F2=0.0	F3=0.0000000	FTOT=0.0000000
F(1.0, -3.5, 3.5)	F1=0.0	F2=0.0	F3=0.0000000	FTOT=0.0000000
F(1.0, -3.5, 4.5)	F1=0.0	F2=0.0	F3=0.0000000	FTOT=0.0000000
F(1.0, -2.5,-4.5)	F1=0.0	F2=0.0	F3=0.0000000	FTOT=0.0000000
F(1.0, -2.5,-3.5)	F1=0.0	F2=0.0	F3=0.0000000	FTOT=0.0000000
F(1.0, -2.5,-2.5)	F1=0.0	F2=0.0	F3=0.0000000	FTOT=0.0000000
F(1.0, -2.5,-1.5)	F1=0.0	F2=0.0	F3=0.0000000	FTOT=0.0000000
F(1.0, -2.5,-0.5)	F1=0.0	F2=0.0	F3=0.0000000	FTOT=0.0000000
F(1.0, -2.5, 0.5)	F1=0.0	F2=0.0	F3=0.0000000	FTOT=0.0000000
F(1.0, -2.5, 1.5)	F1=0.0	F2=0.0	F3=0.0000000	FTOT=0.0000000
F(1.0, -2.5, 2.5)	F1=0.0	F2=0.0	F3=0.0000000	FTOT=0.0000000
F(1.0, -2.5, 3.5)	F1=0.0	F2=0.0	F3=0.0000000	FTOT=0.0000000
F(1.0, -2.5, 4.5)	F1=0.0	F2=0.0	F3=0.0000000	FTOT=0.0000000
F(1.0, -1.5,-4.5)	F1=0.0	F2=0.0	F3=0.0000000	FTOT=0.0000000
F(1.0, -1.5,-3.5)	F1=0.0	F2=0.0	F3=0.0000000	FTOT=0.0000000
F(1.0, -1.5,-2.5)	F1=0.0	F2=0.0	F3=0.0000000	FTOT=0.0000000
F(1.0, -1.5,-1.5)	F1=0.0	F2=0.0	F3=0.0000000	FTOT=0.0000000
F(1.0, -1.5,-0.5)	F1=0.0	F2=0.0	F3=0.0000000	FTOT=0.0000000
F(1.0, -1.5, 0.5)	F1=0.0	F2=0.0	F3=0.0000000	FTOT=0.0000000
F(1.0, -1.5, 1.5)	F1=0.0	F2=0.0	F3=0.0000000	FTOT=0.0000000
F(1.0, -1.5, 2.5)	F1=0.0	F2=0.0	F3=0.0000000	FTOT=0.0000000
F(1.0, -1.5, 3.5)	F1=0.0	F2=0.0	F3=0.0000000	FTOT=0.0000000
F(1.0, -1.5, 4.5)	F1=0.0	F2=0.0	F3=0.0000000	FTOT=0.0000000
F(1.0, -0.5,-4.5)	F1=0.0	F2=0.0	F3=0.0000000	FTOT=0.0000000
F(1.0, -0.5,-3.5)	F1=0.0	F2=0.0	F3=0.0000000	FTOT=0.0000000
F(1.0, -0.5,-2.5)	F1=0.0	F2=0.0000000	F3=0.0000001	FTOT=0.0000001
F(1.0, -0.5,-1.5)	F1=0.0	F2=0.0000000	F3=0.0000002	FTOT=0.0000002
F(1.0, -0.5,-0.5)	F1=0.0	F2=0.0000000	F3=0.0000002	FTOT=0.0000002
F(1.0, -0.5, 0.5)	F1=0.0	F2=0.0000000	F3=0.0000002	FTOT=0.0000002

TABLE AIV.2 LIQUID DROP FLUX AT VARIOUS POSITIONS DOWNSTREAM FROM POINT OF INJECTION

continued ..

Flux at Any Point	Flux due to WL1	Flux due to WL2	Flux due to WL3	Total Flux
F(1.0, -0.5, 1.5)	F1=0.0	F2=0.0000000	F3=0.0000002	FTOT=0.0000002
F(1.0, -0.5, 2.5)	F1=0.0	F2=0.0000000	F3=0.0000001	FTOT=0.0000001
F(1.0, -0.5, 3.5)	F1=0.0	F2=0.0	F3=0.0000000	FTOT=0.0000000
F(1.0, -0.5, 4.5)	F1=0.0	F2=0.0	F3=0.0000000	FTOT=0.0000000
F(1.0, 0.5,-4.5)	F1=0.0	F2=0.0000000	F3=0.0000001	FTOT=0.0000001
F(1.0, 0.5,-3.5)	F1=0.0	F2=0.0000000	F3=0.0000004	FTOT=0.0000004
F(1.0, 0.5,-2.5)	F1=0.0	F2=0.0000000	F3=0.0000011	FTOT=0.0000011
F(1.0, 0.5,-1.5)	F1=0.0	F2=0.0000000	F3=0.0000022	FTOT=0.0000022
F(1.0, 0.5,-0.5)	F1=0.0	F2=0.0000000	F3=0.0000031	FTOT=0.0000031
F(1.0, 0.5, 0.5)	F1=0.0	F2=0.0000000	F3=0.0000031	FTOT=0.0000031
F(1.0, 0.5, 1.5)	F1=0.0	F2=0.0000000	F3=0.0000022	FTOT=0.0000022
F(1.0, 0.5, 2.5)	F1=0.0	F2=0.0000000	F3=0.0000011	FTOT=0.0000011
F(1.0, 0.5, 3.5)	F1=0.0	F2=0.0000000	F3=0.0000004	FTOT=0.0000004
F(1.0, 0.5, 4.5)	F1=0.0	F2=0.0000000	F3=0.0000001	FTOT=0.0000001
F(1.0, 1.5,-4.5)	F1=0.0	F2=0.0000000	F3=0.0000010	FTOT=0.0000010
F(1.0, 1.5,-3.5)	F1=0.0	F2=0.0000000	F3=0.0000039	FTOT=0.0000039
F(1.0, 1.5,-2.5)	F1=0.0	F2=0.0000000	F3=0.0000107	FTOT=0.0000107
F(1.0, 1.5,-1.5)	F1=0.0000000	F2=0.0000001	F3=0.0000208	FTOT=0.0000209
F(1.0, 1.5,-0.5)	F1=0.0000001	F2=0.0000002	F3=0.0000291	FTOT=0.0000293
F(1.0, 1.5, 0.5)	F1=0.0000001	F2=0.0000002	F3=0.0000291	FTOT=0.0000293
F(1.0, 1.5, 1.5)	F1=0.0000000	F2=0.0000001	F3=0.0000208	FTOT=0.0000209
F(1.0, 1.5, 2.5)	F1=0.0	F2=0.0000000	F3=0.0000107	FTOT=0.0000107
F(1.0, 1.5, 3.5)	F1=0.0	F2=0.0000000	F3=0.0000039	FTOT=0.0000039
F(1.0, 1.5, 4.5)	F1=0.0	F2=0.0000000	F3=0.0000010	FTOT=0.0000010
F(1.0, 2.5,-4.5)	F1=0.0	F2=0.0000000	F3=0.0000071	FTOT=0.0000071
F(1.0, 2.5,-3.5)	F1=0.0	F2=0.0000001	F3=0.0000270	FTOT=0.0000271
F(1.0, 2.5,-2.5)	F1=0.0000000	F2=0.0000018	F3=0.0000735	FTOT=0.0000752
F(1.0, 2.5,-1.5)	F1=0.0000089	F2=0.0000096	F3=0.0001433	FTOT=0.0001618
F(1.0, 2.5,-0.5)	F1=0.0046263	F2=0.0000222	F3=0.0002002	FTOT=0.0048487
F(1.0, 2.5, 0.5)	F1=0.0046263	F2=0.0000222	F3=0.0002002	FTOT=0.0048487
F(1.0, 2.5, 1.5)	F1=0.0000089	F2=0.0000096	F3=0.0001433	FTOT=0.0001618
F(1.0, 2.5, 2.5)	F1=0.0000000	F2=0.0000018	F3=0.0000735	FTOT=0.0000752
F(1.0, 2.5, 3.5)	F1=0.0	F2=0.0000001	F3=0.0000270	FTOT=0.0000271
F(1.0, 2.5, 4.5)	F1=0.0	F2=0.0000000	F3=0.0000071	FTOT=0.0000071
F(1.0, 3.5,-4.5)	F1=0.0	F2=0.0000002	F3=0.0000360	FTOT=0.0000363
F(1.0, 3.5,-3.5)	F1=0.0	F2=0.0000071	F3=0.0001372	FTOT=0.0001442
F(1.0, 3.5,-2.5)	F1=0.0000000	F2=0.0000881	F3=0.0003737	FTOT=0.0004618
F(1.0, 3.5,-1.5)	F1=0.0013680	F2=0.0004742	F3=0.0007291	FTOT=0.0025713
F(1.0, 3.5,-0.5)	F1=0.7086405	F2=0.0011003	F3=0.0010183	FTOT=0.7107591
F(1.0, 3.5, 0.5)	F1=0.7086405	F2=0.0011003	F3=0.0010183	FTOT=0.7107591
F(1.0, 3.5, 1.5)	F1=0.0013680	F2=0.0004742	F3=0.0007291	FTOT=0.0025713
F(1.0, 3.5, 2.5)	F1=0.0000000	F2=0.0000881	F3=0.0003737	FTOT=0.0004618
F(1.0, 3.5, 3.5)	F1=0.0	F2=0.0000071	F3=0.0001372	FTOT=0.0001442
F(1.0, 3.5, 4.5)	F1=0.0	F2=0.0000002	F3=0.0000360	FTOT=0.0000363
F(1.0, 4.5,-4.5)	F1=0.0	F2=0.0000042	F3=0.0001356	FTOT=0.0001398
F(1.0, 4.5,-3.5)	F1=0.0	F2=0.0001232	F3=0.0005160	FTOT=0.0006391
F(1.0, 4.5,-2.5)	F1=0.0000000	F2=0.0015383	F3=0.0014059	FTOT=0.0029442
F(1.0, 4.5,-1.5)	F1=0.0004045	F2=0.0082318	F3=0.0027427	FTOT=0.0114290

TABLE AIV.2 LIQUID DROP FLUX AT VARIOUS POSITIONS DOWNSTREAM FROM POINT OF INJECTION

continued ..

Flux at Any Point	Flux due to WL1	Flux due to WL2	Flux due to WL3	Total Flux
F(1.0, 4.5,-0.5)	F1=0.2095453	F2=0.0192159	F3=0.0038307	FTOT=0.2325919
F(1.0, 4.5, 0.5)	F1=0.2095453	F2=0.0192159	F3=0.0038307	FTOT=0.2325919
F(1.0, 4.5, 1.5)	F1=0.0004045	F2=0.0082819	F3=0.0027427	FTOT=0.0114290
F(1.0, 4.5, 2.5)	F1=0.0000000	F2=0.0015383	F3=0.0014059	FTOT=0.0029442
F(1.0, 4.5, 3.5)	F1=0.0	F2=0.0001232	F3=0.0005160	FTOT=0.0006391
F(1.0, 4.5, 4.5)	F1=0.0	F2=0.0000042	F3=0.0001356	FTOT=0.0001398
F(1.0, 5.5,-4.5)	F1=0.0	F2=0.0000262	F3=0.0003771	FTOT=0.0004033
F(1.0, 5.5,-3.5)	F1=0.0	F2=0.0007592	F3=0.0014352	FTOT=0.0021944
F(1.0, 5.5,-2.5)	F1=0.0000000	F2=0.0094838	F3=0.0039105	FTOT=0.0133943
F(1.0, 5.5,-1.5)	F1=0.0000002	F2=0.0510572	F3=0.0076287	FTOT=0.0586862
F(1.0, 5.5,-0.5)	F1=0.0001195	F2=0.1184563	F3=0.0106551	FTOT=0.1292409
F(1.0, 5.5, 0.5)	F1=0.0001196	F2=0.1184563	F3=0.0106551	FTOT=0.1292409
F(1.0, 5.5, 1.5)	F1=0.0000002	F2=0.0510572	F3=0.0076287	FTOT=0.0586862
F(1.0, 5.5, 2.5)	F1=0.0000000	F2=0.0094838	F3=0.0039105	FTOT=0.0133943
F(1.0, 5.5, 3.5)	F1=0.0	F2=0.0007592	F3=0.0014352	FTOT=0.0021944
F(1.0, 5.5, 4.5)	F1=0.0	F2=0.0000262	F3=0.0003771	FTOT=0.0004033
F(1.0, 6.5,-4.5)	F1=0.0	F2=0.0000570	F3=0.0007756	FTOT=0.0008326
F(1.0, 6.5,-3.5)	F1=0.0	F2=0.0016523	F3=0.0029517	FTOT=0.0046041
F(1.0, 6.5,-2.5)	F1=0.0	F2=0.0206402	F3=0.0080426	FTOT=0.0286829
F(1.0, 6.5,-1.5)	F1=0.0000000	F2=0.1111192	F3=0.0156897	FTOT=0.1268088
F(1.0, 6.5,-0.5)	F1=0.0000000	F2=0.2578259	F3=0.0219141	FTOT=0.2797399
F(1.0, 6.5, 0.5)	F1=0.0000000	F2=0.2578259	F3=0.0219141	FTOT=0.2797399
F(1.0, 6.5, 1.5)	F1=0.0000000	F2=0.1111192	F3=0.0156897	FTOT=0.1268088
F(1.0, 6.5, 2.5)	F1=0.0	F2=0.0206402	F3=0.0080426	FTOT=0.0286829
F(1.0, 6.5, 3.5)	F1=0.0	F2=0.0016523	F3=0.0029517	FTOT=0.0046041
F(1.0, 6.5, 4.5)	F1=0.0	F2=0.0000570	F3=0.0007756	FTOT=0.0008326
F(1.0, 7.5,-4.5)	F1=0.0	F2=0.0000438	F3=0.0011795	FTOT=0.0012233
F(1.0, 7.5,-3.5)	F1=0.0	F2=0.0012695	F3=0.0044887	FTOT=0.0057582
F(1.0, 7.5,-2.5)	F1=0.0	F2=0.0158579	F3=0.0122307	FTOT=0.0280885
F(1.0, 7.5,-1.5)	F1=0.0	F2=0.0853727	F3=0.0238598	FTOT=0.1092325
F(1.0, 7.5,-0.5)	F1=0.0	F2=0.1980874	F3=0.0333254	FTOT=0.2314127
F(1.0, 7.5, 0.5)	F1=0.0	F2=0.1980874	F3=0.0333254	FTOT=0.2314127
F(1.0, 7.5, 1.5)	F1=0.0	F2=0.0853727	F3=0.0238598	FTOT=0.1092325
F(1.0, 7.5, 2.5)	F1=0.0	F2=0.0158579	F3=0.0122307	FTOT=0.0280885
F(1.0, 7.5, 3.5)	F1=0.0	F2=0.0012695	F3=0.0044887	FTOT=0.0057582
F(1.0, 7.5, 4.5)	F1=0.0	F2=0.0000438	F3=0.0011795	FTOT=0.0012233
F(1.0, 8.5,-4.5)	F1=0.0	F2=0.0000119	F3=0.0013263	FTOT=0.0013382
F(1.0, 8.5,-3.5)	F1=0.0	F2=0.0003443	F3=0.0050474	FTOT=0.0053917
F(1.0, 8.5,-2.5)	F1=0.0	F2=0.0043010	F3=0.0137528	FTOT=0.0180538
F(1.0, 8.5,-1.5)	F1=0.0	F2=0.0231552	F3=0.0268291	FTOT=0.0499843
F(1.0, 8.5,-0.5)	F1=0.0	F2=0.0537262	F3=0.0374727	FTOT=0.0911989
F(1.0, 8.5, 0.5)	F1=0.0	F2=0.0537262	F3=0.0374727	FTOT=0.0911989
F(1.0, 8.5, 1.5)	F1=0.0	F2=0.0231552	F3=0.0268291	FTOT=0.0499843
F(1.0, 8.5, 2.5)	F1=0.0	F2=0.0043010	F3=0.0137528	FTOT=0.0180538
F(1.0, 8.5, 3.5)	F1=0.0	F2=0.0003443	F3=0.0050474	FTOT=0.0053917
F(1.0, 8.5, 4.5)	F1=0.0	F2=0.0000119	F3=0.0013263	FTOT=0.0013382
F(1.0, 9.5,-4.5)	F1=0.0	F2=0.0000011	F3=0.0011027	FTOT=0.0011038

TABLE AIV.2 LIQUID DROP FLUX AT VARIOUS POSITIONS DOWNSTREAM FROM POINT OF INJECTION

continued ..

Flux at Any Point	Flux due to WL1	Flux due to WL2	Flux due to WL3	Total Flux
F(1.0, 9.5,-3.5)	F1=0.0	F2=0.0000330	F3=0.0041966	FTOT=0.0042295
F(1.0, 9.5,-2.5)	F1=0.0	F2=0.0004118	F3=0.0114345	FTOT=0.0118464
F(1.0, 9.5,-1.5)	F1=0.0	F2=0.0022170	F3=0.0223067	FTOT=0.0245237
F(1.0, 9.5,-0.5)	F1=0.0	F2=0.0051441	F3=0.0311561	FTOT=0.0363003
F(1.0, 9.5, 0.5)	F1=0.0	F2=0.0051441	F3=0.0311561	FTOT=0.0363003
F(1.0, 9.5, 1.5)	F1=0.0	F2=0.0022170	F3=0.0223067	FTOT=0.0245237
F(1.0, 9.5, 2.5)	F1=0.0	F2=0.0004118	F3=0.0114345	FTOT=0.0118464
F(1.0, 9.5, 3.5)	F1=0.0	F2=0.0000330	F3=0.0041966	FTOT=0.0042295
F(1.0, 9.5, 4.5)	F1=0.0	F2=0.0000011	F3=0.0011027	FTOT=0.0011038
F(1.0, 10.5,-4.5)	F1=0.0	F2=0.0000000	F3=0.0006779	FTOT=0.0006780
F(1.0, 10.5,-3.5)	F1=0.0	F2=0.0000011	F3=0.0025799	FTOT=0.0025811
F(1.0, 10.5,-2.5)	F1=0.0	F2=0.0000139	F3=0.0070297	FTOT=0.0070436
F(1.0, 10.5,-1.5)	F1=0.0	F2=0.0000749	F3=0.0137136	FTOT=0.0137885
F(1.0, 10.5,-0.5)	F1=0.0	F2=0.0001739	F3=0.0191540	FTOT=0.0193279
F(1.0, 10.5, 0.5)	F1=0.0	F2=0.0001739	F3=0.0191540	FTOT=0.0193279
F(1.0, 10.5, 1.5)	F1=0.0	F2=0.0000749	F3=0.0137136	FTOT=0.0137885
F(1.0, 10.5, 2.5)	F1=0.0	F2=0.0000139	F3=0.0070297	FTOT=0.0070436
F(1.0, 10.5, 3.5)	F1=0.0	F2=0.0000011	F3=0.0025799	FTOT=0.0025811
F(1.0, 10.5, 4.5)	F1=0.0	F2=0.0000000	F3=0.0006779	FTOT=0.0006780
F(1.0, 11.5,-4.5)	F1=0.0	F2=0.0000000	F3=0.0003082	FTOT=0.0003082
F(1.0, 11.5,-3.5)	F1=0.0	F2=0.0000000	F3=0.0011728	FTOT=0.0011728
F(1.0, 11.5,-2.5)	F1=0.0	F2=0.0000002	F3=0.0031955	FTOT=0.0031957
F(1.0, 11.5,-1.5)	**F1=0.0**	**F2=0.0000009**	**F3=0.0062339**	**FTOT=0.0062347**
F(1.0, 11.5,-0.5)	F1=0.0	F2=0.0000021	F3=0.0087069	FTOT=0.0087090
F(1.0, 11.5, 0.5)	F1=0.0	F2=0.0000021	F3=0.0087069	FTOT=0.0087090
F(1.0, 11.5, 1.5)	F1=0.0	F2=0.0000009	F3=0.0062339	FTOT=0.0062347
F(1.0, 11.5, 2.5)	F1=0.0	F2=0.0000002	F3=0.0031955	FTOT=0.0031957
F(1.0, 11.5, 3.5)	F1=0.0	F2=0.0000000	F3=0.0011728	FTOT=0.0011728
F(1.0, 11.5, 4.5)	F1=0.0	F2=0.0000000	F3=0.0003082	FTOT=0.0003082
F(1.0, 12.5,-4.5)	F1=0.0	F2=0.0000000	F3=0.0001036	FTOT=0.0001036
F(1.0, 12.5,-3.5)	F1=0.0	F2=0.0000000	F3=0.0003942	FTOT=0.0003942
F(1.0, 12.5,-2.5)	F1=0.0	F2=0.0000000	F3=0.0010741	FTOT=0.0010741
F(1.0, 12.5,-1.5)	F1=0.0	F2=0.0000000	F3=0.0020953	FTOT=0.0020953
F(1.0, 12.5,-0.5)	F1=0.0	F2=0.0000000	F3=0.0029266	FTOT=0.0029266
F(1.0, 12.5, 0.5)	F1=0.0	F2=0.0000000	F3=0.0029266	FTOT=0.0029266
F(1.0, 12.5, 1.5)	F1=0.0	F2=0.0000000	F3=0.0020953	FTOT=0.0020953
F(1.0, 12.5, 2.5)	F1=0.0	F2=0.0000000	F3=0.0010741	FTOT=0.0010741
F(1.0, 12.5, 3.5)	F1=0.0	F2=0.0000000	F3=0.0003942	FTOT=0.0003942
F(1.0, 12.5, 4.5)	F1=0.0	F2=0.0000000	F3=0.0001036	FTOT=0.0001036
F(1.0, 13.5,-4.5)	F1=0.0	F2=0.0	F3=0.0000257	FTOT=0.0000257
F(1.0, 13.5,-3.5)	F1=0.0	F2=0.0000000	F3=0.0000980	FTOT=0.0000980
F(1.0, 13.5,-2.5)	F1=0.0	F2=0.0000000	F3=0.0002669	FTOT=0.0002669
F(1.0, 13.5,-1.5)	F1=0.0	F2=0.0000000	F3=0.0005208	FTOT=0.0005208
F(1.0, 13.5,-0.5)	F1=0.0	F2=0.0000000	F3=0.0007273	FTOT=0.0007273
F(1.0, 13.5, 0.5)	F1=0.0	F2=0.0000000	F3=0.0007273	FTOT=0.0007273
F(1.0, 13.5, 1.5)	F1=0.0	F2=0.0000000	F3=0.0005208	FTOT=0.0005208
F(1.0, 13.5, 2.5)	F1=0.0	F2=0.0000000	F3=0.0002669	FTOT=0.0002669
F(1.0, 13.5, 3.5)	F1=0.0	F2=0.0000000	F3=0.0000980	FTOT=0.0000980
F(1.0, 13.5, 4.5)	F1=0.0	F2=0.0	F3=0.0000257	FTOT=0.0000257

TABLE AIV.2 LIQUID DROP FLUX AT VARIOUS POSITIONS DOWNSTREAM FROM POINT OF INJECTION

continued ..

Flux at Any Point	to WL1	to WL2	to WL3	
F(1.0, 14.5,-4.5)	F1=0.0	F2=0.0	F3=0.0000047	FTOT=0.0000047
F(1.0, 14.5,-3.5)	F1=0.0	F2=0.0	F3=0.0000180	FTOT=0.0000180
F(1.0, 14.5,-2.5)	F1=0.0	F2=0.0	F3=0.0000491	FTOT=0.0000491
F(1.0, 14.5,-1.5)	F1=0.0	F2=0.0	F3=0.0000957	FTOT=0.0000957
F(1.0, 14.5,-0.5)	F1=0.0	F2=0.0	F3=0.0001337	FTOT=0.0001337
F(1.0, 14.5, 0.5)	F1=0.0	F2=0.0	F3=0.0001337	FTOT=0.0001337
F(1.0, 14.5, 1.5)	F1=0.0	F2=0.0	F3=0.0000957	FTOT=0.0000957
F(1.0, 14.5, 2.5)	F1=0.0	F2=0.0	F3=0.0000491	FTOT=0.0000491
F(1.0, 14.5, 3.5)	F1=0.0	F2=0.0	F3=0.0000180	FTOT=0.0000180
F(1.0, 14.5, 4.5)	F1=0.0	F2=0.0	F3=0.0000047	FTOT=0.0000047
F(2.0,-14.5,-4.5)	F1=0.0	F2=0.0	F3=0.0	FTOT=0.0
F(2.0,-14.5,-3.5)	F1=0.0	F2=0.0	F3=0.0	FTOT=0.0
F(2.0,-14.5,-2.5)	F1=0.0	F2=0.0	F3=0.0	FTOT=0.0
F(2.0,-14.5,-1.5)	F1=0.0	F2=0.0	F3=0.0	FTOT=0.0
F(2.0,-14.5,-0.5)	F1=0.0	F2=0.0	F3=0.0	FTOT=0.0
F(2.0,-14.5, 0.5)	F1=0.0	F2=0.0	F3=0.0	FTOT=0.0
F(2.0,-14.5, 1.5)	F1=0.0	F2=0.0	F3=0.0	FTOT=0.0
F(2.0,-14.5, 2.5)	F1=0.0	F2=0.0	F3=0.0	FTOT=0.0
F(2.0,-14.5, 3.5)	F1=0.0	F2=0.0	F3=0.0	FTOT=0.0
F(2.0,-14.5, 4.5)	F1=0.0	F2=0.0	F3=0.0	FTOT=0.0
F(2.0,-13.5,-4.5)	F1=0.0	F2=0.0	F3=0.0	FTOT=0.0
F(2.0,-13.5,-3.5)	F1=0.0	F2=0.0	F3=0.0	FTOT=0.0
F(2.0,-13.5,-2.5)	F1=0.0	F2=0.0	F3=0.0	FTOT=0.0
F(2.0,-13.5,-1.5)	F1=0.0	F2=0.0	F3=0.0	FTOT=0.0
F(2.0,-13.5,-0.5)	F1=0.0	F2=0.0	F3=0.0	FTOT=0.0
F(2.0,-13.5, 0.5)	F1=0.0	F2=0.0	F3=0.0	FTOT=0.0
F(2.0,-13.5, 1.5)	F1=0.0	F2=0.0	F3=0.0	FTOT=0.0
F(2.0,-13.5, 2.5)	F1=0.0	F2=0.0	F3=0.0	FTOT=0.0
F(2.0,-13.5, 3.5)	F1=0.0	F2=0.0	F3=0.0	FTOT=0.0
F(2.0,-13.5, 4.5)	F1=0.0	F2=0.0	F3=0.0	FTOT=0.0
F(2.0,-12.5,-4.5)	F1=0.0	F2=0.0	F3=0.0	FTOT=0.0
F(2.0,-12.5,-3.5)	F1=0.0	F2=0.0	F3=0.0	FTOT=0.0
F(2.0,-12.5,-2.5)	F1=0.0	F2=0.0	F3=0.0	FTOT=0.0
F(2.0,-12.5,-1.5)	F1=0.0	F2=0.0	F3=0.0	FTOT=0.0
F(2.0,-12.5,-0.5)	F1=0.0	F2=0.0	F3=0.0	FTOT=0.0
F(2.0,-12.5, 0.5)	F1=0.0	F2=0.0	F3=0.0	FTOT=0.0
F(2.0,-12.5, 1.5)	F1=0.0	F2=0.0	F3=0.0	FTOT=0.0
F(2.0,-12.5, 2.5)	F1=0.0	F2=0.0	F3=0.0	FTOT=0.0
F(2.0,-12.5, 3.5)	F1=0.0	F2=0.0	F3=0.0	FTOT=0.0
F(2.0,-12.5, 4.5)	F1=0.0	F2=0.0	F3=0.0	FTOT=0.0
F(2.0,-11.5,-4.5)	F1=0.0	F2=0.0	F3=0.0	FTOT=0.0
F(2.0,-11.5,-3.5)	F1=0.0	F2=0.0	F3=0.0	FTOT=0.0
F(2.0,-11.5,-2.5)	F1=0.0	F2=0.0	F3=0.0	FTOT=0.0
F(2.0,-11.5,-1.5)	F1=0.0	F2=0.0	F3=0.0	FTOT=0.0
F(2.0,-11.5,-0.5)	F1=0.0	F2=0.0	F3=0.0	FTOT=0.0
F(2.0,-11.5, 0.5)	F1=0.0	F2=0.0	F3=0.0	FTOT=0.0
F(2.0,-11.5, 1.5)	F1=0.0	F2=0.0	F3=0.0	FTOT=0.0
F(2.0,-11.5, 2.5)	F1=0.0	F2=0.0	F3=0.0	FTOT=0.0
F(2.0,-11.5, 3.5)	F1=0.0	F2=0.0	F3=0.0	FTOT=0.0
F(2.0,-11.5, 4.5)	F1=0.0	F2=0.0	F3=0.0	FTOT=0.0

TABLE AIV.2 LIQUID DROP FLUX AT VARIOUS POSITIONS DOWNSTREAM FROM POINT OF INJECTION

continued ..

Any Point	to WL1	to WL2	to WL3	
F(2.0,-10.5,-4.5)	F1=0.0	F2=0.0	F3=0.0	FTOT=0.0
F(2.0,-10.5,-3.5)	F1=0.0	F2=0.0	F3=0.0	FTOT=0.0
F(2.0,-10.5,-2.5)	F1=0.0	F2=0.0	F3=0.0	FTOT=0.0
F(2.0,-10.5,-1.5)	F1=0.0	F2=0.0	F3=0.0	FTOT=0.0
F(2.0,-10.5,-0.5)	F1=0.0	F2=0.0	F3=0.0	FTOT=0.0
F(2.0,-10.5, 0.5)	F1=0.0	F2=0.0	F3=0.0	FTOT=0.0
F(2.0,-10.5, 1.5)	F1=0.0	F2=0.0	F3=0.0	FTOT=0.0
F(2.0,-10.5, 2.5)	F1=0.0	F2=0.0	F3=0.0	FTOT=0.0
F(2.0,-10.5, 3.5)	F1=0.0	F2=0.0	F3=0.0	FTOT=0.0
F(2.0,-10.5, 4.5)	F1=0.0	F2=0.0	F3=0.0	FTOT=0.0
F(2.0, -9.5,-4.5)	F1=0.0	F2=0.0	F3=0.0	FTOT=0.0
F(2.0, -9.5,-3.5)	F1=0.0	F2=0.0	F3=0.0	FTOT=0.0
F(2.0, -9.5,-2.5)	F1=0.0	F2=0.0	F3=0.0	FTOT=0.0
F(2.0, -9.5,-1.5)	F1=0.0	F2=0.0	F3=0.0	FTOT=0.0
F(2.0, -9.5,-0.5)	F1=0.0	F2=0.0	F3=0.0	FTOT=0.0
F(2.0, -9.5, 0.5)	F1=0.0	F2=0.0	F3=0.0	FTOT=0.0
F(2.0, -9.5, 1.5)	F1=0.0	F2=0.0	F3=0.0	FTOT=0.0
F(2.0, -9.5, 2.5)	F1=0.0	F2=0.0	F3=0.0	FTOT=0.0
F(2.0, -9.5, 3.5)	F1=0.0	F2=0.0	F3=0.0	FTOT=0.0
F(2.0, -9.5, 4.5)	F1=0.0	F2=0.0	F3=0.0	FTOT=0.0
F(2.0, -8.5,-4.5)	F1=0.0	F2=0.0	F3=0.0	FTOT=0.0
F(2.0, -8.5,-3.5)	F1=0.0	F2=0.0	F3=0.0	FTOT=0.0
F(2.0, -8.5,-2.5)	F1=0.0	F2=0.0	F3=0.0	FTOT=0.0
F(2.0, -8.5,-1.5)	**F1=0.0**	**F2=0.0**	**F3=0.0**	**FTOT=0.0**
F(2.0, -8.5,-0.5)	F1=0.0	F2=0.0	F3=0.0	FTOT=0.0
F(2.0, -8.5, 0.5)	F1=0.0	F2=0.0	F3=0.0	FTOT=0.0
F(2.0, -8.5, 1.5)	F1=0.0	F2=0.0	F3=0.0	FTOT=0.0
F(2.0, -8.5, 2.5)	F1=0.0	F2=0.0	F3=0.0	FTOT=0.0
F(2.0, -8.5, 3.5)	F1=0.0	F2=0.0	F3=0.0	FTOT=0.0
F(2.0, -8.5, 4.5)	F1=0.0	F2=0.0	F3=0.0	FTOT=0.0
F(2.0, -7.5,-4.5)	F1=0.0	F2=0.0	F3=0.0	FTOT=0.0
F(2.0, -7.5,-3.5)	F1=0.0	F2=0.0	F3=0.0	FTOT=0.0
F(2.0, -7.5,-2.5)	F1=0.0	F2=0.0	F3=0.0	FTOT=0.0
F(2.0, -7.5,-1.5)	F1=0.0	F2=0.0	F3=0.0	FTOT=0.0
F(2.0, -7.5,-0.5)	F1=0.0	F2=0.0	F3=0.0	FTOT=0.0
F(2.0, -7.5, 0.5)	F1=0.0	F2=0.0	F3=0.0	FTOT=0.0
F(2.0, -7.5, 1.5)	F1=0.0	F2=0.0	F3=0.0	FTOT=0.0
F(2.0, -7.5, 2.5)	F1=0.0	F2=0.0	F3=0.0	FTOT=0.0
F(2.0, -7.5, 3.5)	F1=0.0	F2=0.0	F3=0.0	FTOT=0.0
F(2.0, -7.5, 4.5)	F1=0.0	F2=0.0	F3=0.0	FTOT=0.0
F(2.0, -6.5,-4.5)	F1=0.0	F2=0.0	F3=0.0	FTOT=0.0
F(2.0, -6.5,-3.5)	F1=0.0	F2=0.0	F3=0.0	FTOT=0.0
F(2.0, -6.5,-2.5)	F1=0.0	F2=0.0	F3=0.0	FTOT=0.0
F(2.0, -6.5,-1.5)	F1=0.0	F2=0.0	F3=0.0	FTOT=0.0
F(2.0, -6.5,-0.5)	F1=0.0	F2=0.0	F3=0.0	FTOT=0.0
F(2.0, -6.5, 0.5)	F1=0.0	F2=0.0	F3=0.0	FTOT=0.0

TABLE AIV.2 LIQUID DROP FLUX AT VARIOUS POSITIONS DOWNSTREAM FROM POINT OF INJECTION

continued ..

Flux at Any Point	to WL1	to WL2	to WL3	
F(2.0, -6.5, 1.5)	F1=0.0	F2=0.0	F3=0.0	FTOT=0.0
F(2.0, -6.5, 2.5)	F1=0.0	F2=0.0	F3=0.0	FTOT=0.0
F(2.0, -6.5, 3.5)	F1=0.0	F2=0.0	F3=0.0	FTOT=0.0
F(2.0, -6.5, 4.5)	F1=0.0	F2=0.0	F3=0.0	FTOT=0.0
F(2.0, -5.5,-4.5)	F1=0.0	F2=0.0	F3=0.0	FTOT=0.0
F(2.0, -5.5,-3.5)	F1=0.0	F2=0.0	F3=0.0	FTOT=0.0
F(2.0, -5.5,-2.5)	F1=0.0	F2=0.0	F3=0.0	FTOT=0.0
F(2.0, -5.5,-1.5)	F1=0.0	F2=0.0	F3=0.0	FTOT=0.0
F(2.0, -5.5,-0.5)	F1=0.0	F2=0.0	F3=0.0	FTOT=0.0
F(2.0, -5.5, 0.5)	F1=0.0	F2=0.0	F3=0.0	FTOT=0.0
F(2.0, -5.5, 1.5)	F1=0.0	F2=0.0	F3=0.0	FTOT=0.0
F(2.0, -5.5, 2.5)	F1=0.0	F2=0.0	F3=0.0	FTOT=0.0
F(2.0, -5.5, 3.5)	F1=0.0	F2=0.0	F3=0.0	FTOT=0.0
F(2.0, -5.5, 4.5)	F1=0.0	F2=0.0	F3=0.0	FTOT=0.0
F(2.0, -4.5,-4.5)	F1=0.0	F2=0.0	F3=0.0	FTOT=0.0
F(2.0, -4.5,-3.5)	F1=0.0	F2=0.0	F3=0.0	FTOT=0.0
F(2.0, -4.5,-2.5)	F1=0.0	F2=0.0	F3=0.0	FTOT=0.0
F(2.0, -4.5,-1.5)	F1=0.0	F2=0.0	F3=0.0	FTOT=0.0
F(2.0, -4.5,-0.5)	F1=0.0	F2=0.0	F3=0.0	FTOT=0.0
F(2.0, -4.5, 0.5)	F1=0.0	F2=0.0	F3=0.0	FTOT=0.0
F(2.0, -4.5, 1.5)	F1=0.0	F2=0.0	F3=0.0	FTOT=0.0
F(2.0, -4.5, 2.5)	F1=0.0	F2=0.0	F3=0.0	FTOT=0.0
F(2.0, -4.5, 3.5)	F1=0.0	F2=0.0	F3=0.0	FTOT=0.0
F(2.0, -4.5, 4.5)	F1=0.0	F2=0.0	F3=0.0	FTOT=0.0
F(2.0, -3.5,-4.5)	F1=0.0	F2=0.0	F3=0.0	FTOT=0.0
F(2.0, -3.5,-3.5)	F1=0.0	F2=0.0	F3=0.0	FTOT=0.0
F(2.0, -3.5,-2.5)	F1=0.0	F2=0.0	F3=0.0	FTOT=0.0
F(2.0, -3.5,-1.5)	F1=0.0	F2=0.0	F3=0.0	FTOT=0.0
F(2.0, -3.5,-0.5)	F1=0.0	F2=0.0	F3=0.0	FTOT=0.0
F(2.0, -3.5, 0.5)	F1=0.0	F2=0.0	F3=0.0	FTOT=0.0
F(2.0, -3.5, 1.5)	F1=0.0	F2=0.0	F3=0.0	FTOT=0.0
F(2.0, -3.5, 2.5)	F1=0.0	F2=0.0	F3=0.0	FTOT=0.0
F(2.0, -3.5, 3.5)	F1=0.0	F2=0.0	F3=0.0	FTOT=0.0
F(2.0, -3.5, 4.5)	F1=0.0	F2=0.0	F3=0.0	FTOT=0.0
F(2.0, -2.5,-4.5)	F1=0.0	F2=0.0	F3=0.0	FTOT=0.0
F(2.0, -2.5,-3.5)	F1=0.0	F2=0.0	F3=0.0000000	FTOT=0.0000000
F(2.0, -2.5,-2.5)	F1=0.0	F2=0.0	F3=0.0000000	FTOT=0.0000000
F(2.0, -2.5,-1.5)	F1=0.0	F2=0.0	F3=0.0000000	FTOT=0.0000000
F(2.0, -2.5,-0.5)	F1=0.0	F2=0.0	F3=0.0000000	FTOT=0.0000000
F(2.0, -2.5, 0.5)	F1=0.0	F2=0.0	F3=0.0000000	FTOT=0.0000000
F(2.0, -2.5, 1.5)	F1=0.0	F2=0.0	F3=0.0000000	FTOT=0.0000000
F(2.0, -2.5, 2.5)	F1=0.0	F2=0.0	F3=0.0000000	FTOT=0.0000000
F(2.0, -2.5, 3.5)	F1=0.0	F2=0.0	F3=0.0000000	FTOT=0.0000000
F(2.0, -2.5, 4.5)	F1=0.0	F2=0.0	F3=0.0	FTOT=0.0
F(2.0, -1.5,-4.5)	F1=0.0	F2=0.0	F3=0.0000000	FTOT=0.0000000
F(2.0, -1.5,-3.5)	F1=0.0	F2=0.0	F3=0.0000000	FTOT=0.0000000
F(2.0, -1.5,-2.5)	F1=0.0	F2=0.0	F3=0.0000000	FTOT=0.0000000
F(2.0, -1.5,-1.5)	F1=0.0	F2=0.0	F3=0.0000000	FTOT=0.0000000

TABLE AIV.2 LIQUID DROP FLUX AT VARIOUS POSITIONS DOWNSTREAM FROM POINT OF INJECTION

continued ..

Any Point	to WL1	to WL2	to WL3	
F(2.0, -1.5,-0.5)	F1=0.0	F2=0.0	F3=0.0000000	FTOT=0.0000000
F(2.0, -1.5, 0.5)	F1=0.0	F2=0.0	F3=0.0000000	FTOT=0.0000000
F(2.0, -1.5, 1.5)	F1=0.0	F2=0.0	F3=0.0000000	FTOT=0.0000000
F(2.0, -1.5, 2.5)	F1=0.0	F2=0.0	F3=0.0000000	FTOT=0.0000000
F(2.0, -1.5, 3.5)	F1=0.0	F2=0.0	F3=0.0000000	FTOT=0.0000000
F(2.0, -1.5, 4.5)	F1=0.0	F2=0.0	F3=0.0000000	FTOT=0.0000000
F(2.0, -0.5,-4.5)	F1=0.0	F2=0.0	F3=0.0000000	FTOT=0.0000000
F(2.0, -0.5,-3.5)	F1=0.0	F2=0.0	F3=0.0000000	FTOT=0.0000000
F(2.0, -0.5,-2.5)	F1=0.0	F2=0.0	F3=0.0000000	FTOT=0.0000000
F(2.0, -0.5,-1.5)	F1=0.0	F2=0.0	F3=0.0000000	FTOT=0.0000000
F(2.0, -0.5,-0.5)	F1=0.0	F2=0.0	F3=0.0000000	FTOT=0.0000000
F(2.0, -0.5, 0.5)	F1=0.0	F2=0.0	F3=0.0000000	FTOT=0.0000000
F(2.0, -0.5, 1.5)	F1=0.0	F2=0.0	F3=0.0000000	FTOT=0.0000000
F(2.0, -0.5, 2.5)	F1=0.0	F2=0.0	F3=0.0000000	FTOT=0.0000000
F(2.0, -0.5, 3.5)	F1=0.0	F2=0.0	F3=0.0000000	FTOT=0.0000000
F(2.0, -0.5, 4.5)	F1=0.0	F2=0.0	F3=0.0000000	FTOT=0.0000000
F(2.0, 0.5,-4.5)	F1=0.0	F2=0.0	F3=0.0000000	FTOT=0.0000000
F(2.0, 0.5,-3.5)	F1=0.0	F2=0.0	F3=0.0000000	FTOT=0.0000000
F(2.0, 0.5,-2.5)	F1=0.0	F2=0.0	F3=0.0000000	FTOT=0.0000000
F(2.0, 0.5,-1.5)	F1=0.0	F2=0.0	F3=0.0000000	FTOT=0.0000000
F(2.0, 0.5,-0.5)	F1=0.0	F2=0.0	F3=0.0000000	FTOT=0.0000000
F(2.0, 0.5, 0.5)	F1=0.0	F2=0.0	F3=0.0000000	FTOT=0.0000000
F(2.0, 0.5, 1.5)	F1=0.0	F2=0.0	F3=0.0000000	FTOT=0.0000000
F(2.0, 0.5, 2.5)	**F1=0.0**	**F2=0.0**	**F3=0.0000000**	**FTOT=0.0000000**
F(2.0, 0.5, 3.5)	F1=0.0	F2=0.0	F3=0.0000000	FTOT=0.0000000
F(2.0, 0.5, 4.5)	F1=0.0	F2=0.0	F3=0.0000000	FTOT=0.0000000
F(2.0, 1.5,-4.5)	F1=0.0	F2=0.0	F3=0.0000000	FTOT=0.0000000
F(2.0, 1.5,-3.5)	F1=0.0	F2=0.0	F3=0.0000000	FTOT=0.0000000
F(2.0, 1.5,-2.5)	F1=0.0	F2=0.0000000	F3=0.0000000	FTOT=0.0000000
F(2.0, 1.5,-1.5)	F1=0.0	F2=0.0000000	F3=0.0000000	FTOT=0.0000000
F(2.0, 1.5,-0.5)	F1=0.0000000	F2=0.0000000	F3=0.0000001	FTOT=0.0000001
F(2.0, 1.5, 0.5)	F1=0.0000000	F2=0.0000000	F3=0.0000001	FTOT=0.0000001
F(2.0, 1.5, 1.5)	F1=0.0	F2=0.0000000	F3=0.0000000	FTOT=0.0000000
F(2.0, 1.5, 2.5)	F1=0.0	F2=0.0000000	F3=0.0000000	FTOT=0.0000000
F(2.0, 1.5, 3.5)	F1=0.0	F2=0.0	F3=0.0000000	FTOT=0.0000000
F(2.0, 1.5, 4.5)	F1=0.0	F2=0.0	F3=0.0000000	FTOT=0.0000000
F(2.0, 2.5,-4.5)	F1=0.0	F2=0.0000000	F3=0.0000000	FTOT=0.0000000
F(2.0, 2.5,-3.5)	F1=0.0	F2=0.0000000	F3=0.0000001	FTOT=0.0000001
F(2.0, 2.5,-2.5)	F1=0.0	F2=0.0000000	F3=0.0000003	FTOT=0.0000003
F(2.0, 2.5,-1.5)	F1=0.0000000	F2=0.0000000	F3=0.0000006	FTOT=0.0000006
F(2.0, 2.5,-0.5)	F1=0.0000069	F2=0.0000000	F3=0.0000008	FTOT=0.0000077
F(2.0, 2.5, 0.5)	F1=0.0000069	F2=0.0000000	F3=0.0000008	FTOT=0.0000077
F(2.0, 2.5, 1.5)	F1=0.0000000	F2=0.0000000	F3=0.0000006	FTOT=0.0000006
F(2.0, 2.5, 2.5)	F1=0.0	F2=0.0000000	F3=0.0000003	FTOT=0.0000003
F(2.0, 2.5, 3.5)	F1=0.0	F2=0.0000000	F3=0.0000001	FTOT=0.0000001
F(2.0, 2.5, 4.5)	F1=0.0	F2=0.0000000	F3=0.0000000	FTOT=0.0000000
F(2.0, 3.5,-4.5)	F1=0.0	F2=0.0000000	F3=0.0000003	FTOT=0.0000003
F(2.0, 3.5,-3.5)	F1=0.0	F2=0.0000000	F3=0.0000012	FTOT=0.0000012
F(2.0, 3.5,-2.5)	F1=0.0000000	F2=0.0000000	F3=0.0000034	FTOT=0.0000034
F(2.0, 3.5,-1.5)	F1=0.0001116	F2=0.0000002	F3=0.0000066	FTOT=0.0001183

TABLE AIV.2 LIQUID DROP FLUX AT VARIOUS POSITIONS DOWNSTREAM FROM POINT OF INJECTION

continued ..

Any Point	to WL1	to WL2	to WL3	
F(2.0, 3.5,-0.5)	F1=0.0578069	F2=0.0000004	F3=0.0000092	FTOT=0.0578164
F(2.0, 3.5, 0.5)	F1=0.0573069	F2=0.0000004	F3=0.0000092	FTOT=0.0578164
F(2.0, 3.5, 1.5)	F1=0.0001116	F2=0.0000002	F3=0.0000066	FTOT=0.0001183
F(2.0, 3.5, 2.5)	F1=0.0000000	F2=0.0000000	F3=0.0000034	FTOT=0.0000034
F(2.0, 3.5, 3.5)	F1=0.0	F2=0.0000000	F3=0.0000012	FTOT=0.0000012
F(2.0, 3.5, 4.5)	F1=0.0	F2=0.0000000	F3=0.0000003	FTOT=0.0000003
F(2.0, 4.5,-4.5)	F1=0.0	F2=0.0000000	F3=0.0000026	FTOT=0.0000026
F(2.0, 4.5,-3.5)	F1=0.0	F2=0.0000003	F3=0.0000100	FTOT=0.0000103
F(2.0, 4.5,-2.5)	F1=0.0000000	F2=0.0000034	F3=0.0000273	FTOT=0.0000307
F(2.0, 4.5,-1.5)	F1=0.0018132	F2=0.0000184	F3=0.0000532	FTOT=0.0018848
F(2.0, 4.5,-0.5)	F1=0.9392364	F2=0.0000427	F3=0.0000743	FTOT=0.9393533
F(2.0, 4.5, 0.5)	F1=0.9392364	F2=0.0000427	F3=0.0000743	FTOT=0.9393533
F(2.0, 4.5, 1.5)	F1=0.0018132	F2=0.0000184	F3=0.0000532	FTOT=0.0018848
F(2.0, 4.5, 2.5)	F1=0.0000000	F2=0.0000034	F3=0.0000273	FTOT=0.0000307
F(2.0, 4.5, 3.5)	F1=0.0	F2=0.0000003	F3=0.0000100	FTOT=0.0000103
F(2.0, 4.5, 4.5)	F1=0.0	F2=0.0000000	F3=0.0000026	FTOT=0.0000026
F(2.0, 5.5,-4.5)	F1=0.0	F2=0.0000004	F3=0.0000157	FTOT=0.0000161
F(2.0, 5.5,-3.5)	F1=0.0	F2=0.0000116	F3=0.0000598	FTOT=0.0000714
F(2.0, 5.5,-2.5)	F1=0.0000000	F2=0.0001445	F3=0.0001630	FTOT=0.0003075
F(2.0, 5.5,-1.5)	F1=0.0000569	F2=0.0007780	F3=0.0003180	FTOT=0.0011529
F(2.0, 5.5,-0.5)	F1=0.0294598	F2=0.0018051	F3=0.0004442	FTOT=0.0317091
F(2.0, 5.5, 0.5)	F1=0.0294598	F2=0.0018051	F3=0.0004442	FTOT=0.0317091
F(2.0, 5.5, 1.5)	F1=0.0000569	F2=0.0007780	F3=0.0003180	FTOT=0.0011529
F(2.0, 5.5, 2.5)	F1=0.0000000	F2=0.0001445	F3=0.0001630	FTOT=0.0003075
F(2.0, 5.5, 3.5)	F1=0.0	F2=0.0000116	F3=0.0000598	FTOT=0.0000714
F(2.0, 5.5, 4.5)	F1=0.0	F2=0.0000004	F3=0.0000157	FTOT=0.0000161
F(2.0, 6.5,-4.5)	F1=0.0	F2=0.0000060	F3=0.0000695	FTOT=0.0000754
F(2.0, 6.5,-3.5)	F1=0.0	F2=0.0001728	F3=0.0002644	FTOT=0.0004372
F(2.0, 6.5,-2.5)	F1=0.0	F2=0.0021590	F3=0.0007203	FTOT=0.0028793
F(2.0, 6.5,-1.5)	F1=0.0000000	F2=0.0116233	F3=0.0014052	FTOT=0.0130285
F(2.0, 6.5,-0.5)	F1=0.0000018	F2=0.0269691	F3=0.0019627	FTOT=0.0289336
F(2.0, 6.5, 0.5)	F1=0.0000018	F2=0.0269691	F3=0.0019627	FTOT=0.0289336
F(2.0, 6.5, 1.5)	F1=0.0000000	F2=0.0116233	F3=0.0014052	FTOT=0.0130285
F(2.0, 6.5, 2.5)	F1=0.0	F2=0.0021590	F3=0.0007203	FTOT=0.0028793
F(2.0, 6.5, 3.5)	F1=0.0	F2=0.0001728	F3=0.0002644	FTOT=0.0004372
F(2.0, 6.5, 4.5)	F1=0.0	F2=0.0000060	F3=0.0000695	FTOT=0.0000754
F(2.0, 7.5,-4.5)	F1=0.0	F2=0.0000315	F3=0.0002270	FTOT=0.0002584
F(2.0, 7.5,-3.5)	F1=0.0	F2=0.0009116	F3=0.0008637	FTOT=0.0017753
F(2.0, 7.5,-2.5)	F1=0.0	F2=0.0113870	F3=0.0023535	FTOT=0.0137405
F(2.0, 7.5,-1.5)	F1=0.0	F2=0.0513035	F3=0.0045912	FTOT=0.0558947
F(2.0, 7.5,-0.5)	F1=0.0000000	F2=0.1422405	F3=0.0064126	FTOT=0.1486531
F(2.0, 7.5, 0.5)	F1=0.0000000	F2=0.1422405	F3=0.0064126	FTOT=0.1486531
F(2.0, 7.5, 1.5)	F1=0.0	F2=0.0513036	F3=0.0045912	FTOT=0.0658947
F(2.0, 7.5, 2.5)	F1=0.0	F2=0.0113870	F3=0.0023535	FTOT=0.0137405
F(2.0, 7.5, 3.5)	F1=0.0	F2=0.0009115	F3=0.0008637	FTOT=0.0017753
F(2.0, 7.5, 4.5)	F1=0.0	F2=0.0000315	F3=0.0002270	FTOT=0.0002584
F(2.0, 8.5,-4.5)	F1=0.0	F2=0.0000586	F3=0.0005483	FTOT=0.0006068
F(2.0, 8.5,-3.5)	F1=0.0	F2=0.0016973	F3=0.0020866	FTOT=0.0037839

TABLE AIV.2 LIQUID DROP FLUX AT VARIOUS POSITIONS DOWNSTREAM FROM POINT OF INJECTION

continued ..

Any Point	to WL1	to WL2	to WL3	
F(2.0, 8.5,-2.5)	F1=0.0	F2=0.0212015	F3=0.0056855	FTOT=0.0268870
F(2.0, 8.5,-1.5)	F1=0.0	F2=0.1141409	F3=0.0110913	FTOT=0.1252322
F(2.0, 8.5,-0.5)	F1=0.0	F2=0.2648371	F3=0.0154914	FTOT=0.2803285
F(2.0, 8.5, 0.5)	F1=0.0	F2=0.2648371	F3=0.0154914	FTOT=0.2803285
F(2.0, 8.5, 1.5)	F1=0.0	F2=0.1141409	F3=0.0110913	FTOT=0.1252322
F(2.0, 8.5, 2.5)	F1=0.0	F2=0.0212015	F3=0.0056855	FTOT=0.0268870
F(2.0, 8.5, 3.5)	F1=0.0	F2=0.0015973	F3=0.0020866	FTOT=0.0037839
F(2.0, 8.5, 4.5)	F1=0.0	F2=0.0000586	F3=0.0005483	FTOT=0.0006068
F(2.0, 9.5,-4.5)	F1=0.0	F2=0.0000385	F3=0.0009794	FTOT=0.0010179
F(2.0, 9.5,-3.5)	F1=0.0	F2=0.0011156	F3=0.0037273	FTOT=0.0048429
F(2.0, 9.5,-2.5)	F1=0.0	F2=0.0139354	F3=0.0101558	FTOT=0.0240912
F(2.0, 9.5,-1.5)	F1=0.0	F2=0.0750231	F3=0.0198121	FTOT=0.0948352
F(2.0, 9.5,-0.5)	F1=0.0	F2=0.1740735	F3=0.0276719	FTOT=0.2017454
F(2.0, 9.5, 0.5)	F1=0.0	F2=0.1740735	F3=0.0276719	FTOT=0.2017454
F(2.0, 9.5, 1.5)	F1=0.0	F2=0.0750231	F3=0.0198121	FTOT=0.0948352
F(2.0, 9.5, 2.5)	F1=0.0	F2=0.0139354	F3=0.0101558	FTOT=0.0240912
F(2.0, 9.5, 3.5)	F1=0.0	F2=0.0011156	F3=0.0037273	FTOT=0.0048429
F(2.0, 9.5, 4.5)	F1=0.0	F2=0.0000385	F3=0.0009794	FTOT=0.0010179
F(2.0, 10.5,-4.5)	F1=0.0	F2=0.0000089	F3=0.0012936	FTOT=0.0013025
F(2.0, 10.5,-3.5)	F1=0.0	F2=0.0002589	F3=0.0049230	FTOT=0.0051818
F(2.0, 10.5,-2.5)	F1=0.0	F2=0.0032335	F3=0.0134138	FTOT=0.0166473
F(2.0, 10.5,-1.5)	F1=0.0	F2=0.0174079	F3=0.0261678	FTOT=0.0435757
F(2.0, 10.5,-0.5)	F1=0.0	F2=0.0403910	F3=0.0365490	FTOT=0.0769400
F(2.0, 10.5, 0.5)	**F1=0.0**	**F2=0.0403910**	**F3=0.0365490**	**FTOT=0.0769400**
F(2.0, 10.5, 1.5)	F1=0.0	F2=0.0174079	F3=0.0261678	FTOT=0.0435757
F(2.0, 10.5, 2.5)	F1=0.0	F2=0.0032335	F3=0.0134138	FTOT=0.0166473
F(2.0, 10.5, 3.5)	F1=0.0	F2=0.0002589	F3=0.0049230	FTOT=0.0051818
F(2.0, 10.5, 4.5)	F1=0.0	F2=0.0000089	F3=0.0012936	FTOT=0.0013025
F(2.0, 11.5,-4.5)	F1=0.0	F2=0.0000007	F3=0.0012633	FTOT=0.0012641
F(2.0, 11.5,-3.5)	F1=0.0	F2=0.0000212	F3=0.0048078	FTOT=0.0048290
F(2.0, 11.5,-2.5)	F1=0.0	F2=0.0002549	F3=0.0131001	FTOT=0.0133650
F(2.0, 11.5,-1.5)	F1=0.0	F2=0.0014259	F3=0.0255559	FTOT=0.0269819
F(2.0, 11.5,-0.5)	F1=0.0	F2=0.0033085	F3=0.0356944	FTOT=0.0390030
F(2.0, 11.5, 0.5)	F1=0.0	F2=0.0033085	F3=0.0356944	FTOT=0.0390030
F(2.0, 11.5, 1.5)	F1=0.0	F2=0.0014259	F3=0.0255559	FTOT=0.0269819
F(2.0, 11.5, 2.5)	F1=0.0	F2=0.0002549	F3=0.0131001	FTOT=0.0133650
F(2.0, 11.5, 3.5)	F1=0.0	F2=0.0000212	F3=0.0048078	FTOT=0.0048290
F(2.0, 11.5, 4.5)	F1=0.0	F2=0.0000007	F3=0.0012633	FTOT=0.0012641
F(2.0, 12.5,-4.5)	F1=0.0	F2=0.0000000	F3=0.0009123	FTOT=0.0009123
F(2.0, 12.5,-3.5)	F1=0.0	F2=0.0000006	F3=0.0034719	FTOT=0.0034725
F(2.0, 12.5,-2.5)	F1=0.0	F2=0.0000077	F3=0.0094599	FTOT=0.0094676
F(2.0, 12.5,-1.5)	F1=0.0	F2=0.0000412	F3=0.0184546	FTOT=0.0184958
F(2.0, 12.5,-0.5)	F1=0.0	F2=0.0000957	F3=0.0257759	FTOT=0.0258715
F(2.0, 12.5, 0.5)	F1=0.0	F2=0.0000957	F3=0.0257759	FTOT=0.0258715
F(2.0, 12.5, 1.5)	F1=0.0	F2=0.0000412	F3=0.0184546	FTOT=0.0184958
F(2.0, 12.5, 2.5)	F1=0.0	F2=0.0000077	F3=0.0094599	FTOT=0.0094676
F(2.0, 12.5, 3.5)	F1=0.0	F2=0.0000006	F3=0.0034719	FTOT=0.0034725
F(2.0, 12.5, 4.5)	F1=0.0	F2=0.0000000	F3=0.0009123	FTOT=0.0009123
F(2.0, 13.5,-4.5)	F1=0.0	F2=0.0000000	F3=0.0004871	FTOT=0.0004871
F(2.0, 13.5,-3.5)	F1=0.0	F2=0.0000000	F3=0.0018538	FTOT=0.0018538
F(2.0, 13.5,-2.5)	F1=0.0	F2=0.0000001	F3=0.0050511	FTOT=0.0050512

TABLE AIV.2 LIQUID DROP FLUX AT VARIOUS POSITIONS DOWNSTREAM FROM POINT OF INJECTION

Any Point	to WL1	to WL2	to WL3	Total Flux
F(2.0, 13.5,-1.5)	F1=0.0	F2=0.0000004	F3=0.0098539	FTOT=0.0098543
F(2.0, 13.5,-0.5)	F1=0.0	F2=0.0000010	F3=0.0137630	FTOT=0.0137640
F(2.0, 13.5, 0.5)	F1=0.0	F2=0.0000010	F3=0.0137630	FTOT=0.0137640
F(2.0, 13.5, 1.5)	F1=0.0	F2=0.0000004	F3=0.0098539	FTOT=0.0098543
F(2.0, 13.5, 2.5)	F1=0.0	F2=0.0000001	F3=0.0050511	FTOT=0.0050512
F(2.0, 13.5, 3.5)	F1=0.0	F2=0.0000000	F3=0.0018538	FTOT=0.0018538
F(2.0, 13.5, 4.5)	F1=0.0	F2=0.0000000	F3=0.0004871	FTOT=0.0004871
F(2.0, 14.5,-4.5)	F1=0.0	F2=0.0000000	F3=0.0001923	FTOT=0.0001923
F(2.0, 14.5,-3.5)	F1=0.0	F2=0.0000000	F3=0.0007319	FTOT=0.0007319
F(2.0, 14.5,-2.5)	F1=0.0	F2=0.0000000	F3=0.0019942	FTOT=0.0019942
F(2.0, 14.5,-1.5)	F1=0.0	F2=0.0000000	F3=0.0038904	FTOT=0.0038904
F(2.0, 14.5,-0.5)	F1=0.0	F2=0.0000000	F3=0.0054338	FTOT=0.0054338
F(2.0, 14.5, 0.5)	F1=0.0	F2=0.0000000	F3=0.0054338	FTOT=0.0054338
F(2.0, 14.5, 1.5)	F1=0.0	F2=0.0000000	F3=0.0038904	FTOT=0.0038904
F(2.0, 14.5, 2.5)	F1=0.0	F2=0.0000000	F3=0.0019942	FTOT=0.0019942
F(2.0, 14.5, 3.5)	F1=0.0	F2=0.0000000	F3=0.0007319	FTOT=0.0007319
F(2.0, 14.5, 4.5)	F1=0.0	F2=0.0000000	F3=0.0001923	FTOT=0.0001923
F(3.0,-14.5,-4.5)	F1=0.0	F2=0.0	F3=0.0	FTOT=0.0
F(3.0,-14.5,-3.5)	F1=0.0	F2=0.0	F3=0.0	FTOT=0.0
F(3.0,-14.5,-2.5)	F1=0.0	F2=0.0	F3=0.0	FTOT=0.0
F(3.0,-14.5,-1.5)	F1=0.0	F2=0.0	F3=0.0	FTOT=0.0
F(3.0,-14.5,-0.5)	F1=0.0	F2=0.0	F3=0.0	FTOT=0.0
F(3.0,-14.5, 0.5)	F1=0.0	F2=0.0	F3=0.0	FTOT=0.0
F(3.0,-14.5, 1.5)	**F1=0.0**	**F2=0.0**	**F3=0.0**	**FTOT=0.0**
F(3.0,-14.5, 2.5)	F1=0.0	F2=0.0	F3=0.0	FTOT=0.0
F(3.0,-14.5, 3.5)	F1=0.0	F2=0.0	F3=0.0	FTOT=0.0
F(3.0,-14.5, 4.5)	F1=0.0	F2=0.0	F3=0.0	FTOT=0.0
F(3.0,-13.5,-4.5)	F1=0.0	F2=0.0	F3=0.0	FTOT=0.0
F(3.0,-13.5,-3.5)	F1=0.0	F2=0.0	F3=0.0	FTOT=0.0
F(3.0,-13.5,-2.5)	F1=0.0	F2=0.0	F3=0.0	FTOT=0.0
F(3.0,-13.5,-1.5)	F1=0.0	F2=0.0	F3=0.0	FTOT=0.0
F(3.0,-13.5,-0.5)	F1=0.0	F2=0.0	F3=0.0	FTOT=0.0
F(3.0,-13.5, 0.5)	F1=0.0	F2=0.0	F3=0.0	FTOT=0.0
F(3.0,-13.5, 1.5)	F1=0.0	F2=0.0	F3=0.0	FTOT=0.0
F(3.0,-13.5, 2.5)	F1=0.0	F2=0.0	F3=0.0	FTOT=0.0
F(3.0,-13.5, 3.5)	F1=0.0	F2=0.0	F3=0.0	FTOT=0.0
F(3.0,-13.5, 4.5)	F1=0.0	F2=0.0	F3=0.0	FTOT=0.0
F(3.0,-12.5,-4.5)	F1=0.0	F2=0.0	F3=0.0	FTOT=0.0
F(3.0,-12.5,-3.5)	F1=0.0	F2=0.0	F3=0.0	FTOT=0.0
F(3.0,-12.5,-2.5)	F1=0.0	F2=0.0	F3=0.0	FTOT=0.0
F(3.0,-12.5,-1.5)	F1=0.0	F2=0.0	F3=0.0	FTOT=0.0
F(3.0,-12.5,-0.5)	F1=0.0	F2=0.0	F3=0.0	FTOT=0.0
F(3.0,-12.5, 0.5)	F1=0.0	F2=0.0	F3=0.0	FTOT=0.0
F(3.0,-12.5, 1.5)	F1=0.0	F2=0.0	F3=0.0	FTOT=0.0
F(3.0,-12.5, 2.5)	F1=0.0	F2=0.0	F3=0.0	FTOT=0.0
F(3.0,-12.5, 3.5)	F1=0.0	F2=0.0	F3=0.0	FTOT=0.0
F(3.0,-12.5, 4.5)	F1=0.0	F2=0.0	F3=0.0	FTOT=0.0
F(3.0,-11.5,-4.5)	F1=0.0	F2=0.0	F3=0.0	FTOT=0.0
F(3.0,-11.5,-3.5)	F1=0.0	F2=0.0	F3=0.0	FTOT=0.0
F(3.0,-11.5,-2.5)	F1=0.0	F2=0.0	F3=0.0	FTOT=0.0
F(3.0,-11.5,-1.5)	F1=0.0	F2=0.0	F3=0.0	FTOT=0.0

TABLE AIV.2 LIQUID DROP FLUX AT VARIOUS POSITIONS DOWNSTREAM FROM POINT OF INJECTION

continued ..

Any Point	to WL1	to WL2	to WL3	
F(3.0,-11.5,-0.5)	F1=0.0	F2=0.0	F3=0.0	FTOT=0.0
F(3.0,-11.5, 0.5)	F1=0.0	F2=0.0	F3=0.0	FTOT=0.0
F(3.0,-11.5, 1.5)	F1=0.0	F2=0.0	F3=0.0	FTOT=0.0
F(3.0,-11.5, 2.5)	F1=0.0	F2=0.0	F3=0.0	FTOT=0.0
F(3.0,-11.5, 3.5)	F1=0.0	F2=0.0	F3=0.0	FTOT=0.0
F(3.0,-11.5, 4.5)	F1=0.0	F2=0.0	F3=0.0	FTOT=0.0
F(3.0,-10.5,-4.5)	F1=0.0	F2=0.0	F3=0.0	FTOT=0.0
F(3.0,-10.5,-3.5)	F1=0.0	F2=0.0	F3=0.0	FTOT=0.0
F(3.0,-10.5,-2.5)	F1=0.0	F2=0.0	F3=0.0	FTOT=0.0
F(3.0,-10.5,-1.5)	F1=0.0	F2=0.0	F3=0.0	FTOT=0.0
F(3.0,-10.5,-0.5)	F1=0.0	F2=0.0	F3=0.0	FTOT=0.0
F(3.0,-10.5, 0.5)	F1=0.0	F2=0.0	F3=0.0	FTOT=0.0
F(3.0,-10.5, 1.5)	F1=0.0	F2=0.0	F3=0.0	FTOT=0.0
F(3.0,-10.5, 2.5)	F1=0.0	F2=0.0	F3=0.0	FTOT=0.0
F(3.0,-10.5, 3.5)	F1=0.0	F2=0.0	F3=0.0	FTOT=0.0
F(3.0,-10.5, 4.5)	F1=0.0	F2=0.0	F3=0.0	FTOT=0.0
F(3.0, -9.5,-4.5)	F1=0.0	F2=0.0	F3=0.0	FTOT=0.0
F(3.0, -9.5,-3.5)	F1=0.0	F2=0.0	F3=0.0	FTOT=0.0
F(3.0, -9.5,-2.5)	F1=0.0	F2=0.0	F3=0.0	FTOT=0.0
F(3.0, -9.5,-1.5)	F1=0.0	F2=0.0	F3=0.0	FTOT=0.0
F(3.0, -9.5,-0.5)	F1=0.0	F2=0.0	F3=0.0	FTOT=0.0
F(3.0, -9.5, 0.5)	F1=0.0	F2=0.0	F3=0.0	FTOT=0.0
F(3.0, -9.5, 1.5)	F1=0.0	F2=0.0	F3=0.0	FTOT=0.0
F(3.0, -9.5, 2.5)	F1=0.0	F2=0.0	F3=0.0	FTOT=0.0
F(3.0, -9.5, 3.5)	F1=0.0	F2=0.0	F3=0.0	FTOT=0.0
F(3.0, -9.5, 4.5)	F1=0.0	F2=0.0	F3=0.0	FTOT=0.0
F(3.0, -8.5,-4.5)	F1=0.0	F2=0.0	F3=0.0	FTOT=0.0
F(3.0, -8.5,-3.5)	F1=0.0	F2=0.0	F3=0.0	FTOT=0.0
F(3.0, -8.5,-2.5)	F1=0.0	F2=0.0	F3=0.0	FTOT=0.0
F(3.0, -8.5,-1.5)	F1=0.0	F2=0.0	F3=0.0	FTOT=0.0
F(3.0, -8.5,-0.5)	F1=0.0	F2=0.0	F3=0.0	FTOT=0.0
F(3.0, -8.5, 0.5)	F1=0.0	F2=0.0	F3=0.0	FTOT=0.0
F(3.0, -8.5, 1.5)	F1=0.0	F2=0.0	F3=0.0	FTOT=0.0
F(3.0, -8.5, 2.5)	F1=0.0	F2=0.0	F3=0.0	FTOT=0.0
F(3.0, -8.5, 3.5)	F1=0.0	F2=0.0	F3=0.0	FTOT=0.0
F(3.0, -8.5, 4.5)	F1=0.0	F2=0.0	F3=0.0	FTOT=0.0
F(3.0, -7.5,-4.5)	F1=0.0	F2=0.0	F3=0.0	FTOT=0.0
F(3.0, -7.5,-3.5)	F1=0.0	F2=0.0	F3=0.0	FTOT=0.0
F(3.0, -7.5,-2.5)	F1=0.0	F2=0.0	F3=0.0	FTOT=0.0
F(3.0, -7.5,-1.5)	F1=0.0	F2=0.0	F3=0.0	FTOT=0.0
F(3.0, -7.5,-0.5)	F1=0.0	F2=0.0	F3=0.0	FTOT=0.0
F(3.0, -7.5, 0.5)	F1=0.0	F2=0.0	F3=0.0	FTOT=0.0
F(3.0, -7.5, 1.5)	F1=0.0	F2=0.0	F3=0.0	FTOT=0.0
F(3.0, -7.5, 2.5)	F1=0.0	F2=0.0	F3=0.0	FTOT=0.0
F(3.0, -7.5, 3.5)	F1=0.0	F2=0.0	F3=0.0	FTOT=0.0
F(3.0, -7.5, 4.5)	F1=0.0	F2=0.0	F3=0.0	FTOT=0.0
F(3.0, -6.5,-4.5)	F1=0.0	F2=0.0	F3=0.0	FTOT=0.0
F(3.0, -6.5,-3.5)	F1=0.0	F2=0.0	F3=0.0	FTOT=0.0

TABLE AIV.2 LIQUID DROP FLUX AT VARIOUS POSITIONS DOWNSTREAM FROM POINT OF INJECTION

continued ..

	to WL1	to WL2	to WL3	
F(3.0, -6.5,-2.5)	F1=0.0	F2=0.0	F3=0.0	FTOT=0.0
F(3.0, -6.5,-1.5)	F1=0.0	F2=0.0	F3=0.0	FTOT=0.0
F(3.0, -6.5,-0.5)	F1=0.0	F2=0.0	F3=0.0	FTOT=0.0
F(3.0, -6.5, 0.5)	F1=0.0	F2=0.0	F3=0.0	FTOT=0.0
F(3.0, -6.5, 1.5)	F1=0.0	F2=0.0	F3=0.0	FTOT=0.0
F(3.0, -6.5, 2.5)	F1=0.0	F2=0.0	F3=0.0	FTOT=0.0
F(3.0, -6.5, 3.5)	F1=0.0	F2=0.0	F3=0.0	FTOT=0.0
F(3.0, -6.5, 4.5)	F1=0.0	F2=0.0	F3=0.0	FTOT=0.0
F(3.0, -5.5,-4.5)	F1=0.0	F2=0.0	F3=0.0	FTOT=0.0
F(3.0, -5.5,-3.5)	F1=0.0	F2=0.0	F3=0.0	FTOT=0.0
F(3.0, -5.5,-2.5)	F1=0.0	F2=0.0	F3=0.0	FTOT=0.0
F(3.0, -5.5,-1.5)	F1=0.0	F2=0.0	F3=0.0	FTOT=0.0
F(3.0, -5.5,-0.5)	F1=0.0	F2=0.0	F3=0.0	FTOT=0.0
F(3.0, -5.5, 0.5)	F1=0.0	F2=0.0	F3=0.0	FTOT=0.0
F(3.0, -5.5, 1.5)	F1=0.0	F2=0.0	F3=0.0	FTOT=0.0
F(3.0, -5.5, 2.5)	F1=0.0	F2=0.0	F3=0.0	FTOT=0.0
F(3.0, -5.5, 3.5)	F1=0.0	F2=0.0	F3=0.0	FTOT=0.0
F(3.0, -5.5, 4.5)	F1=0.0	F2=0.0	F3=0.0	FTOT=0.0
F(3.0, -4.5,-4.5)	F1=0.0	F2=0.0	F3=0.0	FTOT=0.0
F(3.0, -4.5,-3.5)	F1=0.0	F2=0.0	F3=0.0	FTOT=0.0
F(3.0, -4.5,-2.5)	F1=0.0	F2=0.0	F3=0.0	FTOT=0.0
F(3.0, -4.5,-1.5)	F1=0.0	F2=0.0	F3=0.0	FTOT=0.0
F(3.0, -4.5,-0.5)	F1=0.0	F2=0.0	F3=0.0	FTOT=0.0
F(3.0, -4.5, 0.5)	**F1=0.0**	**F2=0.0**	**F3=0.0**	**FTOT=0.0**
F(3.0, -4.5, 1.5)	F1=0.0	F2=0.0	F3=0.0	FTOT=0.0
F(3.0, -4.5, 2.5)	F1=0.0	F2=0.0	F3=0.0	FTOT=0.0
F(3.0, -4.5, 3.5)	F1=0.0	F2=0.0	F3=0.0	FTOT=0.0
F(3.0, -4.5, 4.5)	F1=0.0	F2=0.0	F3=0.0	FTOT=0.0
F(3.0, -3.5,-4.5)	F1=0.0	F2=0.0	F3=0.0	FTOT=0.0
F(3.0, -3.5,-3.5)	F1=0.0	F2=0.0	F3=0.0	FTOT=0.0
F(3.0, -3.5,-2.5)	F1=0.0	F2=0.0	F3=0.0	FTOT=0.0
F(3.0, -3.5,-1.5)	F1=0.0	F2=0.0	F3=0.0	FTOT=0.0
F(3.0, -3.5,-0.5)	F1=0.0	F2=0.0	F3=0.0	FTOT=0.0
F(3.0, -3.5, 0.5)	F1=0.0	F2=0.0	F3=0.0	FTOT=0.0
F(3.0, -3.5, 1.5)	F1=0.0	F2=0.0	F3=0.0	FTOT=0.0
F(3.0, -3.5, 2.5)	F1=0.0	F2=0.0	F3=0.0	FTOT=0.0
F(3.0, -3.5, 3.5)	F1=0.0	F2=0.0	F3=0.0	FTOT=0.0
F(3.0, -3.5, 4.5)	F1=0.0	F2=0.0	F3=0.0	FTOT=0.0
F(3.0, -2.5,-4.5)	F1=0.0	F2=0.0	F3=0.0	FTOT=0.0
F(3.0, -2.5,-3.5)	F1=0.0	F2=0.0	F3=0.0	FTOT=0.0
F(3.0, -2.5,-2.5)	F1=0.0	F2=0.0	F3=0.0	FTOT=0.0
F(3.0, -2.5,-1.5)	F1=0.0	F2=0.0	F3=0.0	FTOT=0.0
F(3.0, -2.5,-0.5)	F1=0.0	F2=0.0	F3=0.0	FTOT=0.0
F(3.0, -2.5, 0.5)	F1=0.0	F2=0.0	F3=0.0	FTOT=0.0
F(3.0, -2.5, 1.5)	F1=0.0	F2=0.0	F3=0.0	FTOT=0.0
F(3.0, -2.5, 2.5)	F1=0.0	F2=0.0	F3=0.0	FTOT=0.0
F(3.0, -2.5, 3.5)	F1=0.0	F2=0.0	F3=0.0	FTOT=0.0
F(3.0, -2.5, 4.5)	F1=0.0	F2=0.0	F3=0.0	FTOT=0.0
F(3.0, -1.5,-4.5)	F1=0.0	F2=0.0	F3=0.0	FTOT=0.0

TABLE AIV.2 LIQUID DROP FLUX AT VARIOUS POSITIONS DOWNSTREAM FROM POINT OF INJECTION

continued ..

Any Point	to WL1	to WL2	to WL3	Total Flux
F(3.0, -1.5,-3.5)	F1=0.0	F2=0.0	F3=0.0	FTOT=0.0
F(3.0, -1.5,-2.5)	F1=0.0	F2=0.0	F3=0.0	FTOT=0.0
F(3.0, -1.5,-1.5)	F1=0.0	F2=0.0	F3=0.0	FTOT=0.0
F(3.0, -1.5,-0.5)	F1=0.0	F2=0.0	F3=0.0	FTOT=0.0
F(3.0, -1.5, 0.5)	F1=0.0	F2=0.0	F3=0.0	FTOT=0.0
F(3.0, -1.5, 1.5)	F1=0.0	F2=0.0	F3=0.0	FTOT=0.0
F(3.0, -1.5, 2.5)	F1=0.0	F2=0.0	F3=0.0	FTOT=0.0
F(3.0, -1.5, 3.5)	F1=0.0	F2=0.0	F3=0.0	FTOT=0.0
F(3.0, -1.5, 4.5)	F1=0.0	F2=0.0	F3=0.0	FTOT=0.0
F(3.0, -0.5,-4.5)	F1=0.0	F2=0.0	F3=0.0	FTOT=0.0
F(3.0, -0.5,-3.5)	F1=0.0	F2=0.0	F3=0.0000000	FTOT=0.0000000
F(3.0, -0.5,-2.5)	F1=0.0	F2=0.0	F3=0.0000000	FTOT=0.0000000
F(3.0, -0.5,-1.5)	F1=0.0	F2=0.0	F3=0.0000000	FTOT=0.0000000
F(3.0, -0.5,-0.5)	F1=0.0	F2=0.0	F3=0.0000000	FTOT=0.0000000
F(3.0, -0.5, 0.5)	F1=0.0	F2=0.0	F3=0.0000000	FTOT=0.0000000
F(3.0, -0.5, 1.5)	F1=0.0	F2=0.0	F3=0.0000000	FTOT=0.0000000
F(3.0, -0.5, 2.5)	F1=0.0	F2=0.0	F3=0.0000000	FTOT=0.0000000
F(3.0, -0.5, 3.5)	F1=0.0	F2=0.0	F3=0.0000000	FTOT=0.0000000
F(3.0, -0.5, 4.5)	F1=0.0	F2=0.0	F3=0.0	FTOT=0.0
F(3.0, 0.5,-4.5)	F1=0.0	F2=0.0	F3=0.0000000	FTOT=0.0000000
F(3.0, 0.5,-3.5)	F1=0.0	F2=0.0	F3=0.0000000	FTOT=0.0000000
F(3.0, 0.5,-2.5)	F1=0.0	F2=0.0	F3=0.0000000	FTOT=0.0000000
F(3.0, 0.5,-1.5)	F1=0.0	F2=0.0	F3=0.0000000	FTOT=0.0000000
F(3.0, 0.5,-0.5)	F1=0.0	F2=0.0	F3=0.0000000	FTOT=0.0000000
F(3.0, 0.5, 0.5)	F1=0.0	F2=0.0	F3=0.0000000	FTOT=0.0000000
F(3.0, 0.5, 1.5)	F1=0.0	F2=0.0	F3=0.0000000	FTOT=0.0000000
F(3.0, 0.5, 2.5)	F1=0.0	F2=0.0	F3=0.0000000	FTOT=0.0000000
F(3.0, 0.5, 3.5)	F1=0.0	F2=0.0	F3=0.0000000	FTOT=0.0000000
F(3.0, 0.5, 4.5)	F1=0.0	F2=0.0	F3=0.0000000	FTOT=0.0000000
F(3.0, 1.5,-4.5)	F1=0.0	F2=0.0	F3=0.0000000	FTOT=0.0000000
F(3.0, 1.5,-3.5)	F1=0.0	F2=0.0	F3=0.0000000	FTOT=0.0000000
F(3.0, 1.5,-2.5)	F1=0.0	F2=0.0	F3=0.0000000	FTOT=0.0000000
F(3.0, 1.5,-1.5)	F1=0.0	F2=0.0	F3=0.0000000	FTOT=0.0000000
F(3.0, 1.5,-0.5)	F1=0.0	F2=0.0	F3=0.0000000	FTOT=0.0000000
F(3.0, 1.5, 0.5)	F1=0.0	F2=0.0	F3=0.0000000	FTOT=0.0000000
F(3.0, 1.5, 1.5)	F1=0.0	F2=0.0	F3=0.0000000	FTOT=0.0000000
F(3.0, 1.5, 2.5)	F1=0.0	F2=0.0	F3=0.0000000	FTOT=0.0000000
F(3.0, 1.5, 3.5)	F1=0.0	F2=0.0	F3=0.0000000	FTOT=0.0000000
F(3.0, 1.5, 4.5)	F1=0.0	F2=0.0	F3=0.0000000	FTOT=0.0000000
F(3.0, 2.5,-4.5)	F1=0.0	F2=0.0	F3=0.0000000	FTOT=0.0000000
F(3.0, 2.5,-3.5)	F1=0.0	F2=0.0	F3=0.0000000	FTOT=0.0000000
F(3.0, 2.5,-2.5)	F1=0.0	F2=0.0	F3=0.0000000	FTOT=0.0000000
F(3.0, 2.5,-1.5)	F1=0.0000000	F2=0.0000000	F3=0.0000000	FTOT=0.0000000
F(3.0, 2.5,-0.5)	F1=0.0000000	F2=0.0000000	F3=0.0000000	FTOT=0.0000000
F(3.0, 2.5, 0.5)	F1=0.0000000	F2=0.0000000	F3=0.0000000	FTOT=0.0000000
F(3.0, 2.5, 1.5)	F1=0.0000000	F2=0.0000000	F3=0.0000000	FTOT=0.0000000
F(3.0, 2.5, 2.5)	F1=0.0	F2=0.0	F3=0.0000000	FTOT=0.0000000
F(3.0, 2.5, 3.5)	F1=0.0	F2=0.0	F3=0.0000000	FTOT=0.0000000

TABLE AIV.2 LIQUID DROP FLUX AT VARIOUS POSITIONS DOWNSTREAM FROM POINT OF INJECTION

continued ..

Any Point	to WL1	to WL2	to WL3	
F(3.0, 2.5, 4.5)	F1=0.0	F2=0.0	F3=0.0000000	FTOT=0.0000000
F(3.0, 3.5,-4.5)	F1=0.0	F2=0.0	F3=0.0000000	FTOT=0.0000000
F(3.0, 3.5,-3.5)	F1=0.0	F2=0.0000000	F3=0.0000000	FTOT=0.0000000
F(3.0, 3.5,-2.5)	F1=0.0000000	F2=0.0000000	F3=0.0000000	FTOT=0.0000000
F(3.0, 3.5,-1.5)	F1=0.0000048	F2=0.0000000	F3=0.0000001	FTOT=0.0000049
F(3.0, 3.5,-0.5)	F1=0.0024961	F2=0.0000000	F3=0.0000001	FTOT=0.0024962
F(3.0, 3.5, 0.5)	F1=0.0024961	F2=0.0000000	F3=0.0000001	FTOT=0.0024962
F(3.0, 3.5, 1.5)	F1=0.0000048	F2=0.0000000	F3=0.0000001	FTOT=0.0000049
F(3.0, 3.5, 2.5)	F1=0.0000000	F2=0.0000000	F3=0.0000000	FTOT=0.0000000
F(3.0, 3.5, 3.5)	F1=0.0	F2=0.0000000	F3=0.0000000	FTOT=0.0000000
F(3.0, 3.5, 4.5)	F1=0.0	F2=0.0	F3=0.0000000	FTOT=0.0000000
F(3.0, 4.5,-4.5)	F1=0.0	F2=0.0000000	F3=0.0000000	FTOT=0.0000000
F(3.0, 4.5,-3.5)	F1=0.0	F2=0.0000000	F3=0.0000002	FTOT=0.0000002
F(3.0, 4.5,-2.5)	F1=0.0000000	F2=0.0000000	F3=0.0000004	FTOT=0.0000004
F(3.0, 4.5,-1.5)	F1=0.0011690	F2=0.0000000	F3=0.0000008	FTOT=0.0011699
F(3.0, 4.5,-0.5)	F1=0.6055604	F2=0.0000001	F3=0.0000012	FTOT=0.6055615
F(3.0, 4.5, 0.5)	F1=0.6055604	F2=0.0000001	F3=0.0000012	FTOT=0.6055615
F(3.0, 4.5, 1.5)	F1=0.0011690	F2=0.0000000	F3=0.0000008	FTOT=0.0011699
F(3.0, 4.5, 2.5)	F1=0.0000000	F2=0.0000000	F3=0.0000004	FTOT=0.0000004
F(3.0, 4.5, 3.5)	F1=0.0	F2=0.0000000	F3=0.0000002	FTOT=0.0000002
F(3.0, 4.5, 4.5)	F1=0.0	F2=0.0000000	F3=0.0000000	FTOT=0.0000000
F(3.0, 5.5,-4.5)	F1=0.0	F2=0.0000000	F3=0.0000004	FTOT=0.0000004
F(3.0, 5.5,-3.5)	F1=0.0	F2=0.0000001	F3=0.0000016	FTOT=0.0000017
F(3.0, 5.5,-2.5)	F1=0.0000000	F2=0.0000007	F3=0.0000045	FTOT=0.0000052
F(3.0, 5.5,-1.5)	F1=0.0005475	F2=0.0000038	F3=0.0000087	FTOT=0.0005600
F(3.0, 5.5,-0.5)	F1=0.2836069	F2=0.0000088	F3=0.0000122	FTOT=0.2836279
F(3.0, 5.5, 0.5)	F1=0.2836069	F2=0.0000088	F3=0.0000122	FTOT=0.2836279
F(3.0, 5.5, 1.5)	F1=0.0005475	F2=0.0000038	F3=0.0000087	FTOT=0.0005600
F(3.0, 5.5, 2.5)	F1=0.0000000	F2=0.0000007	F3=0.0000045	FTOT=0.0000052
F(3.0, 5.5, 3.5)	F1=0.0	F2=0.0000001	F3=0.0000016	FTOT=0.0000017
F(3.0, 5.5, 4.5)	F1=0.0	F2=0.0000000	F3=0.0000004	FTOT=0.0000004
F(3.0, 6.5,-4.5)	F1=0.0	F2=0.0000001	F3=0.0000034	FTOT=0.0000035
F(3.0, 6.5,-3.5)	F1=0.0	F2=0.0000035	F3=0.0000128	FTOT=0.0000162
F(3.0, 6.5,-2.5)	F1=0.0000000	F2=0.0000433	F3=0.0000348	FTOT=0.0000780
F(3.0, 6.5,-1.5)	F1=0.0000005	F2=0.0002331	F3=0.0000678	FTOT=0.0003014
F(3.0, 6.5,-0.5)	F1=0.0002564	F2=0.0005408	F3=0.0000947	FTOT=0.0008919
F(3.0, 6.5, 0.5)	F1=0.0002564	F2=0.0005408	F3=0.0000947	FTOT=0.0008919
F(3.0, 6.5, 1.5)	F1=0.0000005	F2=0.0002331	F3=0.0000678	FTOT=0.0003014
F(3.0, 6.5, 2.5)	F1=0.0000000	F2=0.0000433	F3=0.0000348	FTOT=0.0000780
F(3.0, 6.5, 3.5)	F1=0.0	F2=0.0000035	F3=0.0000128	FTOT=0.0000162
F(3.0, 6.5, 4.5)	F1=0.0	F2=0.0000001	F3=0.0000034	FTOT=0.0000035
F(3.0, 7.5,-4.5)	F1=0.0	F2=0.0000025	F3=0.0000193	FTOT=0.0000219
F(3.0, 7.5,-3.5)	F1=0.0	F2=0.0000748	F3=0.0000734	FTOT=0.0001482
F(3.0, 7.5,-2.5)	F1=0.0	F2=0.0009347	F3=0.0001999	FTOT=0.0011346
F(3.0, 7.5,-1.5)	F1=0.0000000	F2=0.0050319	F3=0.0003900	FTOT=0.0054219
F(3.0, 7.5,-0.5)	F1=0.0000000	F2=0.0116754	F3=0.0005448	FTOT=0.0122201
F(3.0, 7.5, 0.5)	F1=0.0000000	F2=0.0116754	F3=0.0005448	FTOT=0.0122201
F(3.0, 7.5, 1.5)	F1=0.0000000	F2=0.0050319	F3=0.0003900	FTOT=0.0054219
F(3.0, 7.5, 2.5)	F1=0.0	F2=0.0009347	F3=0.0001999	FTOT=0.0011346
F(3.0, 7.5, 3.5)	F1=0.0	F2=0.0000748	F3=0.0000734	FTOT=0.0001482
F(3.0, 7.5, 4.5)	F1=0.0	F2=0.0000025	F3=0.0000193	FTOT=0.0000219
F(3.0, 8.5,-4.5)	F1=0.0	F2=0.0000197	F3=0.0000820	FTOT=0.0001017

TABLE AIV.2 LIQUID DROP FLUX AT VARIOUS POSITIONS DOWNSTREAM FROM POINT OF INJECTION

continued ..

Any Point	to WL1	to WL2	to WL3	
F(3.0, 8.5,-3.5)	F1=0.0	F2=0.0005703	F3=0.0003121	FTOT=0.0008824
F(3.0, 8.5,-2.5)	F1=0.0	F2=0.0071240	F3=0.0008504	FTOT=0.0079744
F(3.0, 8.5,-1.5)	F1=0.0	F2=0.0383528	F3=0.0016590	FTOT=0.0400118
F(3.0, 8.5,-0.5)	F1=0.0	F2=0.0889888	F3=0.0023171	FTOT=0.0913059
F(3.0, 8.5, 0.5)	F1=0.0	F2=0.0889888	F3=0.0023171	FTOT=0.0913059
F(3.0, 8.5, 1.5)	F1=0.0	F2=0.0383528	F3=0.0016590	FTOT=0.0400118
F(3.0, 8.5, 2.5)	F1=0.0	F2=0.0071240	F3=0.0008504	FTOT=0.0079744
F(3.0, 8.5, 3.5)	F1=0.0	F2=0.0005703	F3=0.0003121	FTOT=0.0008824
F(3.0, 8.5, 4.5)	F1=0.0	F2=0.0000197	F3=0.0000820	FTOT=0.0001017
F(3.0, 9.5,-4.5)	F1=0.0	F2=0.0000529	F3=0.0002579	FTOT=0.0003109
F(3.0, 9.5,-3.5)	F1=0.0	F2=0.0015345	F3=0.0009816	FTOT=0.0025161
F(3.0, 9.5,-2.5)	F1=0.0	F2=0.0191584	F3=0.0026746	FTOT=0.0218429
F(3.0, 9.5,-1.5)	F1=0.0	F2=0.1031953	F3=0.0052176	FTOT=0.1084129
F(3.0, 9.5,-0.5)	F1=0.0	F2=0.2394405	F3=0.0072875	FTOT=0.2467280
F(3.0, 9.5, 0.5)	F1=0.0	F2=0.2394405	F3=0.0072875	FTOT=0.2467280
F(3.0, 9.5, 1.5)	F1=0.0	F2=0.1031953	F3=0.0052176	FTOT=0.1084129
F(3.0, 9.5, 2.5)	F1=0.0	F2=0.0191584	F3=0.0026746	FTOT=0.0218429
F(3.0, 9.5, 3.5)	F1=0.0	F2=0.0015345	F3=0.0009816	FTOT=0.0025161
F(3.0, 9.5, 4.5)	F1=0.0	F2=0.0000529	F3=0.0002579	FTOT=0.0003109
F(3.0, 10.5,-4.5)	F1=0.0	F2=0.0000503	F3=0.0005998	FTOT=0.0006501
F(3.0, 10.5,-3.5)	F1=0.0	F2=0.0014575	F3=0.0022827	FTOT=0.0037403
F(3.0, 10.5,-2.5)	F1=0.0	F2=0.0182073	F3=0.0062198	FTOT=0.0244271
F(3.0, 10.5,-1.5)	F1=0.0	F2=0.0980216	F3=0.0121337	FTOT=0.1101552
F(3.0, 10.5,-0.5)	F1=0.0	F2=0.2274359	F3=0.0169473	FTOT=0.2443832
F(3.0, 10.5, 0.5)	F1=0.0	F2=0.2274359	F3=0.0169473	FTOT=0.2443832
F(3.0, 10.5, 1.5)	F1=0.0	F2=0.0980216	F3=0.0121337	FTOT=0.1101552
F(3.0, 10.5, 2.5)	F1=0.0	F2=0.0182073	F3=0.0062198	FTOT=0.0244271
F(3.0, 10.5, 3.5)	F1=0.0	F2=0.0014576	F3=0.0022827	FTOT=0.0037403
F(3.0, 10.5, 4.5)	F1=0.0	F2=0.0000503	F3=0.0005998	FTOT=0.0006501
F(3.0, 11.5,-4.5)	F1=0.0	F2=0.0000169	F3=0.0010314	FTOT=0.0010483
F(3.0, 11.5,-3.5)	F1=0.0	F2=0.0004888	F3=0.0039252	FTOT=0.0044139
F(3.0, 11.5,-2.5)	F1=0.0	F2=0.0061053	F3=0.0106951	FTOT=0.0168004
F(3.0, 11.5,-1.5)	F1=0.0	F2=0.0328687	F3=0.0208641	FTOT=0.0537328
F(3.0, 11.5,-0.5)	F1=0.0	F2=0.0762640	F3=0.0291413	FTOT=0.1054053
F(3.0, 11.5, 0.5)	F1=0.0	F2=0.0762640	F3=0.0291413	FTOT=0.1054053
F(3.0, 11.5, 1.5)	F1=0.0	F2=0.0328687	F3=0.0208641	FTOT=0.0537328
F(3.0, 11.5, 2.5)	F1=0.0	F2=0.0061053	F3=0.0106951	FTOT=0.0168004
F(3.0, 11.5, 3.5)	F1=0.0	F2=0.0004888	F3=0.0039252	FTOT=0.0044139
F(3.0, 11.5, 4.5)	F1=0.0	F2=0.0000169	F3=0.0010314	FTOT=0.0010483
F(3.0, 12.5,-4.5)	F1=0.0	F2=0.0000020	F3=0.0013114	FTOT=0.0013134
F(3.0, 12.5,-3.5)	F1=0.0	F2=0.0000579	F3=0.0049906	FTOT=0.0050485
F(3.0, 12.5,-2.5)	F1=0.0	F2=0.0007227	F3=0.0135982	FTOT=0.0143209
F(3.0, 12.5,-1.5)	F1=0.0	F2=0.0038908	F3=0.0265276	FTOT=0.0304184
F(3.0, 12.5,-0.5)	F1=0.0	F2=0.0090277	F3=0.0370515	FTOT=0.0460792
F(3.0, 12.5, 0.5)	F1=0.0	F2=0.0090277	F3=0.0370515	FTOT=0.0460792
F(3.0, 12.5, 1.5)	F1=0.0	F2=0.0038908	F3=0.0265276	FTOT=0.0304184
F(3.0, 12.5, 2.5)	F1=0.0	F2=0.0007227	F3=0.0135982	FTOT=0.0143209
F(3.0, 12.5, 3.5)	F1=0.0	F2=0.0000579	F3=0.0049906	FTOT=0.0050485
F(3.0, 12.5, 4.5)	F1=0.0	F2=0.0000020	F3=0.0013114	FTOT=0.0013134

TABLE AIV.2 LIQUID DROP FLUX AT VARIOUS POSITIONS DOWNSTREAM FROM POINT OF INJECTION

continued ..

Flux at Any Point	Flux due to WL1	Flux due to WL2	Flux due to WL3	Total Flux
F(3.0, 13.5,-4.5)	F1=0.0	F2=0.0000001	F3=0.0012328	FTOT=0.0012329
F(3.0, 13.5,-3.5)	F1=0.0	F2=0.0000024	F3=0.0046918	FTOT=0.0046942
F(3.0, 13.5,-2.5)	F1=0.0	F2=0.0000302	F3=0.0127840	FTOT=0.0128142
F(3.0, 13.5,-1.5)	F1=0.0	F2=0.0001626	F3=0.0249392	FTOT=0.0251018
F(3.0, 13.5,-0.5)	F1=0.0	F2=0.0003773	F3=0.0348330	FTOT=0.0352103
F(3.0, 13.5, 0.5)	F1=0.0	F2=0.0003773	F3=0.0348330	FTOT=0.0352103
F(3.0, 13.5, 1.5)	F1=0.0	F2=0.0001626	F3=0.0249392	FTOT=0.0251018
F(3.0, 13.5, 2.5)	F1=0.0	F2=0.0000302	F3=0.0127840	FTOT=0.0128142
F(3.0, 13.5, 3.5)	F1=0.0	F2=0.0000024	F3=0.0046918	FTOT=0.0046942
F(3.0, 13.5, 4.5)	F1=0.0	F2=0.0000001	F3=0.0012328	FTOT=0.0012329
F(3.0, 14.5,-4.5)	F1=0.0	F2=0.0000000	F3=0.0008570	FTOT=0.0008570
F(3.0, 14.5,-3.5)	F1=0.0	F2=0.0000000	F3=0.0032615	FTOT=0.0032615
F(3.0, 14.5,-2.5)	F1=0.0	F2=0.0000004	F3=0.0088867	FTOT=0.0088871
F(3.0, 14.5,-1.5)	F1=0.0	F2=0.0000024	F3=0.0173363	FTOT=0.0173387
F(3.0, 14.5,-0.5)	F1=0.0	F2=0.0000056	F3=0.0242139	FTOT=0.0242195
F(3.0, 14.5, 0.5)	F1=0.0	F2=0.0000056	F3=0.0242139	FTOT=0.0242195
F(3.0, 14.5, 1.5)	F1=0.0	F2=0.0000024	F3=0.0173363	FTOT=0.0173387
F(3.0, 14.5, 2.5)	F1=0.0	F2=0.0000004	F3=0.0088867	FTOT=0.0088871
F(3.0, 14.5, 3.5)	F1=0.0	F2=0.0000000	F3=0.0032615	FTOT=0.0032615
F(3.0, 14.5, 4.5)	F1=0.0	F2=0.0000000	F3=0.0008570	FTOT=0.0008570

TABLE AIV.2 LIQUID DROP FLUX AT VARIOUS POSITIONS DOWNSTREAM FROM POINT OF INJECTION

VITA AUCTORIS

1944	Born in India, March 5
1960	Received Higher Secondary School Degree from D.A.S. Higher Secondary School, New Delhi, India
1962	Received Intermediate Examination Degree from Panjab University, Chandigarh, India
1966	Received Bachelor's Degree in Chemical Engineering from Panjab University, Chandigarh, India
1968	Worked as Process Engineer with Dyer Meakin Breweries, New Delhi, India
1970	Worked as a Research Fellow at Indian Institute of Technology, New Delhi, India
1972	Worked as a Project Engineer with Turcon India Private Limited, New Delhi, India
1973	Worked as Senior Engineer with Industrial Development Services Private Limited, New Delhi, India
1975	Received Degree of Master of Applied Science in Chemical Engineering from the University of Windsor, Windsor, Ontario